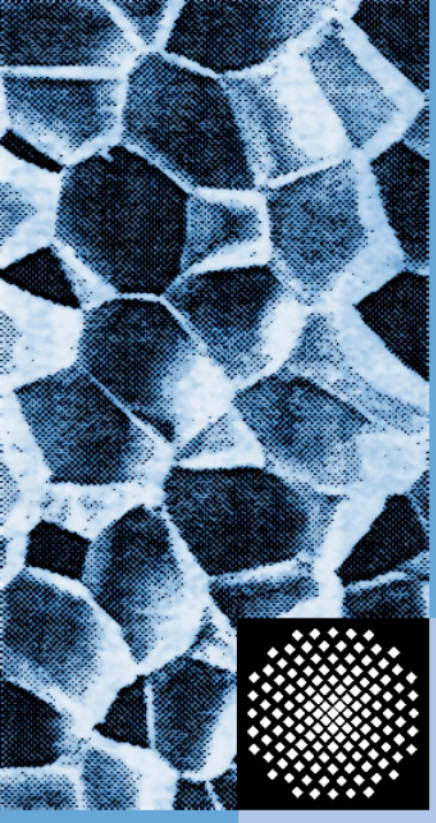

Universität Stuttgart
Germany

Institut für Mechanik (Bauwesen)
Lehrstuhl II, Prof. Dr.-Ing. W. Ehlers

Simulation of Charged Hydrated Porous Materials

Ayhan Yusuf Acartürk

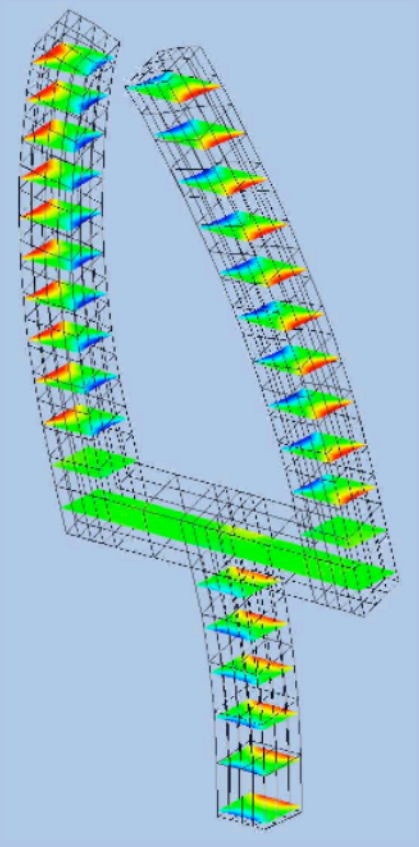

Report No.: II-18 (2009)

Simulation of Charged Hydrated Porous Materials

Von der Fakultät Bau- und Umweltingenieurwissenschaften
der Universität Stuttgart zur Erlangung der Würde
eines Doktor-Ingenieurs (Dr.-Ing.)
genehmigte Abhandlung

vorgelegt von

Dipl.-Ing. Ayhan Yusuf Acartürk

aus
Stuttgart

Hauptberichter:	Prof. Dr.-Ing. Wolfgang Ehlers
1. Mitberichter:	Dr. Ir. Jacques M. R. J. Huyghe
2. Mitberichter:	Prof. Dr.-Ing. Rainer Helmig

Tag der mündlichen Prüfung: 27.03.2009

Institut für Mechanik (Bauwesen) der Universität Stuttgart
Lehrstuhl II, Prof. Dr.-Ing. W. Ehlers
2009

Report No. II-18
Institut für Mechanik (Bauwesen), Lehrstuhl II (Kontinuumsmechanik)
Universität Stuttgart, Germany, 2009

Editor:
Prof. Dr.-Ing. W. Ehlers

Institut für Mechanik (Bauwesen)
Lehrstuhl II (Kontinuumsmechanik)
Universität Stuttgart
Pfaffenwaldring 7
70569 Stuttgart, Germany

VGE Verlag Glückauf Essen
Produced by VGE Verlag GmbH, Essen, Germany
Printed by DIP – Digital Print, Witten, Germany, 2009

ISBN 3–937399–18–6
(D 93 - Dissertation, Universität Stuttgart)

Acknowledgments

The work presented in this doctoral thesis was carried out in the years between 2002 and 2008, when I was working as a research associate at the Institute of Applied Mechanics (Civil Engineering) at the Universität Stuttgart. Numerous people contributed in many ways to the realisation of this work - all their support is most gratefully acknowledged.

First of all I would like to thank my supervisor, Prof. Dr.-Ing. Wolfgang Ehlers, for giving me the opportunity to write this thesis at his institute. Most of all, I want to thank him for the interesting scientific and exciting personal discussions we had. He was a great mentor during my time at the institute. I also want to thank my co-refferee, Jacques Huyghe, for giving me the opportunity of two visits at the department of biomedical engineering at the University of Eindhoven (NL) and for the fruitful time I had together with his team. And last but not least my thank goes to Rainer Helmig for taking on the function of the second co-refferee and also for the open minded scientific discussions.

During my time at the Institute a couple of important people crossed my way. First of all, there was Peter Blome, who has been a good cycling friend and a good mentor for me in the beginning of my academic career. Martin Ammann, Tobias Graf, Bernd Scholz and me spent a lot of time together running around the Bären Seas, discussing scientific stuff - and also just having fun. I also would like to mention Dominik Zimmermann, with whom I had really good conversations during our relaxed evenings in tapas bars - also with Fabian Welschinger. Together with Uwe Rempler we administered the computer network of the institute and had some intense and also good time - uiuiuiui. I thank Famke Kraaijeveld for her support during my stay in the Netherlands, my room mate Yousef Heider for the very good atmosphere and Nils Karajan for the fruitful co-operations and discussions. Finally, I also want to thank my diploma/master students Thomas Hille, Joffrey Mabuma and Arzu Avci who have contributed to this thesis with their great work.

My best friend Martin Reitz has helped me through this time with conversations, prayers and recreative times in the sauna. I also thank Konrad Lazarus for his friendship and prayers. My longtime friend Marc-Oliver Kaiser is always there, whenever I need a friend.

My special thanks I would like to give to my fiancée Miriam Höß for her belief, for always asking the right questions, for the open-minded discussions and simply for the great and eventful time we already spent together up to now.

My brother Tolga Acartürk together with his family has been a great support. And last but not least I would like to thank my parents Musa and Susanne Acartürk for always believing in me, trusting me and supporting me in just the right amount during my life.

Stuttgart, March 2009

Ayhan Acartürk

If you look for truth, you may find comfort in the end;
if you look for comfort, you will not get either comfort or truth,
only soft soap and wishful thinking to begin, and in the end, despair.

C. S. Lewis, Mere Christianity

Deutsche Zusammenfassung

Es ist das Ziel dieser Arbeit, das Verhalten von geladenen, hydratisierten, mehrphasigen Materialien zu verstehen und thermodynamisch konsistent zu modellieren, um anschließend anhand von numerischen Simulationen die Reaktion dieser Materialien auf Veränderungen in ihrer Umgebung wirklichkeitsnah wiedergeben zu können. Das Verständnis über die in diesen Vorgängen enthaltenen Phänomene trägt einerseits dazu bei, Schäden, die durch falschen Umgang mit diesen Materialien entstehen können, zu verhindern. Andererseits ist ein solches Verständnis von essentieller Bedeutung, um die Eigenschaften dieser Materialien gewinnbringend nutzen zu können.

Hydratisierte, poröse Medien sind aus mehreren Konstituierenden zusammengesetzt, d. h. sie bestehen aus einem geladenen Festkörperskelett, in dessen Hohlräumen sich ein viskoses Porenfluid bewegt. Dieses Porenfluid wiederum enthält das Lösungsmittel sowie die gelösten Ionen eines Salzes. Durch diesen speziellen Aufbau antworten solche Medien mit Quell- und Schrumpfprozessen auf elektrische Felder und auf Änderungen der chemischen Zusammensetzung ihrer Umgebung.

Sowohl in der Geomechanik als auch in der Biomechanik sind Materialien mit einer solchen Zusammensetzung relevant. Als Beispiele aus der Geomechanik seien hier Ton und Schiefer genannt. Deren geladener Festkörper setzt sich aus Plättchen zusammen, die aus Aluminium-Silikat-Molekülen bestehen und über Adhäsionskräfte die Festkörpermatrix bilden. Probleme können auftreten, wenn man z. B. bei Bohrungen in tieferen Erdschichten auf Ton oder Schiefer trifft. Hat nun die verwendete Stützflüssigkeit die falsche Konzentration, kommt es zu den oben genannten Quell- und Schrumpfprozessen. Quillt der Boden, verringert sich der Bohrquerschnitt, was dazu führen kann, dass der Bohrer steckenbleibt. Im Falle von Schrumpfungen wird sich ein Hohlraum bilden, der von der vorbeiströmenden Stützflüssigkeit ausgespült werden kann. Beides ist natürlich wegen der damit verbundenen immensen Folgekosten aus Sicht der Bohrfirmen nicht wünschenswert. Die Eigenschaften hydratisierter, porŝer Medien können jedoch auch positiv genutzt werden. Wird durch eine Erdschicht gebohrt, die zwei Wasserschichten voneinander trennt, können quellende Bentonit-Kügelchen in das Bohrloch in der Trennschicht eingebracht werden. Anschließend wird das Bentonit quellen und das Loch somit abgedichten. Auch in der Meerwasserentsalzung finden sich poröse Materialien mit geladenen Festkörperskeletten als Filter wieder.

Im Gegensatz zu Ton und Schiefer bestehen weiche biologische Gewebe, wie z. B. Knorpelgewebe oder der innere Kern der Bandscheiben, der Nucleus Pulposus, aus ungeordneten Kollagenfasern und langkettigen Proteoglykanen mit freien Ladungen. Diese bilden das geladene, isotrope Festkörperskelett, während in den Zwischenräumen eine geladene Porenflüssigkeit strömt. Auch hier spielt die Quellfähigkeit eine immens wichtige Rolle. Lässt beispielsweise altersbedingt die Konzentration der an dem Festkörper haftenden Ladungen in der Bandscheibe nach, so sinkt auch der osmotische Druck darin. Infolge dessen verliert die Bandscheibe an Volumen, bis sich in weit fortgeschrittenem Stadium die Wirbelkörper berühren. Das kann zu sehr starken Rückenbeschwerden führen. Ausgelöst durch einen Unfall, kann das Knorpelgewebe in den Gelenken zerstört werden,

so dass im Laufe der Zeit Knorpelgewebe abgebaut wird und dessen schmierende Wirkung verlorengeht. In diesen Fällen besteht die Möglichkeit, ein künstliches Pendant aus Hydrogel als Ersatz zu verwenden. Beispielsweise kann der Nucleus Pulposus einer degenerierten Bandscheibe durch ein entsprechendes Hydrogel-Kissen ersetzt werden, welches die Dämpfungseigenschaft und auch die Bewegungsfreiheit zum großen Teil wieder herstellt. Im Falle von Gelenkknorpel ist es möglich, biokompatibles Hydrogel mit Stammzellen anzureichern und dieses dann in das Gelenk einzuspritzen. Die Stammzellen werden im Laufe der Zeit neues Knorpelgewebe aufbauen und das biokompatible Hydrogel wird sich zersetzen.

In der Robotik wird Hydrogel aus unterschiedlichen Gründen verwendet. Ein Vorteil ist, dass es künstlich hergestellt wird und somit in der industriellen Produktion mit genau vorgegebenen Eigenschaften produziert werden kann. Des weiteren verfügt es über die Fähigkeit, mit großen Deformationen auf elektrische Felder zu reagieren. Muskeln müssen beispielsweise wiederholt sehr große Deformationen ausüben können. Sie könnten also durch Hydrogel ersetzt werden. Geht man noch einen Schritt weiter und berücksichtigt, dass Hydrogel transparent ist, kann es ebenso in der Optik als künstliche Linse eingesetzt werden, die je nach angelegter elektrischer Spannung ihre optischen Eigenschaften über Deformationen verändert. Resultierend aus der Tatsache, dass Hydrogel ein auf elektrische Felder reagierendes Polymer ist, wird es auch als elektroaktives Polymer (EAP) bezeichnet.

Aus dem bisherigen Überblick über das Vorkommen dieser geladenen, hydratisierten, mehrphasigen Materialien sowohl in der Natur als auch in der Technik und über ihre Einsatzmöglichkeiten lässt sich auf die Größe des Interesses schließen, das Verhalten dieser Materialien zu verstehen sowie Vorhersagen darüber treffen zu können. Für den ingenieursmäßigen Einsatz werden Modelle benötigt, mit deren Hilfe diese Materialien möglichst präzise berechnet werden können. Ebenso folgt aus den bisherigen Betrachtungen, dass nur ein ganzheitliches Modell mit allen individuellen Eigenschaften der Konstituierenden die unterschiedlichen Phänomene, die in geladenen, hydratisierten Materialien vorkommen, abbilden kann. Aus diesem Grund ist es das Ziel dieser Arbeit, ein neues, auf der Theorie Poröser Medien (TPM) basierendes und thermodynamisch konsistentes Modell zu entwickeln, welches alle mechanischen, chemischen und elektrischen Effekte unter Berücksichtigung großer Deformationen einschließt.

An der oben beschriebenen Zusammensetzung der geladenen, hydratisierten, mehrphasigen Materialien wird schon deutlich, dass ein solches Kontinuum eine komplizierte Mikrostruktur aufweist. Zur Modellierung solcher komplexer Mikrostrukturen gibt es unterschiedliche Ansätze. Eine Möglichkeit besteht darin, genau diese Mikrostruktur und die Interaktionen der Konstituierenden über ein diskretes mikroskopisches Modell abzubilden und daraus den Gesamtkörper zusammenzusetzen. Allerdings ist es in so einem Fall schwierig, die benötigten Materialparameter für ein solches Modell anhand von Versuchen zu bestimmen. Außerdem ist der numerische Aufwand für die Simulation eines solchen Modells trotz stetig steigender Computerleistung für realistische Geometrien immer noch zu hoch. Alternativ gibt es die Möglichkeit, motiviert über die Charakteristiken der einzelnen Konstituierenden in der Mikroskale, ein kontinuumsmechanisches Modell direkt auf der Makroskale aufzubauen. Hierbei werden die Eigenschaften der Konstituierenden

über ein bestimmtes repräsentatives Elementarvolumen (REV) gemittelt und kontinuierlich verteilt über das gesamte Volumen angenommen. Der Vorteil eines solchen Vorgehens liegt klar auf der Hand. Zur Modellfindung werden weder die exakte Geometrie der Mikrostruktur noch die Interaktionen der einzelnen Konstituierenden benötigt. Des weiteren können makroskopische Versuche durchgeführt werden, deren Ergebnisse als Materialparameter direkt in das Modell einfließen. Ausgehend von diesen Vorüberlegungen gründet sich die vorliegende Arbeit auf die makroskopische Theorie Poröser Medien (TPM). Die TPM beruht auf der Mischungstheorie, siehe Bowen [27], die um das Konzept der Volumenanteile erweitert wurde. Erste Gedanken hierzu stammen von Woltman [169]. Durch die Verknüpfung der Mischungstheorie, welche *a priori* nur mischbare Konstituierende, wie z. B. Lösungen und Gasgemische kennt, mit dem Konzept der Volumenanteile ist es anhand der TPM möglich, Mischungen aus nichtmischbaren Konstituierenden, wie z. B. Schäume und Geomaterialien, zu beschreiben. Die TPM in ihrer heutigen Form geht zurück auf die Arbeiten von Bowen [28, 29], Mow *et al.* [136], de Boer & Ehlers [24], Ehlers [51, 53, 55, 56] und de Boer [23]. Einen sehr schönen und detaillierten Überblick über die Entwicklung der TPM gibt de Boer [22]. Erste Ansätze zur Modellierung von Quellphänomenen finden sich in Lanir [118]. Später folgen die Arbeiten von Lai *et al.* [116] mit dem ersten Modell, welches die Diffusion einer Ionensorte berücksichtigt. Die Arbeiten von Huyghe & Janssen [107] und Frijns *et al.* [76] beruhen auf den chemischen Potentialen der gelösten Ionen. Dadurch wird es nötig, beide gelösten Ionen separat zu berücksichtigen. Später folgen Arbeiten von van Loon *et al.* [122] und Malakpoor [129], in denen die Elektroneutralitätsbedingung als weitere Bilanzgleichung schwach erfüllt wird. In der vorliegenden Arbeit werden ebenso beide Ionensorten anhand ihrer jeweiligen Bewegungsgleichung beschrieben, wobei hier im Vergleich zu den bereits erwähnten Modellen als Primärvariablen sowohl die Konzentrationen als auch die chemischen Potentiale der Fluidkomponenten gewählt werden können. Des weiteren wird im Gegensatz zu anderen Arbeiten die *Poisson*-Gleichung zur Bestimmung des elektrischen Potentials herangezogen.

Um die eingangs erwähnten Ziele zu erreichen, bietet **Kapitel 1** zunächst eine kurze Einführung in die Thematik der geladenen, hydratisierten Materialien. Außerdem wird die kontinuumsmechanische Herangehensweise der Modellbildung motiviert und es wird ein Überblick über die bisherige Literatur auf diesem Feld gegeben.

Anschließend geht **Kapitel 2** auf die grundlegenden Konzepte, auf denen die Theorie Poröser Medien und somit auch diese Arbeit beruht, ein, um ein allgemeines mehrphasiges Material zu beschreiben. Im Wesentlichen geht es hierbei zunächst um das Konzept der Volumenanteile und der daraus folgenden partiellen Größen, wie die Dichten und die Konzentrationen. Die Kinematik jeder einzelnen Konstituierenden wird anhand ihrer individuellen Bewegungsfunktion beschrieben, aus der sich die individuellen Geschwindigkeiten ermitteln lassen. Ebenso wird in diesem Kapitel auf die Beschreibung der Deformationen und der daraus folgenden Spannungen eingegangen. Abschließend werden die allgemein gültigen Formen der Bilanzrelationen für Mehrphasenmaterialien axiomatisch eingeführt, wobei hier neben den bekannten kontinuumsmechanischen Massen-, Impuls-, Drall-, Energie- und Entropiebilanzen zusätzlich Bilanzrelationen aus der Elektrodynamik eingeführt werden. Die elektrodynamischen Bilanzgleichungen bestehen aus den vier *Maxwell*-Gleichungen und der Ladungsbilanz. Die *Clausius-Planck*-Form der Entropieunglei-

chung wird für den speziellen Fall konstanter und einheitlicher Temperaturen angegeben, die später in dieser Arbeit ausgewertet wird.

Nach diesem allgemeinen, für alle Mehrphasenkontinua gültigen Teil, werden in **Kapitel 3** die axiomatisch eingeführten Bilanzgleichungen anhand von entsprechenden Annahmen an die gegebene Situation angepasst. Dazu zählt beispielsweise, dass das betrachtete Kontinuum zunächst aus zwei nicht mischbaren Phasen, dem Festkörperskelett und dem Porenfluid besteht. Resultierend aus der Tatsache, dass ein sich deformierendes Festkörperskelett beschrieben wird, werden alle kinematischen Größen auf den sich bewegenden Festkörper bezogen. Das betrifft neben den Volumen-, Konzentrations-, Ladungs- und Impulsbilanzen auch die Entropieungleichung. Letztere Bilanz wird noch weiter dahingehend transformiert, dass die zwei nichtmischbaren Phasen, der Festkörper und das Porenfluid, separiert werden können. Dazu wird der Festkörper von den anderen Konstituierenden abgespalten und die Fluidkomponenten, die aufsummiert das Porenfluid ergeben, separat erscheinen. Es gibt zwei starke Restriktionen an das Gesamtaggregat. Das ist zum einen die Sättigungsbedingung, die zu jeder Zeit erfüllt sein muss, d. h. der Fall, dass sich irgendwann in einem Teil des Kontinuums keine Materie befindet, kann nicht vorkommen. Des weiteren ist die Elektroneutralitätsbedingung ebenso zu jeder Zeit an jedem Raumpunkt zu erfüllen. Das bedeutet, dass zu keinem Zeitpunkt eine Ladungsseparation auftreten darf. Diese beiden Restriktionen werden anhand von *Lagrange*-Multiplikatoren in die Entropieungleichung eingearbeitet. Anhand des Konzepts der effektiven Größen werden die Spannungstensoren und die Impulsproduktionen der Konstituierenden in einen von den *Lagrange*-Multiplikatoren bestimmten Anteil und in einen effektiven Anteil aufgeteilt, der sich aus der freien *Helmholtz*schen Energie der Komponente ergibt, d. h. aus einem Potential berechenbar ist. Nach diesen vorbereitenden Maßnahmen müssen für die Konstitutivtheorie die Prozeßvariablen bestimmt werden, von denen die gesuchten Antwortfunktionen abhängen. Anschließend können die gesuchten Ableitungen gebildet werden, und die Entropieungleichung kann ausgewertet werden. Durch diese Vorgehensweise ist sichergestellt, dass die konstitutiven Annahmen die Entropieungleichung nicht verletzen. Aus dieser Auswertung des Gleichgewichtsanteils der Entropieungleichung werden die Definitionen für das chemische Potential und den osmotischen Druck sowohl für jede einzelne Komponente als auch für das gesamte Porenfluid gefunden. Die oben eingeführten *Lagrange*-Multiplikatoren sind an dieser Stelle immer noch unbestimmt. Durch den Vergleich mit anderen Fällen werden diese unbestimmten Größen als der rein mechanische, hydraulische Druck und das elektrische Potential identifiziert. Danach wird der Ungleichgewichtsanteil, der sogenannte dissipative Anteil der Entropieungleichung, ausgewertet. Als Ergebnis erhält man die individuellen Impulsproduktionen der Konstituierenden. Anschließend wird die Bestimmungsgleichung des elektrischen Potentials im Rahmen der Elektrostatik hergeleitet. Nach der Beschreibung des Festkörperskeletts anhand eines erweiterten Materialgesetzes vom Neo-*Hooke*-Typ, werden die Bewegungsgleichungen sowohl der einzelnen Fluidkomponenten als auch die des Porenfluids als Ganzes entwickelt. Den Abschluss dieses Kapitels bildet eine kurze Diskussion der Primärvariablen des Modells. Im späteren Verlauf der Arbeit wird noch intensiver auf die Abhängigkeiten der Primärvariablen eingegangen.

Die im vorherigen Kapitel hergeleitete Theorie besteht aus fünf Bilanzgleichungen und

wird in dem nun folgenden **Kapitel 4** so aufbereitet, dass Anfangs-Randwertprobleme anhand eines numerischen Verfahrens wie der Finite-Elemente-Methode (FEM) gelöst werden können. Dazu werden zunächst die Anfangs- und Randbedingungen für die einzelnen partiellen Differentialgleichungen (PDG) diskutiert. Bei näherer Betrachtung fällt auf, dass sich für die Lösung des PDG-Satzes unterschiedliche Primärvariablensätze auswählen lassen. Bei diesen Variablen handelt es sich um die Festkörperverschiebung, den Gesamtdruck des Porenfluids, die molaren Konzentrationen der dissoziierten Ionen und das elektrische Potential. Hier lassen sich jeweils unabhängig der Gesamtdruck durch den rein hydraulischen Druck ersetzen und die molaren Konzentrationen durch die entsprechenden molaren chemischen Potentiale. Die entsprechend benötigten Gleichungssätze werden diskutiert und die jeweiligen Vor- und Nachteile herausgestellt. Ebenso werden mögliche Vereinfachungen diskutiert, bei denen durch spezielle Annahmen die Anzahl der Primärvariablen und somit die Anzahl der zu lösenden Gleichungen reduziert wird. Des weiteren fällt hier auf, dass je nach Wahl des Primärvariablensatzes die Randbedingungen vom aktuellen Zustand des Gebietes, d. h. von Variablen, die nur innerhalb des Gebietes existieren, abhängen. Das ist beispielsweise der Fall für den Gesamtdruck, die molaren Konzentrationen und das elektrische Potential. Solche Randbedingungen treten auch bei Strömungen mit freien Oberflächen und auch bei der Fluid-Struktur-Interaktion auf. Diese Randbedingungen müssen, damit sie immer dem aktuellen Zustand des Systems entsprechen, mit in die schwachen Formen der Bilanzgleichungen eingebunden werden. Die aus den vier verschiedenen Möglichkeiten des Primärvariablensatzes resultierenden PDG werden alle inklusive ihrer schwachen Formen diskutiert. Auffällig ist hier, dass die Variante mit dem Gesamtdruck und den molaren Konzentrationen bzgl. den Randbedingungen die komplizierteste ist. Um diese Gleichungssätze innerhalb der FEM zu lösen, werden sie sowohl im Raum als auch in der Zeit diskretisiert. Hierbei wird im Wesentlichen von den in gemischten Methoden üblicherweise verwendeten Verfahren Gebrauch gemacht. Für die räumliche Diskretisierung werden *Taylor-Hood*-Elemente verwendet. Somit ergibt sich die Wahl von quadratischen Ansatzfunktionen für die Festkörperverschiebung und von linearen Ansatzfunktionen für den Druckfreiheitsgrad (gesamt oder hydraulisch), die Konzentrationen bzw. chemischen Potentiale und das elektrische Potential. Nach der anschließenden zeitlichen Diskretisierung anhand des impliziten *Euler* Zeitintegrationsverfahrens wird auf die Prozedur zur Lösung des resultierenden Gleichungssystems anhand des *Newton*-Verfahrens eingegangen. Hierbei wird die Systemtangente durch Ableitung des Residuums numerisch bestimmt.

In **Kapitel 5** werden Simulationen anhand des in dieser Arbeit hergeleiteten Modells durchgeführt. In einem ersten Schritt werden zunächst die unterschiedlichen Primärvariablensätze numerisch untersucht. Dabei wird ein besonderes Augenmerk auf die Ergebnisse und die Stabilität des numerischen Lösungsverfahrens gelegt. Dabei zeigt sich, dass der Primärvariablensatz mit den meisten schwach zu erfüllenden Randbedingungen die genaueren Ergebnisse liefert und am stabilsten rechnet. Das ergibt sich aus der Simulation eines eindimensionalen Quellexperiments. Für die Simulation dieses Experiments werden konzentrationsabhängige Aktivitätskoeffizienten eingeführt. Anschließend wird die Reaktion eines EAP auf elektrische Felder anhand von eindimensionalen Rechnungen untersucht. Um die Leistungsfähigkeit des Modells zu demonstrieren, werden abschließend zwei dreidimensionale Simulationen gezeigt. Zum einen handelt es sich dabei um die Si-

mulation eines quellenden Hydrogel-Zylinders mit finiten Deformationen, zum anderen um die Simulation einer Zange aus Hydrogel, einem EAP, die sich durch Anbringen einer elektrischen Spannung schließt.

Abschließend werden die Ergebnisse aus der vorliegenden Arbeit in **Kapitel 6** zusammengefasst. Obwohl die Formulierung anhand des Gesamtdrucks und der molaren Konzentration einen merklichen Mehraufwand für die Programierung bedeutet, lässt sich feststellen, dass dieser Satz an Primärvariablen numerisch weitaus stabiler und schneller ist. Quellversuche können besser nachgerechnet werden und die Simulationszeiten sinken erheblich.

Contents

Nomenclature

Based on well known contributions to tensor calculus such as de Boer [21] and Holzapfel [99], scalar values are denoted by italic letters (a), bold upright roman minuscules are used for vectors ($\mathbf{a}$) and bold roman majuscules to denote tensors ($\mathbf{A}$). Moreover, concerning the naming of the physical quantities, the convention used within this monograph is based on de Boer [22] and Ehlers [56].

Symbols

$(\bar{\cdot})$	given quantities of the external solution
$(\tilde{\cdot})$	boundary terms depending on internal variables
$(\hat{\cdot})$	production terms
$\partial(\cdot)$	surface of the body or boundary of the domain
$\mathrm{d}(\cdot)$	differential element of a quantity
$\delta(\cdot)$	test functions
$(\overset{\prime}{\cdot})_\alpha$, $(\overset{\prime\prime}{\cdot})_\alpha$	first and second material time derivative with respect to the moving constituent α
$(\dot{\cdot})$	time derivative with respect to the overall mixture

Calligraphic letters

$\mathcal{E}$	$[\,\mathrm{V}\,]$	*Lagrange*an multiplier (electric potential)
$\mathcal{P}$	$[\,\mathrm{N/m^2}\,]$	*Lagrange*an multiplier (hydraulic pressure)
$\mathcal{R}$		set of response functions
$\mathcal{S}$		set of process variables
$\mathcal{V}$		set of fundamental process variables

Latin letters

a^α	$[\,\mathrm{mol/m^3}\,]$	activity
$\mathbf{A}_\alpha$	$[-]$	*Almansi*an strain tensor
$\mathbf{b}_e^\alpha$	$[\,\mathrm{T}\,]$	magnetic flux density (magnetic field)
$\mathbf{B}_\alpha$	$[-]$	left *Cauchy-Green* deformation tensor
c_m^α	$[\,\mathrm{mol/m^3}\,]$	molar concentration
$\mathbf{C}_\alpha$	$[-]$	right *Cauchy-Green* deformation tensor

$\mathbf{d}_\alpha$	$[\,\mathrm{m/s}\,]$	diffusion velocity
$\mathbf{d}_e^\alpha$	$[\,\mathrm{C/m^2}\,]$	electric flux density (electric displacement)
D^α	$[\,\mathrm{m^2/s}\,]$	diffusion coefficient
$\mathbf{D}_\alpha$	$[\,\mathrm{1/s}\,]$	strain rate tensor
$\bar{e}$	$[\,\mathrm{V/m}\,]$	electric field at the domain boundary
$\hat{e}^\alpha$	$[\,\mathrm{J/kg\,s}\,]$	total production of internal energy
$\mathbf{e}_e^\alpha$	$[\,\mathrm{V/m}\,]$	electric field
$\mathbf{E}_\alpha$	$[\,-\,]$	*Green* strain tensor
f^α	$[\,-\,]$	activity coefficient
$\boldsymbol{f}$		generalised force vector
F	$[\,\mathrm{C/mol}\,]$	*Faraday* constant
$\boldsymbol{F}$		vector of the residuum
$\mathbf{F}_\alpha$	$[\,-\,]$	deformation gradient
$\mathbf{g}_\alpha$	$[\,\mathrm{m/s^2}\,]$	gravity
$\mathbf{h}_e^\alpha$	$[\,\mathrm{A/m}\,]$	magnetic field intensity
$\hat{\mathbf{h}}^\alpha$	$[\,\mathrm{N/m^2}\,]$	total production of moment of momentum
$\mathbf{i}_e^\alpha$	$[\,\mathrm{C/m^2\,s}\,]$	electric current
I	$[\,\mathrm{mol/m^3}\,]$	ionic strength
$\mathbf{I}$	$[\,-\,]$	identity tensor
$\bar{\jmath}^\alpha$	$[\,\mathrm{mol/m^2\,s}\,]$	ion efflux over the boundary
J_α	$[\,-\,]$	*Jacobi*an determinant
k^α	$[\,\mathrm{m/s}\,]$	*Darcy* permeability
$\boldsymbol{k}$		generalised stiffness vector
$\mathbf{K}^S$	$[\,-\,]$	intrinsic permeability
$\mathbf{K}^\beta$	$[\,\mathrm{J/mol}\,]$	tensor of chemical potential
$\mathbf{L}_\alpha$	$[\,\mathrm{1/s}\,]$	velocity gradient
$\mathbf{m}_e^\alpha$	$[\,\mathrm{A/m}\,]$	magnetic polarisation
$\hat{\mathbf{m}}^\alpha$	$[\,\mathrm{mol/m^3}\,]$	direct production of moment of momentum
M_m^α	$[\,\mathrm{kg/mol}\,]$	molar mass
$\boldsymbol{M}$		generalised mass matrix
n_m^α	$[\,-\,]$	number of moles
$\mathbf{n}$	$[\,-\,]$	outward oriented normal vector
$\mathbf{p}_e^\alpha$	$[\,\mathrm{C/m^2}\,]$	electric polarisation

$\hat{\mathbf{p}}^\alpha$	$[\,\mathrm{N/m^3}\,]$	direct momentum production
$\mathbf{P}^\alpha$	$[\,\mathrm{N/m^2}\,]$	first *Piola-Kirchhoff* stress
$\bar{q}$	$[\,\mathrm{kg/m^2 s}\,]$	fluid efflux over the boundary
$\mathbf{q}^\alpha$	$[\,\mathrm{J/m^2\,s}\,]$	heat influx over the boundary
r^α	$[\,\mathrm{J/kg\,s}\,]$	external heat supply
R	$[\,\mathrm{J/K\,mol}\,]$	universal gas constant
$\bar{R}^\alpha$	$[\,\mathrm{J/K\,kg}\,]$	specific gas constant
$\mathbf{R}_\alpha$	$[-]$	rotation tensor
s^α	$[-]$	saturation
$\hat{\mathbf{s}}^\alpha$	$[\,\mathrm{N/m^3}\,]$	total momentum production
$\mathbf{S}^\alpha$	$[\,\mathrm{N/m^2}\,]$	second *Piola-Kirchhoff* stress
$\mathbf{S}^{\alpha\beta}$	$[-]$	friction tensor
t	$[\,\mathrm{s}\,]$	time
$\bar{\mathbf{t}}$	$[\,\mathrm{N/m^2}\,]$	external load vector (traction force)
$\mathbf{t}^\alpha$	$[\,\mathrm{N/m^2}\,]$	surface traction vector
$\mathbf{T}^\alpha$	$[\,\mathrm{N/m^2}\,]$	*Cauchy* stress
$\boldsymbol{u}$		vector of nodal degrees of freedom
$\mathbf{u}_S$	$[\,\mathrm{m}\,]$	solid displacement
$\mathbf{U}_\alpha$	$[-]$	right *Cauchy* stretch tensor
$V,\ V^\alpha$	$[\,\mathrm{m^3}\,]$	mixture volume and volume of the constituent
$\tilde{V}_m^\alpha$	$[\,\mathrm{mol/m^3}\,]$	partial molar volume
V_m^α	$[\,\mathrm{m^3/mol}\,]$	molar volume
$\mathbf{V}_\alpha$	$[-]$	left *Cauchy* stretch tensor
$\mathbf{w}_\alpha$	$[\,\mathrm{m/s}\,]$	seepage velocity
W^S	$[\,\mathrm{J/m^3}\,]$	strain energy function
$\mathbf{W}_\alpha$	$[\,\mathrm{1/s}\,]$	vorticity tensor
x_m^α	$[-]$	molar fraction
$\mathbf{x}$	$[\,\mathrm{m}\,]$	current position vector
$\mathbf{X}_\alpha$	$[\,\mathrm{m}\,]$	referential position vector
z^α	$[-]$	valence

Greek letters

ϵ_0	$[\,\mathrm{C^2/Nm^2}\,]$	electric permittivity
ϵ	$[\,-\,]$	penalty factor
ε^α	$[\,\mathrm{J/kg}\,]$	mass specific internal energy
$\hat{\varepsilon}^\alpha$	$[\,\mathrm{J/m^3\,s}\,]$	direct energy production
$\hat{\zeta}^\alpha$	$[\,\mathrm{J/K\,m^3\,s}\,]$	direct entropy production
η^α	$[\,\mathrm{J/K\,kg}\,]$	mass specific entropy
γ^α	$[\,\mathrm{N/m^3}\,]$	weight
$\Gamma_{(\,\cdot\,)}$		the domain boundary of a primary variable
$\hat{\kappa}_e^\alpha$	$[\,\mathrm{C/m^3}\,]$	total production of electric flux
θ^α	$[\,\mathrm{K}\,]$	absolute *Kelvin* temperature
$\lambda^S,\ \mu^S$	$[\,\mathrm{N/m^2}\,]$	*Lamé* constants
μ^α	$[\,\mathrm{J/kg}\,]$	chemical potential
μ_0	$[\,\mathrm{N/A^2}\,]$	magnetic permeability
$\pi,\ \pi^\alpha$	$[\,\mathrm{N/m^2}\,]$	overall and partial osmotic pressure
ρ_e^α	$[\,\mathrm{C/m^3}\,]$	charge density of the constituent
$\rho,\ \rho^\alpha$	$[\,\mathrm{kg/m^3}\,]$	mixture density and density of the constituent
$\rho^{\alpha R}$	$[\,\mathrm{kg/m^3}\,]$	effective density of the constituent
σ_η^α	$[\,\mathrm{J/K\,m^3\,s}\,]$	external entropy supply
$\boldsymbol{\tau}^\alpha$	$[\,\mathrm{N/m^2}\,]$	*Kirchhoff* stress
ϕ^j	$[\,-\,]$	basis function of node j
ϕ^γ	$[\,-\,]$	osmotic coefficient
$\varphi,\ \varphi^\alpha$	$[\,-\,]$	entire mixture and the constituent α
$\boldsymbol{\Phi}_\eta^\alpha$	$[\,\mathrm{J/K\,m^2\,s}\,]$	entropy efflux
$\chi_{e1}^F,\ \chi_{e2}^F$	$[\,]$	electric and magnetic susceptibilities
$\boldsymbol{\chi}_\alpha$	$[\,-\,]$	motion function
$\boldsymbol{\psi}^\alpha$	$[\,\mathrm{J/kg}\,]$	mass specific *Helmholtz* free energy
$\boldsymbol{\Psi}_F^\alpha$	$[\,\mathrm{J/m^3}\,]$	*Helmholtz* free energy with respect to the overall fluid volume
ω_e^α	$[\,\mathrm{T}\,]$	total production of magnetic flux

Superscripts

$(\cdot)^{\alpha}$	all constituents
$(\cdot)^{\beta}$	fluid components
$(\cdot)^{\gamma}$	charged fluid components
$(\cdot)^{S}$	solid matrix
$(\cdot)^{F}$	overall fluid
$(\cdot)^{L}$	liquid solvent
$(\cdot)^{+}$	dissolved cations
$(\cdot)^{-}$	dissolved anions
$(\cdot)^{fc}$	fixed charges
$(\cdot)^{\cdot R}$	effective (realistic) quantity

Subscripts

$(\cdot)_{S}$	solid matrix (kinematical quantity)
$(\cdot)_{F}$	overall fluid (kinematical quantity)
$(\cdot)_{L}$	liquid solvent (kinematical quantity)
$(\cdot)_{+}$	dissolved cations (kinematical quantity)
$(\cdot)_{-}$	dissolved anions (kinematical quantity)
$(\cdot)_{E}$	extra quantities
$(\cdot)_{\cdot F}$	quantities with respect to the overall fluid volume
$(\cdot)_{m}$	molar quantities
$(\cdot)_{e}$	electromagnetic quantities
$(\cdot)_{E_{mech.}}$	purely mechanical extra quantities
$(\cdot)_{0S}$	initial quantities by integration with respect to the moving solid

Chapter 1:
Introduction and overview

1.1 Motivation

The last few decades have witnessed a great interest in charged hydrated multiphasic materials. Examples for such kind of materials in the field of geomechanics are chemically active clay and shale. In regions, where such materials can be found, it has been observed that they are able to undergo very high volume changes under varying chemical conditions in the environment. If not treated properly, this characteristic may lead to enormous problems. For example, the ground underneath a construction or a road may be seriously damaged due to swelling phenomena, cf. Figure 1.1 to the left. Difficulties may also arise in drilling processes because of chemically active rock layers. Here, if the drilling fluid does not have an adequate constitution, such a layer may swell so that the drill gets stuck or shrink such that material from layer is rinsed out leading to a collapse of the borehole. Both situations may result in immense costs for the drilling company. Thus, the main objective in these mentioned cases is to prevent the materials from swelling. But it is also possible to utilise the swelling behaviour in a positive sense. Bentonite pellets are used as a sealing when drilling through an impermeable clay layer separating two different water levels. This prevents the water to flow from one region to another, cf. Figure 1.1 to the right.

[geosurvey.state.co.us]

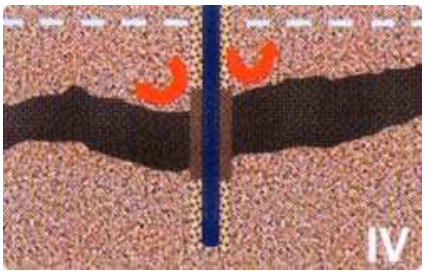

[www.adriatech.com]

Figure 1.1: Swelling of clay underneath a street (left) and use of swelling bentonite pellets as a sealing for the ground water when drilling through a separating clay layer (right).

Concerning biomechanics, there are several charged hydrated porous soft tissues in the human body. The intervertebral discs (IVD) between the vertebrae of the spine and the articular cartilage in the knee joints, cf. Figure 1.2, may serve as examples.

Due to the combination of a charged solid skeleton with a charged interstitial fluid as a solution of dissolved ions, there is a concentration difference between the environmental and the interstitial solution. As a result, an osmotic pressure develops within the material.

The interesting issue here is that not the solid matrix is actually carrying the load, for example, in the IVD or the joints. Instead, the load is carried by the osmotic pressure within interstitial fluid. Due to this and also because of the relatively low volume fraction of the solid, these materials exhibit quite low frictional forces and, moreover, there is almost no abrasion of the solid matrix in a healthy tissue.

But ageing phenomena cause the solid matrix to lose its adherent charges, resulting in a loss of the internal osmotic pressure. In case of the IVD, the damaged soft tissue can be replaced by its artificial analogue, i. e. the inner part of the IVD, the nucleus pulposus, can be replaced by an hydrogel cushion, cf. di Martino *et al.* [132]. Another major cause of the damage of soft tissues, especially in case of articular cartilage, are sports accidents. In order to repair these injuries, Grant *et al.* [82] and Kisiday *et al.* [114] propose to bring in a special kind of hydrogel, which is biocompatible such that new cartilage producing cells, i. e. chondrocytes, may be seeded into it and brought into the corresponding region. As the chondrocytes reproduce the articular cartilage, the biocompatible hydrogel degenerates and, as a result, after a certain time, it will be completely replaced by the newly generated cartilage tissue.

[www.maturespine.com]

[www.eorthopod.com]

Figure 1.2: On the left-hand side, a herniated disc is exhibited and, on the right-hand side, a knee with a cartilage lesion.

Because of its charged constitution, hydrogel also responds to electric fields. Thus, there is also a high interest in using hydrogel in robotics as an artificial muscle or as an artificial lens, which bends or changes its optical characteristics due to deformation according to the applied electric field.

It can be concluded that these materials appear in many engineering fields and that they have a wide range of application. Therefore, it is essential to understand the processes appearing within these materials and their interactions and also to have a tool, which accurately predicts their behaviour under varying external loads and conditions.

1.2 Scope, aims and state of the art

Following above thoughts, only an integral consideration of the multiphasic composition with the individual characteristics of the constituents can unite all the different phenomena appearing in charged hydrated porous media within one model. Thus, the aim of

this thesis is to derive a new and thermodynamically consistent model capturing all the mechanical, chemical and electric effects within the range of finite deformations.

The resulting model consists of several strongly coupled partial differential equations. A numerical solution procedure will be applied to solve the system of equations in a *Lagrange*an frame. Therein, depending on the choice of primary variables, one comes across deformation-dependent boundary conditions. Such boundary conditions are well known in the field of free surface flows and fluid structure interaction (FSI). In order to avoid unsound solutions exhibiting oscillations, these boundary conditions are treated by inclusion into the weak form of the respective balance relation by means of a penalty-like method. As a result, the weakly fulfilled *Dirichlet* boundary conditions acting on a deforming domain are newly applied to several primary variables at once.

In this thesis, the materials are described on the macroscale based on the well-founded continuum-mechanical Theory of Porous Media (TPM). Within this frame, it is possible to model arbitrarily constituted materials, where each constituent of the multiphasic material can have its own state of motion. The characteristics of the individual constituents are captured via constitutive equations based on thermodynamical considerations. In the following, the development of the TPM and the models describing charged hydrated porous materials are briefly reviewed.

First attempts to model binary mixtures consisting of a solid matrix and a interstitial fluid were made by *Woltman*. In his contribution [169] concerning the calculation of the earth pressure on a vertical wall, he introduced the concept of volume fractions. In 1848, the mining engineer Delesse [43] stated a similar concept, while he tried to predict the mineral content of rocks from the mineral fraction on the surface. Thereafter, this concept has been used by many engineers modelling consolidation problems of porous rocks, for example by Biot [14]. *Biot* developed more or less intuitively a theory for porous materials by generalising the consolidation theory of Terzaghi [160]. In contrast to him, Heinrich & Desoyer [94] developed a model based on the work of Fillunger [75]. Thus, this work is based on ensured mechanical principles like the *Euler*ian cut principle and the balance equations. Subsequently, Truesdell & Toupin formed the modern continuum mechanics by constructing a continuum theory based only on few mechanical principles and thermodynamical axioms. In [163] they established the basis for a continuum theory of miscible constituents and stated the well-known "metaphysical principles":

1. All properties of the mixture must be the mathematical consequences of properties of the constituents.

2. So as to describe the motion of a constituent, we may in imagination isolate it from the rest of the mixture, provided we allow properly for the actions of the other constituents upon it.

3. The motion of the mixture is governed by the same equations as is in a single body.

Finally, Bowen [27] can be considered as the final work on the Theory of Mixtures (TM), where all currently valid statements are covered. Thereafter, restricting the general TM by the concept of volume fractions, the TPM has been founded by the works of Bowen

[28, 29]. Therein, Bowen discusses all the kinematics and balance relations valid for mixtures by considering the partial quantities and relations. Note that the term "restricted" refers to the fact that in the case of the TM, developed to describe mixtures with miscible constituents, the response of the overall aggregate does not depend on the volume fraction of its constituents. But in case of the TPM, describing mixtures constituted by immiscible constituents, the response does depend on the respective volume fractions. However, Mow *et al.* [136] independently developed a mixture theory, in which the authors consider biomechanical materials. Subsequently, the application of TPM has been enhanced continuously by de Boer [23], de Boer & Ehlers [24] and Ehlers [51, 53, 55, 56]. De Boer [22] gives in his book a very good insight into the history and the development of the Theory of Porous Media. Following above considerations, the *Biot* theory, apart from some artificial extensions, is *a priori* suitable only for linear models, cf. Schanz & Diebels [148] and citations therein.

However, concerning the modelling of chemically and electrically active materials, Lanir [118] first modelled swelling phenomena under the assumption of slightly changing concentrations within biological tissues, cf. the simplification S IV in Section 4.2.5 and Ehlers *et al.* [64]. This assumption leads to a biphasic model with two primary variables (2-pv), the solid displacement and the pore-fluid pressure, where the ion concentrations reach their equilibrium state immediately. Since only the fluid is moving, the resulting swelling model captures only osmotic effects. Later, Lai *et al.* [116] derive the first so-called triphasic model based on Mow *et al.* [136], where also the diffusion of the ions is considered via their concentration balances. A strong electroneutrality along with a no-electric-current condition is used in this contribution such that only one velocity for both ions is modelled, cf. the simplification S II in Section 4.2.5. A similar model based on the TM with three primary variables (3-pv) has been derived by Snijders *et al.* [155] in 1995. Therein, the authors compute a 2-dimensional (2-d) axisymmetric cylinder and encounter some numerical difficulties resulting from the deformation-dependent pressure and concentration boundary conditions. In their publication, the authors circumvented these difficulties by applying a least squares method at the boundaries. Hon *et al.* [100] reformulated the 3-pv model of Lai *et al.* [116] and also provide a reduction to a 2-pv model.

Later, in 1997, Huyghe & Janssen [107] modelled swelling phenomena by the so-called quadriphasic model with four primary variables (4-pv). In their work, the anions and cations are considered as separate phases with individual velocities. Moreover, in addition to the saturation condition, the electroneutrality condition is incorporated into the *Lagrange*an form of the entropy inequality. In this 4-pv model, the electric potential is included in the electrochemical potentials of the ions. Frijns *et al.* [76] used this 4-pv model to simulate swelling phenomena using the Finite Element Method (FEM) and validated it via the computation of a swelling-compression experiment. Note that in contrast to the 2-d computations of Snijders *et al.* [155] based on molar concentrations and osmotic pressure, the computations in Frijns *et al.* [76] are performed using (electro-)chemical potentials as primary variables. A note on the choice of primary variables will be given later.

Using the Finite Difference Method (FDM), Mow *et al.* [135] analysed the stress-relaxation behaviour based on the theory derived in [116]. The 1-d simulations are based on only

two primary variables, where, in contrast to the above mentioned 2-pv models, the solid displacement and the cation concentration have been used as primary variables. In this publication, only numerical examples of displacement-driven consolidation experiments are given. Following this, it may be speculated that the authors also observed some numerical difficulties from the deformation-dependent boundary conditions and, therefore, they prescribed the displacement at the boundary. In order to avoid these numerical difficulties, Sun *et al.* [159] reformulated the 3-pv model of Lai *et al.* [116] using the modified electrochemical potentials of both ions as primary variables, which leads to a 4-pv model. This model is then solved by use of the FEM to analyse the free swelling behaviour of a hydrated tissue. In 1999, Huyghe & Janssen [108] extended the theoretical model of [107] with regard to temperature effects without giving numerical examples.

The first 3-d computation was published by van Loon *et al.* [122] using the model presented in [107] based on chemical potentials as primary variables. Here, the electric continuity equation, i. e. the electroneutrality condition, is used as the fifth equation to determine the electric potential, i. e., the computations have been performed by a model with five primary variables (5-pv).

Aiming at a higher accuracy of the component velocities, Kaasschieter *et al.* [110] and Malakpoor [129] propose to discretise not only the electrochemical potentials but also the fluid and the ion fluxes within the hybrid finite element scheme. In 2006, Chen *et al.* [37] extended the theory based on Lai *et al.* [116] to apply to finite deformations. They also chose the velocities as primary variables and used the continuity equation to determine the electric potential. Also a 3-d simulation of the deformation of an articular cartilage strip under varying molar concentrations is given. Huyghe *et al.* [109] applied a compressible poromechanics version of the model derived in Huyghe & Janssen [107] to bone tissue to investigate the influence of compressibility in a numerical compression experiment.

In the context of geotechnical applications, based on the empirical *Biot* theory, Sherwood [153] derived a swelling model for chemically active shale, cf. also Heidug & Wong [93] and Loret *et al.* [123].

In the field of electroactive polymers (EAP), which is basically the same as hydrogel (in the field of EAP sometimes also referred to as smart material), Wallmersperger [168] computed the response of such materials to electric and chemical stimulation. In this work, also the solution surrounding the hydrogel is modelled but the fluid motion was not considered, cf. also De & Aluru [41], Li *et al.* [119, 120]. In all of these contributions, the *Poisson* equation of electrostatics is used to compute the electric potential. This is also in agreement with the statement by Samson *et al.* [146] that using the *Poisson* equation is a much more rigorous way compared to the other possibilities. More precisely, as has also been mentioned before, the electric potential may be computed from other conditions actually restricting the ion diffusion, i. e. either the electroneutrality condition or the no electric current condition.

As in the present case and also in several other theories, one has the choice of different sets of primary variables. For example, in continuum mechanics of solids, one can choose between the solid stress and the strain, which are related to each other via a constitutive relation. In theories describing caplillary effects, the capilary pressure and the saturation

are interchangeable primary variables, cf., for example, Helmig [95] and Graf [81]. Also, swelling phenomena may be modelled either by use of hydraulic pressure and chemical potentials or by use of the overall pressure and concentrations as primary variables. The choice of either set of variables is based on the future use of the model. For example, in order to simulate experiments by numerical computations and in order to verify the results, one would choose measureable quantities such as the overall pressure and the concentrations so that both results are directly comparable. In contrast, the purely hydraulic pressure and the chemical potentials are not measureable but instead, they are obtained from measureable quantities by constitutive relations. Thus, based on the interchangeability of the primary variables via their constitutive relations, the choice of either set of primary variables makes no difference within the theory. But stepping onward to numerics, the choice of the set of primary variables describing the fluid and its components has several influences. While the hydraulic pressure and the chemical potentials are continuous over the boundary, the osmotic pressure and the concentrations exhibit a jump. This fact has to be considered by use of weakly fulfilled *Dirichlet* boundary conditions in order to obtain stable and accurate numerical computations, cf. Section 4.3.1. But even though the numerical and the programming effort is higher than in case of continuous boundary conditions, the computations are much faster, cf. Section 5.1.1, and the results are much more accurate, cf. Section 5.2.2. Moreover, the overall number of primary variables may be reduced by additional *a priori* assumptions. But these steps can only be performed for the set using the overall pressure and the concentrations, since in case of chemical potentials, allways both of them are required to compute the concentrations via an aditional equation, cf. Section 4.2.

However, based on the development of the former researchers, the aim of this contribution is to combine the mechanical, chemical and electric properties of charged hydrated porous materials within an integral and thermodynamically consistent continuum-mechanical theory. In contrast to the above mentioned contributions, one of the differences is that the theory is based on the well-founded Theory of Porous Media (TPM). Moreover, each constituent is considered separately by its own motion and, in addition, the electric part is captured by the *Poisson* equation. The advantage of the presented model lies in the combination of these characteristics and, as a result, the model will respond to a mechanical load or to chemical and electric stimulation via a combination of solid deformation, fluid movement, ion diffusion or electric current. Moreover, it will be found that the previously mentioned primary variable sets may easily be interchanged such that the most reliable and effective set may be found by numerical comparison.

1.3 Outline of the thesis

After the introduction and motivation, in **Chapter 2** the continuum-mechanical principles based on the TPM are discussed, considering the multiphasic character of the material. Thus, the basic quantities such as the densities, concentrations and volume fractions are introduced for each constituent. After introducing the kinematic relations based on the concept of superimposed continua, the balance relations of continuum mechanics as well

as electrodynamics of multiphasic materials are introduced axiomatically. Finally, the entropy inequality in its *Clausius-Planck* representation for isothermal conditions.

Given the general material-independent continuum-mechanical fundamentals, the actual model is derived within the constitutive theory in **Chapter 3**. Therefore, the entropy inequality is transformed such that it reflects the constitution of the material with its immiscible phases and its miscible components. Also, the restrictions on the material that it is always saturated and electrically neutral are incorporated into it by means of *Lagrange*an multipliers. From this final version of the entropy principle, the restrictions for the process variables are found by evaluation following the *Coleman-Noll* procedure. Moreover, the chemical potentials and the osmotic pressures are identified as functions of the *Helmholtz* free energies. Finally, the mechanical extra stress of the solid, the velocities of the individual fluid components and the overall fluid and the *Poisson* equation of electrostatics is given. The final model consists of five coupled partial differential equations (PDE).

The general model derived in Chapter 3 is solved numerically using the finite element scheme. Different choices of primary variable sets are possible for the derived set of PDEs. Moreover, based on additional restrictions, the set of primary variables may be reduced. Therefore, in **Chapter 4**, the respective sets of PDEs are given and the advantages and the drawbacks are discussed in detail. Note that depending on the choice of primary variables, some of the corresponding boundary conditions depend on the current state of the domain in the sense that current values of either primary or internal variables are required to compute the boundary condition. Thus, to avoid numerical problems within the *Galerkin* procedure to find the weak forms of the PDEs, the boundary conditions are incorporated into the respective balance relation by a penalty-like method. Next, the discretisation in space and time as well as the actual solution strategy using the *Newton-Raphson* scheme is briefly explained.

In **Chapter 5**, several numerical examples are given. More precisely, the different sets of primary variables are compared with respect to the actual solution and also with respect to numerical aspects such as the computation times and stability within an exemplary 1-d swelling experiment. Additionally, the reduced sets of primary variables and the influence of the activity coefficients are discussed. Moreover, the derived model is validated by comparison with a swelling-compression experiment found in the literature. In order to capture the non-ideal behaviour of solutions of strong electrolytes, the concentration-dependent activity coefficients are incorporated into the model based on the *Debye-Hückel* theory. The effects of an electric stimulation of a hydrogel strip are given by a 1-d experiment. Then, two 3-d computations are given to show the capabilities of the derived model, i. e. a free swelling experiment of a hydrogel disc undergoing finite deformations. Also, the bending behaviour of an electroactive polymer such as gripper deforming under an applied electric field is presented.

Finally, in **Chapter 6**, the results of this thesis are summarised and some aspects for the future research are given.

Chapter 2:
Multiphasic description

As has been pointed out in the introduction, the materials under consideration have a complex multiphasic microstructure. More precisely, in geomechanics chemically active clay and shale pertain to this type. The microstructure of these swelling aluminosilicate minerals, also called smectites, is built up from silicium and aluminium tetrahedra. By sharing ions, the tetrahedra are connected to each other and build negatively charged platelets, cf. Low [125] and van Olphen [140]. In the field of biomechanics, articular cartilage and the intervertebral disc are among charged porous materials. In contrast to the platelets of the smectites, biological soft tissues are composed of fibres consisting proteoglycan aggregates (PGA) immobilised by a collagen fibre meshwork. The negative charge of the PGA chains result from a large number of silicate or carbonate groups along the glycosaminoglycan (GAG) chains, cf. Mow & Ratcliffe [137]. Hence, such charged porous media become more and more important in tissue engineering, since artificially built materials like hydrogel can be used as a replacement of degenerated biological soft tissues. This includes cartilage substitutes in joints with the ability to build up new cartilage (Kisiday *et al.* [114]) or in the intervertebral disc by replacing the inner part of the herniated disc, i. e. the nucleus pulposus (di Martino *et al.* [132]). Additionally, since hydrogel is also an electro active-polymer (EAP), it has the ability to be used as an artificial muscle, for example in robotics or in human bodies, cf. Bar-Cohen [8] or Boyle [31].

In general, such multiphasic and multi-component materials with an unknown microstructure are best described within a macroscopic continuum-mechanical approach. The advantage of such an approach is that neither the microscopic structure of the pores nor the contact interaction of the constituents must be known in particular. Even though the computer power is increasing rapidly, the simulation of realistic problems by discrete models, such as modelling the pore-structure by beams or even molecular simulations, would be totally utopistic. On this account, the model presented in this thesis is based on the continuum-mechanical Theory of Porous Media (TPM), cf. de Boer [22, 23] and Ehlers [56]. By a combination of the Theory of Mixtures (TM), cf. Bowen [27], which has no measure to incorporate any microscopic characteristic of the medium, and the concept of volume fractions, the TPM is obtained. Thus, while the Theory of Mixtures only enables the modelling of general mixtures composed of miscible constituents, the TPM is a convenient tool to model mixtures with immiscible constituents, i. e. the constituents can be locally distinguished on the macroscale. Moreover, by introducing the volume fractions, the constituents and their properties are “smeared” over the spatial domain under consideration. Consequently, the TPM can be understood as the result of either a real or a virtual averaging procedure over representative elementary volumes (REV), cf. Figure 2.1.

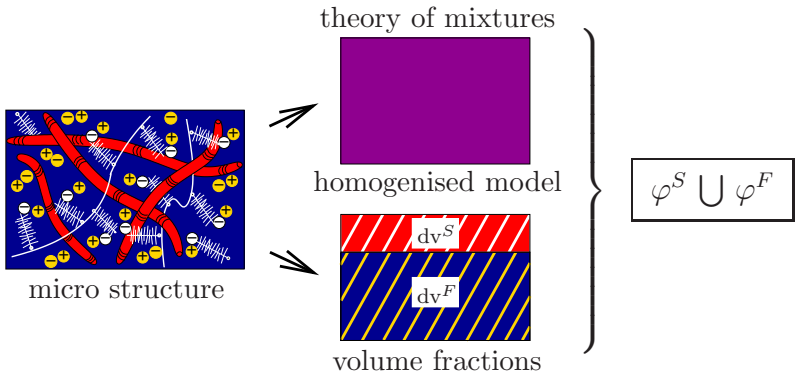

Figure 2.1: Micro structure and macroscopic model.

As mentioned above, the materials under consideration consist of a charged solid matrix which is electrically neutralised and fully saturated by an ionised fluid. Within these materials, it is therefore possible to distinguish between two immiscible phases, namely the charged solid and the ionised fluid. By contrast, since the overall fluid itself is a solution, it is considered to be composed of miscible constituents. Following this, the two phases solid and fluid are modelled within the frame of the TPM, whereas the ionised fluid is modelled by the TM.

In the following sections, the basic quantities such as densities and kinematic variables used for the continuum-mechanical description within this thesis will be introduced. After the introduction of different deformation and stress tensors, the general form of the material independent balance relations will be presented axiomatically.

2.1 Volume fractions, densities and concentrations

In mathematical terms, the mixture φ as a whole is idealised as the sum of all of its constituents denoted by φ^α, where $\alpha = S$ indicates the solid including the mass- and volume-free fixed charges (φ^{fc}), $\alpha = L$ denotes the liquid solvent, $\alpha = +$ and $\alpha = -$ indicate the cations and the anions, respectively, of a salt fully dissolved in the liquid. All three fluid components, φ^L, φ^+ and φ^-, sum up to the overall fluid denoted by $\alpha = F$. In this idealised model, the solid φ^S and the overall fluid φ^F are the immiscible phases, while the fluid components φ^L, φ^+ and φ^- are miscible within the overall fluid. According to this, the relations

$$\varphi = \bigcup_\alpha \varphi^\alpha\,, \quad \alpha = S,\, L,\, +,\, - \qquad \text{and} \qquad \varphi^F = \bigcup_\beta \varphi^\beta\,, \quad \beta = L,\, +,\, - \tag{2.1}$$

describe the constitution of the mixture. Note that the mobile ions only are denoted by φ^γ, where $\gamma = +,\, -$. By summing over the partial volumes of the phases

$$V^\alpha = \int_{\mathcal{B}^\alpha} \mathrm{d}v = \int_{\mathcal{B}} \mathrm{d}v^\alpha \tag{2.2}$$

one obtains the volume of the overall medium $\mathcal{B}$:

$$V = \int_{\mathcal{B}} \mathrm{d}v = \int_{\mathcal{B}} \sum_{\alpha} \mathrm{d}v^{\alpha} = \sum_{\alpha} \int_{\mathcal{B}^{\alpha}} \mathrm{d}v = \sum_{\alpha} V^{\alpha} \,. \tag{2.3}$$

Note that this implies the assumption of immiscible constituents. The ratio of the local constituent volume $\mathrm{d}v^{\alpha}$ to the local bulk volume $\mathrm{d}v$ is defined as the volume fraction:

$$n^{\alpha} := \frac{\mathrm{d}v^{\alpha}}{\mathrm{d}v} \,. \tag{2.4}$$

Even though also the volume fractions n^{β} of the fluid components are defined by (2.4), it is, in general, not possible to compute their volume fractions, since the overall fluid is considered to be a mixture of miscible components. This follows from the fact that all components occupy the whole fluid volume simultaneously. Moreover, the volume of the overall fluid does not change according to the change of its constitution. The corresponding volume change is computed by the partial molar volume, cf. Klotz & Rosenberg [115] and Prigogine & Defay [142],

$$\tilde{V}_m^{\beta} := \frac{\partial V^F}{\partial n_m^{\beta}} \,. \tag{2.5}$$

In other words, the partial molar volume $\tilde{V}_m^{\beta}$ of a fluid component is the volume change of the solution φ^F by changing the amount of component φ^{β} therein. Note that the partial molar volume can be negative as well, meaning that the volume of the overall solution φ^F decreases by adding a certain amount of the component φ^{β}. In the above relation and in what follows, quantities denoted by $(\,\cdot\,)_m$ are molar quantities, such as the number of moles of φ^{β} is denoted by n_m^{β}. The overall volume of the solution is obtained by

$$V^F = \sum_{\beta} n_m^{\beta} \tilde{V}_m^{\beta} \,. \tag{2.6}$$

Following above considerations, it is not possible to specify the molar volume of a component in a solution, but for a single material it is given by

$$V_m^{\beta} := \frac{\mathrm{d}v^{\beta}}{\mathrm{d}n_m^{\beta}} \,. \tag{2.7}$$

For example, in case of a one molar sodium chloride solution, the partial molar volume $\tilde{V}_m^{\mathrm{NaCl}}$ of $\mathrm{Na^+Cl^-}$ is $15\,\mathrm{cm^3/mol}$, while for the crystalline salt the molar volume V_m^{NaCl} is $24\,\mathrm{cm^3/mol}$ (Anderson & Crerar [4]).

Following equation (2.3), the sum of the volume fractions of the constituents leads to the so-called saturation condition

$$\sum_{\alpha} n^{\alpha} = n^S + n^F = n^S + n^L + n^+ + n^- = 1 \,, \tag{2.8}$$

meaning that there is no vacant space in the overall medium. The introduction of the volume fractions leads to two different densities, namely, the realistic (effective or material)

density $\rho^{\alpha R}$ relating the local mass $\mathrm{d}m^\alpha$ of the constituent to its local volume, and the partial (global or bulk) density ρ^α relating the local mass of the constituent to the local bulk volume, namely,

$$\rho^{\alpha R} := \frac{\mathrm{d}m^\alpha}{\mathrm{d}v^\alpha} \quad \text{and} \quad \rho^\alpha := \frac{\mathrm{d}m^\alpha}{\mathrm{d}v} . \tag{2.9}$$

By use of (2.4), one finds that both densities are related to each other by the volume fraction:

$$\rho^\alpha = n^\alpha \rho^{\alpha R} . \tag{2.10}$$

At this point, it becomes obvious that the term material incompressibility acquires a new aspect: even though $\rho^{\alpha R}$ is constant, the partial density ρ^α can change its value during deformation due to a change in the volume fractions. The density of the overall medium is obtained by summing over the partial densities of the constituents

$$\rho = \sum_\alpha \rho^\alpha , \tag{2.11}$$

or for the overall fluid by summing over ρ^β of its components:

$$\rho^F = \sum_\beta \rho^\beta \quad \longrightarrow \quad \rho^{FR} = \sum_\beta s^\beta \rho^{\beta R} . \tag{2.12}$$

Therein, s^β is introduced as the saturation and is defined as

$$s^\beta := \frac{n^\beta}{n^F} , \tag{2.13}$$

which relates the volume fraction of the component to the volume fraction of the overall fluid, cf. Ehlers & Blome [59]. It follows from the definition (2.13) of the saturation s^β that

$$\sum_\beta s^\beta = 1 . \tag{2.14}$$

Finally, an additional density ρ_F^β is defined denoting the density of the fluid component with respect to the overall fluid volume:

$$\rho_F^\beta := s^\beta \rho^{\beta R} = c_m^\beta M_m^\beta \quad \longrightarrow \quad \rho^\beta = n^F \rho_F^\beta , \quad \rho^{FR} = \sum_\beta \rho_F^\beta . \tag{2.15}$$

Therein and in what follows, the variables indicated by the subscript $(\cdot)_F$ denote quantities with respect to the overall fluid volume. Note that the molar mass $M_m^\beta := \mathrm{d}m^\beta / \mathrm{d}n_m^\beta$ is independent of any effects like temperature and pressure changes and, thus, it is always constant. As a chemical measure of the amount of a substance in a mixture, the molar concentration

$$c_m^\beta := \frac{\mathrm{d}n_m^\beta}{\mathrm{d}v^F} \tag{2.16}$$

is introduced. It is the ratio of the local number of moles to the local bulk fluid volume $\mathrm{d}v^F$ and the reciprocal value to the partial molar volume. A further quantity expressing

the amount of a component in a solution in chemistry is the mole fraction

$$x_m^\beta := \frac{\mathrm{d}n_m^\beta}{\sum_\beta \mathrm{d}n_m^\beta} = \frac{c_m^\beta}{\sum_\beta c_m^\beta}\,, \tag{2.17}$$

which also can be expressed in molar concentrations c_m^β instead of the local number of moles $\mathrm{d}n_m^\beta$ by expanding the fraction by the overall fluid volume $\mathrm{d}v^F$. In analogy to the saturation and the volume fractions, all mole fractions add up to one:

$$\sum_\beta x_m^\beta = 1\,. \tag{2.18}$$

As in this thesis charged media are considered, the charges of the solid matrix and the ionised fluid have to be accounted for. While the mass is the basic quantity of mechanics and can only take on positive values, the charge is the basic quantity of electrodynamics and can also take on negative values. The amount of charges contributed by a charged constituent per volume of the overall medium is given by

$$\rho_e^{fc} := n^F \rho_{eF}^{fc} = n^F z^{fc} c_m^{fc} F \qquad \text{and} \qquad \rho_e^\gamma := n^F \rho_{eF}^\gamma = n^F z^\gamma c_m^\gamma F\,. \tag{2.19}$$

Therein, z^{fc} and z^γ are the valences, i. e. the amount of free charges per ion or molecule, of the constituents and F is the *Faraday* constant denoting the amount of elementary charges per mole of a proton. The subscript $(\cdot)_e$ denotes electric quantities. Recall that the fixed charges of the solid are denoted by φ^{fc}. Dealing with charges, an important condition is the electroneutrality condition, stating that there is no charge separation within the medium such that the overall medium is electrically neutral. The condition for the medium itself and for the solution surrounding the medium are given by

$$\rho_e = \sum_\gamma \rho_e^\gamma + \rho_e^{fc} = 0 \qquad \text{and} \qquad \bar{\rho}_e = \sum_\gamma \bar{\rho}_e^\gamma = 0\,, \tag{2.20}$$

where the values denoted by a bar $(\bar{\cdot})$ correspond to the values of the external solution and ρ_e and $\bar{\rho}_e$ denote the respective overall charge densities. In addition to this, dealing with charged ions in solution, i. e. electrolytes, the ionic strength plays an important role:

$$I := \tfrac{1}{2} \sum_\gamma (z^\gamma)^2 c_m^\gamma = \tfrac{1}{2} \sum_\gamma (z^\gamma)^2 \frac{\rho_F^\gamma}{M_m^\gamma}\,. \tag{2.21}$$

This quantity is used in the *Debye-Hückel* theory as well as in the double-layer theory. Note that this value is a common value for all dissolved ions in the solution. Moreover, ions with higher valences contribute more to the ionic strength than the ones with lower valences.

2.2 Kinematics of superimposed continua

2.2.1 Motion functions and velocities

The overall body $\mathcal{B}$ is defined as the manifold of all material points P^α, whereas the boundary and the material points at the boundary are combined into the manifold $\partial\mathcal{B}$. Following the idea of superimposed and interacting continua, at time t_0 indicating the reference configuration, each material point P^α starts from its unique reference coordinate $\mathbf{X}_\alpha$ and moves along its own *Lagrange*an motion function $\boldsymbol{\chi}_\alpha$ to the current configuration:

$$\mathbf{x} = \boldsymbol{\chi}_\alpha(\mathbf{X}_\alpha, t)\,. \tag{2.22}$$

As is shown in Figure 2.2, it is impossible to distinguish the constituents by their location in the current configuration, since the material point P^α is occupied by all constituents

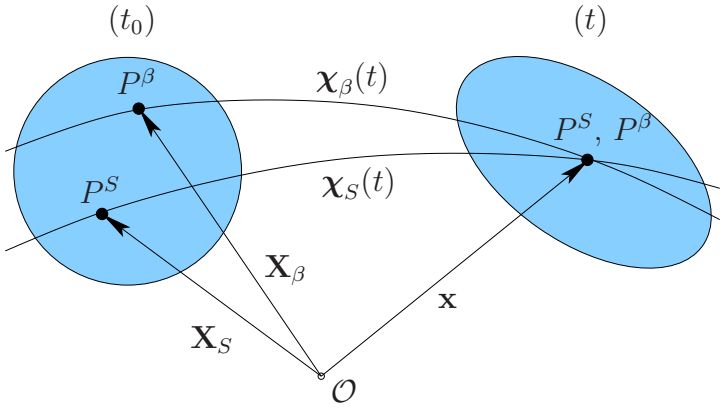

Figure 2.2: Kinematics for the solid φ^S and the fluid components φ^β.

simultaneously. This statement in combination with (2.22) requires the motion function to be unique and uniquely invertible:

$$\mathbf{X}_\alpha = \boldsymbol{\chi}_\alpha^{-1}(\mathbf{x}, t)\,. \tag{2.23}$$

The material gradient $\mathbf{F}_\alpha$ of the motion function with respect to the reference coordinates, i. e. the deformation gradient, and its inverse $\mathbf{F}_\alpha^{-1}$ are given by

$$\mathbf{F}_\alpha := \frac{\partial \boldsymbol{\chi}_\alpha(\mathbf{X}_\alpha, t)}{\partial \mathbf{X}_\alpha} = \operatorname{Grad}_\alpha \mathbf{x} \quad \text{and} \quad \mathbf{F}_\alpha^{-1} = \frac{\partial \boldsymbol{\chi}_\alpha^{-1}(\mathbf{x}, t)}{\partial \mathbf{x}} = \operatorname{grad} \mathbf{X}_\alpha\,. \tag{2.24}$$

Here, the differential operator "$\operatorname{Grad}_\alpha$" denotes the partial differentiation with respect to the reference coordinates $\mathbf{X}_\alpha$ and "grad" the partial differentiation with respect to the current coordinates $\mathbf{x}$. Note that the motion function and, thus, the deformation gradient are only invertible if the *Jacobi*ans differ from zero:

$$J_\alpha := \det \mathbf{F}_\alpha \neq 0\,. \tag{2.25}$$

Following this and taking into consideration that the deformation gradient initially equals the identity tensor, its determinant is restricted to positive values:

$$\mathbf{F}_\alpha(t_0) = \mathbf{I} \quad \longrightarrow \quad J_\alpha = \det \mathbf{F}_\alpha > 0\,. \tag{2.26}$$

Even though it is not possible to distinguish between the constituents by their location $\mathbf{x}$ in the current configuration, each constituent has its own *Lagrange*an velocity and acceleration due to the unique motion function,

$$\overset{\prime}{\mathbf{x}}_\alpha = \frac{\partial \boldsymbol{\chi}_\alpha(\mathbf{X}_\alpha, t)}{\partial t} \quad \text{and} \quad \overset{\prime\prime}{\mathbf{x}}_\alpha = \frac{\partial^2 \boldsymbol{\chi}_\alpha(\mathbf{X}_\alpha, t)}{\partial t^2}\,, \tag{2.27}$$

whereas the *Euler*ian forms are obtained by use of the inverse motion function (2.23):

$$\overset{\prime}{\mathbf{x}}_\alpha = \overset{\prime}{\mathbf{x}}_\alpha[\boldsymbol{\chi}_\alpha^{-1}(\mathbf{x}, t), t] = \overset{\prime}{\mathbf{x}}_\alpha(\mathbf{x}, t) \quad \text{and} \quad \overset{\prime\prime}{\mathbf{x}}_\alpha = \overset{\prime\prime}{\mathbf{x}}_\alpha\,[\boldsymbol{\chi}_\alpha^{-1}(\mathbf{x}, t), t] = \overset{\prime\prime}{\mathbf{x}}_\alpha\,(\mathbf{x}, t)\,. \tag{2.28}$$

Note that the *Lagrange*an position vector $\mathbf{X}_\alpha$ of the reference configuration in (2.27) is constant with respect to time. In order to obtain the *Euler*ian formulation, $\mathbf{X}_\alpha$ in (2.27) is replaced by (2.23), wherein the current position vector $\mathbf{x}$ in (2.28) depends also implicitly on time. Thus, accounting for the different velocities of the constituents, different material time derivatives are defined. Let $\Gamma(\mathbf{x}, t)$ and $\boldsymbol{\Gamma}(\mathbf{x}, t)$ be differentiable scalar- and vector-valued field functions, the corresponding material time derivatives following the motion of φ^α are given by:

$$(\Gamma)'_\alpha = \frac{\partial \Gamma}{\partial t} + \operatorname{grad}\Gamma \cdot \overset{\prime}{\mathbf{x}}_\alpha \quad \text{and} \quad (\boldsymbol{\Gamma})'_\alpha = \frac{\partial \boldsymbol{\Gamma}}{\partial t} + (\operatorname{grad}\boldsymbol{\Gamma})\,\overset{\prime}{\mathbf{x}}_\alpha\,. \tag{2.29}$$

The velocity of the overall fluid is given by the mass averaged velocity of its components, where the densities ρ_F^β of the components, cf. (2.15), are used as weighting factors:

$$\overset{\prime}{\mathbf{x}}_F = \frac{1}{\rho^{FR}} \sum_\beta \rho_F^\beta\, \overset{\prime}{\mathbf{x}}_\beta\,. \tag{2.30}$$

By use of the same procedure, the barycentric velocity of the overall medium

$$\dot{\mathbf{x}} = \frac{1}{\rho} \sum_\alpha \rho^\alpha\, \overset{\prime}{\mathbf{x}}_\alpha \tag{2.31}$$

is obtained. Moreover, the diffusion velocity with respect to the barycentric velocity and the diffusion velocity of the fluid components within the moving fluid are given by:

$$\mathbf{d}_\alpha = \overset{\prime}{\mathbf{x}}_\alpha - \dot{\mathbf{x}} \quad \text{and} \quad \mathbf{d}_{\beta F} = \overset{\prime}{\mathbf{x}}_\beta - \overset{\prime}{\mathbf{x}}_F\,, \tag{2.32}$$

where

$$\sum_\alpha \rho^\alpha\, \mathbf{d}_\alpha = 0 \quad \text{and} \quad \sum_\beta \rho_F^\beta\, \mathbf{d}_{\beta F} = 0\,. \tag{2.33}$$

Generally, in the TPM the solid displacement

$$\mathbf{u}_S := \mathbf{x} - \mathbf{X}_S \tag{2.34}$$

is introduced as the primary kinematic variable of the solid phase. Since the displacement is given with respect to a material point in the initial configuration, it is said to be given in a *Lagrange*an setting. Furthermore, the velocities of the fluid and its components are expressed in a modified *Euler*ian description relative to the moving solid skeleton:

$$\begin{aligned} \mathbf{w}_F &:= \overset{\prime}{\mathbf{x}}_F - \overset{\prime}{\mathbf{x}}_S \quad \text{and} \\ \mathbf{w}_\beta &:= \overset{\prime}{\mathbf{x}}_\beta - \overset{\prime}{\mathbf{x}}_S \;=\; \mathbf{d}_{\beta F} + \mathbf{w}_F \,. \end{aligned} \tag{2.35}$$

Given the solid displacement (2.34) together with (2.24), the solid deformation gradient can be expressed via

$$\mathbf{F}_S = \frac{\partial \mathbf{x}}{\partial \mathbf{X}_S} = \mathbf{I} + \operatorname{Grad}_S \mathbf{u}_S \,. \tag{2.36}$$

From its definition, the deformation gradient is predestined to transport line elements between both configurations, i. e. the reference configuration and the current configuration, cf. Figure 2.2. Note that there is no need to distinguish between the two different derivatives "Grad" and "grad" in linear theories with small deformations[1]. Denoting the referential quantities by majuscules and the quantities of the current configuration by minuscules, it is possible to derive the following relations,

$$\begin{aligned} \mathrm{d}\mathbf{x} &= \mathbf{F}_\alpha \, \mathrm{d}\mathbf{X}_\alpha \,, \\ \mathrm{d}\mathbf{a} &= \det \mathbf{F}_\alpha \, \mathbf{F}_\alpha^{T-1} \, \mathrm{d}\mathbf{A}_\alpha \,, \\ \mathrm{d}v &= \det \mathbf{F}_\alpha \, \mathrm{d}V_\alpha \,, \end{aligned} \tag{2.38}$$

for the line, the area and the volume elements, respectively.

Remark: In the framework of curvilinear coordinates, one finds from its definition that the deformation gradient is a so-called two-field tensor. This term states that one basis of the tensor is situated in the reference configuration, while the other basis is situated in the current configuration. Hence, by a linear combination with the deformation gradient a vector- or a tensor-valued quantity is transported to the respective configuration. Note that within the scope of curvilinear coordinates quantities can be also differentiated as co- and contravariant. For a more detailed description of this topic, the interested reader is referred to de Boer [21], Ehlers [52] and Markert [130]. □

[1] This can be shown by the following relations:

$$\operatorname{grad} \Gamma \;=\; \frac{\partial \Gamma}{\partial \mathbf{x}} \;=\; \Big(\frac{\partial \mathbf{X}_\alpha}{\partial \mathbf{x}} \Big)^T \frac{\partial \Gamma}{\partial \mathbf{X}_\alpha} \;=\; \mathbf{F}_\alpha^T \operatorname{Grad}_\alpha \mathbf{X}_\alpha \,. \tag{2.37}$$

Thus, in case of small deformations with $\mathbf{F}_\alpha \approx \mathbf{I}$ both derivatives approximately coincide ($\operatorname{grad} \Gamma \approx \operatorname{Grad}_\alpha \Gamma$).

2.2.2 Deformation and strain measures

As any other tensor, the deformation tensor $\mathbf{F}_\alpha$ can be factorised by polar decomposition into a rotation tensor and a stretch tensor, viz.,

$$\mathbf{F}_\alpha =: \mathbf{R}_\alpha \, \mathbf{U}_\alpha =: \mathbf{V}_\alpha \, \mathbf{R}_\alpha \, . \tag{2.39}$$

Therein, the tensor $\mathbf{R}_\alpha$ is a proper orthogonal rotation tensor and, since $\mathbf{F}_\alpha$ is unique and uniquely invertible, $\mathbf{U}_\alpha$ and $\mathbf{V}_\alpha$ are the symmetric, positive definite stretch tensors. According to their position in the decomposition, the tensor $\mathbf{U}_\alpha$ is called the right (material) *Cauchy* stretch tensor and $\mathbf{V}_\alpha$ the left (spatial) *Cauchy* stretch tensor. In case $\mathbf{F}_\alpha$ is given in eingenvectors, it is possible to decompose the deformation into a pure rotation and a pure stretch. Figure 2.3 depicts the effect of the tensors on a line element.

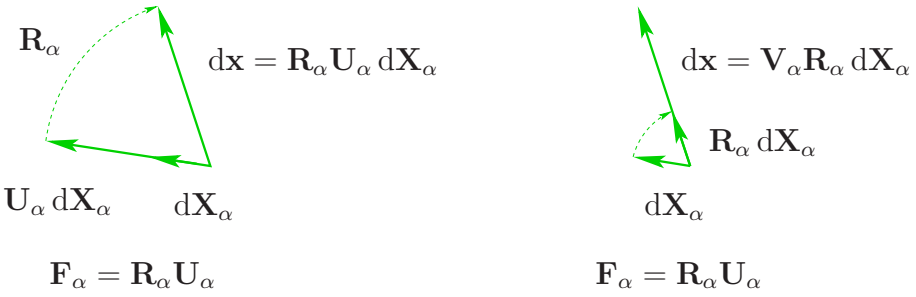

Figure 2.3: Polar decomposition of $\mathbf{F}_\alpha$ into a rotation tensor $\mathbf{R}_\alpha$ and either a referential stretch tensor $\mathbf{U}_\alpha$ or a stretch $\mathbf{V}_\alpha$ in the current configuration.

Like $\mathbf{F}_\alpha$, the rotation tensor $\mathbf{R}_\alpha$ is also a so-called two-field tensor. Thus, by a linear combination with $\mathbf{R}_\alpha$ the stretch tensors $\mathbf{V}_\alpha$ and $\mathbf{U}_\alpha$ are transported to the reference and the current configuration by a backward and a forward rotation:

$$\mathbf{U}_\alpha = \mathbf{R}_\alpha^T \, \mathbf{V}_\alpha \, \mathbf{R}_\alpha \quad \text{and} \quad \mathbf{V}_\alpha = \mathbf{R}_\alpha \, \mathbf{U}_\alpha \, \mathbf{R}_\alpha^T \, . \tag{2.40}$$

The deformation tensors are obtained by the squares of line elements $\mathrm{d}\mathbf{x}$ and $\mathrm{d}\mathbf{X}_\alpha$ and the corresponding transport theorems given by $(2.38)_1$. Thus, one ends up with:

$$\begin{aligned} \mathrm{d}\mathbf{x} \cdot \mathrm{d}\mathbf{x} \;&=\; \mathbf{F}_\alpha \mathrm{d}\mathbf{X}_\alpha \cdot \mathbf{F}_\alpha \mathrm{d}\mathbf{X}_\alpha \;=\; \mathrm{d}\mathbf{X}_\alpha \cdot (\mathbf{F}_\alpha^T \mathbf{F}_\alpha) \, \mathrm{d}\mathbf{X}_\alpha \;=\; \mathrm{d}\mathbf{X}_\alpha \cdot \mathbf{C}_\alpha \, \mathrm{d}\mathbf{X}_\alpha \quad \text{and} \\ \mathrm{d}\mathbf{X}_\alpha \cdot \mathrm{d}\mathbf{X}_\alpha \;&=\; \mathbf{F}_\alpha^{-1} \mathrm{d}\mathbf{x} \cdot \mathbf{F}_\alpha^{-1} \mathrm{d}\mathbf{x} \;=\; \mathrm{d}\mathbf{x} \cdot (\mathbf{F}_\alpha^{T-1} \mathbf{F}_\alpha^{-1}) \, \mathrm{d}\mathbf{x} \;=\; \mathrm{d}\mathbf{x} \cdot \mathbf{B}_\alpha^{-1} \, \mathrm{d}\mathbf{x} \, . \end{aligned} \tag{2.41}$$

Therein, the right and the left *Cauchy-Green* deformation tensors have been defined as:

$$\mathbf{C}_\alpha := \mathbf{F}_\alpha^T \mathbf{F}_\alpha \quad \text{and} \quad \mathbf{B}_\alpha := \mathbf{F}_\alpha \, \mathbf{F}_\alpha^T \, . \tag{2.42}$$

With the aid of (2.39), the relations

$$\mathbf{C}_\alpha = \mathbf{U}_\alpha^T \mathbf{R}_\alpha^T \, \mathbf{R}_\alpha \mathbf{U}_\alpha = \mathbf{U}_\alpha^2 \quad \text{and} \quad \mathbf{B}_\alpha = \mathbf{V}_\alpha \mathbf{R}_\alpha \, \mathbf{R}_\alpha^T \mathbf{V}_\alpha^T = \mathbf{V}_\alpha^2 \tag{2.43}$$

are found, and it becomes obvious that the right *Cauchy-Green* deformation tensor $\mathbf{C}_\alpha$ is

a deformation measure of the reference configuration, while the left one $\mathbf{B}_\alpha$ acts on the current configuration. Note that the deformation gradient and the left and the right *Cauchy* stretch tensors have the same eigenvalues, while the eigenvalues of the *Cauchy-Green* deformation tensors are the squares of the former ones. For a more detailed information on this topic, the reader is referred to, for example, Holzapfel [99] and many others.

It follows from the definitions of the deformation tensors that they are equal to the identity tensor $\mathbf{I}$ for the deformation free situation. In contrast, the strain measures are zero in this situation. They are obtained by the difference of the squares of the line elements and, again, using the corresponding transport theorems $(2.38)_1$:

$$\mathrm{d}\mathbf{x}\cdot\mathrm{d}\mathbf{x}-\mathrm{d}\mathbf{X}_\alpha\cdot\mathrm{d}\mathbf{X}_\alpha \;=\; \mathrm{d}\mathbf{X}_\alpha\cdot(\mathbf{C}_\alpha-\mathbf{I})\,\mathrm{d}\mathbf{X}_\alpha \;=\; \mathrm{d}\mathbf{x}\cdot(\mathbf{I}-\mathbf{B}_\alpha^{-1})\,\mathrm{d}\mathbf{x}\,. \tag{2.44}$$

Now, the referential *Green* strain tensor $\mathbf{E}_\alpha$ and the *Almansi*an strain tensor $\mathbf{A}_\alpha$ acting on the current configuration are defined as

$$\mathbf{E}_\alpha := \tfrac{1}{2}(\mathbf{C}_\alpha-\mathbf{I}) \quad\text{and}\quad \mathbf{A}_\alpha := \tfrac{1}{2}(\mathbf{I}-\mathbf{B}_\alpha^{-1})\,. \tag{2.45}$$

By use of a push-forward, the *Green* strain tensor is transported to the current configuration and by a pull-back the *Almansi*an strain tensor is pulled back to the reference configuration, i. e.

$$\mathbf{A}_\alpha=\mathbf{F}_\alpha^{T-1}\,\mathbf{E}_\alpha\,\mathbf{F}_\alpha^{-1} \quad\text{and}\quad \mathbf{E}_\alpha=\mathbf{F}_\alpha^{T}\,\mathbf{A}_\alpha\,\mathbf{F}_\alpha\,. \tag{2.46}$$

The *Karni-Reiner* strain measures will not be derived within this thesis, because they are not of relevance for the further discussions. For a detailed discussion of deformation and strain measures and the corresponding rates, the interested reader is referred to the works of, for example, Ehlers [51, 52] and Holzapfel [99].

2.2.3 Deformation rates

In order to obtain the rate of the deformation, one usually starts from the material time derivative of the line element $\mathrm{d}\mathbf{x}$. Using the definition of the deformation gradient and using $(2.38)_1$,

$$\mathrm{d}\overset{\prime}{\mathbf{x}}_\alpha=(\mathbf{F}_\alpha)'_\alpha\,\mathrm{d}\mathbf{X}_\alpha=(\mathbf{F}_\alpha)'_\alpha\,\mathbf{F}_\alpha^{-1}\mathrm{d}\mathbf{x}=:\mathbf{L}_\alpha\mathrm{d}\mathbf{x}\,, \tag{2.47}$$

the definition for the spatial velocity gradient $\mathbf{L}_\alpha$ (current configuration) is obtained, where the relations

$$\mathbf{L}_\alpha=\operatorname{grad}\overset{\prime}{\mathbf{x}}_\alpha \quad\text{and}\quad \mathbf{L}_\alpha\cdot\mathbf{I}=\operatorname{div}\overset{\prime}{\mathbf{x}}_\alpha \tag{2.48}$$

hold. In the above relation, $\operatorname{div}(\cdot)$ denotes the divergence operator corresponding to $\operatorname{grad}(\cdot)$. Like any other tensor, $\mathbf{L}_\alpha$ can be uniquely decomposed into a symmetric and a skew-symmetric part,

$$\mathbf{L}_\alpha=\mathbf{D}_\alpha+\mathbf{W}_\alpha\,, \tag{2.49}$$

where the symmetric part

$$\mathbf{D}_\alpha=\tfrac{1}{2}(\mathbf{L}_\alpha+\mathbf{L}_\alpha^T) \tag{2.50}$$

is called the strain rate tensor. The skew-symmetric part

$$\mathbf{W}_\alpha = \tfrac{1}{2}(\mathbf{L}_\alpha - \mathbf{L}_\alpha^T) \tag{2.51}$$

is named vorticity or spin tensor. Also, the transport theorems for the velocities of area and volume elements are obtained from the definitions (2.38):

$$\begin{aligned} (\mathrm{d}\mathbf{a})'_\alpha &= [\,(\,\mathbf{L}_\alpha \cdot \mathbf{I}\,)\,\mathbf{I} \,-\, \mathbf{L}_\alpha^T\,]\,\mathrm{d}\mathbf{a}\,, \\ (\mathrm{d}v)'_\alpha &= (\,\mathbf{L}_\alpha \cdot \mathbf{I}\,)\,\mathrm{d}v\,. \end{aligned} \tag{2.52}$$

Note that the transport corresponding to the velocity of a line element is given by relation (2.47).

2.2.4 Stress measures

External forces act on the surface $\partial\mathcal{B}$ of the medium under consideration. These forces, resulting from the external vicinity (contact forces), are represented by the surface traction vector $\mathbf{t}^\alpha$. By the *Cauchy* theorem

$$\mathbf{t}^\alpha(\mathbf{x}, \mathbf{n}, t) := \mathbf{T}^\alpha(\mathbf{x}, t)\,\mathbf{n}, \tag{2.53}$$

the partial *Cauchy* stress $\mathbf{T}^\alpha$ acting on the constituent φ^α is defined. In the above relation, $\mathbf{n}$ is the outward oriented unit normal vector of the surface $\partial\mathcal{B}$. Note that the *Cauchy* stress represents the so-called *true stress*, because it relates the current force vector $\mathbf{t}^\alpha$ to the current area element $\mathrm{d}a$. By use of the differential representation of the surface force $\mathrm{d}\mathbf{k}^\alpha$, namely,

$$\mathrm{d}\mathbf{k}^\alpha = \mathbf{t}^\alpha \mathrm{d}a = \mathbf{T}^\alpha \mathbf{n}\,\mathrm{d}a = \mathbf{T}^\alpha \mathrm{d}\mathbf{a}\,, \tag{2.54}$$

further representations of the stress tensors can be defined. More precisely, in order to obtain the *Kirchhoff* stress tensor, the surface force $\mathrm{d}\mathbf{k}^\alpha$ is related to a weighted surface element $\mathrm{d}\bar{\mathbf{a}}_\alpha = \det \mathbf{F}_\alpha^{-1}\mathrm{d}\mathbf{a}$, i. e.

$$\mathrm{d}\mathbf{k}^\alpha = \mathbf{T}^\alpha \det \mathbf{F}_\alpha\, \mathrm{d}\bar{\mathbf{a}}_\alpha =: \boldsymbol{\tau}^\alpha\, \mathrm{d}\bar{\mathbf{a}}_\alpha\,. \tag{2.55}$$

Following this, the *Kirchhoff* stress represents a weighted *Cauchy* stress ($\boldsymbol{\tau} = \det \mathbf{F}_\alpha\, \mathbf{T}^\alpha$). By additionally relating $\mathrm{d}\mathbf{k}^\alpha$ to a surface element of the reference configuration, i. e. $\mathrm{d}\mathbf{A} = (\det \mathbf{F})^{-1}\,\mathbf{F}^T\mathrm{d}\mathbf{a}$, one obtains the first *Piola-Kirchhoff* stress tensor:

$$\mathrm{d}\mathbf{k}^\alpha = \mathbf{T}^\alpha \det \mathbf{F}_\alpha\, \mathbf{F}_\alpha^{T-1}\mathrm{d}\mathbf{A}_\alpha =: \mathbf{P}^\alpha\, \mathrm{d}\mathbf{A}_\alpha\,. \tag{2.56}$$

Therein, the transport theorem for a surface element given by $(2.38)_2$ has been used. Note that the first *Piola-Kirchhoff* stress tensor is a two-field tensor as well, since only one basis is transported to the reference configuration ($\mathbf{P}^\alpha = \boldsymbol{\tau}^\alpha\,\mathbf{F}_\alpha^{T-1}$). Moreover, $\mathbf{P}^\alpha$ relates the force vector of the current configuration to the area element of the reference

configuration. By another transport of the second tensor basis one obtains

$$\mathbf{S}^{\alpha} = \mathbf{F}_{\alpha}^{-1}\,\mathbf{P}^{\alpha}\,, \tag{2.57}$$

i. e. the second *Piola-Kirchhoff* stress. The full (covariant) pull-back of the current *Kirchhoff* stress to the referential second *Piola-Kirchhoff* stress is given by:

$$\mathbf{S}^{\alpha} = \mathbf{F}_{\alpha}^{-1}\,\boldsymbol{\tau}^{\alpha}\,\mathbf{F}_{\alpha}^{T-1}\,. \tag{2.58}$$

Note that the stress tensors $\boldsymbol{\tau}$ and $\mathbf{S}$ are not relevant from the physical point of view, because they represent, in contrast to $\mathbf{T}^{\alpha}$ and $\mathbf{P}^{\alpha}$, artificial quantities.

2.3 Balance relations

In this section, the balance relations of continuum mechanics and electrodynamics are briefly presented. They are introduced axiomatically within the frame of the master balance principle (Ehlers [53], Eringen & Maugin [72], Hutter & Jönk [103]). In case of electrodynamics, besides the volume balance relations balancing volume-specific physical quantities, also relations balancing area-specific quantities on a surface are required. Based on physical observations, the balance equations relate the temporal change of a physical quantity to long and short range effects from outside the region under consideration. More precisely, from a continuum-mechanical point of view, the balanced quantities are the mass, the momentum, the moment of momentum (m. o. m.), the energy and the entropy, while, concerning the electrodynamics, the balanced quantities are the charge, the magnetic field intensity and the electric flux density. Gravity, radioactivity and microwaves acting on a mass element of the body $\mathcal{B}$ and the electric current through an area element at the surface $\partial\mathcal{B} \equiv \mathcal{S}$ are examples for the long range effects, while contact forces and heat conducted through the surface $\mathcal{S}$ as well as electric and magnetic fields on a circuit line element $\partial\mathcal{S} \equiv \mathcal{L}$ at the surface belong to the short range effects. Also note that the balance relations are independent of the material, i. e. they are valid for all kind of matter in any circumstance.

Concerning porous materials, one has to account for their multiphasic character, i. e. the constituents can have their own physical quantity and are able to exchange this physical quantity among each other. Nevertheless, following the metaphysical principles as given on page 3, the balance relation of the overall medium is obtained by summing over the corresponding balance relation of all constituents. The resulting balance of φ has to be the same as the corresponding balance for a single-phasic material.

2.3.1 Master balance principle

Volume balance relations

Firstly, the master balance is introduced for the overall body $\mathcal{B}$ with the surface $\partial\mathcal{B} = \mathcal{S}$. Therein, the temporal change of the volume specific scalar- and vector-valued quantity Ψ

and $\boldsymbol{\Psi}$ in the domain is balanced with the efflux $\boldsymbol{\phi}\cdot\mathbf{n}$ and $\boldsymbol{\Phi}\,\mathbf{n}$ of the mechanical quantity over the surface $\mathcal{S}$ to the external vicinity, the supply σ and $\boldsymbol{\sigma}$ to the body from a distance affecting the whole body and, finally, the production $\hat{\Psi}$ and $\hat{\boldsymbol{\Psi}}$ of the physical quantity due to the couplings of φ with its surrounding (cf. Ehlers [54, 56]):

$$\begin{aligned}\frac{\mathrm{d}}{\mathrm{d}t}\int_{\mathcal{B}}\Psi\,\mathrm{d}v &= \int_{\mathcal{S}}(\boldsymbol{\phi}\cdot\mathbf{n})\,\mathrm{d}a + \int_{\mathcal{B}}\sigma\,\mathrm{d}v + \int_{\mathcal{B}}\hat{\Psi}\,\mathrm{d}v\,,\\ \frac{\mathrm{d}}{\mathrm{d}t}\int_{\mathcal{B}}\boldsymbol{\Psi}\,\mathrm{d}v &= \int_{\mathcal{S}}(\boldsymbol{\Phi}\,\mathbf{n})\,\mathrm{d}a + \int_{\mathcal{B}}\boldsymbol{\sigma}\,\mathrm{d}v + \int_{\mathcal{B}}\hat{\boldsymbol{\Psi}}\,\mathrm{d}v\,.\end{aligned} \tag{2.59}$$

Given the above global forms of the general balance relations, the corresponding local forms valid for the material point are obtained by moving the time derivative into the integral[2] on the left-hand side and calculating its time derivative by use of (2.52). Also, the surface integral on the right-hand side is transformed to a volume integral via the *Gauß* theorem as given in Ehlers [57]. Following this and assuming sufficiently smooth integrands one obtains

$$\begin{aligned}\dot{\Psi} + \Psi\,\mathrm{div}\,\dot{\mathbf{x}} &= \mathrm{div}\,\boldsymbol{\phi} + \sigma + \hat{\Psi}\,,\\ \dot{\boldsymbol{\Psi}} + \boldsymbol{\Psi}\,\mathrm{div}\,\dot{\mathbf{x}} &= \mathrm{div}\,\boldsymbol{\Phi} + \boldsymbol{\sigma} + \hat{\boldsymbol{\Psi}}\end{aligned} \tag{2.60}$$

as the local forms of the global master balances.

The balance relations of the constituents have the same appearance as the ones of the overall medium:

$$\begin{aligned}\frac{\mathrm{d}_\alpha}{\mathrm{d}t}\int_{\mathcal{B}}\Psi^\alpha\,\mathrm{d}v &= \int_{\mathcal{S}}(\boldsymbol{\phi}^\alpha\cdot\mathbf{n})\,\mathrm{d}a + \int_{\mathcal{B}}\sigma^\alpha\,\mathrm{d}v + \int_{\mathcal{B}}\hat{\Psi}^\alpha\,\mathrm{d}v\,,\\ \frac{\mathrm{d}_\alpha}{\mathrm{d}t}\int_{\mathcal{B}}\boldsymbol{\Psi}^\alpha\,\mathrm{d}v &= \int_{\mathcal{S}}(\boldsymbol{\Phi}^\alpha\,\mathbf{n})\,\mathrm{d}a + \int_{\mathcal{B}}\boldsymbol{\sigma}^\alpha\,\mathrm{d}v + \int_{\mathcal{B}}\hat{\boldsymbol{\Psi}}^\alpha\,\mathrm{d}v\,.\end{aligned} \tag{2.61}$$

The only difference is that the quantities introduced in (2.59) are now denoted by an additional superscript $(\,\cdot\,)^\alpha$. As for the overall medium, also for the single constituent the local forms of the balance relations may be derived:

$$\begin{aligned}(\Psi)'_\alpha + \Psi^\alpha\,\mathrm{div}\,\overset{\prime}{\mathbf{x}}_\alpha &= \mathrm{div}\,\boldsymbol{\phi}^\alpha + \sigma^\alpha + \hat{\Psi}^\alpha\,,\\ (\boldsymbol{\Psi})'_\alpha + \boldsymbol{\Psi}^\alpha\,\mathrm{div}\,\overset{\prime}{\mathbf{x}}_\alpha &= \mathrm{div}\,\boldsymbol{\Phi}^\alpha + \boldsymbol{\sigma}^\alpha + \hat{\boldsymbol{\Psi}}^\alpha\,,\end{aligned} \tag{2.62}$$

They are obtained by the same procedure as for the overall medium, namely, a time differentiation of the left-hand side integral and transforming the surface integral on the right-hand side to a volume integral via the *Gauß* theorem.

From the fact that the local forms of the overall balances (2.60) of the medium are given, on the one hand, by the balance relations of a single-phase material and, on the other hand, by summing up the local partial balances (2.62) of all constituents, one can find

[2] For the a *Lagrange*an formulation, as it is the case within this contribution, this is possible.

the following constraints between the global and the partial quantities:

$$\begin{aligned} \Psi &= \sum_\alpha \Psi^\alpha\,, \quad \boldsymbol{\phi}\cdot\mathbf{n} = \sum_\alpha [\boldsymbol{\phi}^\alpha - \Psi^\alpha\,\mathbf{d}_\alpha]\cdot\mathbf{n}\,, \quad \sigma = \sum_\alpha \sigma^\alpha\,, \quad \hat{\Psi} = \sum_\alpha \hat{\Psi}^\alpha\,, \\ \boldsymbol{\Psi} &= \sum_\alpha \boldsymbol{\Psi}^\alpha\,, \quad \boldsymbol{\Phi}\,\mathbf{n} = \sum_\alpha [\boldsymbol{\Phi}^\alpha - \boldsymbol{\Psi}^\alpha\otimes\mathbf{d}_\alpha]\,\mathbf{n}\,, \quad \boldsymbol{\sigma} = \sum_\alpha \boldsymbol{\sigma}^\alpha\,, \quad \hat{\boldsymbol{\Psi}} = \sum_\alpha \hat{\boldsymbol{\Psi}}^\alpha\,. \end{aligned} \tag{2.63}$$

Note that in order to obtain the restrictions $(2.63)_2$ and $(2.63)_6$ the relations

$$(\Psi^\alpha)'_\alpha = \dot{\Psi}^\alpha + \operatorname{grad}\Psi^\alpha\cdot\mathbf{d}_\alpha \quad\text{and}\quad (\boldsymbol{\Psi}^\alpha)'_\alpha = \dot{\boldsymbol{\Psi}}^\alpha + \operatorname{grad}\boldsymbol{\Psi}^\alpha\,\mathbf{d}_\alpha \tag{2.64}$$

and the diffusion velocity $(2.32)_1$ have been used.

Surface balance relations

In analogy to the previously introduced volume balance relations, physical quantities may also be balanced at surfaces. Thus, the general form of a vectorial quantity $\boldsymbol{\Psi}$ piercing a surface $\mathcal{S}$ with its boundary $\partial\mathcal{S}\equiv\mathcal{L}$ is given by, cf. Eringen & Maugin [72],

$$\frac{\mathrm{d}}{\mathrm{d}t}\int_{\mathcal{S}}\boldsymbol{\Psi}\cdot\mathbf{n}\,\mathrm{d}a = \oint_{\mathcal{L}}(\boldsymbol{\phi}\cdot\mathbf{n})\,\mathrm{d}s + \int_{\mathcal{S}}\boldsymbol{\sigma}\cdot\mathbf{n}\,\mathrm{d}a + \int_{\mathcal{S}}\hat{\boldsymbol{\Psi}}\cdot\mathbf{n}\,\mathrm{d}a\,. \tag{2.65}$$

The local form is again obtained by computation of the time derivative of the surface integral on the left-hand side by use of material time derivative of an areal element, cf. (2.52), and by transformation of the line integral to a surface integral:

$$\dot{\boldsymbol{\Psi}} + \left(\operatorname{div}\dot{\mathbf{x}}\,\mathbf{I} - \mathbf{L}^T\right)\boldsymbol{\Psi} = \operatorname{rot}\boldsymbol{\phi} + \boldsymbol{\sigma} + \hat{\boldsymbol{\Psi}}\,. \tag{2.66}$$

In analogy, the partial surface balance relation of the constituent φ^α reads

$$\frac{\mathrm{d}_\alpha}{\mathrm{d}t}\int_{\mathcal{S}}\boldsymbol{\Psi}^\alpha\cdot\mathbf{n}\,\mathrm{d}a = \oint_{\mathcal{L}}(\boldsymbol{\phi}^\alpha\cdot\mathbf{n})\,\mathrm{d}s + \int_{\mathcal{S}}\boldsymbol{\sigma}^\alpha\cdot\mathbf{n}\,\mathrm{d}a + \int_{\mathcal{S}}\hat{\boldsymbol{\Psi}}^\alpha\cdot\mathbf{n}\,\mathrm{d}a\,. \tag{2.67}$$

Note that the quantities introduced in the above relation have the same physical meaning as mentioned before but are belonging to the constituent φ^α denoted by the additional superscript $(\,\cdot\,)^\alpha$. The relation

$$(\boldsymbol{\Psi})'_\alpha + \left(\operatorname{div}\overset{\prime}{\mathbf{x}}_\alpha\,\mathbf{I} - \mathbf{L}_\alpha^T\right)\boldsymbol{\Psi}^\alpha = \operatorname{rot}\boldsymbol{\phi}^\alpha + \boldsymbol{\sigma}^\alpha + \hat{\boldsymbol{\Psi}}^\alpha \tag{2.68}$$

represents the local form of (2.67). Also here, the summation over the partial surface balance relations of the constituents must lead to the surface balance relation of the overall medium. Thus, one finds the restrictions

$$\boldsymbol{\Psi} = \sum_\alpha \boldsymbol{\Psi}^\alpha\,, \quad \boldsymbol{\phi}\cdot\mathbf{n} = \sum_\alpha [\boldsymbol{\phi}^\alpha - \boldsymbol{\Psi}^\alpha\times\mathbf{d}_\alpha]\cdot\mathbf{n}\,, \quad \boldsymbol{\sigma} = \sum_\alpha \boldsymbol{\sigma}^\alpha\,, \quad \hat{\boldsymbol{\Psi}} = \sum_\alpha \hat{\boldsymbol{\Psi}}^\alpha \tag{2.69}$$

and, in addition,

$$\sum_{\alpha} \left[2\,\mathrm{skw}(\mathrm{grad}\,\mathbf{d}_\alpha)\,\boldsymbol{\Psi}^\alpha + \mathbf{d}_\alpha\,\mathrm{div}\,\boldsymbol{\Psi}^\alpha \right] = 0 \tag{2.70}$$

for the area specific quantities of the surface balance relations, cf. also (2.63).

2.3.2 Balance relations of continuum mechanics

Concerning the particular balances of the overall medium, the corresponding physical quantities are listed in Table 2.1. Therein, $\rho\,\dot{\mathbf{x}}$ denotes the momentum of the overall medium, $\mathbf{T}$ the overall *Cauchy* stress tensor and $\rho\,\mathbf{g}$ the volume specific body force, where $\mathbf{g}$ can generally be interpreted as the gravity, and $\mathbf{x} \times (\rho\,\dot{\mathbf{x}})$ denotes the m. o. m. of the entire mixture. Concerning the energy balance, which is also referred to as the first law of thermodynamics, ε is the internal energy, $\mathbf{q}$ is the heat influx over the boundary and r denotes the external heat supply. In the entropy balance, the second law of thermodynamics, the quantities indicated by η, $\boldsymbol{\phi}_\eta \cdot \mathbf{n}$ and σ_η are, respectively, the entropy itself, the efflux of entropy over the surface of the body and the external entropy supply from a distance. Note that due to the fact that the system is assumed to be closed, all production terms are equal to zero - except the non-negative entropy production ($\hat{\eta} \geq 0$).

balance of	Ψ, $\boldsymbol{\Psi}$	$\boldsymbol{\phi}$, $\boldsymbol{\Phi}$	σ, $\boldsymbol{\sigma}$	$\hat{\Psi}$, $\hat{\boldsymbol{\Psi}}$
mass	ρ	$\mathbf{0}$	0	0
momentum	$\rho\,\dot{\mathbf{x}}$	$\mathbf{T}$	$\rho\,\mathbf{g}$	$\mathbf{0}$
m. o. m.	$\mathbf{x} \times (\rho\,\dot{\mathbf{x}})$	$\mathbf{x} \times \mathbf{T}$	$\mathbf{x} \times (\rho\,\mathbf{g})$	$\mathbf{0}$
energy	$\rho\,\varepsilon + \frac{1}{2}\dot{\mathbf{x}} \times (\rho\,\dot{\mathbf{x}})$	$\mathbf{T}^T\dot{\mathbf{x}} - \mathbf{q}$	$\dot{\mathbf{x}} \cdot (\rho\,\mathbf{g}) + \rho\,r$	0
entropy	$\rho\,\eta$	$\boldsymbol{\phi}_\eta$	σ_η	$\hat{\eta}$

Table 2.1: Continuum-mechanical volume balance relations of the overall medium.

In order to obtain the local forms of the specific balance relations related to the overall medium, the quantities given in Table 2.1 are inserted into the local master balance given in (2.60). By additionally using the so-called respective "lower" balances one obtains the balances for mass, momentum, moment of momentum, energy and entropy:

$$\begin{aligned}
&\text{mass} && \dot{\rho} + \rho\,\mathrm{div}\,\dot{\mathbf{x}} = 0\,, \\
&\text{momentum} && \rho\,\ddot{\mathbf{x}} = \mathrm{div}\,\mathbf{T} + \rho\,\mathbf{g}\,, \\
&\text{m. o. m.} && \mathbf{0} = \mathbf{I} \times \mathbf{T} \quad \longrightarrow \quad \mathbf{T} = \mathbf{T}^T\,, \\
&\text{energy} && \rho\,\dot{\varepsilon} = \mathbf{T} \cdot \mathbf{L} - \mathrm{div}\,\mathbf{q} + \rho\,r\,, \\
&\text{entropy} && \rho\,\dot{\eta} = \mathrm{div}\,\boldsymbol{\phi}_\eta + \sigma_\eta\,.
\end{aligned} \tag{2.71}$$

Note that above balances are equal to the well-known forms generally used in the field of continuum mechanics of single-phase materials. As given in $(2.71)_3$, the result of the balance of m. o. m. is the symmetry *Cauchy* stress tensor of the overall medium. But note that in the case of electromagnetic interactions, the stress tensor is in general not symmetric, cf. Eringen & Maugin [72] and Hutter *et al.* [104] and also the footnote on page 59 for more details.

In order to obtain the specific balance relations corresponding to φ^α, the quantities listed in Table 2.2 are inserted into the local form of the master balance of the constituents given by (2.62). The additional quantities, i. e. the production terms, in the table allow for interactions amongst the constituents. Here, $\hat{\rho}^\alpha$ denotes the mass production, $\hat{\mathbf{s}}^\alpha$ denotes the total momentum production, $\hat{\mathbf{h}}^\alpha$ is the total production of m. o. m. , $\hat{e}^\alpha$ is the total energy production term and, finally, $\hat{\eta}^\alpha$ denotes the entropy production of φ^α. Note that, in contrast to the overall aggregate, the entropy production of a single constituent may also be negative. Moreover, following Ehlers [56], the *a priori* constitutive assumptions

$$\boldsymbol{\phi}_\eta^\alpha = -\frac{1}{\theta^\alpha}\,\mathbf{q}^\alpha \quad \text{and} \quad \sigma_\eta^\alpha = \frac{1}{\theta^\alpha}\,\rho^\alpha\, r^\alpha \tag{2.72}$$

for the entropy efflux and for the entropy supply are made. Therein, θ^α denotes the absolute *Kelvin*'s temperature of φ^α and allows for separate temperatures for each of the constituents.

balance of	Ψ^α, $\boldsymbol{\Psi}^\alpha$	$\boldsymbol{\phi}^\alpha$, $\boldsymbol{\Phi}^\alpha$	σ^α, $\boldsymbol{\sigma}^\alpha$	$\hat{\Psi}^\alpha$, $\hat{\boldsymbol{\Psi}}^\alpha$
mass	ρ^α	$\mathbf{0}$	0	$\hat{\rho}^\alpha$
momentum	$\rho^\alpha\, \overset{\prime}{\mathbf{x}}_\alpha$	$\mathbf{T}^\alpha$	$\rho^\alpha\, \mathbf{g}^\alpha$	$\hat{\mathbf{s}}^\alpha$
m. o. m.	$\mathbf{x} \times (\rho^\alpha\, \overset{\prime}{\mathbf{x}}_\alpha)$	$\mathbf{x} \times \mathbf{T}^\alpha$	$\mathbf{x} \times (\rho^\alpha\, \mathbf{g}^\alpha)$	$\hat{\mathbf{h}}^\alpha$
energy	$\rho^\alpha\, \varepsilon^\alpha + \frac{1}{2}\, \overset{\prime}{\mathbf{x}}_\alpha \times (\rho^\alpha\, \overset{\prime}{\mathbf{x}}_\alpha)$	$(\mathbf{T}^\alpha)^T\, \overset{\prime}{\mathbf{x}}_\alpha - \mathbf{q}^\alpha$	$\overset{\prime}{\mathbf{x}}_\alpha \cdot (\rho^\alpha\, \mathbf{g}^\alpha) + \rho^\alpha\, r^\alpha$	$\hat{e}^\alpha$
entropy	$\rho^\alpha\, \eta^\alpha$	$\boldsymbol{\phi}_\eta^\alpha$	σ_η^α	$\hat{\eta}^\alpha$

Table 2.2: Continuum-mechanical volume balance relations of the constituent.

Summarising above considerations, one obtains the local forms of the individual balances of the constituent φ^α:

$$\begin{aligned}
&\text{mass} && (\rho^\alpha)'_\alpha + \rho^\alpha \operatorname{div} \overset{\prime}{\mathbf{x}}_\alpha = \hat{\rho}^\alpha\,, \\
&\text{momentum} && \rho^\alpha\, \overset{\prime\prime}{\mathbf{x}}_\alpha = \operatorname{div} \mathbf{T}^\alpha + \rho^\alpha\, \mathbf{g}^\alpha + \hat{\mathbf{p}}^\alpha\,, \\
&\text{m. o. m.} && \mathbf{0} = \mathbf{I} \times \mathbf{T}^\alpha + \hat{\mathbf{m}}^\alpha\,, \\
&\text{energy} && \rho^\alpha\, (\varepsilon^\alpha)'_\alpha = \mathbf{T}^\alpha \cdot \mathbf{L}_\alpha - \operatorname{div} \mathbf{q}^\alpha + \rho^\alpha\, r^\alpha + \hat{\varepsilon}^\alpha\,, \\
&\text{entropy} && \rho^\alpha\, (\eta^\alpha)'_\alpha = \operatorname{div} \left(-\frac{1}{\theta^\alpha}\, \mathbf{q}^\alpha\right) + \frac{1}{\theta^\alpha}\, \rho^\alpha\, r^\alpha + \hat{\zeta}^\alpha\,.
\end{aligned} \tag{2.73}$$

Again, the above balances are obtained with the aid of the respective "lower" balances. Note that in contrast to single-phase materials, the partial *Cauchy* stress in $(2.73)_4$ is not *a priori* symmetric anymore. The additional term $\hat{\mathbf{m}}^\alpha$ denotes the direct m. o. m. production resulting from the rotational degree of freedom of the constituent or from electromagnetic interactions, cf. also the footnote on page 59. Note that for non-polar materials (*Boltzmann* continua), as given in this contribution, the m. o. .m. production vanishes and, as a consequence, the partial *Cauchy* stress is symmetric. Concerning micro-polar materials (*Cosserat* continua), the interested reader is referred to the works of Diebels [44], Ehlers [56], Scholz [149] and Volk [164]. In addition to $\hat{\mathbf{m}}^\alpha$ in relations (2.73), some further direct production terms occur. Namely, the direct momentum production $\hat{\mathbf{p}}^\alpha$, the direct energy production $\hat{\varepsilon}^\alpha$ and the direct entropy production $\hat{\zeta}^\alpha$. They are related to the total production terms given in Table 2.2 via

$$\begin{aligned}
&\text{momentum} && \hat{\mathbf{s}}^\alpha = \hat{\mathbf{p}}^\alpha + \hat{\rho}^\alpha \overset{\prime}{\mathbf{x}}_\alpha \,, \\
&\text{m. o. m.} && \hat{\mathbf{h}}^\alpha = \hat{\mathbf{m}}^\alpha + \mathbf{x} \times (\hat{\mathbf{p}}^\alpha + \hat{\rho}^\alpha \overset{\prime}{\mathbf{x}}_\alpha) \,, \\
&\text{energy} && \hat{e}^\alpha = \hat{\varepsilon}^\alpha + \hat{\mathbf{p}}^\alpha \cdot \overset{\prime}{\mathbf{x}}_\alpha + \hat{\rho}^\alpha (\varepsilon^\alpha + \tfrac{1}{2} \overset{\prime}{\mathbf{x}}_\alpha \cdot \overset{\prime}{\mathbf{x}}_\alpha) \,, \\
&\text{entropy} && \hat{\eta}^\alpha = \hat{\zeta}^\alpha + \hat{\rho}^\alpha \eta^\alpha \,.
\end{aligned} \tag{2.74}$$

The additional terms on the right-hand side are the so-called indirect productions due to the productions of the "lower" physical quantities, for example, $\hat{\rho}^\alpha \overset{\prime}{\mathbf{x}}_\alpha$ denotes the momentum production due to mass production $\hat{\rho}^\alpha$.

Recalling that summing a partial balance relation over all constituents the result has to be equal to the single-phase balance, the total production terms have to satisfy the following restrictions:

$$\sum_\alpha \hat{\rho}^\alpha = 0 \,, \quad \sum_\alpha \hat{\mathbf{s}}^\alpha = \mathbf{0} \,, \quad \sum_\alpha \hat{\mathbf{h}}^\alpha = \mathbf{0} \,, \quad \sum_\alpha \hat{e}^\alpha = 0 \,, \quad \sum_\alpha \hat{\eta}^\alpha \geq 0 \,. \tag{2.75}$$

See Table 2.1 for the production terms of the overall medium. Note that the entropy production is the only term which must be greater than or equal to zero. The inequality form of the entropy balance was the reason why the correct form for multiphasic materials was not found till the late sixties of the last century. During the intense discussions between the researchers, it has been found to be too restrictive, that the entropy production of each constituent has to be positive. As a result of these considerations, the only restriction to the entropy production is now that the sum of all $\hat{\eta}^\alpha$ has to be non-negative. Thereafter, this principle has been repeatedly and successfully applied to the mixture theory as well as to the TPM, cf., for example, de Boer & Ehlers [24], Bowen [27], Bowen & Wiese [30], Ehlers [51], Huyghe & Janssen [108], Lai *et al.* [116] and Markert [130].

2.3.3 Entropy principle of multiphasic materials

Aiming at the appropriate representation of the entropy balance for multiphasic materials, its local form $(2.73)_5$ is summed over all constituents to obtain the corresponding relation

for the overall medium. Then, the total entropy production $(2.74)_4$ and restriction $(2.75)_5$ are inserted. After a rearrangement, the inequality

$$\sum_{\alpha} \left[\rho^{\alpha}(\eta^{\alpha})'_{\alpha} + \hat{\rho}^{\alpha}\eta^{\alpha} + \operatorname{div}\left(\frac{1}{\theta^{\alpha}} \mathbf{q}^{\alpha} \right) - \frac{1}{\theta^{\alpha}} \rho^{\alpha} r^{\alpha} \right] \geq 0 \tag{2.76}$$

is obtained, i. e. the entropy production of the overall medium is always greater than zero. After introducing the *Helmholtz* free energy via the *Legendre* transformation

$$\psi^{\alpha} := \varepsilon^{\alpha} - \theta^{\alpha}\eta^{\alpha} , \tag{2.77}$$

as well as inserting the partial energy balance $(2.73)_4$ and its total energy production $(2.74)_3$, one arrives at the *Clausius-Duhem* representation of the entropy inequality:

$$\begin{aligned} \sum_{\alpha} \frac{1}{\theta^{\alpha}} \Big\{ & \mathbf{T}^{\alpha} \cdot \mathbf{L}_{\alpha} - \rho^{\alpha} \left[(\psi^{\alpha})'_{\alpha} - (\theta^{\alpha})'_{\alpha}\eta^{\alpha} \right] - \hat{\mathbf{p}}^{\alpha} \cdot \overset{\prime}{\mathbf{x}}_{\alpha} \\ & - \hat{\rho}^{\alpha}(\psi^{\alpha} + \tfrac{1}{2} \overset{\prime}{\mathbf{x}}_{\alpha} \cdot \overset{\prime}{\mathbf{x}}_{\alpha}) - \frac{1}{\theta^{\alpha}} \mathbf{q}^{\alpha} \cdot \operatorname{grad} \theta^{\alpha} + \hat{e}^{\alpha} \Big\} \geq 0 . \end{aligned} \tag{2.78}$$

In the remainder of this thesis, it is assumed that the thermodynamic temperature θ^{α} of each constituent is equal and constant ($\theta^{\alpha} \equiv \theta \equiv$ const.). Following this, and taking advantage of restriction $(2.75)_5$, one ends up with

$$\sum_{\alpha} \left[\mathbf{T}^{\alpha} \cdot \mathbf{L}_{\alpha} - \rho^{\alpha}(\psi^{\alpha})'_{\alpha} - \hat{\mathbf{p}}^{\alpha} \cdot \overset{\prime}{\mathbf{x}}_{\alpha} - \hat{\rho}^{\alpha}(\psi^{\alpha} + \tfrac{1}{2} \overset{\prime}{\mathbf{x}}_{\alpha} \cdot \overset{\prime}{\mathbf{x}}_{\alpha}) \right] \geq 0 , \tag{2.79}$$

which is the *Clausius-Planck* form of the entropy inequality for heterogeneous materials.

2.3.4 Balance relations of Electrodynamics

The differential form of the *Maxwell* equations together with the balance of charge, i. e. the so-called electric continuity equation, will be introduced within the framework of the master balance principle presented in Section 2.3.1. In fact, the equations known as *Maxwell* equations were already known as separate relations before *Maxwell* summarised them. Anyway, in this section, the balance relations for the overall body initially and, thereafter, the partial balance relations for the individual constituent will be introduced axiomatically.

Balancing physical quantities of electrodynamics, there exist two types of balance relations. The volume balance relations for volumetric quantities and the surface balance relations used for area specific ones. As for the continuum-mechanical balance relations, the relevant quantities of the overall aggregate, which have to be inserted into the master balance, are given in Table 2.3 and Table 2.4.

In Table 2.3, the introduced quantities are denoted as follows. As has already been mentioned, ρ_e stands for the overall charge density, $\mathbf{d}_e$ is the electric flux density (also denoted as electric displacement) and $\mathbf{b}_e$ denotes the magnetic flux density. In Table 2.4 $\mathbf{h}_e$ stands for the magnetic field intensity, $\mathbf{i}_e$ denotes the electric current and $\mathbf{e}_e$ denotes

balance relation	Ψ	$\boldsymbol{\phi}$	σ	$\hat{\Psi}$
charge balance	ρ_e	$\mathbf{0}$	0	0
electric flux continuity	0	$\mathbf{d}_e$	$-\rho_e$	0
magnetic flux continuity	0	$\mathbf{b}_e$	0	0

Table 2.3: Electrodynamic volume balance relations of the overall medium.

induction law of	$\boldsymbol{\Psi}$	$\boldsymbol{\Phi}$	$\boldsymbol{\sigma}$	$\hat{\boldsymbol{\Psi}}$
Ampère	$\mathbf{d}_e$	$\mathbf{h}_e$	$-\mathbf{i}_e$	$\mathbf{0}$
Faraday	$\mathbf{b}_e$	$-\mathbf{e}_e$	$\mathbf{0}$	$\mathbf{0}$

Table 2.4: Electrodynamic surface balance relations of the overall medium.

the electric field (strength).

Going through the procedure of time derivation of the left-hand side integral and transformation of the first integral at the right-hand side via the *Gauß* theorem, the local forms are obtained. In particular, for the non-relativistic case of a deformable material, the volume balance relations are given by

$$\begin{aligned} &\text{charge} && \dot{\rho}_e + \rho_e \operatorname{div} \dot{\mathbf{x}} = 0 \,, \\ &\text{electric flux continuity} && 0 = \operatorname{div} \mathbf{d}_e - \rho_e \,, \\ &\text{magnetic flux continuity} && 0 = \operatorname{div} \mathbf{b}_e \,, \end{aligned} \tag{2.80}$$

whereas the derivation of the local forms of the surface balance relations results in:

$$\begin{aligned} &\textit{Ampère}\text{'s law} && \dot{\mathbf{d}}_e + \left(\operatorname{div} \dot{\mathbf{x}}\, \mathbf{I} - \mathbf{L}^T \right) \mathbf{d}_e = \operatorname{rot} \mathbf{h}_e - \mathbf{i}_e \,, \\ &\textit{Faraday}\text{'s law} && \dot{\mathbf{b}}_e + \left(\operatorname{div} \dot{\mathbf{x}}\, \mathbf{I} - \mathbf{L}^T \right) \mathbf{b}_e = -\operatorname{rot} \mathbf{e}_e \,. \end{aligned} \tag{2.81}$$

Therein, the additional second term on the left-hand side stems from the time derivation of the area element. Note that even though *Faraday*'s and *Ampère*'s law belong to the surface balance relations, they are valid for the overall aggregate, i. e. for each surface within the material.

Remark: In contrast to the charge balance, the continuity of the electric and the magnetic flux are no balance relations in the sense of the master balance (2.62), since they do actually not balance any quantity, i. e. $\boldsymbol{\Psi}^\alpha = \mathbf{0}$. In particular, they relate the efflux of a quantity to its sources in the medium. Moreover, *Ampère*'s and *Faraday*'s law are surface balances relating either the temporal change of the electric field to the rotation of the magnetic field intensity $\mathbf{b}_e$ on the surface around the electric field and the electric

current $\mathbf{i}_e$ through the surface or the temporal change of the magnetic flux density to the circulating electric field $\mathbf{e}_e$ at the surface, cf. Eringen & Maugin [72] and Grot [84]. Note that the minus sign in *Faraday*'s law is based on *Lenz* law and states that the induced $\mathbf{b}_e$ field opposes the inducing electric field.

Moreover, the above equations make obvious that the *Maxwell* equations in the above representation are not *Galilei* invariant, i. e. they depend on the position of the observer. This can be illustrated by the following description. Imagine a moving charge in space, where the inertial system is fixed at a point in space. Following *Ampère*'s law, this moving charge produces a magnetic field. Now, changing the perspective by placing the inertial system into the centre of the moving charge, the charge has no velocity and, therefore, it does not produce any magnetic field anymore.

This inconsistency was well known at the end of the 19$^{\text{th}}$ century. Einstein was the one who published in his work [67] the solution for this inconsistency. He used *Lorentz* transformations instead of the *Galilei*an ones to transform the different inertial systems into each other. By use of the *Lorentz* transformations, not only space is transformed but also time. Following this, the three-dimensional space is combined with time to a quadruple. Moreover, *Lorentz* transformations are limited to systems whose relative velocity does not exceed a certain maximum, i. e. the speed of light (Hutter *et al.* [104]). In the textbooks of, for example, Eringen & Maugin [72] and Maugin *et al.* [134] the *Galilei*an invariant representation of the *Maxwell* equations can be found. □

Actually, in the above relations, the electric flux continuity, also denoted as *Gauß* law, states that there exists a electric monopole and that each unbalanced net charge ρ_e results in an electric flux density $\mathbf{d}_e$, cf. $(2.80)_1$ and $(2.80)_2$. In contrast, as one can see from the magnetic flux continuity, also denoted as *Gauß* law of magnetism, the magnetic flux density $\mathbf{b}_e$ does not have a source, i. e. magnetic fields do not have a starting and an end point, such as electric fields have. Furthermore, *Ampère*'s law states that a magnetic field is produced by varying electric fields and *Faraday*'s law states that an electric field is produced by changing magnetic fields. In addition, the second term considering magnetic fields due to electric currents has been introduced by *Maxwell*. This equation is also known as *Ampère*'s circuital law (with *Maxwell*'s extension).

Stepping over to the partial relations of the individual constituents, the relevant quantities are summarised in Table 2.5 for the volume balance relations and in Table 2.6 for the surface balance relations. Note that the partial balance relations imply the electromagnetic fields are individually applied for each conducting constituent.

balance relation	Ψ^α	$\boldsymbol{\phi}^\alpha$	σ^α	$\hat{\Psi}^\alpha$
charge balance	ρ_e^α	$\mathbf{0}$	0	$\hat{\rho}_e^\alpha$
electric flux continuity	0	$\mathbf{d}_e^\alpha$	$-\rho_e^\alpha$	$\hat{\kappa}_e^\alpha$
magnetic flux continuity	0	$\mathbf{b}_e^\alpha$	0	$\hat{\omega}_e^\alpha$

Table 2.5: Electrodynamic volume balance relations of the constituent.

induction law of	$\boldsymbol{\Psi}^\alpha$	$\boldsymbol{\Phi}^\alpha$	$\boldsymbol{\sigma}^\alpha$	$\hat{\boldsymbol{\Psi}}^\alpha$
Ampère	$\mathbf{d}_e^\alpha$	$\mathbf{h}_e^\alpha$	$-\mathbf{i}_e^\alpha$	$\hat{\mathbf{d}}_e^\alpha$
Faraday	$\mathbf{b}_e^\alpha$	$-\,\mathbf{e}_e^\alpha$	$\mathbf{0}$	$\hat{\mathbf{b}}_e^\alpha$

Table 2.6: Electrodynamic surface balance relations of the constituent.

All quantities in the above tables have the same physical interpretation as in case of the overall aggregate, where the additional superscript denotes the belonging to a constituent and the non-zero production terms. In particular, $\hat{\rho}_e^\alpha$ denotes the total charge production, $\hat{\omega}_e^\alpha$ and $\hat{\kappa}_e^\alpha$ represent the total productions terms, $\hat{\mathbf{d}}_e^\alpha$ is the total production of electric field and $\hat{\mathbf{b}}_e^\alpha$ denotes the total production of magnetic field. The local forms of the volume balance relations are given by

$$\begin{aligned}
&\text{charge} && (\rho_e^\alpha)'_\alpha + \rho_e^\alpha \operatorname{div} \overset{\prime}{\mathbf{x}}_\alpha = \hat{\rho}_e^\alpha \,, \\
&\text{electric flux continuity} && 0 = \operatorname{div} \mathbf{d}_e^\alpha - \rho_e^\alpha + \hat{\kappa}_e^\alpha \,, \\
&\text{magnetic flux continuity} && 0 = \operatorname{div} \mathbf{b}_e^\alpha + \hat{\omega}_e^\alpha \,,
\end{aligned} \tag{2.82}$$

and the local forms surface balance relations are represented by

$$\begin{aligned}
&\textit{Ampère}\text{'s law} && (\mathbf{d}_e^\alpha)'_\alpha + \left(\operatorname{div} \overset{\prime}{\mathbf{x}}_\alpha \mathbf{I} - \mathbf{L}_\alpha^T\right) \mathbf{d}_e^\alpha = \operatorname{rot} \mathbf{h}_e^\alpha - \mathbf{i}_e^\alpha + \hat{\mathbf{d}}_e^\alpha \,, \\
&\textit{Faraday}\text{'s law} && (\mathbf{b}_e^\alpha)'_\alpha + \left(\operatorname{div} \overset{\prime}{\mathbf{x}}_\alpha \mathbf{I} - \mathbf{L}_\alpha^T\right) \mathbf{b}_e^\alpha = -\operatorname{rot} \mathbf{e}_e^\alpha + \hat{\mathbf{b}}_e^\alpha \,.
\end{aligned} \tag{2.83}$$

Concerning the production terms, it follows from the fact of the non-existence of magnetic monopoles that $\hat{\omega}_e^\alpha = 0$. The relations for the production terms are summarised as follows:

$$\hat{\rho}_e^\alpha = \hat{z}^\alpha + \frac{z^\alpha F}{M_m^\alpha} \hat{\rho}^\alpha \,, \qquad \hat{\omega}_e^\alpha = 0 \,. \tag{2.84}$$

wherein the overall charge production $\hat{\rho}_e^\alpha$ consists of two parts, i. e. the first term representing the direct charge production of the constituent denoted by $\hat{z}^\alpha$ and the second term representing the charge production due to mass production.

Recalling that summing a balance relation over all constituents has to result in the balance relation of the overall medium, one obtains the following restrictions for the production terms:

$$\sum_\alpha \hat{\rho}_e^\alpha = 0 \,, \qquad \sum_\alpha \hat{\kappa}_e^\alpha = 0 \,, \qquad \hat{\omega}_e^\alpha = 0 \,, \qquad \sum_\alpha \hat{\mathbf{b}}_e^\alpha = \mathbf{0} \,, \qquad \sum_\alpha \hat{\mathbf{d}}_e^\alpha = \mathbf{0} \,. \tag{2.85}$$

Chapter 3:
Constitutive theory of finite swelling

The general framework of the TPM has been illustrated in the previous chapter. Based on these general statements concerning the concept of volume fractions, the kinematics of superimposed continua and the material independent balance relations, it is possible to model various kinds of different materials. This can include biphasic continua with an elastic (Eipper [68]), a viscoelastic (Markert [130]), a elastoplastic (Blome [17] and Mahnkopf [127]) solid matrix or biphasic continua with different temperatures and partially compressible constituents (Ghadiani [77]) and even multiphasic continua with different temperatures of the partially compressible constituents and phase exchanges (Graf [81] and Ricken & Ustohalova [145]). But before, one has to particularise the general equations so as to be able to describe the specific behaviour of the material under consideration.

As already mentioned in the introduction of Chapter 2, the materials discussed in this contribution belong to the group of charged hydrated porous media. The challenge is to derive an accurate continuum-mechanical model which considers all the different effects occurring in processes where such materials are involved. More precisely, the final model will incorporate mechanical, chemical as well as electric effects within the frame of finite elastic deformations. It is the aim of the constitutive theory to achieve all these demands on the model on the one hand and to ensure that the developed model is thermodynamically consistent and to reconcile the different topics with the TPM on the other.

In particular, in the following sections the balance relations and the entropy principle will be rearranged to suit the needs of the material under consideration. By evaluating the entropy inequality near the thermodynamical equilibrium, quantities such as the chemical potential and the osmotic pressure will be identified and restrictions for the *Helmholtz* free energies, for the stress tensors and, moreover, for the momentum productions of the constituents will be obtained. Putting all findings together, the relations specific for the constituents, i. e. the solid stress, the motion of the overall fluid and its components as well as the electric potential will be specified.

3.1 Adapting the balance relations

Before the actual evaluation of the entropy principle, the respective balances (2.73) and the entropy inequality (2.79) will be rearranged to reflect the given facts of the considered media. These are, for example, that the medium consists of both miscible and immiscible constituents. Moreover, restrictions which must be obeyed by the model, such as the saturation condition and the electroneutrality condition, will be incorporated into the entropy inequality. Note that the materials under consideration are non-polar ($\hat{\mathbf{m}}^{\alpha} \equiv 0$)

and that isothermal conditions are assumed ($\theta^\alpha \equiv \theta \equiv \text{const.}$). As a result, the balance of moment of momentum reduces to the statement that the stress tensors are symmetric and, since the temperature state of the overall domain is known, there is no need to consider the energy balances.

3.1.1 Volume and concentration balances

Within this thesis, mass exchanges like phase transitions and chemical reactions between the constituents are excluded ($\hat{\rho}^\alpha \equiv 0$) and all the constituents are assumed to be incompressible in the range of moderate pressures ($\rho^{\alpha R} \equiv \text{const.}$). But note that equation (2.15) shows that even though the overall fluid is incompressible, it changes its effective density due to changes in its composition, cf. (2.12). Starting with the mass balance of the solid constituent, the above assumptions yield to the volume balance

$$(n^S)'_S + n^S \operatorname{div} \mathbf{x}'_S = 0\,. \tag{3.1}$$

By an analytical time-integration of the above relation, one immediately finds a condition for the current solidity

$$\boxed{n^S = n^S_{0S} \left(\det \mathbf{F}_S\right)^{-1},} \tag{3.2}$$

cf. Appendix B.2. Therein, the value denoted by $(\,\cdot\,)_{0S}$ is the initial value corresponding to the variable $(\,\cdot\,)$, where the time-integration is performed with respect to φ^S [1].

The remaining mass balances of the fluid components need a transformation as well. In particular, the occurring time derivatives will be replaced by ones with respect to the moving solid. Therefore, by again excluding mass exchanges, the mass balance of φ^β is given by

$$(\rho^\beta)'_\beta + \rho^\beta \operatorname{div} \mathbf{x}'_\beta = 0\,. \tag{3.3}$$

Recalling that the fluid components represent the miscible constituents, the partial density ρ^β is expressed by use of (2.15) via the density with respect to the fluid volume ρ^β_F such that

$$n^F (\rho^\beta_F)'_\beta + (n^F)'_\beta \rho^\beta_F + \rho^\beta_F n^F \operatorname{div} \mathbf{x}'_\beta = 0\,. \tag{3.4}$$

In a first instance, the material time derivative of the second term is transformed to a time derivative with respect to the moving solid. For this, the general transformation

$$\boxed{(\,\cdot\,)'_\alpha = (\,\cdot\,)'_S + \operatorname{grad}(\,\cdot\,) \cdot \mathbf{w}_\alpha} \tag{3.5}$$

is of great benefit. By incorporating the saturation condition $n^F = 1 - n^S$ and the volume balance of the solid, one obtains

$$n^F (\rho^\beta_F)'_\beta + \rho^\beta_F \operatorname{div}(\mathbf{x}'_S + n^F \mathbf{w}_\beta) = 0\,. \tag{3.6}$$

[1] Following this argumentation, the initial value of the fluid volume fraction (porosity) is given by

$$n^F_{0S} = 1 - n^S_{0S}\,.$$

Herein, use was made of the divergence theorem [57]. The divergence term in the above relation can further be transformed to

$$\operatorname{div}(\overset{\prime}{\mathbf{x}}_S + n^F \mathbf{w}_\beta) = n^S \operatorname{div} \overset{\prime}{\mathbf{x}}_S + n^F \operatorname{div} \overset{\prime}{\mathbf{x}}_\beta + \operatorname{grad} n^F \cdot \mathbf{w}_\beta \,. \tag{3.7}$$

In a second step, the remaining time-derivative with respect to φ^β of the first term is also transformed to one with respect to the moving solid. Thus, by use of (3.5) and (2.34), the final representation of the mass balance of the fluid components can be extracted from above relation:

$$\boxed{n^F (\rho_F^\beta)'_S + \rho_F^\beta \operatorname{div}(\mathbf{u}_S)'_S + \operatorname{div}(n^F \rho_F^\beta \mathbf{w}_\beta) = 0 \,.} \tag{3.8}$$

The form of this relation equals to a mass balance belonging to a hybrid model, which is characterised by an incompressible solid matrix and compressible fluid constituents, cf. Diebels [44].

Following the considerations concerning the composition of the overall aggregate, i. e., the interstitial fluid is build by the liquid solvent and the mobile ions, the volume balance of the overall fluid is obtained by summing over the concentration balances of its components. More precisely, summing (3.3) over all φ^β yields

$$\sum_\beta \left[(\rho^\beta)'_\beta + \rho^\beta \operatorname{div} \overset{\prime}{\mathbf{x}}_\beta \right] = 0 \,. \tag{3.9}$$

Transforming the time derivatives with respect to the motion of φ^β to ones following the motion of the overall fluid φ^F by use of an equation analogous to (3.5) and by use of the diffusion velocities $(2.32)_2$ and the divergence theorem, one obtains finally

$$(\rho^F)'_F + \rho^F \operatorname{div} \overset{\prime}{\mathbf{x}}_F = 0 \tag{3.10}$$

as the volume balance of the overall fluid. For later use, material incompressibility is assumed, i. e. $(\rho^{FR})'_S \approx 0$, cf. also Chapter 3.6, and the time derivatives are again transformed to ones with respect to the moving solid φ^S. Moreover, with the aid of equations (3.1) and (3.5) the above relation can be transformed to

$$\boxed{\operatorname{div}\left[(\mathbf{u}_S)'_S + n^F \mathbf{w}_F \right] = 0 \,,} \tag{3.11}$$

which represents the final representation of the volume balance of the overall fluid. Note that to obtain above relation the the solid displacement (2.34) has been used.

3.1.2 Charge balances

The balance of charge used in electromagnetism is quite similar to the mass balance of continuum mechanics, cf. Bennethum & Cushman [12] and Eringen [71]. More precisely, it also balances the basic quantity and, therefore, it neither exists a corresponding influx

over the boundary nor a supply from a distance. Anyway, recalling that mass exchanges are excluded and, furthermore, also ruling out direct production of charges $\hat{z}^\gamma$, as they occur for example in plasma[2], the charge balances for all free charges φ^+, φ^- and φ^{fc},

$$(\rho_e^\gamma)'_\gamma + \rho_e^\gamma \operatorname{div} \overset{\prime}{\mathbf{x}}_\gamma = 0 \quad \text{and} \quad (\rho_e^{fc})'_S + \rho_e^{fc} \operatorname{div} \overset{\prime}{\mathbf{x}}_S = 0\,, \tag{3.12}$$

are obtained. Under these conditions, i. e. no mass and no charge productions, the charge balances are similar to the mass balances multiplied by the corresponding valence and the *Faraday* constant. Note that the mass- and volume-free fixed charges φ^{fc} are attached to the solid and, thus, both of them have the same motion function. Applying the same procedure to the charge balance of φ^{fc} as to the solid volume balance, i. e. analytical time-integration, leads to

$$\boxed{\rho_{eF}^{fc} = n_{0S}^F \, \rho_{eF0S}^{fc} \, (\det \mathbf{F}_S - n_{0S}^S)^{-1}\,,} \tag{3.13}$$

wherein equation $(2.19)_1$ has been used.

3.1.3 Momentum balances

Concerning the momentum balances, one again starts from its general representation $(2.73)_3$. Since in this contribution only quasi-static processes are examined, the acceleration terms are considered as negligible, i. e. $\rho^\alpha \overset{\prime\prime}{\mathbf{x}}_\alpha \approx 0$. Thus,

$$\mathbf{0} = \operatorname{div} \mathbf{T}^\alpha + \rho^\alpha \mathbf{g}^\alpha + \hat{\mathbf{p}}^\alpha \tag{3.14}$$

is the momentum balance of the constituent. Postulating that the acceleration $\mathbf{g}^\alpha$ is the same for all constituents ($\mathbf{g}^\alpha \equiv \mathbf{g}$), the summation over φ^α leads to the momentum balance of the overall aggregate

$$\boxed{\mathbf{0} = \operatorname{div} \mathbf{T} + \rho \, \mathbf{g}\,.} \tag{3.15}$$

Note that therein the restriction $(2.75)_3$, has been regarded.

3.1.4 Separation of the solid and fluid quantities

As was mentioned above, the general entropy inequality will be rearranged in this section to fit the needs of the material under consideration. At this stage, this is mainly that the overall aggregate is composed of miscible as well as immiscible constituents. To start with, the momentum production $(2.74)_2$ together with its corresponding restriction $(2.75)_3$ and

[2] Plasma is an ionised and, therefore, conducting gas. In particular, it consists of charged particles like ions or molecules and also of free electrons and protons. As long as energy is contributed to the plasma by, for example, electromagnetic fields, the electrons and the charged particles are separated from each other. Plasma is also referred to as the fourth state of matter.

the seepage velocity $(2.35)_2$ are inserted into the *Clausius-Planck* inequality (2.79) such that

$$\boxed{\mathbf{T}^S \cdot \mathbf{L}_S - \rho^S (\psi^S)'_S \,+\, \sum_\beta \left[\, \mathbf{T}^\beta \cdot \mathbf{L}_\beta - \rho^\beta (\psi^\beta)'_\beta - \hat{\mathbf{p}}^\beta \cdot \mathbf{w}_\beta \,\right] \,\geq\, 0\,.} \tag{3.16}$$

In the above relation, the contributions of both immiscible phases, i. e. the solid and the overall fluid, to the entropy production are separated from each other. Recalling that the pore-fluid is a chemical solution of miscible components and, thus, each fluid component always occupies the overall fluid volume element $\mathrm{d}v^F$, the mass specific *Helmholtz* free energy ψ^β of the fluid components is modified to reflect this situation:

$$\rho^\beta \psi^\beta \;=\; n^F (\,\rho^\beta_F \psi^\beta\,) \;=:\; n^F \Psi^\beta_F \qquad \longrightarrow \qquad \boxed{\Psi^\beta_F \;:=\; \rho^\beta_F \psi^\beta\,,} \tag{3.17}$$

Therein, as for the densities (2.15), the variables indicated by a subscript $(\,\cdot\,)_F$ denote quantities with respect to the overall fluid volume. Summing over the energies of all components leads to the *Helmholtz* free energy of the overall fluid:

$$\boxed{\Psi^F_F \;=\; \sum_\beta \Psi^\beta_F \;=\; \sum_\beta \rho^\beta_F \psi^\beta\,.} \tag{3.18}$$

With the aid of the partially transformed mass balance of the components (3.6) and (3.7), the material time derivatives of the *Helmholtz* free energies of the components in (3.16) are transformed with respect to the moving overall fluid:

$$\begin{aligned} \rho^\beta (\psi^\beta)'_\beta \;&=\; n^F (\Psi^\beta_F)'_\beta \;-\; n^F \psi^\beta (\rho^\beta_F)'_\beta \\ &=\; n^F\, (\Psi^\beta_F)'_\beta \;+\; n^S\, \Psi^\beta_F \operatorname{div} \mathbf{x}'_S \;+\; n^F\, \Psi^\beta_F \operatorname{div} \mathbf{x}'_\beta \;+\; \Psi^\beta_F \operatorname{grad} n^F \cdot \mathbf{w}_\beta\,, \end{aligned} \tag{3.19}$$

where

$$(\Psi^\beta_F)'_\beta \;=\; (\Psi^\beta_F)'_F + \operatorname{grad} \Psi^\beta_F \cdot \mathbf{d}_{\beta F}\,. \tag{3.20}$$

Putting this together, one comes along with the entropy inequality of a biphasic material saturated with a solution φ^F made up of several components φ^β:

$$\begin{aligned} &(\,\mathbf{T}^S - n^S\, \Psi^F_F \mathbf{I}\,) \cdot \mathbf{L}_S \;-\; \rho^S (\psi^S)'_S \;+\; \sum_\beta (\,\mathbf{T}^\beta - n^F \Psi^\beta_F \mathbf{I}\,) \cdot \mathbf{L}_\beta \;-\; n^F (\Psi^F_F)'_F \;- \\ &\quad - n^F \sum_\beta \operatorname{grad} \Psi^\beta_F \cdot \mathbf{d}_{\beta F} \;-\; \sum_\beta (\,\hat{\mathbf{p}}^\beta \;+\; \Psi^\beta_F \operatorname{grad} n^F\,) \cdot \mathbf{w}_\beta \;\geq\; 0\,. \end{aligned} \tag{3.21}$$

3.1.5 Constraining saturation and electroneutrality conditions

According to Liu [121], any linear combination of field equations yielding zero and acting as a restriction on the thermodynamic process can be incorporated into the entropy in-

equality by means of a *Lagrange*an multiplier. In the case considered in this contribution, two distinct restrictions have to be considered. First, a purely mechanical constraint on the mixture, i. e. the saturation condition (2.8), cf. Bowen [28], Lai *et al.* [116] and Mow *et al.* [136], and, second, an electrostatic constraint, i. e. the electroneutrality condition (2.20), cf. Bennethum & Cushman [13], Gu *et al.* [85] and Huyghe & Janssen [108]. The material time derivative with respect to the moving solid of both conditions will be incorporated into the entropy inequality (3.21).

First, the corresponding relation to the material time derivative $(\,\cdot\,)'_S$ of the saturation condition is obtained by transforming the time derivatives of the volume fractions of φ^β by use of relation (3.5). Next, the volume balances of the materially incompressible constituents given in analogy to (3.1) are inserted. Following this, the saturation constraint leads to:

$$\boxed{-\,(\,n^S + \sum_\beta n^\beta\,)'_S \;=\; n^S \operatorname{div} \mathbf{x}'_S \;+\; \sum_\beta (n^\beta \operatorname{div} \mathbf{x}'_\beta + \operatorname{grad} n^\beta \cdot \mathbf{w}_\beta) \;=\; 0\,.} \tag{3.22}$$

In the literature, this relation is also referred to as the incompressibility constraint. The same procedure is applied to the overall charge density in the medium to obtain the material time derivative of the electroneutrality condition with respect to the solid:

$$\boxed{-\,(\,\rho_e^{fc} + \sum_\gamma \rho_e^\gamma\,)'_S \;=\; \rho_e^{fc} \operatorname{div} \mathbf{x}'_S \;+\; \sum_\gamma (\,\rho_e^\gamma \operatorname{div} \mathbf{x}'_\gamma + \operatorname{grad} \rho_e^\gamma \cdot \mathbf{w}_\gamma\,) \;=\; 0\,.} \tag{3.23}$$

Moreover, replacing ρ_e^{fc} by the sum of the charge densities of the mobile ions, in other words, using the electroneutrality condition, the above relation can further be reduced to yield

$$\operatorname{div}(\sum_\gamma \rho_e^\gamma \mathbf{w}_\gamma) \;=\; 0\,. \tag{3.24}$$

The obtained expression is the continuity equation of electrostatics.

Finally, both of the equations, (3.22) and (3.23), are multiplied by their corresponding *Lagrange*an multipliers $\mathcal{P}$ and $\mathcal{E}$, respectively, and incorporated into the entropy inequality:

$$\begin{aligned}
&(\,\mathbf{T}^S \;+\; n^S \mathcal{P}\,\mathbf{I} \;+\; \rho_e^{fc}\,\mathcal{E}\,\mathbf{I} \;-\; n^S\,\Psi_F^F\,\mathbf{I}\,)\cdot\mathbf{L}_S \;-\; \rho^S(\psi^S)'_S \;+\\
&\quad +\,(\,\mathbf{T}^L \;+\; n^L \mathcal{P}\,\mathbf{I} \;-\; n^F\,\Psi_F^L\,\mathbf{I}\,)\cdot\mathbf{L}_L \;-\; n^F(\Psi_F^F)'_F \;+\\
&\quad +\sum_\gamma (\,\mathbf{T}^\gamma \;+\; n^\gamma \mathcal{P}\,\mathbf{I} \;+\; \rho_e^\gamma\,\mathcal{E}\,\mathbf{I} \;-\; n^F\,\Psi_F^\gamma\,\mathbf{I}\,)\cdot\mathbf{L}_\gamma \;-\\
&-\; n^F \sum_\beta \operatorname{grad}\Psi_F^\beta \cdot \mathbf{d}_{\beta F} \;-\; (\,\hat{\mathbf{p}}^L \;-\; \mathcal{P}\operatorname{grad} n^L \;+\; \Psi_F^L \operatorname{grad} n^F\,)\cdot\mathbf{w}_L \;-\\
&-\sum_\gamma (\,\hat{\mathbf{p}}^\gamma \;-\; \mathcal{P}\operatorname{grad} n^\gamma \;-\; \mathcal{E}\operatorname{grad}\rho_e^\gamma \;+\; \Psi_F^\gamma \operatorname{grad} n^F\,)\cdot\mathbf{w}_\gamma \;\geq\; 0\,.
\end{aligned} \tag{3.25}$$

3.1.6 Effective quantities

The effective stress principle, cf. Bishop [15], Skempton [154] and de Boer & Ehlers [25], is extended in such a way that the contribution of the multiple *Lagrange*an multipliers to the stress tensors and the momentum productions of the constituents are gathered in the effective quantities denoted by $(\,\cdot\,)_E$. In particular,

$$\boxed{\begin{aligned} &\mathbf{T}^S_E := n^S \mathcal{P}\,\mathbf{I} + \rho^{fc}_e\,\mathcal{E}\,\mathbf{I} + \mathbf{T}^S\,, \\ &\mathbf{T}^L_E := n^L \mathcal{P}\,\mathbf{I} + \mathbf{T}^L\,, \qquad\qquad \mathbf{T}^\gamma_E := n^\gamma \mathcal{P}\,\mathbf{I} + \rho^\gamma_e\,\mathcal{E}\,\mathbf{I} + \mathbf{T}^\gamma\,, \\ &\hat{\mathbf{p}}^L_E := -\mathcal{P}\,\mathrm{grad}\,n^L + \hat{\mathbf{p}}^L \quad \text{and} \quad \hat{\mathbf{p}}^\gamma_E := -\mathcal{P}\,\mathrm{grad}\,n^\gamma - \mathcal{E}\,\mathrm{grad}\,\rho^\gamma_e + \hat{\mathbf{p}}^\gamma \end{aligned}} \tag{3.26}$$

are replaced in (3.25) such that

$$\begin{aligned} &(\,\mathbf{T}^S_E - n^S\,\Psi^F_F\,\mathbf{I}\,)\cdot\mathbf{L}_S \;-\; \rho^S(\psi^S)'_S \;+\; \sum_\beta (\,\mathbf{T}^\beta_E - n^F\Psi^\beta_F\,\mathbf{I}\,)\cdot\mathbf{L}_\beta \;-\; n^F(\Psi^F_F)'_F \;- \\ &\quad - \sum_\beta (\,\hat{\mathbf{p}}^\beta_E \;+\; \Psi^\beta_F\,\mathrm{grad}\,n^F\,)\cdot\mathbf{w}_\beta \;-\; n^F \sum_\beta \mathrm{grad}\,\Psi^\beta_F\cdot\mathbf{d}_{\beta F} \;\geq\; 0\,. \end{aligned} \tag{3.27}$$

Moreover, the above relation is the final form of the entropy inequality for a biphasic medium consisting of a charged solid matrix saturated and neutralised by a charged fluid mixture, whereas the pore-fluid is composed of miscible and incompressible constituents. In the following sections, this inequality will be evaluated by the *Coleman-Noll* procedure.

3.2 Evaluation of the entropy principle

Aiming at an accurate model covering all the mentioned effects, it is essential to utilise the entropy principle. By use of this principle, the otherwise arbitrary choice of constitutive equations will be restricted so that they fulfil the entropy inequality and the restrictions incorporated therein. This procedure, evaluating the entropy principle to obtain more information for the constitutive equations, was first applied by Coleman & Noll [38] in 1963 to single-phasic materials.

In the following sections, the process variables on which the response functions depend will be specified, such that a calculation of the material time derivatives of the *Helmholtz* free energies is possible. Subsequently, the corresponding derivatives in (3.27) will be replaced so as to enable the evaluation of the entropy inequality. Moreover, definitions for the chemical potentials as well as for the osmotic pressures of the fluid components, which are consistent with both the classical thermodynamics in chemistry and the continuum mechanics, will be established.

3.2.1 Process variables

In order to close the model for the material under consideration, constitutive equations have to be found for the members of the set of undetermined response functions $\mathcal{R}$, such

that they satisfy the entropy principle (3.27). In this regard, an arbitrary introduction of constitutive equations is avoided by the determination of the response functions and the process variables based on well-known thermodynamical principles, namely, the *principle of determinism*, *equipresence*, *local actions*, *material frame indifference* and *dissipation*, cf. Coleman & Noll [38], Ehlers [51]. Following Ehlers [56], the set of response functions fulfilling the *principle of determinism* for isothermal conditions of non-polar materials is given by

$$\mathcal{R} = \{ \psi^S,\, \Psi_F^\beta,\, \mathbf{T}_E^S,\, \mathbf{T}_E^\beta,\, \hat{\mathbf{p}}_E^\beta \}\,. \tag{3.28}$$

Note that all the above mentioned, up to now undetermined quantities show up in the entropy inequality except for the energy potential Ψ_F^F of the overall fluid. Recall that Ψ_F^F is the sum of Ψ_F^β, cf. equation (3.18). The *principle of equipresence* states that each element of $\mathcal{R}$ can be a function of the whole set of constitutive or process variables,

$$\mathcal{R} := \mathcal{R}(\mathcal{S})\,, \tag{3.29}$$

unless the second law of thermodynamics requires otherwise. Here, the set $\mathcal{S}$ of process variables is a subset of the fundamental process variables $\mathcal{V}$ derived by gradually decreasing the amount of independent process variables via *a priori* assumptions specifying the process under consideration. Note that these assumptions achieve a restriction of the considered thermodynamical process. The set $\mathcal{V}$ for a general porous medium is given by, cf. Ehlers [51]:

$$\begin{aligned} \mathcal{V} = \{ &\theta^\alpha\,,\, \operatorname{grad}\theta^\alpha\,,\, n^\beta\,,\, \operatorname{grad} n^\beta\,,\, \rho^{\alpha R}\,,\, \operatorname{grad}\rho^{\alpha R}\,,\\ &\mathbf{F}_\alpha\,,\, \operatorname{Grad}_\alpha \mathbf{F}_\alpha\,,\, \overset{\prime}{\mathbf{x}}_\alpha\,,\, \operatorname{Grad}_\alpha \overset{\prime}{\mathbf{x}}_\alpha\,,\, \mathbf{X}_\alpha \}\,. \end{aligned} \tag{3.30}$$

On the basis of this set, a saturated porous medium with multiple constituents is fully described, where non-isothermal processes are considered as well as inhomogeneities. Following this, the temperature field θ^α of the constituents is included as well as the referential position vector $\mathbf{X}_\alpha$. Note that in the above set, the gradients of all variables are considered to be able to model materials of second grade. In such materials, the state of a constituent may depend on the state of the others and it is also possible to capture non-local effects. Note as well that one of the volume fractions, i. e. the one of the solid, has not been taken into consideration in the above list, because it is uniquely determined by the saturation condition (2.8). Moreover, in contrast to single-phasic materials, where the complete motion is given by the deformation gradient alone, the variables n^α and $\rho^{\alpha R}$ have to be taken into account for a general porous medium besides the deformation gradients $\mathbf{F}_\alpha$. This follows from the fact that there is no mass production in case of a single-phasic material and, therefore, the mass balance can be integrated to calculate the current density $\rho^{\alpha R}$. Needless to say that the volume fraction of a single-phasic material equals to unity. Note that, in contrast, it is not possible to integrate the mass balance $(2.73)_1$ of a porous material with existing mass productions. Apart from the deformation variables, the velocities $\overset{\prime}{\mathbf{x}}_\alpha$ and their gradients $\operatorname{Grad}_\alpha \overset{\prime}{\mathbf{x}}_\alpha$ are considered in (3.30) to capture viscous effects of the constituents.

Starting with the reduction of the above set $\mathcal{V}$ of process variables, only isothermal conditions are taken into consideration, i. e. the temperature θ^α and its gradient $\operatorname{grad}\theta^\alpha$ may

be abandoned from the above list. Concerning the fluid components, and to satisfy the *principle of material frame indifference*, the seepage velocities $\mathbf{w}_\beta$ and the symmetric part of the velocity gradient $\mathbf{D}_\beta$ will be used instead of the velocities $\overset{\prime}{\mathbf{x}}_\beta$ and the gradients of the velocities of the fluid components $\operatorname{Grad}_\beta \overset{\prime}{\mathbf{x}}_\beta$. Moreover, the description of the deformation of a fluid by its deformation gradient can be replaced by the determinant of $\mathbf{F}_\beta$. This can be shown by a multiplicative split of the deformation gradient into a purely volumetric part $\det \mathbf{F}_\beta$ and an isochoric part $\tilde{\mathbf{F}}_\beta$,

$$\mathbf{F}_\beta \;=\; (\det \mathbf{F}_\beta)^{1/3}\, \tilde{\mathbf{F}}_\beta \,. \tag{3.31}$$

Regarding that fluids at rest sense only volumetric changes, the multiplicative split of a fluid deformation gradient can be expressed via

$$\mathbf{F}_\beta \;=\; (\det \mathbf{F}_\beta)^{1/3}\, \mathbf{I} \,. \tag{3.32}$$

Therefore, $\mathbf{F}_\beta$ may be replaced by $\det \mathbf{F}_\beta$. However, following Cross [39], the deformation variables of a fluid are not influenced by a possible mass production. On this basis, $\det \mathbf{F}_\beta$ can further be replaced by $\rho^{\beta R}$ using the mass balance. Summing up the discussed considerations results in the following intermediate subset of process variables:

$$\tilde{\mathcal{V}} \;=\; \{\, n^\beta \,,\, \operatorname{grad} n^\beta \,,\, \rho^{\alpha R} \,,\, \operatorname{grad} \rho^{\alpha R} \,,\, \mathbf{F}_S \,,\, \operatorname{Grad}_S \mathbf{F}_S \,,\, \overset{\prime}{\mathbf{x}}_S \,,\, \operatorname{Grad}_S \overset{\prime}{\mathbf{x}}_S \,,\, \mathbf{w}_\beta \,,\, \mathbf{D}_\beta \} \,. \tag{3.33}$$

Generally, in case of compressible constituents, the densities ρ^α are computed from two variables, the volume fractions n^α and the effective densities $\rho^{\alpha R}$. By assuming materially incompressible solid and fluid components, the effective densities $\rho^{\alpha R}$ degenerate to constants and, in case of a homogeneous reference configuration, also the gradients $\operatorname{grad} \rho^{\alpha R}$ vanish. Hence, they can be discarded from the set above. In case of a biphasic material incorporating a compressible fluid, n^F represents the part depending on the solid deformation and ρ^{FR} stands for the part depending on the volumetric compression of the fluid, cf. (2.10). Recalling that this contribution deals with a fluid being a mixture of miscible but individually incompressible components, their densities are computed by

$$\rho^\beta \;=\; n^\beta\, \rho^{\beta R} \;=\; n^F\, \rho_F^\beta \,, \tag{3.34}$$

wherein n^F is still the part depending on the solid deformation and ρ_F^β is the new variable describing the state of the fluid component replacing its volume fraction n^β. Concerning the solid matrix, it is assumed that it behaves purely elastic. Thus, the solid velocity and its gradient can be cancelled from the set of independent variables as well. Moreover, following Bowen [28], the gradients of the process variables ρ_F^β and $\mathbf{F}_S$ only influence the production terms. Following the considerations made up to now,

$$\mathcal{S} \;=\; \{\, \rho_F^\beta \,,\, \mathbf{F}_S \,,\, \mathbf{w}_\beta \,,\, \mathbf{D}_\beta \} \tag{3.35}$$

represents the final set of process variables. Now, given the relevant subset $\mathcal{S}$ of constitutive variables describing the thermodynamical process under consideration, the dependencies of the response functions are known. Following the *principle of equipresence*,

each member of the set of response functions $\mathcal{R}$ depends on the whole set of constitutive variables, cf. (3.29),

$$\boxed{\{\,\psi^S,\ \Psi_F^\beta,\ \mathbf{T}_E^S,\ \mathbf{T}_E^\beta,\ \hat{\mathbf{p}}_E^\beta\} \;=\; \mathcal{R}\,\{\,\rho_F^\beta\,,\,\mathbf{F}_S\,,\,\mathbf{w}_\beta\,,\,\mathbf{D}_\beta\}\,.} \tag{3.36}$$

3.2.2 *Helmholtz* free energies of the constituents

If the above subset (3.35) would be used as process variables for the *Helmholtz* free energies, one would assert that ψ^S and Ψ_F^β must be independent from the variables $\mathbf{w}_\beta$ and $\mathbf{D}_\beta$ to satisfy the entropy inequality, cf. Ehlers [51]. Therefore, for the sake of convenience, the *a priori* assumption is made that the *Helmholtz* free energies do not depend upon these variables. Moreover, the demand for the above mentioned *principle of material frame indifference* requires that $\psi^S(\mathbf{F}_S)$ is expressed in such a way that $\mathbf{F}_S$ can be replaced by the right *Cauchy-Green* deformation tensor $\mathbf{C}_S$ ($\psi^S(\mathbf{F}_S) \;=\; \psi^S(\mathbf{C}_S)$). In contrast, the the assumption of an isotropic response of the solid requires that the free energy of the solid can equally be described by the left *Cauchy-Green* deformation tensor $\mathbf{B}_S$ ($\psi^S(\mathbf{F}_S) \;=\; \psi^S(\mathbf{B}_S)$). In order to fulfil both requirements simultaneously, the solid deformation should be formulated in the invariants of the deformation tensors, since the invariants of both deformation tensors are equal. For more details, cf. Section 3.3.

Nevertheless, one further *a priori* assumption can be made on the basis of the idea of the *principle of constituent separation* without circumventing the *principle of equipresence*, cf. Ehlers [50] and Ehlers [53]. This principle predicates that the *Helmholtz* free energy of the constituent φ^α only depends on the variables brought into the process by the constituent itself. Consequently, it is assumed that

$$\psi^S = \psi^S(\mathbf{F}_S)\,, \qquad \Psi_F^F = \Psi_F^F\big(\,\rho_F^L\,,\rho_F^-\,,\rho_F^-\,\big) \;=\; \textstyle\sum_\beta \Psi_F^\beta\big(\,\rho_F^\beta\,\big)\,. \tag{3.37}$$

Thus, ψ^S depends only on its deformation gradient[3] and the *Helmholtz* free energy of the fluid component only on its density via ρ_F^β, i. e. its concentration in the fluid. Following Bowen [26], weighing a model that way implies that it can only represent ideal solutions. Therefore, he suggests that the most general form to specify the state of a fluid mixture is when the thermodynamical potentials of the fluid components may also depend on the state of the other components, i. e. $\Psi_F^F = \sum_\beta \Psi_F^\beta(\rho_F^L\,,\,\rho_F^+\,,\,\rho_F^-)$. However, considering such a model would lead to a quite complex evaluation of the entropy principle. In contrast, Green & Naghdi [83] criticise Bowen's contribution for making statements without any mathematical evidence and showed how to derive a general model of a binary fluid mixture that is not restricted to simple cases. In their model, as in the one suggested here, the potential of the fluid component only depends on its own amount in the overall fluid, i. e. $\Psi_F^\beta = \Psi_F^\beta(\rho_F^\beta)$, cf. also Atkin & Craine [6]. Anyway, note that the density ρ_F^β of the one component is coupled with the density of the other components via the overall fluid volume $\mathrm{d}v^F$.

Taking above considerations into account, the material time derivatives of the *Helmholtz*

[3] Note that ψ^S depends on the fixed charge density ρ_F^{fc} via (3.13).

free energies, which are actually needed in the entropy inequality, can be computed. Hence, one obtains for the solid constituent

$$\rho^S(\psi^S)'_S = \rho^S \frac{\partial \psi^S}{\partial \mathbf{F}_S} (\,\mathbf{F}_S\,)'_S \;=\; \rho^S \frac{\partial \psi^S}{\partial \mathbf{F}_S}\, \mathbf{F}_S^T \cdot \mathbf{L}_S \tag{3.38}$$

and for the overall fluid

$$\begin{aligned} n^F(\Psi_F^F)'_F \;&=\; n^F \sum_\beta \frac{\partial \Psi_F^F}{\partial \rho_F^\beta} \left[\, (\,\rho_F^\beta\,)'_\beta \;-\; \operatorname{grad} \rho_F^\beta \cdot \mathbf{d}_{\beta F} \,\right] \\ &= -\sum_\beta \rho_F^\beta \frac{\partial \Psi_F^F}{\partial \rho_F^\beta} (\, n^S \operatorname{div} \overset{\prime}{\mathbf{x}}_S + n^F \operatorname{div} \overset{\prime}{\mathbf{x}}_\beta + \operatorname{grad} n^F \cdot \mathbf{w}_\beta \,) - \\ &\quad - n^F \sum_\beta \frac{\partial \Psi_F^F}{\partial \rho_F^\beta} \operatorname{grad} \rho_F^\beta \cdot \mathbf{d}_{\beta F}\,. \end{aligned} \tag{3.39}$$

In order to derive the above relations, (2.47), (3.6) and (3.7) were used. Now, the time derivatives in (3.27) can be replaced to result in

$$\boxed{\begin{aligned} &\left[\, \mathbf{T}_E^S \;-\; n^S\, \Psi_F^F\, \mathbf{I} \;+\; n^S \sum_\beta \rho_F^\beta \frac{\partial \Psi_F^F}{\partial \rho_F^\beta}\, \mathbf{I} \;-\; \rho^S \frac{\partial \psi^S}{\partial \mathbf{F}_S}\, \mathbf{F}_S^T \,\right] \cdot \mathbf{D}_S \;+ \\ &\qquad + \sum_\beta \left[\, \mathbf{T}_E^\beta \;-\; n^F\, \Psi_F^\beta\, \mathbf{I} \;+\; n^F \rho_F^\beta \frac{\partial \Psi_F^F}{\partial \rho_F^\beta}\, \mathbf{I} \,\right] \cdot \mathbf{D}_\beta \;- \\ &\quad - \sum_\beta \left[\, \hat{\mathbf{p}}_E^\beta \;+\; \Psi_F^\beta \operatorname{grad} n^F \;-\; \rho_F^\beta \frac{\partial \Psi_F^F}{\partial \rho_F^\beta} \operatorname{grad} n^F \,\right] \cdot \mathbf{w}_\beta \;- \\ &\qquad - n^F \sum_\beta \left[\, \operatorname{grad} \Psi_F^\beta \;-\; \frac{\partial \Psi_F^F}{\partial \rho_F^\beta} \operatorname{grad} \rho_F^\beta \,\right] \cdot \mathbf{d}_{\beta F} \;\geq\; 0\,. \end{aligned}} \tag{3.40}$$

Therein, since only non-polar constituents are considered in this contribution, i. e. $\mathbf{T}^\alpha = (\,\mathbf{T}^\alpha\,)^T$, the velocity gradient is replaced by its symmetric part $\mathbf{D}_\alpha$, cf. (2.50).

Equation (3.40) is the inequality, which must be satisfied by any admissible thermodynamical process. This inequality will now be evaluated near the thermodynamical equilibrium[4] by the standard arguments given, for example, in Coleman & Noll [38], Diebels [44] and Ehlers [56]. The inequality does not need to be satisfied by the process as a whole. It is a sufficient (not a necessary) condition for each single term to fulfil the inequality, i. e. being either equal to or greater than zero. A thermodynamical process at a specific spatial position is given by the values of the variables in $\mathcal{S}$. But note that their derivatives, which come into play via the derivative of the response functions, i. e. the *Helmholtz* free energies, can have arbitrary values at this position. The reason is that the derivatives depend on the guidance of the process under consideration. Thus, the terms in front of the derivatives of the process variables, i. e. the velocity gradient $\mathbf{D}_\alpha$, must vanish. Otherwise, the results obtained by evaluation of the above inequality would depend on the

[4] The thermodynamical potentials are only valid near the equilibrium, cf., for example, Hille [96]

guidance of the process.

Moreover, the entropy inequality generally consists of two parts. The first two expressions connected to the velocity gradients are referred to as the equilibrium (reversible) part. On the basis of these two expressions, the restrictions for the stress tensors are found. Note that generally the second term, i. e. the stress contribution of the fluid components, is classified as dissipative. But in the case given above, it is not a mechanical friction part. As it will be discussed in detail later, this term consists only of reversible chemical contributions and, therefore, it is counted to the equilibrium portion. The second two expressions connected to the velocities $\mathbf{w}_\beta$ and $\mathbf{d}_{\beta F}$ are referred to as the dissipative (irreversible) part. These two terms are the expressions which always provide positive values during the process. Therefore, this portion of the entropy inequality is also referred to as the dissipation inequality. In case of equilibrium, the seepage and diffusion velocities vanish and, therefore, this part is zero as well. By evaluation of the dissipation inequality further restrictions for the remaining response functions are obtained, particularly, the momentum productions of the fluid and its components.

3.2.3 Tensor of chemical potential

First of all, a closer look is taken at the second term in (3.40) corresponding to the fluid components φ^β. Following the above mentioned argument according to which this term has to vanish, a rearrangement yields

$$\mathbf{T}_E^\beta \,-\, n^F\,\Psi_F^\beta\,\mathbf{I} \;=\; -n^F\,\rho_F^\beta\,\frac{\partial \Psi_F^F}{\partial \rho_F^\beta}\,\mathbf{I}\,. \tag{3.41}$$

Moreover, recalling the definition of the tensor of chemical potential $\mathbf{K}^\beta$ by Bowen [26] in 1967, i. e.

$$\boxed{\rho^\beta\,\mathbf{K}^\beta \;:=\; \rho^\beta\,\psi^\beta\,\mathbf{I} \,-\, (\mathbf{T}_E^\beta)^T\,,} \tag{3.42}$$

However, following (3.41), the fluid component is fully described by a scalar valued chemical potential μ^β. Thus,

$$\mathbf{K}^\beta = \mu^\beta\,\mathbf{I}\,. \tag{3.43}$$

Following this, one finds from the definition of $\mathbf{K}^\beta$ with the aid of (2.15):

$$n^F(\rho_F^\beta\,\mu^\beta) \;=\; n^F\,\rho_F^\beta\,\frac{\partial \Psi_F^F}{\partial \rho_F^\beta}\,. \tag{3.44}$$

Consequently, the derivative of the entire *Helmholtz* free energy of the overall fluid Ψ_F^F with respect to the component density in the fluid ρ_F^β is the chemical potential. Moreover,

$$\boxed{\mu^\beta \;:=\; \frac{\partial \Psi_F^\beta}{\partial \rho_F^\beta} \;=\; \frac{\partial \Psi_F^F}{\partial \rho_F^\beta}\,,} \tag{3.45}$$

since Ψ_F^F is just the sum of Ψ_F^β.

3.2.4 *Helmholtz* free energy of the fluid and its components

To continue with the evaluation of the entropy principle, a *Helmholtz* free energy for the overall fluid will be postulated within this section, i. e.

$$\boxed{\Psi_F^F := \sum_\beta \left[\mu_0^\beta \, \rho_F^\beta + \bar{R}^\beta \theta \, \rho_F^\beta \, (\ln \rho_F^\beta - 1) \right].} \tag{3.46}$$

Moreover, in (3.46), μ_0^β denotes the reference potential (standard state potential), $\bar{R}^\beta$ denotes specific gas constant, which is related to the universal gas constant R via the molar mass of the component φ^β ($\bar{R}^\beta = R/M_m^\beta$) and ln represents the natural logarithm to the basis $e \approx 2.71828$. This potential function is the *Helmholtz* free energy of the overall fluid from which the chemical potentials are obtained by derivation.

Given the *Helmholtz* free energy of the overall fluid mixture (3.46), it is also possible to particularise the contributions of the components of the overall fluid. Thus, the potential function corresponding to the individual fluid component is

$$\boxed{\Psi_F^\beta = \mu_0^\beta \, \rho_F^\beta + \bar{R}^\beta \theta \, \rho_F^\beta \, (\ln \rho_F^\beta - 1).} \tag{3.47}$$

3.2.5 Chemical potentials of the components

The mass specific chemical potentials μ^β of the fluid components can be calculated by taking the derivative of either (3.46) or of the component contribution (3.47) with respect to the component density ρ_F^β:

$$\boxed{\mu^\beta = \frac{\partial \Psi_F^F}{\partial \rho_F^\beta} = \frac{\partial \Psi_F^\beta}{\partial \rho_F^\beta} = \mu_0^\beta + \bar{R}^\beta \theta \ln \rho_F^\beta .} \tag{3.48}$$

The chemical potentials given above are formulated in the densities ρ_F^β. This expressions are related to the molar chemical potential μ_m^β generally used in chemistry via (2.15):

$$\mu^\beta = \frac{\partial \Psi_F^F}{\partial \rho_F^\beta} = \frac{1}{M_m^\beta} \frac{\partial \Psi_F^F}{\partial c_m^\beta} = \frac{1}{M_m^\beta} \mu_m^\beta := \frac{1}{M_m^\beta} (\mu_{m0}^\beta + R\theta \, \ln c_m^\beta). \tag{3.49}$$

3.2.6 Osmotic pressures of the components

Taking again a closer look at the term concerning the fluid components in the equilibrium part of the entropy inequality, i. e. the second term in (3.40), one finds:

$$\mathbf{T}_E^\beta = n^F (\Psi_F^\beta - \rho_F^\beta \, \mu^\beta) \, \mathbf{I} = -n^F \, \pi^\beta \, \mathbf{I} . \tag{3.50}$$

This relation is based on the assumption of isotropic and, therefore, scalar valued chemical potentials, which in turn result in a scalar valued partial stress. Thus, the partial osmotic pressure π^β of the fluid component φ^β can be identified as

$$\boxed{\pi^\beta := \rho_F^\beta \, \mu^\beta - \Psi_F^\beta \, .} \tag{3.51}$$

The extra stress of the overall fluid is given by the sum of the extra stresses of its components:

$$\mathbf{T}_E^F := \sum_\beta \mathbf{T}_E^\beta = -n^F \sum_\beta \pi^\beta \, \mathbf{I} \, . \tag{3.52}$$

Taking into account the equilibrium part related to the solid matrix in (3.40), one finds with the definition of the chemical potential (3.45)

$$\mathbf{T}_E^S = n^S \sum_\beta \left(\Psi_F^\beta - \rho_F^\beta \, \mu^\beta \right) \mathbf{I} + \rho^S \frac{\partial \psi^S}{\partial \mathbf{F}_S} \, \mathbf{F}_S^T \tag{3.53}$$

or simply

$$\mathbf{T}_E^S = -n^S \, \pi \, \mathbf{I} + \rho^S \, \frac{\partial \psi^S}{\partial \mathbf{F}_S} \, \mathbf{F}_S^T \, , \tag{3.54}$$

wherein the sum of the partial osmotic pressures,

$$\boxed{\pi := \sum_\beta \pi^\beta = \sum_\beta \left(\rho_F^\beta \, \mu^\beta - \Psi_F^\beta \right) ,} \tag{3.55}$$

is the overall osmotic pressure. Given the partial osmotic pressure (3.51), the chemical potential of the fluid component (3.48) and its *Helmholtz* free energy (3.47), the partial osmotic pressure of the φ^β yields

$$\pi^\beta = \bar{R}^\beta \theta \rho_F^\beta \, . \tag{3.56}$$

Note in passing that the osmotic pressures introduced above are derived from the thermodynamical considerations made before. In Chapter 3.2.12, the different osmotic pressures and their practical relevance will be discussed in detail.

3.2.7 *Lagrange*an multipliers

Recall that in Section 3.1.5 certain restrictions on the overall medium, namely the saturation and the electroneutrality condition, have been incorporated into the entropy principle by means of *Lagrange*an multipliers. In particular, the saturation condition has been multiplied by $\mathcal{P}$ and the electroneutrality condition by $\mathcal{E}$. Both of the multipliers still have to be identified.

For simplification, starting from a binary model including a compressible constituent, the *Lagrange*an multiplier $\mathcal{P}$ can be specified. In such a case, one obtains additional terms

in the entropy inequality, where $\mathcal{P}$ appears together with the derivative of the *Helmholtz* free energy of the fluid constituent with respect to its density. This term is known as the thermodynamical pressure, cf. Drumheller & Bedford [49], Green & Naghdi [83], see the remark below. In contrast, in case of incompressible constituents, as regarded within this thesis, the multiplier $\mathcal{P}$ has no such counterpart and degenerates to an additional unknown to be calculated from the boundary conditions. Nevertheless, on the basis of this knowledge, $\mathcal{P}$ is identified as the effective hydraulic pressure acting on the overall mixture:

$$\boxed{\mathcal{P} \;:\; \text{effective hydraulic pressure}\,.} \tag{3.57}$$

Cf. also Chapter 3.2.12 for a detailed discussion of the different pressures introduced up to now and their correlation.

The second *Lagrange*an multiplier $\mathcal{E}$ is interpreted as the electrostatic force acting on a electric charge, i. e.

$$\boxed{\mathcal{E} \;:\; \text{electric potential}\,.} \tag{3.58}$$

Note that in Gu *et al.* [85], Huyghe & Janssen [107, 108] and Bennethum & Cushman [13], the *Lagrange*an multiplier is identified as the electrostatic force acting on one mole of ions, which therefore is the combination of $\mathcal{E}$ with the *Faraday* constant F. F in turn denotes the electric charge (*Coulomb*, C) per mole of protons. This is because they used the concentration balances of the free charges to calculate the electroneutrality, while in this contribution, the charge balances have been used. Note furthermore that Bennethum [11] claims that $\mathcal{E}$ does not correspond to the electrostatic force since it seemingly has no counterpart in case of constituents with changing valences, as is the case in plasma. But in her contribution, she combines the chemical potential with the *Lagrange*an multiplier to the electrochemical potential. In contrast, in my opinion, the electrochemical potential is an artificial construct, which combines two distinct quantities.

Remark: In the case of compressible constituents, cf., for example, Ghadiani [77], Graf [81], Markert [130], the mass balances of the constituents have to be inserted into the material time derivative of the saturation condition. Based on the example of a binary model consisting of a solid phase φ^S and a fluid phase φ^F, one obtains after some rearrangements for the mass balance, cf. (3.8):

$$n^F (\rho^{FR})'_S + \rho^{FR} \operatorname{div} \overset{\prime}{\mathbf{x}}_S + \operatorname{div} (n^F \rho^{FR} \mathbf{w}_F) = 0\,.$$

By use of this equation in the material time derivative of the saturation condition, one arrives (in contrast to (3.22)) at

$$-\,(\,n^S + n^F\,)'_S \;=\; n^S \operatorname{div} \overset{\prime}{\mathbf{x}}_S \;+\; n^F \operatorname{div} \overset{\prime}{\mathbf{x}}_F \;+\; \operatorname{grad} n^F \cdot \mathbf{w}_F \;+\; n^F \,\frac{(\rho^{FR})'_F}{\rho^{FR}} \;=\; 0\,.$$

Note the rightmost additional term with $(\rho^{FR})'_F$. Inserting the above restriction into the entropy inequality of a biphasic model, one obtains additional terms compared to the

equation given by (3.22), i. e.

$$\dots\, n^F \Big(\frac{\mathcal{P}}{\rho^{FR}} \,-\, \rho^{FR} \frac{\partial \psi^F}{\partial \rho^{FR}} \Big) \, (\rho^{FR})'_F \,\dots\,.$$

Since the *Helmholtz* free energy of the compressible fluid depends on its effective density, as opposed to the incompressible case, by factoring out the time-derivative of the process variable ρ^{FR}, the term stemming from the saturation condition falls together with the derivative of ψ^F. Note that, for convenience, only the relevant term is given here. Following the standard arguments given in Section 3.2.2 that each process must satisfy the entropy inequality, this term ought to be zero. Therefore, one finds

$$\mathcal{P} \,=\, (\rho^{FR})^2 \, \frac{\partial \psi^F}{\partial \rho^{FR}} \,, \tag{3.59}$$

whereas in the related literature, it is referred to this expression as the *thermodynamic pressure*, cf., for example, Bowen [29]. Moreover, note that, if all constituents are compressible, there are not enough equations to solve all unknowns. In such a case, one needs an evolution equation for one of the volume fractions (Diebels [44, 45]). Another concept is to split the deformation gradient into a part deforming the pore structure and a part changing densities (Bluhm [18]). For more detailed information about compressible models, cf. Diebels [44] and Bluhm [19]. □

3.2.8 Mechanical part of the effective quantities

Up to this point, the terms in the entropy principle consisting of the *Helmholtz* free energies Ψ_F^β and Ψ_F^F and their derivatives have been identified, i. e. the chemical potentials μ^β and the osmotic pressures π^β of the fluid components. In this section, new quantities referring to the purely mechanical part of the *Cauchy* stresses and the momentum productions are introduced, i. e.

$$\boxed{\begin{aligned}
\mathbf{T}^S_{E\,mech.} &:= -n^S \sum_\beta \Psi_F^\beta \, \mathbf{I} \,+\, n^S \sum_\beta \rho_F^\beta \, \mu^\beta \, \mathbf{I} \,+\, \mathbf{T}^S_E \,, \\
\mathbf{T}^\beta_{E\,mech.} &:= -n^F \, \Psi_F^\beta \, \mathbf{I} \,+\, n^F \rho_F^\beta \, \mu^\beta \, \mathbf{I} \,+\, \mathbf{T}^\beta_E \,, \\
\hat{\mathbf{p}}^\beta_{E\,mech.} &:= \Psi_F^\beta \operatorname{grad} n^F \,-\, \rho_F^\beta \, \mu^\beta \operatorname{grad} n^F \,+\, \hat{\mathbf{p}}^\beta_E \,.
\end{aligned}} \tag{3.60}$$

As a consequence, the entropy inequality (3.40) can be rewritten as

$$\begin{aligned}
\Big(\mathbf{T}^S_{E\,mech.} - \rho^S \frac{\partial \psi^S}{\partial \mathbf{F}_S} \, \mathbf{F}_S^T \Big) \cdot \mathbf{D}_S \,+\, \sum_\beta \mathbf{T}^\beta_{E\,mech.} \cdot \mathbf{D}_\beta \,-\, \sum_\beta \hat{\mathbf{p}}^\beta_{E\,mech.} \cdot \mathbf{w}_\beta \,- \\
- \, n^F \sum_\beta \Big(\operatorname{grad} \Psi_F^\beta \,-\, \frac{\partial \Psi_F^F}{\partial \rho_F^\beta} \operatorname{grad} \rho_F^\beta \Big) \cdot \mathbf{d}_{\beta F} \geq 0 \,.
\end{aligned} \tag{3.61}$$

The above relation clearly shows that the purely mechanical solid extra stress is given by

$$\mathbf{T}^S_{E\text{mech.}} = \rho^S \frac{\partial \psi^S}{\partial \mathbf{F}_S} \mathbf{F}_S^T , \tag{3.62}$$

i. e. the derivative of ψ^S with respect to the solid deformation gradient. Concerning the fluid components, the friction force $\operatorname{div} \mathbf{T}^\beta_{E\text{mech.}}$ appearing in the momentum balance of φ^β develops from the viscous flux of the component. Moreover, it can be shown from a dimensional analysis, cf. Ehlers *et al.* [62] and Markert [131], that in case of a porous medium, the contribution of the friction force of the fluid phase to its momentum, cf. $(2.73)_3$, can usually be assumed to be negligible in comparison to the contribution of its interaction force $\hat{\mathbf{p}}^F$. This considerations are directly adopted within this thesis for the liquid components. Consequently, the purely mechanical part of the extra stresses of all fluid components can be treated to be negligible:

$$\mathbf{T}^\beta_{E\text{mech.}} \approx \mathbf{0} . \tag{3.63}$$

3.2.9 Principle of dissipation

Summarising the above statements, the equilibrium part of the entropy inequality is fulfilled. The remaining part of the inequality, i. e. the dissipation inequality

$$\mathcal{D} = - \sum_\beta \hat{\mathbf{p}}^\beta_{E\text{mech.}} \cdot \mathbf{w}_\beta - n^F \sum_\beta \big(\operatorname{grad} \Psi^\beta_F - \frac{\partial \Psi^F_F}{\partial \rho^\beta_F} \operatorname{grad} \rho^\beta_F \big) \cdot \mathbf{d}_{\beta F} \geq 0 , \tag{3.64}$$

will be discussed in this section. First, the second term is considered by recalling that the *Helmholtz* free energy Ψ^β_F is a function of ρ^β_F. Following this, and taking into account that the derivatives of both *Helmholtz* free energies Ψ^β_F and Ψ^F_F are equivalent, cf. (3.45), their gradients are given by

$$\operatorname{grad} \Psi^\beta_F = \frac{\partial \Psi^F_F}{\partial \rho^\beta_F} \operatorname{grad} \rho^\beta_F , \tag{3.65}$$

and, therefore, the last term in (3.64) vanishes. As a result, only the term

$$\mathcal{D} = - \sum_\beta \hat{\mathbf{p}}^\beta_{E\text{mech.}} \cdot \mathbf{w}_\beta \geq 0 \tag{3.66}$$

is left in the dissipation inequality. To fulfil this equation in all circumstances, an appropriate constitutive assumption will be made for $\hat{\mathbf{p}}^\beta_{E\text{mech.}}$ such that the result is always positive in case the process under consideration is not in equilibrium, or zero otherwise ($\mathbf{w}_\beta \equiv 0$). This can be guaranteed if $\hat{\mathbf{p}}^\beta_{E\text{mech.}}$ is modelled as a positive definite quadratic expression:

$$\hat{\mathbf{p}}^\beta_{E\text{mech.}} \propto \mathbf{w}_\beta . \tag{3.67}$$

Hence, the following ansatz is made for the purely mechanical momentum interaction term of the fluid component:

$$\begin{aligned}\hat{\mathbf{p}}^{\beta}_{E_{mech.}} = -\sum_{\alpha} \mathbf{S}^{\beta\alpha}\,(\,\overset{\prime}{\mathbf{x}}_{\beta} - \overset{\prime}{\mathbf{x}}_{\alpha}\,) = &-\mathbf{S}^{\beta S}\,(\,\overset{\prime}{\mathbf{x}}_{\beta} - \overset{\prime}{\mathbf{x}}_{S}\,) - \mathbf{S}^{\beta L}\,(\,\overset{\prime}{\mathbf{x}}_{\beta} - \overset{\prime}{\mathbf{x}}_{L}\,)\\ &- \mathbf{S}^{\beta +}\,(\,\overset{\prime}{\mathbf{x}}_{\beta} - \overset{\prime}{\mathbf{x}}_{+}\,) - \mathbf{S}^{\beta -}\,(\,\overset{\prime}{\mathbf{x}}_{\beta} - \overset{\prime}{\mathbf{x}}_{-}\,)\,.\end{aligned} \tag{3.68}$$

Therein, $\mathbf{S}^{\beta\alpha}$ are the positive definite second order friction tensors describing the resistance of relative movement among the constituents which, in general, can be anisotropic. By inserting this ansatz into the dissipation inequality (3.66), one obtains after some rearrangements

$$\begin{aligned}\mathcal{D} = \mathbf{S}^{LS}\,\mathbf{w}_L\cdot\mathbf{w}_L + \mathbf{S}^{+S}\,\mathbf{w}_+\cdot\mathbf{w}_L + \mathbf{S}^{-S}\,\mathbf{w}_-\cdot\mathbf{w}_L +\\ +\mathbf{S}^{L+}\,(\,\mathbf{w}_L - \mathbf{w}_+\,)\cdot(\,\mathbf{w}_L - \mathbf{w}_+\,) + \mathbf{S}^{L-}\,(\,\mathbf{w}_L - \mathbf{w}_-\,)\cdot(\,\mathbf{w}_L - \mathbf{w}_-\,) \geq 0\,.\end{aligned} \tag{3.69}$$

Provided that the friction among the ions is negligible and that the friction among the remaining components is symmetric, i. e.

$$\mathbf{S}^{+-} = \mathbf{S}^{-+} = \mathbf{0} \quad \text{and} \quad \mathbf{S}^{L\gamma} = \mathbf{S}^{\gamma L}\,, \tag{3.70}$$

the result for the mechanical interaction term can be summarised by

$$\begin{aligned}\hat{\mathbf{p}}^{L}_{E_{mech.}} &= -\mathbf{S}^{LS}\,\mathbf{w}_L + \sum_{\gamma}\mathbf{S}^{L\gamma}\,(\,\overset{\prime}{\mathbf{x}}_{\gamma} - \overset{\prime}{\mathbf{x}}_{L}\,)\,,\\ \hat{\mathbf{p}}^{\gamma}_{E_{mech.}} &= -\mathbf{S}^{\gamma S}\,\mathbf{w}_{\gamma} - \mathbf{S}^{L\gamma}\,(\,\overset{\prime}{\mathbf{x}}_{\gamma} - \overset{\prime}{\mathbf{x}}_{L}\,)\,,\end{aligned} \tag{3.71}$$

and, thus,

$$\hat{\mathbf{p}}^{F}_{E_{mech.}} = \sum_{\beta}\hat{\mathbf{p}}^{\beta}_{E_{mech.}} = -\mathbf{S}^{LS}\,\mathbf{w}_L - \sum_{\gamma}\mathbf{S}^{\gamma S}\,\mathbf{w}_{\gamma}\,. \tag{3.72}$$

In equation (3.71), one can clearly differentiate between two distinct parts in the momentum interaction. The first expression corresponds to the flux of the fluid component relative to the moving solid, i. e. the friction between the solid φ^S and the fluid component φ^{β}, while the second term corresponds to the diffusion of the components within the liquid. Moreover, by making the following ansatz for the remaining friction tensors, one obtains

$$\boxed{\begin{aligned}\mathbf{S}^{LS} &:= n^F\left[\,n^L\mu^{LR}\,(\mathbf{K}^S)^{-1}\,\right]\frac{\mathbf{w}_F\otimes\mathbf{w}_F}{\mathbf{w}_F\cdot\mathbf{w}_F}\,,\\ \mathbf{S}^{\gamma S} &:= n^F\left[\,n^{\gamma}\mu^{\gamma R}\,(\mathbf{K}^S)^{-1}\,\right]\frac{\mathbf{w}_F\otimes\mathbf{w}_F}{\mathbf{w}_F\cdot\mathbf{w}_F}\,,\\ \mathbf{S}^{L\gamma} &:= n^F\,\frac{n^F\rho^{\gamma}_F\,\bar{R}^{\gamma}\theta}{D^{\gamma}}\,\frac{\mathbf{d}_{\gamma F}\otimes\mathbf{d}_{\gamma F}}{\mathbf{d}_{\gamma F}\cdot\mathbf{d}_{\gamma F}}\,.\end{aligned}} \tag{3.73}$$

Following above findings, the momentum interaction of the overall fluid can be written as

$$\boxed{\hat{\mathbf{p}}^F_{E_{mech.}} = -n^F \, (\mathbf{K}^F)^{-1} \, \mathbf{w}_F \,, \quad \text{where} \quad (\mathbf{K}^F)^{-1} := \sum_\beta \frac{n^\beta \mu^{\beta R} \, \mathbf{w}_F \cdot \mathbf{w}_\beta}{\mathbf{w}_F \cdot \mathbf{w}_F} \, (\mathbf{K}^S)^{-1} \,.} \tag{3.74}$$

In the above relations, D^γ is the diffusion coefficient of φ^γ moving within the liquid solvent, R is the universal gas constant, $\mu^{\beta R}$ are the effective viscosities of φ^β, and $\mathbf{K}^S$ is the positive definite tensor characterising the intrinsic permeability of the solid skeleton. This material parameter is, in contrast to the positive definite hydraulic permeability tensor $\mathbf{K}^F$, independent of the fluid properties. Considering that the solution is mainly composed of the liquid solvent and that the ions play a subsidiary role with respect to the volume fraction, i. e.

$$n^\gamma \ll n^L \quad \longrightarrow \quad s^\gamma \ll s^L \,, \tag{3.75}$$

it can be deduced from the effective density ρ^{FR} of the overall fluid that, cf. (2.12),

$$\rho^\gamma_F \ll \rho^L_F \approx \rho^{FR} \,. \tag{3.76}$$

Moreover, from the velocity $\overset{\prime}{\mathbf{x}}_F$ of the overall fluid, cf. (2.30), it follows that

$$\overset{\prime}{\mathbf{x}}_L \approx \overset{\prime}{\mathbf{x}}_F \,. \tag{3.77}$$

Pursuing this further, it may be assumed that the influence of the dissolved salt to the material properties of the overall fluid is marginal. Thus, $\mu^{LR} \approx \mu^{FR}$ and $\gamma^{LR} \approx \gamma^{FR}$. Following this considerations, $(3.74)_2$ can be rewritten as

$$(\mathbf{K}^F)^{-1} \approx n^F \mu^{FR} \, (\mathbf{K}^S)^{-1} \,. \tag{3.78}$$

This is also the correlation given in Ehlers *et al.* [62] and Markert [131]. For isotropic conditions, i. e. $\mathbf{K}^S = K^S \, \mathbf{I}$, the *Darcy* permeability is defined via

$$k^F := \frac{\gamma^{FR}}{\mu^{FR}} \, K^S \,. \tag{3.79}$$

Thus,

$$\boxed{\hat{\mathbf{p}}^F_{E_{mech.}} = -(n^F)^2 \frac{k^F}{\gamma^{FR}} \, \mathbf{w}_F \,.} \tag{3.80}$$

For a more detailed discussion on all the different permeabilities, the interested reader is referred to Markert [131]. Note that in above considerations, even though the friction stress of the fluid and its components is neglected, cf. (3.63), the viscosity of the liquid is included into the model via its momentum interaction, also known as the drag force [56]. Concerning the interaction term of the fluid components φ^β, one obtains by inserting the

friction tensors $(3.73)_3$ into the production terms $(3.71)_2$

$$\boxed{\hat{\mathbf{p}}^{\gamma}_{E_{mech.}} = -n^F\,(\mathbf{D}^{\gamma})^{-1}\,\mathbf{d}_{\gamma F}\,, \qquad \text{where} \quad \mathbf{D}^{\gamma} := \frac{D^{\gamma}}{n^F\,\rho^{\gamma}_F\,\bar{R}^{\gamma}\theta}\,\mathbf{I}\,.} \tag{3.81}$$

Therein, $\mathbf{D}^{\gamma}$ is the diffusion tensor corresponding to φ^{γ}. In order to arrive at the above statement, the assumptions in (3.76) and (3.77) were used. In particular, since $n^{\gamma} \ll n^L$, the friction tensor $\mathbf{S}^{\gamma S}$ has been neglected compared to $\mathbf{S}^{L\gamma}$. Moreover, since $\overset{\prime}{\mathbf{x}}_L \approx \overset{\prime}{\mathbf{x}}_F$, it follows that $\overset{\prime}{\mathbf{x}}_{\gamma} - \overset{\prime}{\mathbf{x}}_L \approx \mathbf{d}_{\gamma F}$.

3.2.10 Stress tensors

Having defined $\mathbf{T}^{\alpha}_{E_{mech.}}$, the stress tensors will be summarised for later use in this section. Aiming at such a summary, relations $(3.60)_1$ and $(3.60)_2$ are rearranged and inserted into the overall stress tensors $(3.26)_1$ to $(3.26)_3$ yielding

$$\boxed{\begin{aligned}
\mathbf{T}^S &= -n^S\,\mathcal{P}\,\mathbf{I} + n^S\,\Psi^F_F\,\mathbf{I} - n^S\,\textstyle\sum_{\beta}\,\rho^{\beta}_F\,\mu^{\beta}\,\mathbf{I} - \rho^{fc}_e\,\mathcal{E}\,\mathbf{I} + \mathbf{T}^S_{E_{mech.}}\,,\\
\mathbf{T}^L &= -n^L\mathcal{P}\,\mathbf{I} + n^F\,\Psi^L_F\,\mathbf{I} - n^F\,\rho^L_F\,\mu^L\,\mathbf{I} + \mathbf{T}^L_{E_{mech.}}\,,\\
\mathbf{T}^{\gamma} &= -n^{\gamma}\mathcal{P}\,\mathbf{I} + n^F\,\Psi^{\gamma}_F\,\mathbf{I} - n^F\,\rho^{\gamma}_F\,\mu^{\gamma}\,\mathbf{I} - \rho^{\gamma}_e\,\mathcal{E}\,\mathbf{I} + \mathbf{T}^{\gamma}_{E_{mech.}}\,.
\end{aligned}} \tag{3.82}$$

Additionally, by use of the osmotic pressure (3.51), the stress tensors can be represented alternatively as:

$$\begin{aligned}
\mathbf{T}^S &= -n^S\,\mathcal{P}\,\mathbf{I} - n^S\,\pi\,\mathbf{I} - \rho^{fc}_e\,\mathcal{E}\,\mathbf{I} + \mathbf{T}^S_{E_{mech.}}\,,\\
\mathbf{T}^L &= -n^L\mathcal{P}\,\mathbf{I} - n^F\,\pi^L\,\mathbf{I} + \mathbf{T}^L_{E_{mech.}}\,,\\
\mathbf{T}^{\gamma} &= -n^{\gamma}\mathcal{P}\,\mathbf{I} - n^F\,\pi^{\gamma}\,\mathbf{I} - \rho^{\gamma}_e\,\mathcal{E}\,\mathbf{I} + \mathbf{T}^{\gamma}_{E_{mech.}}\,.
\end{aligned} \tag{3.83}$$

The stress tensor $\mathbf{T}^F$ of the overall fluid is obtained from the sum of the stress tensors of its components φ^{β}, viz.:

$$\boxed{\mathbf{T}^F = \sum_{\beta}\mathbf{T}^{\beta} = -n^F\,(\,\mathcal{P} + \pi\,)\,\mathbf{I} - \sum_{\gamma}\,\rho^{\gamma}_e\,\mathcal{E}\,\mathbf{I} + \mathbf{T}^F_{E_{mech.}}\,.} \tag{3.84}$$

Moreover, to get the stress tensor of the overall medium, the above $\mathbf{T}^F$ is summed up with $\mathbf{T}^S$ such that

$$\mathbf{T} = -\,(\,\mathcal{P} + \pi\,)\,\mathbf{I} + \mathbf{T}^S_{E_{mech.}}\,, \tag{3.85}$$

From the above equations, one can see that the stress tensor of a constituent consists of several parts. In particular, it has contributions from the hydraulic pressure and from the osmotic pressure, which in turn is represented by the chemical potentials. Furthermore, it has a contribution from the electrostatic force $\mathcal{E}$. Finally, the solid also responses

via stresses to mechanical deformations. Note in passing that the liquid does not have a contribution from the electroneutrality condition, since it is not electrically charged. Also, from $\mathbf{T}^F$ it is obvious that the hydraulic pressure $\mathcal{P}$ can be merged with the osmotic pressure π into the overall effective pressure p:

$$\boxed{p := \mathcal{P} + \pi\,.} \tag{3.86}$$

3.2.11 Momentum productions

Concerning the interaction terms, the extra terms given by $(3.60)_3$ are rearranged and inserted into the momentum productions defined in $(3.26)_4$ and $(3.26)_5$ which results in

$$\boxed{\begin{aligned} \hat{\mathbf{p}}^L &= \mathcal{P}\operatorname{grad} n^L - \Psi_F^L \operatorname{grad} n^F + \rho_F^L\,\mu^L \operatorname{grad} n^F + \hat{\mathbf{p}}^L_{E\text{mech.}}\,, \\ \hat{\mathbf{p}}^\gamma &= \mathcal{P}\operatorname{grad} n^\gamma - \Psi_F^\gamma \operatorname{grad} n^F + \rho_F^\gamma\,\mu^\gamma \operatorname{grad} n^F + \mathcal{E}\operatorname{grad}\rho_e^\gamma + \hat{\mathbf{p}}^\gamma_{E\text{mech.}}\,. \end{aligned}} \tag{3.87}$$

Alternatively, using the osmotic pressure (3.51), the above relations yield

$$\begin{aligned} \hat{\mathbf{p}}^L &= \mathcal{P}\operatorname{grad} n^L + \pi^L \operatorname{grad} n^F + \hat{\mathbf{p}}^L_{E\text{mech.}}\,, \\ \hat{\mathbf{p}}^\gamma &= \mathcal{P}\operatorname{grad} n^\gamma + \pi^\gamma \operatorname{grad} n^F + \mathcal{E}\operatorname{grad}\rho_e^\gamma + \hat{\mathbf{p}}^\gamma_{E\text{mech.}}\,. \end{aligned} \tag{3.88}$$

Again, summing over the interaction terms of the fluid components, one obtains the corresponding term for the overall fluid, i. e.

$$\boxed{\hat{\mathbf{p}}^F = \mathcal{P}\operatorname{grad} n^F + \pi \operatorname{grad} n^F + \mathcal{E}\sum_\gamma \operatorname{grad}\rho_e^\gamma + \hat{\mathbf{p}}^F_{E\text{mech.}}\,.} \tag{3.89}$$

Also in the case of the interaction terms, it can be seen that they consist of three distinct contributions, namely, the mechanical hydraulic pressure, the chemical osmotic pressure (chemical potential), the electrostatic force and the purely mechanical friction part. Having discussed the *Helmholtz* free energies, the stress tensors and the momentum productions of the constituents, the next step is the computation of the corresponding relations for the constituents. In particular, the corresponding relations to compute the mechanical solid extra stress, the seepage velocities of the overall fluid and its components will be introduced in Section 3.3 *et sequens*.

3.2.12 Pressures in the overall fluid

But before going further, some remarks on the pressures introduced in the previous chapters will be given. In the overall derivation of the theory, three different pressures could be identified. The first one introduced in Chapter 3.2.6 is the osmotic pressure. It develops only from the chemical constitution of the overall fluid solution and, thus, it is computed

from the amount of the component in the fluid, i. e. the concentrations of its components, by use of relation

$$\pi \;=\; \sum_{\beta} \pi^{\beta} \;=\; \sum_{\beta} \bar{R}^{\beta} \theta \, \rho_F^{\beta} \,.$$

Therein, the distinction of the partial osmotic pressures π^{β} is a result of the theoretical considerations made before. However, the above relation represents the value of the partial osmotic pressures π^{β} and, thus, of the osmotic pressure π at any material point within the continuum. As any other pressure, it cannot be measured on its own, but only in comparison to another solution. For example, in chemistry very often the case of a chemical solution (denoted by 1) and a pure solvent (denoted by 2) separated by a semipermeable membrane is used to explain the osmotic pressure. This example is comparable to two "point-solutions" in continuum physics without the existence of any gradients. The osmotic pressure is measured by the difference of the water level heights at equilibrium state. Thus, it is always the result of a comparison of both solutions, cf. also Section 4.1. However, together with the assumption that the liquid concentration is constant, cf. Section 3.6, and that the concentration ρ_2^{γ} of the ions is zero in the pure solvent solution denoted by 2, one obtains

$$\Delta\pi \;=\; \pi^1 - \pi^2 \;=\; (\bar{R}^L \theta \rho_1^L + \sum_{\gamma} \bar{R}^{\gamma} \theta \rho_1^{\gamma}) \;-\; (\bar{R}^L \theta \rho_2^L + \sum_{\gamma} \bar{R}^{\gamma} \theta \rho_2^{\gamma}) \;=\; \sum_{\gamma} \bar{R}^{\gamma} \theta \rho_1^{\gamma} \,.$$

The above relation exactly represents the *van't Hoff* equation generally used in textbooks of chemistry, cf., for example, Adam *et al.* [2], Klotz & Rosenberg [115] and Ott & Boerio-Goates [141]. The second pressure introduced in Section 3.2.7 and identified from the *Lagrange*an multipliers is the purely mechanical hydraulic pressure $\mathcal{P}$. In case of incompressible fluids the value of $\mathcal{P}$ develops from the given boundary conditions, whereas in the general case of a compressible fluid $\mathcal{P}$ is computed from its potential by derivation, cf. (3.59). This topic has already been discussed in several contributions, cf., for example, Bowen [29]. In the absence of chemical effects, this pressure can also be measured relative to the pressure surrounding the overall body by inserting a pressure transducer.

The consequence of the above considerations is that both the hydraulic pressure as well as the osmotic pressure can be combined to one overall pressure p using the relation

$$p \;=\; \mathcal{P} + \pi$$

introduced in Section 3.2.10. This is also the measured pressure value if a pressure transducer is inserted into the interstitial fluid in the overall aggregate in case of combined chemical and mechanical processes. With the knowledge of the constitutive relation for the osmotic pressure π, its value can be computed and subtracted from the overall pressure leading to the value of the hydraulic pressure $\mathcal{P}$.

Note in passing that up to Section 3.2.8 inclusively no distinction is made between a solvent and the solutes in the derivation of the overall theory and, therefore, all the fluid components are represented by the same chemical potential. In contrast, in contributions such as Lai *et al.* [116] and Huyghe & Janssen [107] *a priori* a special chemical potential for the solvent is introduced, which either depends on the hydraulic pressure ($p - R\theta \sum c_m^{\gamma}$),

cf. [116], or on the overall pressure (p), cf. [107].

3.3 The solid skeleton

Among the materials under consideration within this thesis are, from the area of biomechanics, articular cartilage, intervertebral disc as well as hydrogel, and, from the area of geomechanics, chemically active clay and shale. From this list, it is clear that those materials can be subdivided into two categories according to the behaviour of the solid matrix. While the materials from the area of biomechanics are mostly composed of entangled collagen fibres and large charged molecules, cf., for example, Mow & Ratcliffe [137], the materials which are part of the field of geomechanics are mostly made up of silicate platelets, cf., e. g., van Olphen [140]. This fact clearly shows that different models need to be used for the two categories.

More precisely, it is well known from literature that biological tissues and their artificial replacements such as hydrogel clearly exhibit viscoelastic behaviour (Grant *et al.* [82]). This behaviour originates from different properties of the materials. First of all, the multiphasic composition results in macroscopic viscous effects due to the fact that the fluid is flowing within the solid skeleton while the overall aggregate undergoes volume changing effects such as compression, tension, swelling or shrinking. The second reason is the intrinsic viscoelastic property of the solid matrix of these materials (Hayes & Bodine [91] and Mak [128]), i. e. the single collagen fibres exhibit viscoelastic properties with tension-compression nonlinearities (Huang *et al.* [101]). For a modelling of the viscoelastic properties of multiphasic materials, a thermodynamically consistent model for finite deformations has been developed by Markert [130], see also Ehlers & Markert [65].

In contrast, the materials from geomechanics, such as chemically active clay and shale behave plastic, cf., for example, Hueckel [102] and Loret *et al.* [123]. The plastic material behaviour results from the fact that the silicate platelets are able to slide on each other. Note that in this case, one can also observe viscous effects. But here, they are only a result of the multiphasic composition, since the single platelet itself can be considered as stiff. The model postulated in Ehlers [53] can be chosen to describe plasticity in the geomechanical context by a thermodynamically consistent single surface yield criterion, see also Blome [17].

Moreover, depending on the global arrangement of the fibres and the platelets in the medium, biomaterials as well as geomaterials may exhibit anisotropic behaviour, cf. Ehlers *et al.* [63] and Karajan *et al.* [111]. For a detailed introduction on anisotropy, the interested reader is referred to the works of Apel [5], Boehler [20], Schröder [150], Schröder *et al.* [151], Spencer [156] and the citations therein. For a general introduction to material nonlinearity, the reader is referred to the textbooks of Haupt [90] and Holzapfel [99].

The above considerations clearly show that the choice of an adequate material model heavily depends on the medium studied. Thus, in order to preserve a certain flexibility concerning the underlying material, this thesis will consider the solid material as isotropic and elastic in the range of finite deformations. In this scope, a strain energy function is

customarily defined as

$$W^S := \rho^S_{0S}\,\psi^S \tag{3.90}$$

weighting the *Helmholtz* free energy ψ^S with the initial density of the solid. This newly defined function also has to obey the thermodynamical principles already mentioned in Section 3.2.2. In order to make this possible, the process variable $\mathbf{F}_S$ of the solid skeleton has to be modified further. More precisely, so as to satisfy the *principle of material symmetry*, which states that for isotropy the response of a material should be independent of a superimposed rotation of the body in the reference configuration, it can be shown that W^S has to depend in such a way on $\mathbf{F}_S$ that it can also be expressed by the left *Cauchy-Green* deformation tensor $(2.42)_1$ acting on the current configuration. Thus,

$$W^S = W^S(\,\mathbf{B}_S\,)\,. \tag{3.91}$$

Moreover, the *principle of material frame indifference*, stating that the response of a material is independent on the position of the observer in the current configuration, is fulfilled, if W^S depends on $\mathbf{F}_S$ so that this dependency can also be replaced by the right *Cauchy-Green* deformation tensor $(2.42)_2$ acting on the reference configuration:

$$W^S = W^S(\,\mathbf{C}_S\,)\,. \tag{3.92}$$

For a more detailed discussion on this topic, the interested reader is referred to the works by Truesdell & Toupin [163] and Truesdell & Noll [162]. Nevertheless, both of the above principles are satisfied at once if the strain energy function is given in the invariants of the deformation tensors $\mathbf{C}_S$ and $\mathbf{B}_S$, because both tensors have the same invariants[5]. As already discussed in Section 3.2.8, the purely mechanical solid extra stress is obtained from (3.62) which transfers to

$$\mathbf{T}^S_{E\,mech.} = \frac{1}{J_S}\,\frac{\partial W^S}{\partial \mathbf{F}_S}\,\mathbf{F}_S^T \tag{3.94}$$

by use of (3.90) and

$$\rho^S = \rho^S_{0S}\,(\,\det\,\mathbf{F}_S\,)^{-1}\,, \tag{3.95}$$

which is the result of the time-integration of the solid mass balance without mass productions, cf. (3.2). In (3.94), J_S denotes the *Jacobi*an $\det\,\mathbf{F}_S$. At this point, it becomes obvious that by the definition of the strain energy function, the *Cauchy* stress can be

[5]It can be shown that, based on the definition of the left and the right *Cauchy-Green* deformation tensors, the fundamental invariants of both tensors are equal:

$$\begin{aligned} I &= \mathbf{C}_S\cdot\mathbf{I} &&= \mathbf{B}_S\cdot\mathbf{I}\,,\\ II &= \tfrac{1}{2}\,(\,I^2 - \mathbf{C}_S\,\mathbf{C}_S\cdot\mathbf{I}\,) &&= \tfrac{1}{2}\,(\,I^2 - \mathbf{B}_S\,\mathbf{B}_S\cdot\mathbf{I}\,)\,,\\ III &= \det\,\mathbf{C}_S &&= \det\,\mathbf{B}_S\,. \end{aligned} \tag{3.93}$$

replaced by the *Kirchhoff* stress via (2.55) yielding

$$\boldsymbol{\tau}^S_{E\,mech.} = \frac{\partial W^S}{\partial \mathbf{F}_S}\,\mathbf{F}_S^T\,. \tag{3.96}$$

Note that this quantity can be transported via a covariant transport from the current to the reference configuration and back again, cf., for example, Ehlers [51, 52], Holzapfel [99] and Section 2.2.4, to convert between the different stress measures. Continuing, by actually replacing the process variable $\mathbf{F}_S$ by $\mathbf{C}_S$, i. e. $W^S = W^S(\mathbf{C}_S)$, one finds by use of the tensor calculus

$$\boldsymbol{\tau}^S_{E\,mech.} = \Big(\frac{\partial \mathbf{C}_S}{\partial \mathbf{F}_S}\Big)^T \frac{\partial W^S}{\partial \mathbf{C}_S}\,\mathbf{F}_S^T = \mathbf{F}_S\Big(2\,\frac{\partial W^S}{\partial \mathbf{C}_S}\Big)\,\mathbf{F}_S^T \tag{3.97}$$

or in analogy by expressing W^S in the right *Cauchy-Green* deformation tensor, i. e. $W^S = W^S(\mathbf{B}_S)$,

$$\boldsymbol{\tau}^S_{E\,mech.} = \Big(\frac{\partial \mathbf{B}_S}{\partial \mathbf{F}_S}\Big)^T \frac{\partial W^S}{\partial \mathbf{B}_S}\,\mathbf{F}_S^T = 2\,\frac{\partial W^S}{\partial \mathbf{B}_S}\,\mathbf{B}_S\,. \tag{3.98}$$

According to Ehlers & Eipper [60], the following constitutive assumption of a Neo-*Hooke* type is chosen for the strain energy function of the solid matrix:

$$W^S := \frac{1}{2}\,\mu^S(\mathbf{B}_S\cdot\mathbf{I}-3) - \mu^S\,\ln J_S + \lambda^S(1-n^S_{0S})^2\Big(\frac{J_S-1}{1-n^S_{0S}} - \ln\frac{J_S-n^S_{0S}}{1-n^S_{0S}}\Big) \tag{3.99}$$

Therein, μ^S and λ^S denote the *Lamé* constants. Moreover, in the above relation, the first two terms belong to the strain energy function of a standard Neo-*Hooke* type model, where the last term on the right-hand side is an extension which reflects a special characteristic of incompressible porous solids, i. e. the compression point. This point is reached, if all the pore fluid or gas is pressed out of the porous medium, such that the volume fraction of the solid matrix reaches unity and any further compression would lead to infinite stresses. Following the above considerations about the derivative of W^S, i. e. (3.97) and (3.98), the result is

$$\boxed{\boldsymbol{\tau}^S_{E\,mech.} = \mu^S\,(\,\mathbf{B}_S - \mathbf{I}\,) + \lambda^S\,(\,1 - n^S_{0S}\,)^2\Big(\frac{J_S}{1-n^S_{0S}} - \frac{J_S}{J_S-n^S_{0S}}\Big)\,\mathbf{I}\,,} \tag{3.100}$$

where, once again, the volumetric expansion term is found at the rightmost part.

3.4 The fluid components

The entropy inequality has been evaluated and all previously undetermined response functions have been specified, i. e. the *Helmholtz* free energies, the stress tensors and the momentum productions have been found, cf. Section 3.2.2, Section 3.2.10 and Section 3.2.11. Now, the stress tensors and the momentum productions can be inserted into the corresponding momentum balances. By doing so, one obtains in case of quasi-static

processes ($\rho^\alpha \overset{''}{\mathbf{x}}_\alpha \equiv 0$) functions describing the flow and the diffusion of the fluid and its components.

3.4.1 Liquid flow

In a first step, the liquid stress tensor $(3.82)_2$ and the liquid momentum production $(3.87)_1$ are inserted into the quasi-static form of the momentum balance of the liquid $(2.73)_3$. This leads to

$$\mathbf{0} = -n^L \operatorname{grad} \mathcal{P} + n^F \operatorname{grad} (\Psi^L_F - \rho^L_F \mu^L) + \operatorname{div} \mathbf{T}^L_{E\,mech.} + \rho^L \mathbf{g} + \hat{\mathbf{p}}^L_{E\,mech.} , \tag{3.101}$$

where, the divergence theorem as given in Ehlers [57] has been used. Utilising the fact that the Ψ^L_F is a function of ρ^L_F, the second term on the right-hand side can further be reformulated:

$$\begin{aligned} \operatorname{grad} (\Psi^L_F - \rho^L_F \mu^L) &= \frac{\partial \Psi^L_F}{\partial \rho^L_F} \operatorname{grad} \rho^L_F - \mu^L \operatorname{grad} \rho^L_F - \rho^L_F \operatorname{grad} \mu^L \\ &= - \rho^L_F \operatorname{grad} \mu^L . \end{aligned} \tag{3.102}$$

Replacing the corresponding term in the above momentum balance yields

$$\mathbf{0} = -n^L \operatorname{grad} \mathcal{P} - n^F \rho^L_F \operatorname{grad} \mu^L + n^F \rho^L_F \mathbf{g} + \hat{\mathbf{p}}^L_{E\,mech.} . \tag{3.103}$$

Therein, the vanishing mechanical extra stress (3.63) of the liquid has been considered.

3.4.2 Ion diffusion

The same procedure as for the liquid is also applied to the mobile ions. Therefore, their stress tensor $(3.82)_3$ and their momentum production $(3.87)_2$ are inserted into the quasi-static form of the momentum balance of the ions $(2.73)_3$. Moreover, with the aid of (3.102) and the vanishing mechanical extra stresses (3.63),

$$\mathbf{0} = -n^\gamma \operatorname{grad} \mathcal{P} - n^F \rho^\gamma_F \operatorname{grad} \mu^\gamma - \rho^\gamma_e \operatorname{grad} \mathcal{E} + n^F \rho^\gamma_F \mathbf{g} + \hat{\mathbf{p}}^\gamma_{E\,mech.} \tag{3.104}$$

is obtained. Note that this momentum balance has an additional contribution from the electrostatic fields. To find the relation actually responsible for the ion diffusion, the mechanical momentum production (3.81) is inserted into the above function to yield

$$n^F \rho^\gamma_F \mathbf{d}_{\gamma F} = -\frac{D^\gamma}{\bar{R}^\gamma \theta} \big(s^\gamma \operatorname{grad} \mathcal{P} - \rho^\gamma_F \mathbf{g} + \rho^\gamma_F \operatorname{grad} \mu^\gamma + \rho^\gamma_{eF} \operatorname{grad} \mathcal{E} \big) . \tag{3.105}$$

Following the assumption (3.75), the first term including the gradient of the hydraulic pressure $\mathcal{P}$ is neglected in the following. Moreover, since the relative velocity of the ions with respect to the moving solid is needed, the diffusion velocity of the ions within the

overall fluid is replaced by

$$\mathbf{d}_{\gamma F} = \mathbf{w}_\gamma - \mathbf{w}_F \tag{3.106}$$

such that

$$\boxed{n^F \rho_F^\gamma \mathbf{w}_\gamma = -\frac{D^\gamma}{\bar{R}^\gamma \theta}\left(\rho_F^\gamma \operatorname{grad} \mu^\gamma - \rho_F^\gamma \mathbf{g} + \rho_{eF}^\gamma \operatorname{grad} \mathcal{E} \right) + n^F \rho_F^\gamma \mathbf{w}_F \,.} \tag{3.107}$$

The above relation is referred to as extended *Nernst-Planck* equation, as it additionally includes the fluid velocity.

3.4.3 Fluid flow

Next, the momentum balances of the fluid components are summed up yielding the momentum balance of the overall fluid. Firstly,

$$\mathbf{0} = -n^F \operatorname{grad} \mathcal{P} + n^F \sum_\beta \rho_F^\beta \operatorname{grad} \mu^\beta + n^F \sum_\gamma \rho_{eF}^\gamma \operatorname{grad} \mathcal{E} + n^F \rho^{FR} \mathbf{g} + \hat{\mathbf{p}}_{E\,\text{mech.}}^F \,, \tag{3.108}$$

is obtained by summing over (3.103) and (3.104). In the above relation, use has also been made of (3.72). By inserting (3.80), one ends up with the extended *Darcy*-type equation:

$$\boxed{n^F \mathbf{w}_F = -\frac{k^F}{\gamma^{FR}} \left(\operatorname{grad} \mathcal{P} - \rho^{FR} \mathbf{g} + \sum_\beta \rho_F^\beta \operatorname{grad} \mu^\beta + \sum_\gamma \rho_{eF}^\gamma \operatorname{grad} \mathcal{E} \right) .} \tag{3.109}$$

3.5 Electric potential

The electrical potential $\mathcal{E}$, i. e. the *Lagrange*an multiplier, is still undetermined. In order to derive a corresponding relation, the *Maxwell* relations introduced in Section 2.3.4 are consulted. Within this monograph, it is assumed that the same electromagnetic fields are applied to all of the constituents, i. e. no distinction is made between quantities of the constituents in case of electrodynamic balance relations. Summarising the relations found in Section 2.3.4 , the relevant equations for the nonrelativistic case of uniform electric and magnetic fields $\mathbf{e}_e$ and $\mathbf{h}_e$ applied to a deforming material are given by

$$\begin{aligned}
&\text{electric flux continuity:} && \operatorname{div} \mathbf{d}_e &&= \rho_e \,, \\
&\textit{Ampère}\text{'s law of induction:} && \dot{\mathbf{d}}_e + \left(\operatorname{div} \dot{\mathbf{x}}\, \mathbf{I} - \mathbf{L}^T \right) \mathbf{d}_e &&= \operatorname{rot} \mathbf{h} - \mathbf{i}_e \,, \\
&\textit{Faraday}\text{'s law of induction:} && \dot{\mathbf{b}}_e + \left(\operatorname{div} \dot{\mathbf{x}}\, \mathbf{I} - \mathbf{L}^T \right) \mathbf{b}_e &&= -\operatorname{rot} \mathbf{e}_e \,, \\
&\text{magnetic flux continuity:} && \operatorname{div} \mathbf{b}_e &&= 0 \,.
\end{aligned} \tag{3.110}$$

along with the restrictions given in Section 2.3.1 and Section 2.3.4. Moreover, $\mathbf{d}_e$ and $\mathbf{b}_e$ are given as

$$\begin{aligned} \text{electric flux density}: \qquad \mathbf{d}_e &= \epsilon_0\,\mathbf{e}_e + \textstyle\sum_\gamma \mathbf{p}_e^\gamma\,, \\ \text{magnetic field strength}: \qquad \mathbf{b}_e &= \mu_0\,(\,\mathbf{h}_e + \textstyle\sum_\gamma \mathbf{m}_e^\gamma\,)\,, \end{aligned} \tag{3.111}$$

where $\mathbf{p}_e^\gamma$ and $\mathbf{m}_e^\gamma$ are the material dependent electric and magnetic polarisations:

$$\mathbf{p}_e^\gamma = \epsilon_0\,\chi_{e1}^F\,\mathbf{e}_e \qquad \text{and} \qquad \mathbf{m}_e^\gamma = \chi_{e2}^F\,\mathbf{h}_e\,. \tag{3.112}$$

In the above relations, ϵ_0 denotes the electric permittivity of a vacuum and μ_0 is the magnetic permeability of a vacuum. Moreover, χ_{e1}^F and χ_{e2}^F are the electric and magnetic susceptibilities of the overall fluid[6], which denote the ability of the medium to polarise in response to a given electric or magnetic field.

Remark: In their above representation, the *Maxwell* equations are given in SI[7] units. By writing the *Maxwell* equations in cgs units (centimetre-gramme-second), it appears a number c in above equations, cf., for example, O'Handley [139] and Maugin [133]. This number denotes the velocity of light in a vacuum and is defined as $c = 1/\sqrt{\epsilon_0\,\mu_0}$. □

Considering only static or slowly changing electric and magnetic fields, the time derivatives of the $\mathbf{d}_e$ and $\mathbf{b}_e$ fields can be neglected and, in addition, restricting the considerations to uniform and quasi static deformations, the spatial derivatives of the velocity may be neglected. Thus, the four *Maxwell* relations for electromagnetics are completely decoupled. Following this, and in the absence of magnetic fields, only the first *Maxwell* equation is needed. Therein, the electric flux density can be transformed by use of

$$\epsilon^F \;=\; \epsilon_0\,(\,1 + \chi_{e1}^F\,) \tag{3.113}$$

in $(3.111)_1$, such that a linear relation between the electric field density $\mathbf{d}_e$ and the electric field strength $\mathbf{e}_e$ is derived. Note that this linear case of electrodynamics corresponds to situations where only moderate electric fields are present. Thus,

$$\mathbf{d}_e = \epsilon^F\,\mathbf{e}_e\,, \tag{3.114}$$

where ϵ^F is the constant permittivity of the overall fluid. In electrostatics, the gradient of the electric potential is directly related to the electric field via

$$\mathbf{e}_e = -\operatorname{grad}\mathcal{E}\,. \tag{3.115}$$

Note that the electric potential only exists in electrostatics[8]. Finally, inserting above

[6] Eringen [71] suggests susceptibilities $\chi_e^{\gamma F}$ such that the resistance of each component to polarise can be captured separately. Following Ellison *et al.* [69] and Nörtemann *et al.* [138], the susceptibilities of the ions are measured together, cf. also the argumentation in case of the activity coefficients in Section A.2.

[7] SI units are also denoted as mks units (metre-kilogramme-second).

[8] In case of electrodynamics with oscillating electric and magnetic fields, the electromagnetic force (EMF) has to be introduced. The EMF is actually a vector denoting the force acting on a charge per unit

relations into the first *Maxwell* equation, one finds the *Poisson* equation of the electric potential:

$$\boxed{\operatorname{div}\operatorname{grad}\mathcal{E} = -\frac{1}{\epsilon^F}\,\rho_e\,.} \tag{3.116}$$

Given the above relation, the *Laplace*an of the electric potential of electrostatics is obtained from the sum of all free charges, cf., for example, Avci [7] and Wallmersperger [168].

3.6 Primary variables of the model

Summarising all the considerations made up to now, charged hydrated porous media are fully described by the model derived in this monograph. In particular, the momentum balance of the overall mixture (3.15) and the corresponding stress tensor (3.85) provide a partial differential equation corresponding to the solid displacement $\mathbf{u}_S$. The hydraulic pressure $\mathcal{P}$ corresponds to the overall fluid balance (3.11) and the densities ρ_F^β (or the concentrations c_m^β) to the concentration balances of the fluid components (3.8). Furthermore, the seepage velocities $\mathbf{w}_F$ and $\mathbf{w}_\beta$ are obtained by the relations (3.109), (3.103) and (3.107), while the electric potential $\mathcal{E}$ is obtained from the *Poisson* equation (3.116). Hence, the model is constituted by ten variables:

$$\mathbf{u}_S\,, \quad \mathcal{P}\,, \quad \mathbf{w}_F\,, \quad \rho_F^\beta\,, \quad \mathbf{w}_\beta \quad \text{and} \quad \mathcal{E}\,. \tag{3.117}$$

Note that the displacement and the velocities are even vectorial variables consisting of one element corresponding to each spatial direction. However, this huge amount of unknowns can be reduced by inserting the seepage velocities of φ^F and φ^β into the associated volume and concentration balances. Thus,

$$\mathbf{u}_S\,, \quad \mathcal{P}\,, \quad \rho_F^\beta \quad \text{and} \quad \mathcal{E} \tag{3.118}$$

is the reduced set of primary variables. Concerning the numerical treatment discussed in the next section, the obvious advantage of the second set is that the amount of unknowns is by far less then in the first one. However, if one is interested in highly accurate values of the velocities, the first set should be used within the frame of hybrid finite elements, cf., e. g., Malakpoor [129]. The higher accuracy is achieved by directly discretising the gradients as additional primary variables such that the velocities may be computed by this values instead of calculating them via the derivatives of the primary variables. However, concerning the second set some further considerations are possible. As the saturation of the solutes in the solution is much lower then the saturation of the liquid, cf. (3.75), it can

volume and contributes to the momentum balance of the charged component. Moreover, if the medium under consideration is micropolar or consists of electric and magnetic dipoles, there is an electromagnetic couple force acting on a charged particle and contributing to the balance of moment of momentum. Note that in this case, the *Cauchy* stress in not symmetric anymore. For a detailed introduction into electromagnetism of deformable continua, the interested reader is referred to the textbooks of Eringen & Maugin [72], Maugin [133] and Maugin *et al.* [134].

be assumed that the density (concentration) of the liquid is constant ($\rho_F^L, c_m^L \approx$ const.). This argument can be strengthened by computing the volume of the overall solution via the following volume function of a NaCl solution given in the concentration scale, cf. Klotz & Rosenberg [115],

$$V^F = 1001.38 + 16.2553\,(c_m) + 1.7738\,(c_m)^{3/2} + 0.1194\,(c_m)^2\,, \tag{3.119}$$

where c_m is the molarity of the solution, i. e. the number of moles of NaCl dissolved in the solvent. From the corresponding curve plotted in Figure 3.1 it is apparent that the volume of the overall fluid changes only minimally between the both extreme cases, i. e. pure solvent at $c_m = 0\,\text{mol/l}$ and saturated NaCl solution at $c_m = 6.14\,\text{mol/l}$.

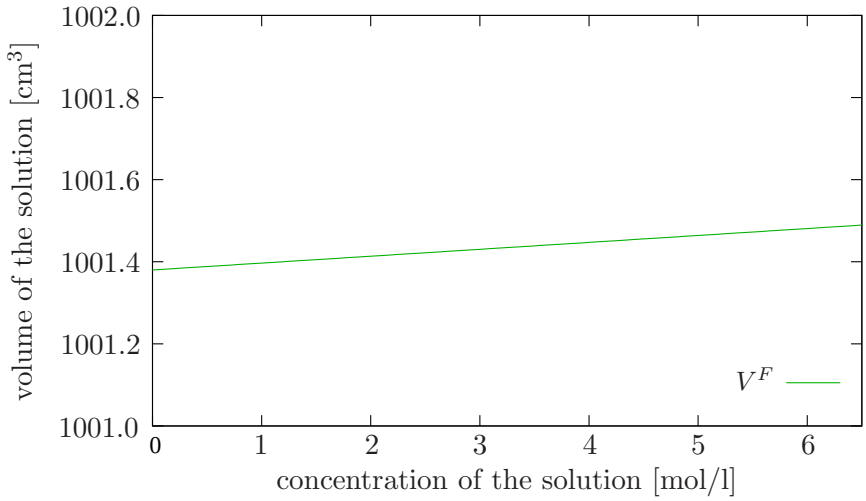

Figure 3.1: The volume of the overall solution at 25 °C in the range of pure solvent (H_2O) to a saturated NaCl solution. The volume changes of the order of 10^{-2} %.

Hence, ρ_F^L (c_m^L), relating the mass (the number of moles) of the component φ^L to the volume of the overall solution, is considered as constant and, therefore, also its chemical potential. By this argumentation, the set of primary variables can further be reduced to five:

$$\boxed{\mathbf{u}_S\,, \quad \mathcal{P}\,, \quad \rho_F^\gamma \quad \text{and} \quad \mathcal{E}\,.} \tag{3.120}$$

Chapter 4:
Numerical treatment

Given the model derived in Chapter 3, the general characteristics of swelling media have been captured within a thermodynamically consistent model based on the TPM. The task in this chapter is to solve the derived set of equations within a numerical approximation scheme such as the Finite Element Method (FEM). As one could already recognise from the different stress tensors and the momentum production terms presented in Section 3.2.10 and Section 3.2.11, different representations of the model are possible. In the next sections, these models corresponding to different choices of primary variables and the respective boundary conditions will be discussed.

To solve the resulting sets of partial differential equations (PDE) within a variational scheme, their weak formulations are required. They will be presented by applying the standard *Galerkin* procedure. Moreover, depending on the chosen set of the primary variables, the boundary conditions need a special treatment. In particular, choosing the overall pressure or the molar concentrations of the ions and also the electric potential as primary variables, one discovers that the corresponding boundary conditions implicitly depend on other primary variables or even on internal variables. The numerical simulations obtained by a conventional treatment of these boundary conditions result in oscillating and, therefore, unsound results. Hence, these boundary conditions will be treated especially as weakly imposed *Dirichlet* boundary conditions using a penalty-like method.

Thereafter, the actual discretisation of the PDE will be briefly discussed. As usual in the FE procedure, two different discretisation schemes will be applied subsequently. The spatial discretisation will be done within the finite element scheme, whereas the time domain is discretised using the finite difference scheme.

Note that in what follows, the densities ρ_F^β will be replaced by the molar concentrations c_m^β via (2.15). From this relation, it is obvious that the choice of either variable is completely interchangeable. But aiming more into the direction of biomechanical applications, the standard quantity used in this area is the molar concentration. Therefore, the following relations are given by use of the variable c_m^β.

4.1 Electrical and chemical relations as initial and boundary conditions

From a chemical point of view, the materials under consideration are immiscible aggregates of macro molecules forming the solid and an interstitial liquid solution. For such an aggregate, Donnan [47] derived the so-called *Donnan* equation, which states that the

product of the ion concentrations in the internal solution in case of equilibrium and the external solution surrounding the medium are equal:

$$c_m^+ \, c_m^- \;=\; \bar{c}_m^+ \, \bar{c}_m^- \,. \tag{4.1}$$

Therein, and in what follows, the values indicated by a bar, i. e. $(\bar{\cdot})$, correspond to values of the external solution. Additionally, using the electroneutrality condition of either solution, cf. (2.20), the following coherences between the concentrations are derived:

$$\begin{aligned} &\text{external solution:} \quad \sum_\gamma \bar{\rho}_e^\gamma \;=\; 0 \qquad \longrightarrow \quad \bar{c}_m^- \;=\; -\frac{z^+}{z^-}\bar{c}_m^+ \,, \\ &\text{internal solution:} \quad \sum_\gamma \rho_e^\gamma \;+\; \rho_e^{fc} \;=\; 0 \quad \longrightarrow \quad c_m^- \;=\; -\frac{1}{z^-}\left(z^+ c_m^+ \;+\; z^{fc} c_m^{fc} \right). \end{aligned} \tag{4.2}$$

Inserting above findings into the *Donnan* equation, the quadratic equation is resolved to calculate the cation and the anion concentration

$$\boxed{c_m^\gamma \;=\; \frac{1}{2\,|z^\gamma|}\sqrt{\left(z^{fc}\, c_m^{fc} \right)^2 \;-\; 4\, z^+ z^- \left(\bar{c}_m^\gamma \right)^2} \;-\; \frac{z^{fc}\, c_m^{fc}}{2\, z^\gamma} \,,} \tag{4.3}$$

respectively. With these relations, one is able to compute the ion concentrations in the equilibrium case, which can be used as initial and boundary conditions. As a result of this consideration, it is assumed that initially the overall aggregate and during the computations the boundary is electrically neutral.

Another initial and boundary condition to describe the state of the solution is the osmotic pressure. Figure 4.1 depicts the situation concerning the pressure at the boundary between the internal and the external solution. Therein, the hydraulic pressure $\mathcal{p}$ is continuous over the boundary, while the osmotic pressure π exhibits a jump. This jump is captured by

$$\Delta\pi \;=\; p \;-\; \bar{p} \;=\; \pi \;-\; \bar{\pi} \,. \tag{4.4}$$

Note that in order to compute $\Delta\pi$, one has to take care of the fact that the solution is composed of multiple dissolved components by using the osmolarity of the solution, i. e. the sum of all concentrations $(\sum_\gamma c_m^\gamma)$. By inserting the osmotic pressures (3.56), one obtains

$$\boxed{\Delta\pi \;=\; R\theta \left[(c_m^+ + c_m^-) - (\bar{c}_m^+ + \bar{c}_m^-) \right] .} \tag{4.5}$$

Since the concentration of the liquid is assumed to be constant, it does not appear in the above equation. For a discussion of the different pressures occurring in the interstitial fluid, cf. also Section 3.2.12.

The third quantity describing the state of an electrolyte solution in equilibrium is the electric potential. Donnan also showed in his contribution from 1911 that the electric

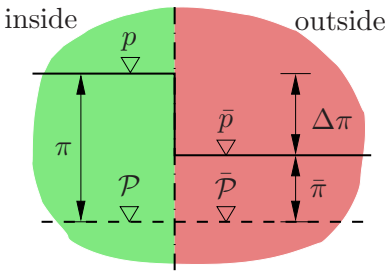

Figure 4.1: The pressure evolution across the interfacial boundary. The difference between the pressures in both regions is the osmotic pressure $\Delta\pi$.

potential difference at the domain boundary is given by

$$\boxed{\Delta\mathcal{E} = \mathcal{E} - \bar{\mathcal{E}} = \frac{R\theta}{z^\gamma F} \ln \frac{\bar{c}_m^\gamma}{c_m^\gamma}.} \tag{4.6}$$

In the literature, the above equation is referred to as the *Donnan* potential and also as the *Nernst* potential (Ott & Boerio-Goates [141]). Note that the choice of the component φ^γ is irrelevant for the value of $\Delta\mathcal{E}$. The electric potential is a quantity which can only be computed or measured relative to a chosen reference point. This is why there exists no absolute value of the electric potential[1]. Additionally, as one can see from all relevant equations, only the gradient of $\mathcal{E}$ plays a role and not its actual value. However, in the general case, where the concentrations on the boundaries differ, the above given concentration-dependent value $\Delta\mathcal{E}$ has to be used as initial and boundary condition. And since the concentration at the boundary is deformation-dependent, cf. (4.3), the value of $\Delta\mathcal{E}$ will change according to the deformation. As a consequence, this deformation-dependent boundary condition has always to be considered irrespective of the choice of the remaining primary variables, cf. next section. Moreover, the electric potential is a *Lagrange*an multiplier just like the hydraulic pressure $\mathcal{P}$ and, therefore, also the value of $\mathcal{E}$ develops only from the value at the boundary. So, if the value of $\mathcal{E}$ at the boundary does not change with the concentration or the deformation, it will not change in the domain as well, except within the non-equilibrium state.

It is important to say that all three of the above equations, i. e. (4.3), (4.5) and (4.6), are only used as initial conditions and as boundary conditions, since during the computations, it is assumed that the boundary layer elements are immediately in equilibrium with the external solution.

4.2 Alternative formulations

As was already mentioned in the introduction of this chapter, the chemical and electric stimulation of charged hydrated porous media can be modelled by use of different sets of primary variables. Regarding the stress tensors in Section 3.2.10 and the momentum

[1] This is also the case for the chemical potentials μ_m^γ.

production terms in Section 3.2.11, it is apparent that different choices are possible. For example, concerning the description of the overall fluid phase, it is possible to choose between the overall pore-fluid pressure p and the hydraulic pressure $\mathcal{P}$. The similar holds for the fluid components, where one can choose between the molar concentrations c_m^γ of the ions and their corresponding chemical potentials μ_m^γ[2], cf. equation (3.48). It is the aim of this section, to summarise these different formulations and to highlight the similarities and the differences.

Before going into details, some remarks have to be given with respect to the boundary conditions. As will be explained in detail later in Section 4.3.1, the boundary corresponding to each PDE is separated into two parts. These are the *Dirichlet* boundaries denoted by $\Gamma_{(\cdot)}$, where the primary variable corresponding to the respective PDE is prescribed, and the *Neumann* boundaries, with prescribed fluxes out of the domain. In the following, the discussed boundary conditions are only valid for the values of the primary variables at *Dirichlet* boundaries[3].

4.2.1 Model variant I

The corresponding set of equations for the first variant of the primary variable combination can already be found in the previous chapter, where the only change made here is the reformulation of the equations in the molar concentrations c_m^β. For convenience, the corresponding stress tensors

$$\begin{aligned}
\mathbf{T}^S &= -n^S\,\mathcal{P}\,\mathbf{I} + n^S\,\Psi_F^F\,\mathbf{I} - n^S\,\textstyle\sum_\beta\, c_m^\beta\,\mu_m^\beta\,\mathbf{I} - \rho_e^{fc}\,\mathcal{E}\,\mathbf{I} + \mathbf{T}^S_{E\text{mech.}}\,,\\
\mathbf{T}^L &= -n^L\mathcal{P}\,\mathbf{I} + n^F\,\Psi_F^L\,\mathbf{I} - n^F c_m^L\,\mu_m^L\,\mathbf{I} + \mathbf{T}^L_{E\text{mech.}}\,,\\
\mathbf{T}^\gamma &= -n^\gamma\mathcal{P}\,\mathbf{I} + n^F\,\Psi_F^\gamma\,\mathbf{I} - n^F c_m^\gamma\,\mu_m^\gamma\,\mathbf{I} - \rho_e^\gamma\,\mathcal{E}\,\mathbf{I} + \mathbf{T}^\gamma_{E\text{mech.}}
\end{aligned} \tag{4.7}$$

and the momentum productions

$$\begin{aligned}
\hat{\mathbf{p}}^L &= \mathcal{P}\,\operatorname{grad} n^L - \Psi_F^L\,\operatorname{grad} n^F + c_m^L\,\mu_m^L\,\operatorname{grad} n^F + \hat{\mathbf{p}}^L_{E\text{mech.}}\,,\\
\hat{\mathbf{p}}^\gamma &= \mathcal{P}\,\operatorname{grad} n^\gamma - \Psi_F^\gamma\,\operatorname{grad} n^F + c_m^\gamma\,\mu_m^\gamma\,\operatorname{grad} n^F + \mathcal{E}\,\operatorname{grad}\rho_e^\gamma + \hat{\mathbf{p}}^\gamma_{E\text{mech.}}
\end{aligned} \tag{4.8}$$

are briefly summarised here. Utilising the above equations in the momentum balances and taking advantage of

$$\operatorname{grad}\left(\,\Psi_F^\beta - c_m^\beta\,\mu_m^\beta\,\right) = -\,c_m^\beta\,\operatorname{grad}\mu_m^\beta\,, \tag{4.9}$$

cf. also (3.102), one obtains a model formulated in the solid displacement $\mathbf{u}_S$, the hydraulic pressure $\mathcal{P}$, the molar chemical potentials μ_m^γ of the ions and the electric potential $\mathcal{E}$. The resulting set of PDE is summarised in Table 4.1. Recalling that the chemical potential of φ^L is constant since $c_m^L \approx$ const., the chemical part of $n^F\mathbf{w}_F$ only depends on μ_m^γ.

[2] Alternatively, one can choose between the densities ρ_F^β and the chemical potentials μ^β, cf. (2.15).
[3] And also as initial conditions within the overall domain.

equation:	variant I: formulation in $\mathbf{u}_S$, $\mathcal{P}$, μ_m^γ, $\mathcal{E}$
momentum:	$\operatorname{div}\left(\mathbf{T}^S_{E\,mech.} - \mathcal{P}\,\mathbf{I} - \pi\,\mathbf{I}\right) + \rho\,\mathbf{g} = \mathbf{0}$
volume:	$\operatorname{div}\left[\,(\mathbf{u}_S)'_S + n^F\mathbf{w}_F\,\right] = 0$
concentration:	$n^F(c_m^\gamma)'_S + c_m^\gamma \operatorname{div}\mathbf{x}'_S + \operatorname{div}\left(n^F c_m^\gamma \mathbf{w}_\gamma\right) = 0$
Poisson:	$\operatorname{div}\operatorname{grad}\mathcal{E} = -\dfrac{1}{\epsilon^F}\,\rho_e$
Darcy:	$n^F\mathbf{w}_F = -\dfrac{k^F}{\gamma^{FR}}\left(\operatorname{grad}\mathcal{P} - \rho^{FR}\mathbf{g} + \sum_\gamma c_m^\gamma \operatorname{grad}\mu_m^\gamma + \sum_\gamma \rho_{eF}^\gamma \operatorname{grad}\mathcal{E}\right)$
Nernst-Planck:	$n^F c_m^\gamma \mathbf{w}_\gamma = -\dfrac{D^\gamma}{R\theta}\left(c_m^\gamma \operatorname{grad}\mu_m^\gamma - c_m^\gamma M_m^\gamma \mathbf{g} + \rho_{eF}^\gamma \operatorname{grad}\mathcal{E}\right) + n^F c_m^\gamma \mathbf{w}_F$

Table 4.1: Set of equations for the formulation in the primary variables $\mathbf{u}_S$, $\mathcal{P}$, μ_m^γ, $\mathcal{E}$.

As is apparent from the set in Table 4.1, if the chemical potentials are chosen as primary variables, one has to find a relation between the chemical potentials μ_m^γ and the concentrations c_m^γ, because their values and material time derivatives are actually needed in the concentration balances. However, since the amount of the ions in the solution also depends on the amount of fixed charges, the relation can not be found by simply inverting μ_m^γ. Instead, it has to be derived by taking care of the electroneutrality constraint. Summing over the chemical potentials of both ions and rearranging the resulting relation leads to

$$c_m^+\,c_m^- = \exp\left(\frac{\Delta\mu_m^+ + \Delta\mu_m^-}{R\theta}\right), \quad \text{where} \quad \Delta\mu_m^\gamma = \mu_m^\gamma - \mu_{m0}^\gamma\,. \tag{4.10}$$

Multiplying equation (2.20) by c_m^γ, the above relation can be incorporated into the electroneutrality condition. From this expression, the missing relation is obtained as

$$c_m^\gamma = \frac{1}{2\,|z^\gamma|}\sqrt{(z^{fc}c_m^{fc})^2 - 4\,z^+z^-\exp\left(\frac{\Delta\mu_m^+ + \Delta\mu_m^-}{R\theta}\right)} - \frac{z^{fc}\,c_m^{fc}}{2\,z^\gamma}\,. \tag{4.11}$$

Considering that the fixed charges concentration c_m^{fc} is a function of the solid displacement, cf. (3.13), the above finding is an expression depending on three of the primary variables, i. e. $c_m^\gamma = c_m^\gamma\left(c_m^{fc}(\mathbf{u}_S)\,,\,\mu_m^+\,,\,\mu_m^-\right)$. Hence, the chain rule has to be applied in order to find its material time derivative,

$$(c_m^\gamma)'_S = \frac{\partial c_m^\gamma}{\partial c_m^{fc}}\left(c_m^{fc}(\mathbf{u}_S)\right)'_S + \sum_{\delta=+,-}\frac{\partial c_m^\gamma}{\partial \mu_m^\delta}\,(\mu_m^\delta)'_S\,. \tag{4.12}$$

Therein the derivatives of c_m^γ with respect to c_m^{fc} and μ_m^γ and the material time derivative

of the fixed charge concentration c_m^{fc} are given by (Mabuma [126]),

$$\begin{aligned}
\frac{\partial c_m^\gamma}{\partial c_m^{fc}} &= \frac{(z^{fc})^2\, c^{fc}}{2|z^\gamma|\sqrt{(z^{fc}c^{fc})^2 \;-\; 4\, z^+ z^-\, \exp\Big(\dfrac{\Delta\mu_m^+ \,+\, \Delta\mu_m^-}{R\theta}\Big)}} \;-\; \frac{z^{fc}}{2\, z^\gamma}\,, \\
\frac{\partial c_m^\gamma}{\partial \mu_m^\delta} &= \frac{z^\gamma \exp\Big(\dfrac{\Delta\mu_m^+ \,+\, \Delta\mu_m^-}{R\theta}\Big)}{|z^\gamma|\, R\theta \sqrt{(z^{fc}c_m^{fc})^2 \;-\; 4\, z^+ z^-\, \exp\Big(\dfrac{\Delta\mu_m^+ \,+\, \Delta\mu_m^-}{R\theta}\Big)}}\,, \qquad (4.13) \\
\big(c_m^{fc}(\mathbf{u}_S)\big)'_S &= \frac{c_{m0S}^{fc}\,(1-n_{0S}^S)}{n^F(\det\mathbf{F}_S - n_{0S}^S)}\,\mathbf{F}_S^{T-1}\,\big(\mathbf{F}_S^{T-1}\,\mathrm{Grad}_S\,(\mathrm{Grad}_S\,\mathbf{u}_S)\big)^{\underline{1}}\,(\mathbf{u}_S)'_S\,.
\end{aligned}$$

At this point, the set of equations for the first variant is complete. Nevertheless, if one pursues the strategy of using electrochemical potentials, above relations are only valid for solutions with uni-valent electrolytes[4], i. e. both of the dissolved ions have the same valences.

The *Dirichlet* boundary conditions for this set of equations are given by

$$\begin{aligned}
\mathbf{u}_S(\mathbf{x},t) &= \bar{\mathbf{u}}_S && \text{on } \Gamma_{\mathbf{u}_S}\,, \\
\mathcal{P}\big(\,\bar{c}_m^\gamma(\mathbf{x},t),\,\bar{\mathcal{P}}(\mathbf{x},t)\,\big) &= \bar{p} \;-\; R\theta \sum_\gamma \bar{c}_m^\gamma && \text{on } \Gamma_{\mathcal{P}}\,, \\
\mu_m^\gamma\big(\,\bar{c}_m^\gamma(\mathbf{x},t)\,\big) &= \bar{\mu}_{m0}^\gamma \,+\, R\theta\, \ln \bar{c}_m^\gamma && \text{on } \Gamma_{\mu_m^\gamma}\,, \\
\tilde{\mathcal{E}}\big(\,c_m^\gamma(\mathbf{u}_S,\,\mu_m^+,\,\mu_m^-),\,\bar{c}_m^\gamma(\mathbf{x},t),\,\bar{\mathcal{E}}(\mathbf{x},t)\,\big) &= \bar{\mathcal{E}} \,+\, \frac{R\theta}{z^\gamma F}\,\ln\frac{\bar{c}_m^\gamma}{c_m^\gamma} && \text{on } \Gamma_{\mathcal{E}}\,,
\end{aligned} \qquad (4.14)$$

where in the above relation and in what follows, $(\tilde{\cdot})$ denotes deformation-dependent *Dirichlet* boundary conditions. The hydraulic pressure boundary condition is obtained by rearranging (4.4) and the one for $\mathcal{E}$ by rearranging (4.6). Moreover, the corresponding relation to compute the chemical potentials from the concentration of the external solution is given by (3.48) and the one for the osmotic pressure by (3.56). From the above relations, it is evident that, in contrast to the boundary conditions of $\mathbf{u}_S$, $\mathcal{P}$ and μ_m^γ, which only depend on known external quantities, the one for the electric potential

[4]For solutions with arbitrary electrolytes based on electrochemical potentials, resolving the sum of the electrochemical potentials results in the exponential function

$$c_m^+\, c_m^- \;=\; \exp\Big(\frac{\Delta\mu_m^+ \,+\, \Delta\mu_m^- \,-\, (z^+ + z^-)F\mathcal{E}}{R\theta}\Big)$$

for the concentrations, i. e. $c_m^\gamma \,=\, c_m^\gamma\,(\,\mathbf{u}_S\,,\,\mu_m^+\,,\,\mu_m^-\,,\,\mathcal{E}\,)$. Note that by use of the electrochemical potential instead of chemical potentials as primary variables, the contribution of the electric potential to the ion diffusion may change, cf. the usage of the chemical potentials as primary variables in Section 5.1 in comparison to the other possible primary variable sets.

additionally depends on the internal variable $c_m^\gamma = c_m^\gamma(c_m^{fc}(\mathbf{u}_S), \mu_m^+, \mu_m^-)$. As a result, the value of $\tilde{\mathcal{E}}$ at the boundary will be concentration- and, therefore, deformation dependent. This kind of boundary conditions need a special treatment, cf. the discussion about deformation-dependent *Dirichlet* boundary conditions in Section 4.3.1 and also the considerations about the electric potential in Section 4.1.

This set of primary variables is quite similar to the one widely used in the literature, cf. Gu *et al.* [86], van Loon *et al.* [122], Sun *et al.* [159]. The reason is that the *Dirichlet* boundary conditions for $\mathbf{u}_S$, $\mathcal{P}$ and μ_m^γ can be imposed strongly, i. e. they may be treated in the standard way, since they are computed only from known external values. In contrast to van Loon *et al.* [122], where the continuity equation (3.24) is used under open-circuit conditions as the determining equation for the electric potential $\mathcal{E}$, $\mathcal{E}$ is computed from the *Poisson* equation in this thesis. Note that the continuity equation yields no additional information (Samson *et al.* [146]), since both of the ion velocities are already solved by insertion into the corresponding volume balances.

4.2.2 Model variant II

Another representation of the model can be found by actually calculating the gradients of the chemical potentials. By this additional step, the concentrations c_m^γ will replace the chemical potentials μ_m^γ as primary variables. Computing the gradients of the molar chemical potentials of the ions given by (3.48), one obtains

$$c_m^\gamma \operatorname{grad} \mu_m^\gamma \;=\; R\theta \operatorname{grad} c_m^\gamma \,. \tag{4.15}$$

Due to the interchange of primary variables, also the set of PDE changes slightly, cf. Table 4.2.

equation	variant II : formulation in $\mathbf{u}_S$, $\mathcal{P}$, c_m^γ, $\mathcal{E}$
momentum:	$\operatorname{div}\left(\mathbf{T}^S_{E\text{mech.}} - \mathcal{P}\,\mathbf{I} - \pi\,\mathbf{I}\right) + \rho\,\mathbf{g} = \mathbf{0}$
volume:	$\operatorname{div}\left[\,(\mathbf{u}_S)'_S + n^F \mathbf{w}_F\,\right] = 0$
concentration:	$n^F (c_m^\gamma)'_S + c_m^\gamma \operatorname{div} \overset{\prime}{\mathbf{x}}_S + \operatorname{div}\left(n^F c_m^\gamma \mathbf{w}_\gamma\right) = 0$
Poisson:	$\operatorname{div}\operatorname{grad}\mathcal{E} = -\dfrac{1}{\epsilon^F}\,\rho_e$
Darcy:	$n^F \mathbf{w}_F = -\dfrac{k^F}{\gamma^{FR}}\left(\operatorname{grad}\mathcal{P} - \rho^{FR}\mathbf{g} + \sum_\gamma \left(R\theta \operatorname{grad} c_m^\gamma + \rho_{eF}^\gamma \operatorname{grad}\mathcal{E}\right)\right)$
Nernst-Planck:	$n^F c_m^\gamma \mathbf{w}_\gamma = -\dfrac{D^\gamma}{R\theta}\left(R\theta \operatorname{grad} c_m^\gamma - c_m^\gamma M_m^\gamma \mathbf{g} + \rho_{eF}^\gamma \operatorname{grad}\mathcal{E}\right) + n^F c_m^\gamma \mathbf{w}_F$

Table 4.2: Set of equations for the formulation in the primary variables $\mathbf{u}_S$, $\mathcal{P}$, c_m^γ, $\mathcal{E}$.

Moreover, also the boundary conditions for the concentration balances have to be adapted:

$$\begin{aligned}
\mathbf{u}_S(\mathbf{x},t) &= \bar{\mathbf{u}}_S && \text{on } \Gamma_{\mathbf{u}_S}\,,\\
\mathcal{P}\big(\,\bar{c}_m^\gamma(\mathbf{x},t),\,\bar{\mathcal{P}}(\mathbf{x},t)\,\big) &= \bar{p} - \sum_\gamma \bar{\pi}^\gamma && \text{on } \Gamma_{\mathcal{P}}\,,\\
\tilde{c}_m^\gamma\big(\,c_m^{fc}(\mathbf{u}_S),\bar{c}_m^\gamma(\mathbf{x},t)\,\big) &= \frac{1}{2\,|z^\gamma|}\sqrt{\big(\,z^{fc}\,c_m^{fc}\,\big)^2 - 4\,z^+z^-\,(\bar{c}_m^\gamma)^2} - \frac{z^{fc}\,c_m^{fc}}{2\,z^\gamma} && \\
& && \text{on } \Gamma_{c_m^\gamma}\,,\\
\tilde{\mathcal{E}}\big(\,c_m^\gamma,\bar{c}_m^\gamma(\mathbf{x},t),\bar{\mathcal{E}}(\mathbf{x},t)\,\big) &= \bar{\mathcal{E}} + \frac{R\theta}{z^\gamma F}\,\ln\frac{\bar{c}_m^\gamma}{c_m^\gamma} && \text{on } \Gamma_{\mathcal{E}}\,.
\end{aligned} \tag{4.16}$$

Therein, the boundary condition for the hydraulic pressure is obtained by rearranging (4.4):

$$p = \bar{p} + \Delta\pi \quad\longrightarrow\quad p - \pi = \bar{p} - \bar{\pi} \quad\longrightarrow\quad \mathcal{P} = \bar{p} - \bar{\pi} \tag{4.17}$$

As is the case in the variant I, the *Dirichlet* boundary condition for the electric potential $\tilde{\mathcal{E}}$ does not only depend on known external values. Instead, it also depends on the primary variable c_m^γ. However, in addition to $\tilde{\mathcal{E}}$ also the *Dirichlet* boundary conditions of the molar concentrations $\tilde{c}_m^\gamma$ are deformation depend, i. e. they depend on the internal variable $c_m^{fc} = c^{fc}(\mathbf{u}_S)$.

4.2.3 Model variant III

Using the alternative representation of the stress tensors and the momentum productions given in Section 3.2.10 and Section 3.2.11, respectively, one obtains a formulation in the primary variables $\mathbf{u}_S$, p, μ^γ and $\mathcal{E}$, where, compared to the variant I, the primary variable $\mathcal{P}$ is substituted by the overall pressure p. More precisely, using the definition of the osmotic pressure (3.51), one finds that

$$\operatorname{grad}\big(\,\Psi_F^\gamma - c_m^\gamma\,\mu_m^\gamma\,\big) = -\operatorname{grad}\pi^\gamma = -c_m^\gamma\operatorname{grad}\mu_m^\gamma\,. \tag{4.18}$$

Thus, by a combination of both pressures, the hydraulic and the osmotic pressure, occurring in the current set of PDE via expression (3.86), one obtains the overall pressure as the primary variable governing the overall fluid.

The corresponding set of PDE for this formulation is summarised in Table 4.3. Note that the missing relations between the chemical potentials and the concentrations have been derived in Section 4.2.1. Finally, also the boundary conditions have to be brought in

equation	variant III : formulation in $\mathbf{u}_S$, p, μ_m^γ, $\mathcal{E}$
momentum:	$\operatorname{div}\left(\mathbf{T}^S_{E\,mech.} - p\,\mathbf{I}\right) + \rho\,\mathbf{g} = \mathbf{0}$
volume:	$\operatorname{div}\left[\,(\mathbf{u}_S)'_S + n^F\mathbf{w}_F\,\right] = 0$
concentration:	$n^F(c_m^\gamma)'_S + c_m^\gamma \operatorname{div}\overset{\prime}{\mathbf{x}}_S + \operatorname{div}\left(n^F c_m^\gamma \mathbf{w}_\gamma\right) = 0$
Poisson:	$\operatorname{div}\operatorname{grad}\mathcal{E} = -\dfrac{1}{\epsilon^F}\,\rho_e$
Darcy:	$n^F\mathbf{w}_F = -\dfrac{k^F}{\gamma^{FR}}\left(\operatorname{grad} p - \rho^{FR}\mathbf{g} + \sum_\gamma \rho_{eF}^\gamma \operatorname{grad}\mathcal{E}\right)$
Nernst-Planck:	$n^F c_m^\gamma \mathbf{w}_\gamma = -\dfrac{D^\gamma}{R\theta}\left(c_m^\gamma \operatorname{grad}\mu_m^\gamma - c_m^\gamma M_m^\gamma\,\mathbf{g} + \rho_{eF}^\gamma \operatorname{grad}\mathcal{E}\right) + n^F c_m^\gamma \mathbf{w}_F$

Table 4.3: Set of equations for the formulation in the primary variables $\mathbf{u}_S$, p, μ_m^γ, $\mathcal{E}$.

accordance with the primary variables:

$$\boxed{\begin{aligned}
\mathbf{u}_S(\mathbf{x},t) &= \bar{\mathbf{u}}_S && \text{on } \Gamma_{\mathbf{u}_S}\,,\\
\tilde{p}\big(\,c_m^\gamma(\mathbf{u}_S,\,\mu_m^+,\,\mu_m^-),\,\bar{c}_m^\gamma(\mathbf{x},t),\,\bar{\mathcal{P}}(\mathbf{x},t)\,\big) &= \bar{p} + \Delta\,\pi && \text{on } \Gamma_p\,,\\
\mu_m^\gamma\big(\,\bar{c}_m^\gamma(\mathbf{x},t)\,\big) &= \bar{\mu}_{m0}^\gamma + R\theta\,\ln\bar{c}_m^\gamma && \text{on } \Gamma_{\mu_m^\gamma}\,,\\
\tilde{\mathcal{E}}\big(\,c_m^\gamma(\mathbf{u}_S,\,\mu_m^+,\,\mu_m^-),\,\bar{c}_m^\gamma(\mathbf{x},t),\,\bar{\mathcal{E}}(\mathbf{x},t)\,\big) &= \bar{\mathcal{E}} + \frac{R\theta}{z^\gamma F}\,\ln\frac{\bar{c}_m^\gamma}{c_m^\gamma} && \text{on } \Gamma_\mathcal{E}\,.
\end{aligned}} \tag{4.19}$$

As is evident from the above relations, by use of this set of primary variables, compared to the variant I, besides $\tilde{\mathcal{E}}$ also the *Dirichlet* boundary condition $\tilde{p}$ corresponding to the overall pressure p depends on internal variables. In particular, the pressure boundary condition consists of two terms, the applied hydraulic pressure in the external solution and the difference in the osmotic pressure, cf. equation (4.5).

4.2.4 Model variant IV

The last model variant is the combination of model variants II and III, where the primary variables μ_m^γ are replaced by c_m^γ and the hydraulic pressure $\mathcal{P}$ by the overall pressure p. From an engineering point of view, both of these quantities are rather easy to measure and this fact is especially useful for the comparison with experimental results. The gradients of the chemical potentials are calculated via (4.15), which finally leads to the resulting set of equations given in Table 4.4.

Regarding the boundary conditions, this formulation is the most sophisticated case. In

equation	variant IV : formulation in $\mathbf{u}_S$, p, c_m^γ, $\mathcal{E}$
momentum:	$\operatorname{div}\left(\mathbf{T}^S_{E\,mech.} - p\,\mathbf{I}\right) + \rho\,\mathbf{g} = \mathbf{0}$
volume:	$\operatorname{div}\left[\,(\mathbf{u}_S)'_S + n^F\mathbf{w}_F\,\right] = 0$
concentration:	$n^F(c_m^\gamma)'_S + c_m^\gamma \operatorname{div}\overset{\prime}{\mathbf{x}}_S + \operatorname{div}\left(n^F c_m^\gamma \mathbf{w}_\gamma\right) = 0$
Poisson:	$\operatorname{div}\operatorname{grad}\mathcal{E} = -\dfrac{1}{\epsilon^F}\,\rho_e$
Darcy:	$n^F\mathbf{w}_F = -\dfrac{k^F}{\gamma^{FR}}\left(\operatorname{grad}p - \rho^{FR}\mathbf{g} + \sum\limits_\gamma \rho_{eF}^\gamma \operatorname{grad}\mathcal{E}\right)$
Nernst-Planck:	$n^F c_m^\gamma \mathbf{w}_\gamma = -\dfrac{D^\gamma}{R\theta}\left(R\theta \operatorname{grad} c_m^\gamma - c_m^\gamma M_m^\gamma \mathbf{g} + \rho_{eF}^\gamma \operatorname{grad}\mathcal{E}\right) + n^F c_m^\gamma \mathbf{w}_F$

Table 4.4: Set of equations for the formulation in the primary variables $\mathbf{u}_S$, p, c_m^γ, $\mathcal{E}$.

particular, the *Dirichlet* boundary conditions for this set of primary variables are given by

$$
\begin{aligned}
\mathbf{u}_S(\mathbf{x},t) &= \bar{\mathbf{u}}_S && \text{on } \Gamma_{\mathbf{u}_S}\,,\\
\tilde{p}\big(c_m^\gamma,\, \bar{c}_m^\gamma(\mathbf{x},t),\, \bar{\mathcal{P}}(\mathbf{x},t)\big) &= \bar{p} + \Delta\pi && \text{on } \Gamma_p\,,\\
\tilde{c}_m^\gamma\big(c_m^{fc}(\mathbf{u}_S), \bar{c}_m^\gamma(\mathbf{x},t)\big) &= \frac{1}{2\,|z^\gamma|}\sqrt{\left(z^{fc}\,c_m^{fc}\right)^2 - 4\,z^+z^-\,(\bar{c}_m^\gamma)^2} - \frac{z^{fc}\,c_m^{fc}}{2\,z^\gamma} && \\
& && \text{on } \Gamma_{c_m^\gamma}\,,\\
\tilde{\mathcal{E}}\big(c_m^\gamma,\, \bar{c}_m^\gamma(\mathbf{x},t),\, \bar{\mathcal{E}}(\mathbf{x},t)\big) &= \bar{\mathcal{E}} + \frac{R\theta}{z^\gamma F}\,\ln\frac{\bar{c}_m^\gamma}{c_m^\gamma} && \text{on } \Gamma_{\mathcal{E}}\,.
\end{aligned}
\tag{4.20}
$$

As one can see from the above set, all boundary conditions except the one for the displacement either depend on internal or on primary variables. As has already been mentioned in the previous sections, this kind of boundary conditions have to be treated in a special way as described in Section 4.3.1.

4.2.5 Additional possibilities

The models presented in the previous four subsections are capable to capture all effects appearing in charged hydrated porous media. In particular, deformations resulting from mechanical forces, fluid movement based on pressure, concentration and electric potential gradients, ion diffusion generated by varying concentrations and electric potentials as well as electric currents due to changes in concentrations and electric potentials are covered. Based on several further assumptions, these aforementioned most general models can

be reduced. It is the aim of this subsection to give an overview of possible additional assumptions with the resulting set of equations and the corresponding set of primary variables.

All the following considerations are based on the model variant IV, since this is the version which is most suitable for simplifications. Considering the model variants I and II, it has been observed during numerical simulations, that by neglecting electric currents the computations based on the chemical potentials as primary variables get unstable and lead to wrong results. The reason is that, firstly, the concentrations of the ions are computed from the square root of exponential functions, which may lead to numerical difficulties, and, secondly, the second derivative of the solid displacement $\mathbf{u}_S$ is needed to compute the material time derivatives $(c_m^\gamma)'_S$ of the ion concentrations. Moreover, using such a model, both of the chemical potentials are needed to compute the concentrations of the ions. Therefore, it is not possible to reduce the variants I and II to models governed by less than four primary variables.

Simplification I: No electric current

In order to model electro-osmotic effects within charged hydrated porous media, small deviations from the electroneutrality condition are required, i. e. the electroneutrality condition has to be fulfilled weakly by use of the *Poisson* equation. Otherwise, no voltage can be applied at the boundary and, thus, no electric currents will occur. To allow this small deviations, all charged constituents need to be regarded. In contrast, the swelling behaviour of these materials is fully captured without explicitly considering electric quantities. Thus, the first obvious possibility to simplify the model is to exclude electric currents over the surface resulting from potential differences. Note that within the specimen, the electric current originates from different sources which are not assumed to vanish individually. In particular, convection current occurs because of changes of the hydraulic as well as of the osmotic pressure ($\operatorname{grad}\mathcal{P}$ and $\operatorname{grad} c_m^\gamma$), whereas diffusion current is caused by concentration differences ($\operatorname{grad} c_m^\gamma$). Both of these currents compete with the conduction current resulting from differences of the electrostatic force within the specimen ($\operatorname{grad}\mathcal{E}$). For a more detailed explanation, the interested reader is referred to Lai *et al.* [117]. Following this argumentation, the *Poisson* equation can be omitted from the list of partial differential equations. Also in *Darcy*'s law, the sum of ρ_e^γ has to be replaced by $-\rho_e^{fc}$ via the electroneutrality condition[5]. As a result of this assumption, the electric potential can not be computed anymore and its gradient has to be obtained from the condition that no net electric current occurs within the domain. The corresponding

[5]This step is important for numerical stability reasons.

relation for the electric current is[6], cf. Lai *et al.* [116] and Sun *et al.* [159],

$$\mathbf{i} = \sum_{\gamma} \rho_e^{\gamma} \mathbf{w}_{\gamma} = \mathbf{0} \,. \tag{4.21}$$

Inserting the extended *Nernst-Planck* equations into the above relation, the gradient of the electric potential can be computed:

$$\begin{aligned} F \operatorname{grad} \mathcal{E} \;=\; & \Big[z^{fc} D^L \operatorname{grad} p + \big(z^+ D^+ \rho_F^+ + z^- D^- \rho_F^- - z^{fc} D^L \rho^{FR} \big) \mathbf{g} - \\ & - \sum_{\gamma} \big(z^{\gamma} D^{\gamma} R\theta \operatorname{grad} c_m^{\gamma} \big) \Big] \Big/ \Big[(z^+)^2 D^+ c_m^+ + (z^-)^2 D^- c_m^- + (z^{fc})^2 D^L c_m^{fc} \Big] \,. \end{aligned} \tag{4.22}$$

Thereafter, the gradient of $\mathcal{E}$ can be replaced in the *Darcy*'s law and the *Nernst-Planck* equations. An alternative representation of (4.22) formulated in the hydraulic pressure is given in Appendix B.2. Moreover, in the above relation, the abbreviation

$$D^L = \frac{k^F c^{fc} R\theta}{\gamma^{FR}} \tag{4.23}$$

has been used, where D^L can be interpreted as the diffusion coefficient of the liquid solvent (Sun *et al.* [159]). By the above procedure, net electric currents within the domain and over the surface are excluded and the set of primary variables is reduced by one to

$$\mathbf{u}_S \,, \quad p \,, \quad c_m^{\gamma} \,. \tag{4.24}$$

The set of boundary conditions for this set of primary variables is not explicitly listed here, since they are the same as for the variant IV, except that there is no need for a boundary condition for $\mathcal{E}$, cf. Table 4.4.

Simplification II: Locally fulfilled electroneutrality

The restrictions (2.20) can be utilised once more to further reduce the number of primary variables. Considering equation (4.2) and, in the case of a negatively charged solid matrix, choosing the cation concentration c_m^+ as the primary variable c_m, the anion concentration

[6] A way to derive this relation is via the weak formulation of the continuity equation (3.24). Concerning weak formulations cf. Section 4.3.1. Multiplying the equation by a test function $\delta\iota$, integrating this product partially over the volume and shifting the integral containing the divergence term onto the surface, the condition for the electric current over the surface is obtained:

$$\int_{\Omega} \operatorname{grad} \delta\iota \cdot \big(\sum_{\gamma} \rho_e^{\gamma} \mathbf{w}_{\gamma} \big) \, \mathrm{d}v = \int_{\Gamma} \delta\iota \big(\sum_{\gamma} \rho_e^{\gamma} \mathbf{w}_{\gamma} \big) \cdot \mathrm{d}\mathbf{a} \,.$$

In case of isolated conditions, there is no electric current over the surface and the right-hand side, i. e. the surface integral, is zero. Following this, the left-hand side has to be zero as well for arbitrary values of $\operatorname{grad} \delta\iota$. Thus, the term in the braces has to vanish, i. e. $\sum_{\gamma} \rho_e^{\gamma} \mathbf{w}_{\gamma} = \mathbf{0}$. Based on this relation it is possible to compute the gradient of $\mathcal{E}$.

may be computed directly from the electroneutrality conditions:

$$\begin{aligned} &\text{external solution:} \quad \sum_{\gamma} \bar{\rho}_e^{\gamma} = 0 \qquad \longrightarrow \quad \bar{c}_m^- = -\frac{z^+}{z^-}\,\bar{c}_m\,, \\ &\text{internal solution:} \quad \sum_{\gamma} \rho_e^{\gamma} + \rho_e^{fc} = 0 \quad \longrightarrow \quad c_m^- = -\frac{1}{z^-}\,(\,z^+\,c_m + z^{fc}\,c_m^{fc}\,)\,. \end{aligned} \tag{4.25}$$

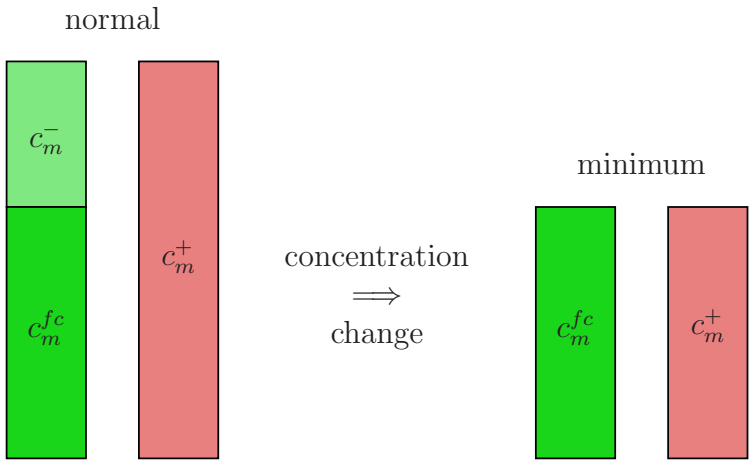

Figure 4.2: Normal concentration distribution for negatively charged solids on the left. Residual concentration distribution fulfilling the electroneutrality condition on the right.

The choice of the cations as the primary variable for such a model is based on numerical reasons. In normal situations, as depicted for a negatively charged solid skeleton on the left-hand side of Figure 4.2, each concentration will have a certain value. Considering an infinite dilute external solution, c_m^+ within the medium will tend to the amount of c_m^{fc} to maintain electroneutrality, while the amount of the anions c_m^- will reach zero; and vice versa for a positively charged solid matrix. Following the above considerations, the anion concentration is not a primary variable anymore and the corresponding concentration balance can be omitted from the list of equations to be solved. The set of PDE of the remaining model, consisting of the three primary variables

$$\mathbf{u}_S\,, \quad p\,, \quad c_m\,, \tag{4.26}$$

is summarised in Table 4.5. Note that also for this model, (4.22) is required to compute the gradient of $\mathcal{E}$. But, in addition, the second derivative of the solid displacement $\mathbf{u}_S$ has to be used therein, cf. $(4.13)_2$. The reason is that only one of the ions is modelled and, thus, the anion concentration in (4.22) has to be expressed via $(4.25)_2$.

Moreover, the anion diffusion velocity may be computed using $(4.25)_2$ in relation (3.107) of φ^-. Thus, the model is characterised by a strongly fulfilled electroneutrality condition, i. e. locally at each point, and at every instance of time. The *Dirichlet* boundary conditions

equation	simplification II: formulation in $\mathbf{u}_S$, p, c_m
momentum:	$\operatorname{div}\left(\mathbf{T}^S_{E\,mech.} - p\,\mathbf{I}\right) + \rho\,\mathbf{g} = \mathbf{0}$
volume:	$\operatorname{div}\left[\,(\mathbf{u}_S)'_S + n^F\mathbf{w}_F\,\right] = 0$
concentration:	$n^F(c_m)'_S + c_m \operatorname{div}\mathbf{x}'_S + \operatorname{div}\left(n^F c_m \mathbf{w}_+\right) = 0$
Darcy:	$n^F\mathbf{w}_F = -\dfrac{k^F}{\gamma^{FR}}\left(\operatorname{grad} p - \rho^{FR}\mathbf{g} - \rho^{fc}_{eF}\operatorname{grad}\mathcal{E}\right)$
Nernst-Planck:	$n^F c_m\mathbf{w}_+ = -\dfrac{D^+}{R\theta}\left(R\theta\operatorname{grad} c_m - c^\gamma_m M^\gamma_m\mathbf{g} + \rho^+_{eF}\operatorname{grad}\mathcal{E}\right) + n^F c_m\mathbf{w}_F$

Table 4.5: Set of equations for the formulation in the primary variables $\mathbf{u}_S$, p, c_m.

corresponding to this set of primary variables are given by

$$\boxed{\begin{aligned} \mathbf{u}_S(\mathbf{x},t) &= \bar{\mathbf{u}}_S && \text{on } \Gamma_{\mathbf{u}_S}\,, \\ \tilde{p}\big(c_m,\,\bar{c}_m(\mathbf{x},t),\,\bar{\mathcal{P}}(\mathbf{x},t)\big) &= \bar{p} + \Delta\pi && \text{on } \Gamma_p\,, \\ \tilde{c}_m\big(c^{fc}_m(\mathbf{u}_S),\bar{c}_m(\mathbf{x},t)\big) &= \frac{1}{2\,z^+}\sqrt{\left(z^{fc}\,c^{fc}_m\right)^2 - 4\,z^+z^-\,(\bar{c}_m)^2} - \frac{z^{fc}\,c^{fc}_m}{2\,z+} \\ & && \text{on } \Gamma_{c_m}\,. \end{aligned}} \tag{4.27}$$

Simplification III: Chemical potential of the liquid

Starting from the reduced model previously introduced, it is possible to assume that the chemical potential μ^L_m of the liquid solvent is not constant. To achieve this, c^L_m is, firstly, replaced by the partial liquid pressure p^L via the ideal gas law (A.5) and, secondly, the pressure is exchanged by the mole fraction x^L_m with the aid of *Raoult*'s law ($p^L = x^L_m\,p^L_0$), cf. also the remark on page 117 in Appendix A.1. The molar fraction of the liquid in turn is expressed via the molar concentrations of all fluid components, cf. (2.17). By this step, and still assuming that the molar concentration c^L_m of the liquid is constant, the chemical potential is formulated using the quantities of the solutes:

$$\mu^L_m = \mu^L_{m0} + R\theta\,\ln\frac{c^L_m}{c^L_m + c^+_m + c^-_m}\,. \tag{4.28}$$

For more details on this formulation cf. Ehlers & Acartürk [58] and Ehlers *et al.* [66]. But note that such a formulation with a chemical potential depending on the quantities of other fluid components is not consistent with the *Helmholtz* free energy derived within this thesis.

Simplification IV: Slightly changing concentrations

Generally, in biological tissues, only very low concentration changes will occur. Following this argumentation, the lastly described model may further be reduced by assuming that the equilibrium within the domain is reached immediately. This fact directly leads to the statement of rapidly diffusing ions such that the corresponding volume balance of the cations may be neglected and dropped from the list. This assumption is also called *Lanir*'s assumption (Lanir [118]) and is discussed in detail in the frame of the TPM along with finite visco-elasticity and anisotropy in Karajan [113] and in Ehlers *et al.* [63, 64]. The result is an extended two-phase model capable of describing osmotic effects. The advantage of this model with only two primary variables is that the behaviour of biological soft tissues such as the intervertebral disc is captured quite well. Moreover, real scale computations with complex and realistic geometries may be performed. However, this model will not be discussed further on within this thesis. Instead, the interested reader is referred to the contributions cited above.

4.3 Finite Element Method

The models previously derived and given by their respective set of PDE will be solved within the FEM. Therefore, after the introduction of the ansatz and test functions corresponding to each primary variable, the weak forms of the previously found PDE will be derived. Since the model variant IV is the most sophisticated one with respect to the boundary conditions, this variant is exemplary chosen for the derivation of the weak forms. Therein, the deformation-dependent *Dirichlet* boundary conditions will be treated especially by incorporation into the weak forms using a penalty-like method.

After having found the weak form of the corresponding PDE, they will firstly be discretised in the spatial domain. The spatial integration of the semi-discrete system will be carried out by the *Gauß* quadrature. Moreover, after applying the time discretisation by the implicit *Euler* scheme, the numerical solution procedure by the *Newton* method will be discussed briefly.

For a more general introduction into the Finite Element Method, the interested reader is referred to the works by, for example, Bathe [10], Braess [32], Schwarz [152] and Zienkiewicz & Taylor [172]. Concerning the Finite Element procedure applied to porous materials, cf., for example, Ammann [3], Ehlers & Ellsiepen [61] and Ellsiepen [70].

4.3.1 Weak formulations and weakly fulfilled *Dirichlet* boundary conditions

The discussions within this section are based on the set of PDE given in Table 4.4. Therein, the equations are given in their strong representations valid for each spatial point $\mathbf{x}$. Since this is too strict for a numerical solution strategy, the equations in this set will be transformed into their corresponding weak formulations. The resulting set will then be valid for the whole considered domain in an integral manner and not for each

spatial point.

Dirichlet and *Neumann* boundaries

First, the boundary $\Gamma = \partial\Omega$ of the considered domain Ω is splitted into to two regions: the *Dirichlet* boundaries where the primary variable itself is prescribed and the *Neumann* boundaries with the prescribed efflux over the boundary. Following this argumentation, each PDE has its own boundary Γ, which is the set union of its *Dirichlet* and *Neumann* boundaries, i. e.

$$\begin{aligned} \Gamma_S &= \Gamma_{\mathbf{u}_S} \cup \Gamma_{\bar{\mathbf{t}}}\,, & \Gamma_F &= \Gamma_p \cup \Gamma_{\bar{q}}\,, & \Gamma_\gamma &= \Gamma_{c_m^\gamma} \cup \Gamma_{\bar{\jmath}^\gamma}\,, & \Gamma_P &= \Gamma_\varepsilon \cup \Gamma_{\bar{e}}\,, \\ \emptyset &= \Gamma_{\mathbf{u}_S} \cap \Gamma_{\bar{\mathbf{t}}}\,, & \emptyset &= \Gamma_p \cap \Gamma_{\bar{q}}\,, & \emptyset &= \Gamma_{c_m^\gamma} \cap \Gamma_{\bar{\jmath}^\gamma}\,, & \emptyset &= \Gamma_\varepsilon \cap \Gamma_{\bar{e}}\,, \end{aligned} \tag{4.29}$$

where, as denoted by the empty set $\emptyset$, only either of the conditions can be applied to one part of the boundary, cf. Figure 4.3. The *Dirichlet* boundary conditions are also referred as the essential and the *Neumann* ones also as the natural boundary conditions. Moreover,

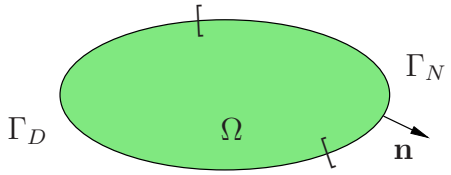

Figure 4.3: Domain Ω with mutually exclusive *Dirichlet* boundaries Γ_D and *Neumann* boundaries Γ_N.

in above relations, besides the *Dirichlet* boundaries denoted by the primary variables as subscripts, the subscript $\bar{\mathbf{t}}$ indicates the boundary with applied stresses, $\bar{q}$ the boundaries with fluid efflux, $\bar{\jmath}^\gamma$ the boundaries with ion effluxes and $\bar{e}$ the applied electric field.

Ansatz and test functions

The trial and test spaces appropriate to the primary variables and the test functions, respectively, will be defined within this section. In particular, the trial (ansatz) functions of the primary variables are given within their spaces by

$$\begin{aligned} \mathcal{S}_{\mathbf{u}_S}(t) &:= \{\ \mathbf{u}_S \in H^1(\Omega)^d : \mathbf{u}_S(\mathbf{x}) = \bar{\mathbf{u}}_S(\mathbf{x},t) && \text{on } \Gamma_{\mathbf{u}_S}\ \} \subset H^1(\Omega)^d\,, \\ \mathcal{S}_p(t) &:= \{\ p \in H^1(\Omega)\ :\ p(\mathbf{x}) = \tilde{p}\big(c_m^\gamma(\mathbf{x}),\, \bar{c}_m^\gamma(\mathbf{x},t),\, \bar{\mathcal{P}}(\mathbf{x},t)\big) && \text{on } \Gamma_p\ \} \subset H^1(\Omega)\,, \\ \mathcal{S}_{c_m^\gamma}(t) &:= \{\ c_m^\gamma \in H^1(\Omega)\ : c_m^\gamma(\mathbf{x}) = \tilde{c}_m^\gamma\big(c_m^{fc}(\mathbf{u}_S), \bar{c}_m^\gamma(\mathbf{x},t)\big) && \text{on } \Gamma_{c_m^\gamma}\ \} \subset H^1(\Omega)\,, \\ \mathcal{S}_\varepsilon(t) &:= \{\ \mathcal{E} \in H^1(\Omega)\ :\ \mathcal{E}(\mathbf{x}) = \tilde{\mathcal{E}}\big(c_m^\gamma(\mathbf{x}),\, \bar{c}_m^\gamma(\mathbf{x},t),\, \bar{\mathcal{E}}(\mathbf{x},t)\big) && \text{on } \Gamma_\varepsilon\ \} \subset H^1(\Omega)\,, \end{aligned} \tag{4.30}$$

where H^1 denotes the *Sobolev* spaces corresponding to functions, which first derivatives are square integrable within the domain Ω, cf. Braess [32] and Steeb [158], and d denotes

the dimension of the problem ($d \in \{1, 2, 3\}$). At the domain boundary, the trial functions are given by their *Dirichlet* values. In case of $\mathbf{u}_S$, the function directly fulfils the applied displacement $\bar{\mathbf{u}}_S(\mathbf{x}, t)$ at the boundary. In contrast, the respective values for the overall pressure, the ion concentrations and the electric potential depend on other primary or internal variables and have to be computed via the relations (4.20). In addition, the test spaces corresponding to the test functions are defined by

$$\begin{aligned}
\mathcal{T}_{\mathbf{u}_S} &:= \{\ \delta\mathbf{u}_S \in H^1(\Omega)^d\ :\ \delta\mathbf{u}_S(\mathbf{x}) = \mathbf{0}\ \text{ on }\ \Gamma_{\mathbf{u}_S}\ \}\,, \\
\mathcal{T}_{p} &:= \{\ \delta p \in H^1(\Omega)\ :\ \delta p(\mathbf{x}) = 0\ \text{ on }\ \Gamma_{p}\ \}\,, \\
\mathcal{T}_{c_m^\gamma} &:= \{\ \delta c_m^\gamma \in H^1(\Omega)\ :\ \delta c_m^\gamma(\mathbf{x}) = 0\ \text{ on }\ \Gamma_{c_m^\gamma}\ \}\,, \\
\mathcal{T}_{\varepsilon} &:= \{\ \delta\mathcal{E} \in H^1(\Omega)\ :\ \delta\mathcal{E}(\mathbf{x}) = 0\ \text{ on }\ \Gamma_{\varepsilon}\ \}\,.
\end{aligned} \tag{4.31}$$

Following this, the test functions are defined in a subspace of H^1, where the corresponding functions disappear at the *Dirichlet* boundaries.

Weak imposition of *Dirichlet* boundary conditions

As has already been mentioned in Section 4.1 and Section 4.2, some of the essential boundary conditions of the PDE depend on the current state of the domain. Considering the variant IV, these dependencies result either from the need of internal variables or of other primary variables to compute the *Dirichlet* value at the boundary of the PDE under consideration. While the former case applies to the molar concentration $(4.20)_3$ depending on $c_m^{fc}(\mathbf{u}_S)$, the latter one applies to the boundary conditions of the overall pressure $\tilde{p}$ and the electric potential $\tilde{\mathcal{E}}$ both depending on the molar concentrations c_m^γ.

If these boundary conditions are applied by use of a standard scheme, where the prescribed *Dirichlet* value at the boundary is simply matched through the degrees of freedom, the numerical simulations will start to oscillate apparently around the equilibrium state, cf. also Section 4.3.6. This numerical instabilities resulting from such deformation-dependent concentration and pressure boundary conditions have also been observed by other authors, cf. Snijders *et al.* [155]. In their contribution, the authors regarded these problems by use of a *Lagrange*-multiplier method. But note that this method increases the number of unknowns by one for each restriction to be applied and, hence, increases the numerical effort to solve the system of equations. Other possibilities which have been tried to overcome the numerical difficulties were to average the value of c_m^{fc} over adjacent nodes or to use the value of this variable from an inner element layer, cf. Acartürk *et al.* [1]. By use of these first approaches, the oscillations could be avoided and the problem could be isolated.

Such deformation-dependent boundary conditions are also known in the field of modelling fluid-structure interactions (FSI), moving boundaries or free surfaces (Dowell & Hall [48], Tezduyar [161], Wall [166]). From the fluid-mechanical point of view, in case of FSI, the conditions at the fluid boundary change with the deformation of the structure. There are three different possible solutions for such problems, cf. Felippa & Park

[73], Felippa *et al.* [74] or Wall [166]: (1) simultaneous methods, (2) partitioned methods and (3) field-elimination methods. In the case of a simultaneous solution, both the fluid and the structure are solved simultaneously within one combined computational algorithm considering all physical properties, i. e. use is made of a monolithic solution of the strongly coupled problem. In contrast, applying the partitioned solution strategy, both parts, the structure and the fluid solution, are computed in an iterative manner (staggered scheme) using different specialised and effective algorithms by applying the solution of one domain as a load on the other domain. The third possibility, when all the governing equations concerning one component are eliminated such as describing the interaction between a fluid and a stiff solid structure, is usually avoided in the field of FSI [166] since there is no interaction anymore.

In case of free surface flow problems, there is also an additional restriction needed to model moving boundaries. Depending on the basic choice of the setting, i. e., *Lagrange*an, *Eule*rian or arbitrary *Lagrange*an-*Eule*rian, different possibilities for the implementation of the additional condition are possible, cf., e. g., Scardovelli & Zaleski [147] for a review in *Eule*rian settings. Considering firstly the *Lagrange*an setting, which is also used in the present contribution, the governing equations are given such that the FE mesh moves with the free surface. For this formulation, Hirt *et al.* [98] introduced additional primary variables maintaining the extra conditions at the free surface boundary. Later, Hansbo [88], Ramaswamy & Kawahara [144] and Radovitzky & Ortiz [143] incorporated the boundary condition for the free surface into the *Lagrange*an weak form of the *Navier-Stokes* equation for single-phasic fluids. Considering secondly the *Eule*rian setting with a fixed mesh, as it is usually chosen in fluid mechanics, one proceeds from methods like the surface marker method to locate the boundary. Currently, the arbitrary *Lagrange*an-*Eule*rian (ALE) formulation is mostly used, where the boundary is described in an *Lagrange*an and the domain in an *Eule*rian setting, cf., e. g., Hirt *et al.* [97], Wall *et al.* [167].

From these facts, it has been found to be the best procedure to impose the *Dirichlet* boundary conditions weakly, cf. also Ehlers & Acartürk [58]. This will be achieved in the following section by incorporation of the boundary conditions into the weak formulation of the corresponding balance relation via a penalty-like method, cf. Hansbo & Hermansson [89] and Zienkiewicz *et al.* [173]. By use of this procedure, the boundary conditions are always calculated within the element-wise routine of the residuum within each *Newton* step, cf. also Section 4.4. As a result, they always coincide with the current state of the primary variables, thus, overcoming the problem of spurious oscillations. Note in passing that the weak imposition of *Dirichlet* boundary conditions is performed for four primary variables simultaneously, i. e. the overall pressure p, both of the molar concentrations c_m^γ and the electric potential $\mathcal{E}$.

Weak formulations (Variant IV)

Each balance relation as well as the *Poisson* equation given in Table 4.4 is related to one primary variable. In particular, the momentum balance of the mixture is directly connected with the solid displacement $\mathbf{u}_S$, the fluid volume balance with the overall pressure

p, the concentration balances with the concentration of the corresponding ion c^γ_m and the *Poisson* equation with the electric potential $\mathcal{E}$. The weak forms of these relations are obtained by multiplying each relation by an arbitrary test function, i. e. $\delta\mathbf{u}_S$, δp, δc^γ_m and $\delta\mathcal{E}$, respectively, and integrating the resulting relations over the domain Ω. Thereafter, carrying out integration by parts, a divergence term appears, which is then shifted onto the surface via the *Gauß*ian integral theorem, cf. Ehlers [57]. A more detailed introduction concerning the weak formulation of PDE is given in, for example, Bathe [10], Ehlers *et al.* [62] and Zienkiewicz & Taylor [172]. By this procedure, the balance relations do not need to be fulfilled locally (strongly) for each spatial point $\mathbf{x}$ but in an integral (weak) manner for the overall domain Ω. Moreover, by integration by parts also the order of appearing spatial derivatives is decreased by one. For example in case of the momentum balance, the second derivative of the primary variable $\mathbf{u}_S$ is needed in its strong representation, whereas in its weak form only the first derivative of $\mathbf{u}_S$ will appear. Moreover, recalling that the test functions are defined to be zero on *Dirichlet* boundaries, cf. (4.31), the application of the *Gauß* theorem results in a term related to the *Neumann* boundary, which appears on the right-hand side of each weak form, while the term corresponding to the *Dirichlet* boundaries vanishes.

To start with, the above mentioned *Galerkin* procedure is first applied to the momentum balance of the overall mixture. This leads to the form well-known from a standard two-phase model. Thus, concerning the momentum balance, the problem can be summarised as follows:

$$\boxed{\begin{array}{c}\text{Find } \mathbf{u}_S \in \mathcal{S}_{\mathbf{u}_S} \;\; \forall \;\; \delta\mathbf{u}_S \in \mathcal{T}_{\mathbf{u}_S} \text{ such that} \\ \displaystyle\int_\Omega (\mathbf{T}^S_{E\,mech.} - p\,\mathbf{I}) \cdot \operatorname{grad}\delta\mathbf{u}_S \,\mathrm{d}v \;-\; \int_\Omega (\rho^S + \rho^F)\,\mathbf{b}\cdot\delta\mathbf{u}_S \,\mathrm{d}v \;=\; \int_{\Gamma_t} \bar{\mathbf{t}}\cdot\delta\mathbf{u}_S \,\mathrm{d}a\end{array}} \tag{4.32}$$

With respect to this equation, the computations start from a stress-free and, therefore, from an undeformed reference state. Following this, the referential solid extra stress is set zero:

$$\mathbf{T}^S_{E\,mech.0} = \mathbf{0}\,. \tag{4.33}$$

Recalling that the pressure is initialised by p_0, cf. equation (4.39), the overall medium is in this case initially not in equilibrium. Thus, the equilibrium state will only be reached after a certain computation time. In fact, this is a specific characteristic of materials consisting of a charged solid matrix. Since there is always a concentration difference between the ambient solution and the internal one, there will also always be an osmotic pressure within the material. As a result, there exists no stress-free and undeformed state of this materials. Only if the external concentration reaches infinite concentration, the internal osmotic pressure tends to zero, and only in this case the solid matrix can be assumed to be stress-free. But note that there is no such case for biological tissues, as *in vivo* conditions only physiological concentrations occur and, therefore, these tissues are generally prestressed. On the other hand, it is also possible to start from an imaginary

equilibrium state by applying the initial (osmotic) pressure to the solid matrix via

$$\mathbf{T}^S_{E_{mech.0}} = p_0 \, \mathbf{I} \, . \tag{4.34}$$

Considering a finite description of the solid with a non-linear stress-strain curve, the above assumption may lead to inaccurate results because of the non-matching initial displacement, cf. Karajan *et al.* [112]. However, this error can also be circumvented by adopting the material parameters to the prestressed situation. In (4.32), the traction boundary condition is given by

$$\bar{\mathbf{t}} = (\mathbf{T}^S_{E_{mech.}} - p \, \mathbf{I} \,) \, \mathbf{n} \, . \tag{4.35}$$

where $\mathbf{n}$ denotes the outward-oriented unit normal vector.

Applying the *Galerkin* procedure to the volume balance of the overall fluid given in Table 4.4 yields

$$\int_\Omega n^F \mathbf{w}_F \cdot \operatorname{grad} \delta p \, \mathrm{d}v \; - \; \int_\Omega \operatorname{div} (\mathbf{u}_S)'_S \, \delta p \, \mathrm{d}v \; = \; \int_{\Gamma_{\bar{q}}} \bar{q} \, \delta p \, \mathrm{d}a \, . \tag{4.36}$$

Therein, δp is the test function fulfilling the homogeneous *Dirichlet* conditions and the *Neumann* boundary condition $\bar{q}$ is the scalar value of fluid volume efflux over the *Neumann* boundary given by

$$\bar{q} \; = \; n^F \mathbf{w}_F \cdot \mathbf{n} \, . \tag{4.37}$$

Using (4.36), the *Dirichlet* boundary conditions are strongly fulfilled, i. e. within the numerical procedure, the primary variable fulfils the prescribed value. Note that this is actually directly connected with the definition of the trial functions (4.30) for the primary variables. Hence, the above representation of the weak form can only be used for the model variants I and III, where the hydraulic pressure can directly be applied. But because of the previously mentioned reasons, a penalty-like method needs to be used for the model variants II and IV to impose the *Dirichlet* boundary conditions for the overall pressure weakly.

Therefore, the jump condition $(4.20)_2$ for the osmotic pressure at the boundary is rearranged to yield zero, multiplied by the test function δp, integrated over the *Dirichlet* boundary Γ_p and inserted into the previously derived weak form of the overall fluid volume balance:

$$\begin{aligned} &\int_\Omega n^F \mathbf{w}_F \cdot \operatorname{grad} \delta p \, \mathrm{d}v \; - \; \int_\Omega \operatorname{div} (\mathbf{u}_S)'_S \, \delta p \, \mathrm{d}v \, + \\ &+ \int_{\Gamma_p} \kappa^p \left[p - \bar{p} - R\theta \left[(c^+_m + c^-_m) - (\bar{c}^+_m + \bar{c}^-_m) \right] \right] \delta p \, \mathrm{d}a \; = \; \int_{\Gamma_{\bar{q}}} \bar{q} \, \delta p \, \mathrm{d}a \, . \end{aligned} \tag{4.38}$$

Therein, the third term on the left-hand side corresponds to the weak imposition of the *Dirichlet* boundary condition. The parameter κ^p denotes the penalty parameter of the pressure boundary condition, which has to be chosen appropriately for the problem, i. e. as large as possible to reach high accuracy, but also as low as possible to obtain convergence.

Finally, the initial condition for the overall pressure p_0 is given by

$$p_0 \;=\; \bar{p}_0 \;+\; \Delta\pi_0\,, \tag{4.39}$$

where

$$\Delta\pi_0 = R\theta\left[(c^+_{m0} + c^-_{m0}) - (\bar{c}^+_{m0} + \bar{c}^-_{m0})\right] \tag{4.40}$$

denotes the non-zero initial osmotic pressure. Concerning the overall fluid volume balance, the task may be summarised as follows:

$$\begin{gathered}
\text{Find } p \in \mathcal{S}_p \;\; \forall \;\; \delta p \in \mathcal{T}_p \text{ such that} \\
\int_\Omega n^F \mathbf{w}_F \cdot \operatorname{grad}\delta p \,\mathrm{d}v \;-\; \int_\Omega \operatorname{div}(\mathbf{u}_S)'_S \,\delta p \,\mathrm{d}v + \\
+ \int_{\Gamma_p} \kappa^p \left[\, p - \bar{p} - R\theta\left[(c^+_m + c^-_m) - (\bar{c}^+_m + \bar{c}^-_m)\right]\right] \delta p \,\mathrm{d}a \;=\; \int_{\Gamma_{\bar{q}}} \bar{q}\,\delta p \,\mathrm{d}a\,.
\end{gathered} \tag{4.41}$$

Switching now to the concentration balances of the ions, the derivation of their standard weak form results in

$$\int_\Omega n^F c^\gamma_m \mathbf{w}_\gamma \cdot \operatorname{grad}\delta c^\gamma_m \,\mathrm{d}v \;-\; \int_\Omega [\, n^F (c^\gamma_m)'_S \;+\; c^\gamma_m \operatorname{div}(\mathbf{u}_S)'_S \,]\,\delta c^\gamma_m \,\mathrm{d}v \;=\; \int_{\Gamma_{\bar{j}^\gamma}} \bar{j}^\gamma \,\delta c^\gamma_m \,\mathrm{d}a\,, \tag{4.42}$$

where δc^γ_m is the test function and

$$\bar{j}^\gamma \;=\; n^F c^\gamma_m \mathbf{w}_\gamma \cdot \mathbf{n} \tag{4.43}$$

is the scalar value of the ion efflux out of the domain Ω over the *Neumann* boundary $\Gamma_{\bar{j}^\gamma}$. Also in case of this weak formulation, the *Dirichlet* boundary conditions are strongly fulfilled within the numerical procedure. Following this, the above expression can only be used for the model variants I and III. In case of the model variants II and IV, the concentration boundary has to be treated in a special way. Therefore, the same procedure is applied to the ions as has been done for the fluid, i. e. rearranging $(4.20)_3$ to yield zero, multiplying the result by the test function δc^γ_m, integrating over the *Dirichlet* boundary $\Gamma_{c^\gamma_m}$ and inserting the resulting expression into (4.42), yields the weak form of the ion concentration balances including the weak imposition of the *Dirichlet* boundary conditions:

$$\begin{aligned}
&\int_\Omega n^F c^\gamma_m \mathbf{w}_\gamma \cdot \operatorname{grad}\delta c^\gamma_m \,\mathrm{d}v \;-\; \int_\Omega [\, n^F (c^\gamma_m)'_S \;+\; c^\gamma_m \operatorname{div}(\mathbf{u}_S)'_S \,]\,\delta c^\gamma_m \,\mathrm{d}v + \\
&+ \int_{\Gamma_{c^\gamma_m}} \kappa^c \left[\, c^\gamma_m - \frac{1}{2\,|z^\gamma|}\sqrt{\left(z^{fc}\,c^{fc}_m\right)^2 - 4\,z^+ z^-\,(\,\bar{c}^\gamma_m\,)^2} + \frac{z^{fc}\,c^{fc}_m}{2\,z^\gamma}\right] \delta c^\gamma_m \,\mathrm{d}a = \\
&\qquad = \int_{\Gamma_{\bar{j}^\gamma}} \bar{j}^\gamma \,\delta c^\gamma \,\mathrm{d}a\,.
\end{aligned} \tag{4.44}$$

Therein, κ^c denotes a penalty parameter of the concentration boundary conditions, which has to be chosen properly. The initial condition for the cation concentration c_{m0} is given by

$$c^\gamma_{m0} \;=\; \frac{1}{2\,|z^\gamma|}\,\sqrt{\left(\,z^{fc}\,c^{fc}_{m0}\,\right)^2 \;-\; 4\,z^+ z^-\,(\,\bar{c}^\gamma_{m0}\,)^2} \;-\; \frac{z^{fc}\,c^{fc}_{m0}}{2\,z^\gamma}\,. \tag{4.45}$$

Following this, the problem for the ion concentration balances is summarised as follows:

$$\begin{gathered}
\text{For } \gamma = \{+,-\} \text{ find } \; c^\gamma_m \,\in\, \mathcal{S}_{c^\gamma_m} \;\; \forall \;\; \delta c^\gamma_m \,\in\, \mathcal{T}_{c^\gamma_m} \text{ such that} \\
\int_\Omega n^F c^\gamma_m \mathbf{w}_\gamma \cdot \operatorname{grad}\delta c^\gamma_m \,\mathrm{d}v \;-\; \int_\Omega [\, n^F (c^\gamma_m)'_S \;+\; c^\gamma_m \operatorname{div}(\mathbf{u}_S)'_S \,]\,\delta c^\gamma_m \,\mathrm{d}v + \\
+ \int_{\Gamma_{c^\gamma_m}} \kappa^c \left[\, c^\gamma_m - \frac{1}{2\,|z^\gamma|}\,\sqrt{\left(\,z^{fc}\,c^{fc}_m\,\right)^2 - 4\,z^+ z^-\,(\,\bar{c}^\gamma_m\,)^2} + \frac{z^{fc}\,c^{fc}_m}{2\,z^\gamma} \,\right] \delta c^\gamma_m \,\mathrm{d}a \;= \\
= \int_{\Gamma_{\bar{\jmath}^\gamma}} \bar{\jmath}^\gamma\,\delta c^\gamma \,\mathrm{d}a\,.
\end{gathered} \tag{4.46}$$

Moreover, the application of the *Galerkin* procedure to the *Poisson* equation yields:

$$\int_\Omega \operatorname{grad}\mathcal{E}\cdot\operatorname{grad}\delta\mathcal{E}\,\mathrm{d}v \;-\; \int_\Omega \frac{n^F F}{\epsilon^F}\Big(\sum_\gamma z^\gamma c^\gamma_m + z^{fc} c^{fc}_m\Big)\delta\mathcal{E}\,\mathrm{d}v \;=\; -\int_{\Gamma_{\bar{e}}} \bar{e}\,\delta\mathcal{E}\,\mathrm{d}a\,, \tag{4.47}$$

wherein

$$\bar{e} \;=\; -\operatorname{grad}\mathcal{E}\cdot\mathbf{n} \tag{4.48}$$

is the applied electric field on the *Neumann* boundary and $\delta\mathcal{E}$ is the test function.

Note that the weak formulation of the $\mathcal{E}$ boundary condition is needed for any of the models. However, in case of simple 1-d situations with very low concentration changes, it can be decided to neglect the influence of the concentrations on the electric potential and, thus, the external electric potential $\bar{\mathcal{E}}$ may be applied directly using the standard conventional method for *Dirichlet* boundary conditions[7].

Nevertheless, considering an non-uniformly deforming material with varying concentrations at the boundary, equation $(4.20)_4$ states that $\mathcal{E}$ at the boundary changes as well. By varying electric potentials on the boundaries, gradients arise within the domain, which in turn influence the ion movements. Therefore, for general cases, the electric potential at the boundary needs to be imposed weakly.

[7]To apply $\mathcal{E}$ strongly on $\Gamma_\mathcal{E}$, one can follow this argumentation: Equation (4.6) can be rearranged with the aid of the chemical potential to yield

$$\mathcal{E}(\mathbf{x},t) \;=\; \bar{\mathcal{E}} \;+\; \frac{1}{z^\gamma F}\,(\,\bar{\mu}^\gamma_m \;-\; \mu^\gamma_m) \;=\; \bar{\mathcal{E}}\,,$$

since the chemical potentials at the boundary are directly fulfilled by the trial functions, cf. $(4.20)_3$. But note that in this case, the information about the deformation dependency of the electric potential at the boundary is lost.

Thus, the relation given by $(4.20)_4$ is rearranged, multiplied by its test function, integrated over the *Dirichlet* boundary Γ_ε and inserted into the above standard weak form. Following the above considerations, the task for the *Poisson* equation may be summarised as follows:

$$\boxed{\begin{aligned} &\text{Find } \mathcal{E} \in \mathcal{S}_\varepsilon \;\; \forall \;\; \delta\mathcal{E} \in \mathcal{T}_\varepsilon \text{ such that} \\ &\int_\Omega \operatorname{grad}\mathcal{E} \cdot \operatorname{grad}\delta\mathcal{E}\,\mathrm{d}v \;-\; \int_\Omega \frac{n^F F}{\epsilon^F}\Big(\sum_\gamma z^\gamma c_m^\gamma + z^{fc} c_m^{fc}\Big)\delta\mathcal{E}\,\mathrm{d}v + \\ &+ \int_{\Gamma_\varepsilon} \kappa^\varepsilon \Big(\mathcal{E} \;-\; \bar{\mathcal{E}} \;-\; \frac{R\theta}{z^\gamma F}\,\ln\frac{\bar{c}_m^\gamma}{c_m^\gamma}\Big)\,\delta\mathcal{E}\,\mathrm{d}a \;=\; \int_{\Gamma_{\bar{e}}} \bar{e}\,\delta\mathcal{E}\,\mathrm{d}a\,. \end{aligned}} \tag{4.49}$$

In the above relation, the overall charge density ρ_e has been replaced by (2.19). As before, κ^ε is the penalty factor of the electric potential boundary condition and $\bar{\mathcal{E}}$ is the applied electric potential at the corresponding boundary. Moreover, the electric potential is initialised by

$$\mathcal{E}_0 \;=\; \bar{\mathcal{E}}_0 \;+\; \frac{R\theta}{z^\gamma F}\,\ln\frac{\bar{c}_{m0}^\gamma}{c_{m0}^\gamma}\,. \tag{4.50}$$

In contrast to the *Poisson* equation used in this thesis to compute $\mathcal{E}$ as well as in Li *et al.* [119], Wallmersperger [168], Zhou *et al.* [170], the continuity equation of the charges (3.24) is used in the literature of swelling materials quite often to determine the electric potential, cf., for example, cf. Gu *et al.* [86], van Loon *et al.* [122], Sun *et al.* [159]. But this equation does not provide any additional information to compute the actual value of the electric potential, since the seepage velocities of the ions are already inserted into the corresponding concentration balances. Thus, it just restricts the ions diffusion. Moreover, regarding the weak form of the continuity equation, cf. the footnote on page 72, the respective *Neumann* boundary condition would be the sum of $\Gamma_{\bar{j}^\gamma}$, which already correspond to the concentration balances. Note furthermore that, mathematically spoken, the *Neumann* boundary condition is the normal derivative, i. e. the flux, of the primary variable. But considering the electric potential $\mathcal{E}$ as the primary variable, then the gradient is the electric field $\mathbf{e}$, cf. (3.115), and not the electric current $\mathbf{i}$.

4.3.2 Spatial discretisation

For the spatial discretisation, the domain Ω containing the overall body $\mathcal{B}$ is approximated by its discrete counterpart Ω^h, where Ω^h is obtained by a fragmentation of the overall domain into subdomains by so-called elements $\mathcal{L}$:

$$\Omega \;\approx\; \Omega^h = \bigcup_{e=1}^{N_e} \mathcal{L}\,. \tag{4.51}$$

Following this, the discretised overall domain Ω^h is the set union of its elements $\mathcal{L}$, cf. also the sketch of a meshed domain in Figure 4.4. In a next step, the spatially continuous weak formulations are discretised by defining new discrete and finite dimensional subspaces $\mathcal{S}_{dof}^h$

and $\mathcal{T}^h_{dof}$ of the continuous and infinite dimensional trial and test spaces $\mathcal{S}_{dof}$ and $\mathcal{T}_{dof}$ given in (4.30) and (4.31), whereas the subscript *dof* is one element of the set union of all primary variables, i. e. $dof \in \{\, \mathbf{u}_S,\, p,\, c_m^+,\, c_m^-,\, \mathcal{E} \,\}$, cf., for example, Ammann [3].

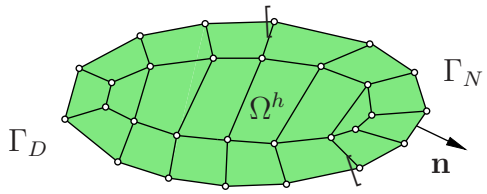

Figure 4.4: Sketch of the discretised domain Ω^h with its elements and nodes.

As a result of the discretisation, the domain Ω^h now consists of N_e elements and N_n nodes, which leads to N_n-dimensional subspaces of the discrete trial and test functions. Within this subspaces, the discrete counterparts of the primary variables corresponding to the exemplary chosen model variant IV can be summarised as

$$\begin{aligned}
\mathbf{u}_S(\mathbf{x},t) &\approx \mathbf{u}_S^h(\mathbf{x},t) = \bar{\mathbf{u}}_S^h(\mathbf{x},t) &&+ \sum_{j=1}^{N_n} \boldsymbol{\phi}_u^j(\mathbf{x})\; \mathbf{u}_S^j(t) \;\in \mathcal{S}^h_{\mathbf{u}_S}(t)\,,\\
p(\mathbf{x},t) &\approx p^h(\mathbf{x},t) = \tilde{p}^h\big(c_m^\gamma,\, \bar{c}_m^\gamma(\mathbf{x},t),\, \bar{\mathcal{P}}(\mathbf{x},t)\big) &&+ \sum_{j=1}^{N_n} \phi_p^j(\mathbf{x})\; p^j(t) \;\in \mathcal{S}^h_p(t)\,,\\
c_m^\gamma(\mathbf{x},t) &\approx c_m^{\gamma\,h}(\mathbf{x},t) = \tilde{c}_m^{\gamma\,h}\big(c_m^{fc}(\mathbf{u}_S), \bar{c}_m^\gamma(\mathbf{x},t)\big) &&+ \sum_{j=1}^{N_n} \phi_c^j(\mathbf{x})\; c_m^{\gamma\,j}(t) \;\in \mathcal{S}^h_{c_m^\gamma}(t)\,,\\
\mathcal{E}(\mathbf{x},t) &\approx \mathcal{E}^h(\mathbf{x},t) = \tilde{\mathcal{E}}^h\big(c_m^\gamma,\, \bar{c}_m^\gamma(\mathbf{x},t),\, \bar{\mathcal{E}}(\mathbf{x},t)\big) &&+ \sum_{j=1}^{N_n} \phi_\mathcal{E}^j(\mathbf{x})\; \mathcal{E}^j(t) \;\in \mathcal{S}^h_\mathcal{E}(t)\,.
\end{aligned} \tag{4.52}$$

Furthermore, the test functions are given by

$$\begin{aligned}
\delta\mathbf{u}_S(\mathbf{x}) &\approx \delta\mathbf{u}_S^h(\mathbf{x}) = &&\sum_{j=1}^{N_n} \boldsymbol{\phi}_u^j(\mathbf{x})\; \delta\mathbf{u}_S^j \;\in \mathcal{T}^h_{\mathbf{u}_S}\,,\\
\delta p(\mathbf{x}) &\approx \delta p^h(\mathbf{x}) = &&\sum_{j=1}^{N_n} \phi_p^j(\mathbf{x})\; \delta p^j \;\in \mathcal{T}^h_p\,,\\
\delta c_m^\gamma(\mathbf{x}) &\approx \delta c_m^{\gamma\,h}(\mathbf{x}) = &&\sum_{j=1}^{N_n} \phi_c^j(\mathbf{x})\; \delta c_m^{\gamma\,j} \;\in \mathcal{T}^h_{c_m^\gamma}\,,\\
\delta\mathcal{E}(\mathbf{x}) &\approx \delta\mathcal{E}^h(\mathbf{x}) = &&\sum_{j=1}^{N_n} \phi_\mathcal{E}^j(\mathbf{x})\; \delta\mathcal{E}^j \;\in \mathcal{T}^h_\mathcal{E}\,.
\end{aligned} \tag{4.53}$$

For example, the continuous field function $\mathbf{u}_S$ is approximated by its discrete counterpart $\mathbf{u}_S^h$, whereas the values on the domain boundary are given by the discrete versions $\bar{\mathbf{u}}_S^h$ of the *Dirichlet* boundary conditions. In contrast, as the definition of the test spaces implies,

the corresponding discrete test functions are zero at the domain boundary, i. e. they fulfil the homogeneous *Dirichlet* boundary conditions.

Within the domain, the functions are represented by the product of their global basis functions $\boldsymbol{\phi}_u^j$, ϕ_p^j, ϕ_c^j and ϕ_ε^j corresponding to the node j and the nodal values of the primary variables. The solid displacement as a vectorial quantity is approximated individually in each spatial direction by separate basis functions, i. e. $\boldsymbol{\phi}_u^j = \{\phi_{u1}^j, \ldots, \phi_{ud}^j\}$ with d denoting the spatial dimension of the problem. Within the finite element procedure, the unknown nodal values of the discretised primary variables are also called degree of freedom (DOF). Note that while the basis functions only depend on the spatial position, the nodal values of the primary variables only depend on time. As a result within a FE procedure, the dependence of the variables on time and spatial coordinates is fully separated.

Based on the concept of *partition of unity*, the basis functions are defined as functions with the maximum value of one at their corresponding node j and zero at all other nodes. Following this, one obtains a system of N_n linearly independent equations with N_n nodal unknowns for each primary variable.

From (4.52) and (4.53), it can be seen that equal approximations, i. e. the same basis functions, have been used for the trial and test functions. This procedure of using equal approximation spaces is called *Bubnov-Galerkin* or just *Galerkin* method. On the other hand, it is also possible to use different basis functions for the approximation of the above functions. This more general approach is called *Petrov-Galerkin* method and is generally applied in situations where stabilisation techniques are required such as in fluid dynamics, cf. Graf [80], Helmig [95], or in porous materials, cf. Ehlers *et al.* [62].

The weak formulations given in Section 4.3.1 must hold for any choice of test functions. Thus, in order to obtain one separate equation corresponding to each DOF, the discrete forms of the test functions are inserted. Following the definitions of the test functions (4.53) and recalling that the values of the test functions are one at their corresponding node and zero else, one obtains the $N_n \times N_{dof}$ linearly independent equations. These equations are summarised in the residuum vector with each row corresponding to one test function. For more details on this procedure, cf. Ammann [3] and Ellsiepen [70].

4.3.3 Mixed finite elements

In contrast to the standard finite element scheme, where only one equation for one primary variable has to be solved, all five equations of the strongly coupled system have to be solved simultaneously in this thesis. The appropriate FE method for this case is called mixed finite element method (MFEM). In particular, for the exemplary chosen model variant IV the variables p, c_m^+, c_m^- and $\mathcal{E}$ have to be considered besides the variable solid displacement $\mathbf{u}_S$.

To find appropriate approximation functions for the degrees of freedom, the balance relations can be consulted in a first step. In the momentum balance, the overall pressure, i. e. the sum of the hydraulic and the osmotic pressures (the latter obtained from the sum of the molar concentrations), appears together with the stress tensor. The stress tensor

itself is obtained from the derivative of the solid displacement and from both of this terms the divergence needs to be computed. Therefore, to obtain equal order approximations of these derivatives, a quadratic approximation should be chosen for $\mathbf{u}_S$ and a linear one for the overall pressure p, or for $\mathcal{P}$, and c_m^γ.

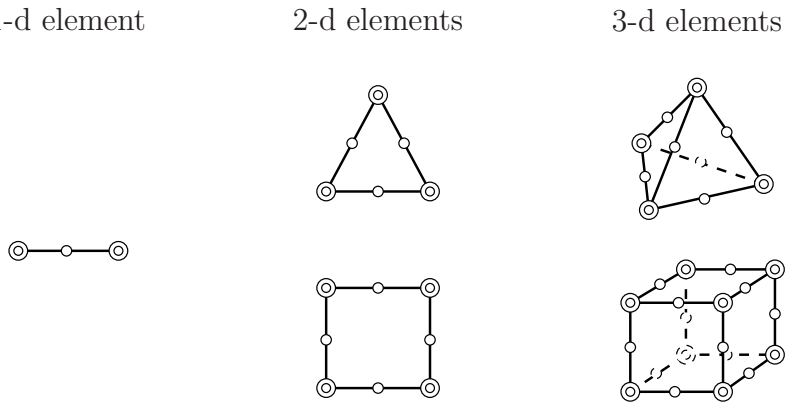

Figure 4.5: Spatial discretisation using extended *Taylor-Hood* elements.

A more mathematical argumentation is based on the solvability of the resulting system of equations. In particular, the patch test or, more general, the inf-sup condition, also referred as *Ladyshenskaya-Babuška-Brezzi* or LBB condition, has to be fulfilled, cf. Zienkiewicz *et al.* [171] and Chapelle & Bathe [36]. This conditions demand that the number of unknown nodal displacement values minus the given *Dirichlet* values at the boundary is higher than the unknown nodal values of the pressure, cf. also Brezzi & Bathe [34]. As a result, the upper left submatrix corresponding to the solid displacement is larger then the submatrix corresponding to the pressure. This conditions are satisfied, if the approximation of the displacement is chosen one order higher than the other ones. Therefore, as depicted in Figure 4.5, the spatial discretisation proceeds from a quadratic approximation of the solid displacement and linear approximations for the overall pore-fluid pressure, the cation and anion concentrations and the electric potential (Q2P1C1A1X1). This type of mixed finite elements is known as extended *Taylor-Hood* elements.

4.3.4 Numerical integration

The weak formulations of the governing balance relations and the *Poisson* equation are given in an integral representation. For the numerical treatment of such integrals, the *Gauß* quadrature is appropriate, cf. Zienkiewicz & Taylor [172]. Within the *Gauß* quadra-

ture, a continuous integral is transformed to a summation via

$$\int_{\mathcal{L}} f(\boldsymbol{\xi})\,\mathrm{d}\boldsymbol{\xi} = \sum_{q=1}^{N_q} f(\boldsymbol{\xi}_q)\,w_q\,. \tag{4.54}$$

Therein, the function f expressed in the element coordinates $\boldsymbol{\xi}$ is integrated over the element volume. By use of the *Gauß* quadrature, this integration can also be carried out by evaluating the function f at the discrete *Gauß* point $\boldsymbol{\xi}_q$ and weighting the result with the corresponding weighting function w_q. Summing the results of all *Gauß* points within the element leads to the sought-after integral. The advantage of this procedure compared to others like the *Newton-Cotes* formulae is that it is much more accurate and the evaluation of f at $\boldsymbol{\xi}_q$ and the summation of this terms is numerically quite easy to handle.

Moreover, by use of N_q so-called *Gauß* points, a function of order $(2N_q - 1)$ can be integrated exactly. The coordinates of the mentioned points for different types of elements in several dimensions with the corresponding weighting values can be found, for example, in Zienkiewicz & Taylor [172].

4.3.5 Semidiscrete initial-value problem

Summarising the above considerations, the continuous weak forms of the the momentum balance (4.32), the overall fluid volume balance (4.41), the concentration balances (4.46) and the *Poisson* equation (4.49) are now spatially discretised. Such a system is also referred as semi-discrete, since only the spatial discretisation has been carried out up to now. In this subsection, following Ehlers & Ellsiepen [61], Ellsiepen [70] and Ammann [3], the semi-discrete system will be written in an abstract formulation. For this, all DOF of the system, these are the N_n nodal unknowns of each primary variable, are gathered in the vector $\boldsymbol{u}$, i. e.

$$\boldsymbol{u} = [\,(\,\mathbf{u}_S^1\,,\,p^1\,,\,c_m^{+1}\,,\,c_m^{-1}\,,\,\mathcal{E}^1\,)\,,\ldots,(\,\mathbf{u}_S^{N_n}\,,\,p^{N_n}\,,\,c_m^{+N_n}\,,\,c_m^{-N_n}\,,\,\mathcal{E}^{N_n}\,)\,]^T\,. \tag{4.55}$$

Note that, for convenience, it has been assumed in the above vector $\boldsymbol{u}$ that all DOFs are approximated in the same order. Recall that $\mathbf{u}_S^j$ is a vectorial quantity with one element for each spatial direction. Following this and expressing the only appearing time derivative in the relevant equations, i. e. the material time derivative with respect to the deforming solid skeleton $(\,\cdot\,)'_S$, via $(\,\cdot\,)'$, this so-called semi-discrete system can be written in an abstract description via

$$\boldsymbol{F}(t,\boldsymbol{u},\boldsymbol{u}') = \big[\,\boldsymbol{M}\,\boldsymbol{u}' + \boldsymbol{k}(\boldsymbol{u}) - \boldsymbol{f}\,\big] \stackrel{!}{=} \mathbf{0}\,, \quad \text{where} \quad \boldsymbol{u}(t_0) = \boldsymbol{u}_0\,. \tag{4.56}$$

Therein, $\boldsymbol{M}$ is the generalised mass matrix, $\boldsymbol{k}$ the generalised stiffness vector and $\boldsymbol{f}$ the generalised force vector consisting of the *Neumann* boundary conditions. In particular, $\boldsymbol{M}$ is composed of the time derivatives of the primary variables. Since only the solid displacement and the ion concentrations have velocities in their weak forms, the mass

matrix is singular. Following this, the above system is a differential-algebraic system (DAE). For the solution of DAE systems, cf. the very good text book by Brenan *et al.* [33]. In cases, where the generalised mass matrix would not be singular, the above set of equations would be called a partial differential equation (PDE). For a more detailed discussion on the topic solving above equation and efficient adaptive time integration methods, the interested reader is referred to the works of Diebels *et al.* [46], Ehlers & Ellsiepen [61] and Ellsiepen [70].

4.3.6 Temporal discretisation

The above derived semi-discrete system still needs to be discretised in the time domain. For this purpose, the implicit (backward) *Euler* method defined by the backward *Taylor* series evaluated at the current time step t_{n+1}

$$\boldsymbol{u}_n \;=\; \boldsymbol{u}_{n+1} \;-\; \boldsymbol{u}'_{n+1}\,(\,t_{n+1} - t_n\,) \quad\longrightarrow\quad \boldsymbol{u}'_{n+1} \;=\; \frac{\boldsymbol{u}_{n+1} \;-\; \boldsymbol{u}_n}{t_{n+1} - t_n} \tag{4.57}$$

will be used. Therein, the n denotes the old time step. Since this scheme is unconditionally stable, this is the time integration strategy, which is applied to the set (4.56) of DAE introduced in the previous subsection.

An alternative possibility for the discretisation in the time domain is to use explicit methods. The corresponding scheme to the above mentioned one is the explicit (forward) *Euler* scheme defined by the forward *Taylor* series evaluated at the last time step t_n

$$\boldsymbol{u}_{n+1} \;=\; \boldsymbol{u}_n \;+\; \boldsymbol{u}'_n\,(\,t_{n+1} - t_n\,) \quad\longrightarrow\quad \boldsymbol{u}'_n \;=\; \frac{\boldsymbol{u}_{n+1} \;-\; \boldsymbol{u}_n}{t_{n+1} - t_n}\,. \tag{4.58}$$

The above scheme is not unconditionally stable. Instead, one has to take advantage of the maximum time step size to keep the numerical computations stable. For a more detailed discussion on time discretisation techniques, cf., for instance, Ammann [3] and Ellsiepen [70] and also the works by Danilov [40] and Heider [92].

Moreover, knowing the above classifications of time integration schemes, some further considerations can be made about the deformation-dependent boundary conditions. Taking a closer look at the explicit *Euler* scheme (4.58), one can see that the current value of the variables $\boldsymbol{u}_{n+1}$ is extrapolated by use of the known values of the variables $\boldsymbol{u}_n$ of the former time step. Concerning the boundary conditions, in a first attempt, the values of the concentrations $(c_m^\gamma)_{n+1}$ and the osmotic pressure $(\Delta\pi)_{n+1}$ for the boundary conditions at the current time step have been computed based on the value of the fixed charge concentration $(c_m^{fc})_n$ of the last accepted time step. But from the above relation, it gets now obvious that the usage of the values of variables from the old time step leads to an explicit behaviour, even though a strictly implicit scheme such as the implicit *Euler* is used for the time integration. As a result, the computations lead to unsound numerical oscillations. To avoid these problems, the corresponding boundary conditions have been incorporated into the weak formulations, such that the boundary conditions are always inline with the current deformation, cf. Section 4.3.1, and also with the current values of

the variables within each *Newton* iteration step, cf. Section 4.4.

4.4 Numerical solution procedure

In the previous section, the governing set of partial differential equations has been fully discretised in the spatial as well as in the temporal domain. To avoid stability problems, the implicit *Euler* time integration scheme (4.57) is inserted into the DAE. Thereafter, the resulting set of nonlinear equations, i. e.

$$\boldsymbol{F}_{n+1}\left(t_{n+1}, \boldsymbol{u}_{n+1}, \boldsymbol{u}'_{n+1}(\boldsymbol{u}_{n+1})\right) \;=\; \boldsymbol{M}(\boldsymbol{u}_{n+1})\,\boldsymbol{u}'_{n+1} + \boldsymbol{k}(\boldsymbol{u}_{n+1}) - \boldsymbol{f}_{n+1} \;=\; \boldsymbol{0}\,, \tag{4.59}$$

has to be solved. This can only be done iteratively by a *Newton* iteration scheme within each time integration step. To go through the iteration procedure, the global tangent of the system will be computed numerically in this thesis. By derivation of (4.59) with respect to its variables, which are the unknowns of the current time step $\boldsymbol{u}_{n+1}$ and also the corresponding velocities $\boldsymbol{u}'_{n+1}$, one obtains the global tangent of the system:

$$\mathrm{D}\boldsymbol{F}^k_{n+1} \;:=\; \frac{\mathrm{d}\boldsymbol{F}^k_{n+1}}{\mathrm{d}\boldsymbol{u}^k_{n+1}} \;=\; \frac{\partial \boldsymbol{F}^k_{n+1}}{\partial \boldsymbol{u}^k_{n+1}} \;+\; \frac{1}{\Delta t_{n+1}} \frac{\partial \boldsymbol{F}^k_{n+1}}{\partial (\boldsymbol{u}')^k_{n+1}}\,. \tag{4.60}$$

Therein, the derivative of $\boldsymbol{u}'_{n+1}$ with respect to $\boldsymbol{u}_{n+1}$ has been computed with the aid of (4.57), i. e.

$$\frac{\partial \boldsymbol{u}'_{n+1}}{\partial \boldsymbol{u}_{n+1}} \;=\; \frac{1}{\Delta t_{n+1}}\,\mathbf{I}\,. \tag{4.61}$$

Following this the global *Jacobi*an of the system also depends on the time integration scheme. Having found the global tangent of the system $\mathrm{D}\boldsymbol{F}^k_{n+1}$, the following linear system of equations has to be solved for the current *Newton* iteration step k:

$$\mathrm{D}\boldsymbol{F}^k_{n+1}\,\Delta\boldsymbol{u}^k_{n+1} \;=\; -\boldsymbol{F}^k_{n+1}\,. \tag{4.62}$$

This can be done either by direct solvers such as SPARSE or SuperLU, or by iterative solvers in combination with preconditioners such as, for example, Incomplete LU-factorisation (ILU) in combination with Generalised Minimal Residual (GMRES). A nice overview over iterative solvers with preconditioners is given in the work of Barrett *et al.* [9]. The advantage of iterative solvers is that they are much faster in case of large systems and need far less memory than a direct solver. But in case of systems with less number of DOF, the cost of the preconditioning procedure by, for example, an ILU sweeps off the advantages of iterative solvers. Therefore, direct solvers should be used in such a case.

Having found the above solution, i. e. the vector $\Delta\boldsymbol{u}^k_{n+1}$ of the current *Newton* iteration step, the solution vector is updated via

$$\boldsymbol{u}^{k+1}_{n+1} \;=\; \boldsymbol{u}^k_{n+1} + \Delta\,\boldsymbol{u}^k_{n+1} \tag{4.63}$$

and the next *Newton* step may be solved. This procedure is repeated until the L_2-norm

of the residuum is less than a certain tolerance:

$$||\boldsymbol{F}_{n+1}^{k+1}|| < \varepsilon_{tol} \,. \tag{4.64}$$

Note that in case of the standard *Newton* method, the *Jacobi*an is newly computed for each *Newton* step. In contrast, if the *Jacobi*an once calculated is used for several *Newton* steps, the method is called simplified *Newton*. The advantage is here that by using the the old system tangent several times, also the LU factorisation of the last step may also be used again. This is again of particular interest for large systems.

Chapter 5:
Numerical examples

The thermodynamically consistent model derived in Chapter 3 with the different possible sets of primary variables presented in Chapter 4 including the simplifications S I, S II and S III[1] have been implemented into the FE-tool PANDAS[2]. As it has already been pointed out in Ehlers & Acartürk [58] and in Section 4.3.1, the weak imposition of the *Dirichlet* boundary conditions is of great importance for the stability of the numerical computations. Thus, this procedure has been applied for all relevant primary variables. The healing process by comparing the different approaches of strongly and weakly imposed *Dirichlet* boundary conditions is presented in Ehlers & Acartürk [58].

Within this chapter, the results of the initial boundary-value problems (IBVP) by use of the different variants of the set of primary variables and the simplifications will be compared. While a particular emphasis will be laid on numerical aspects such as stability and computation times, the evolution of the displacement and the concentrations within the domain will be investigated. In these numerical experiments, it is found that the variant IV includes the most reliable set of primary variables. To achieve a higher accuracy of the computations in comparison to the experiments, concentration-dependent activity coefficients based on the *Debye-Hückel* theory are introduced and their influence is discussed. Thereafter, the numerical result obtained is also compared with a swelling-compression experiment found in Frijns *et al.* [76].

Since also the electric effects can be simulated by this model, a numerical example of a two-dimensional (2-d) specimen deforming under an electric stimulation will be computed. Effectively including one-dimensional (1-d) loading conditions, the response of the overall aggregate to an applied voltage can be observed.

Finally, to show the capabilities of the model derived within this thesis, two three-dimensional (3-d) simulations of the free swelling experiment of a hydrogel disc and the bending of a gripper based on hydrogel are presented.

5.1 Comparison of the different approaches

As it has been mentioned above, the different sets of primary variables and the simplifications will be initially compared with respect to the obtained results and the numerical effectivity. Since all of the different sets are based on the same thermodynamical model derived in Chapter 3, the results should, in principle, be the same. However, as different

[1] For simplification IV, cf. Ehlers *et al.* [64].

[2] **P**orous media **A**daptive **N**onlinear finite element solver based on **D**ifferential **A**lgebraic **S**ystems (`www.get-pandas.com`)

variables with different internal dependencies are discretised, the results may differ. Also in other porous material formulations, such as the model of multiphasic flow and transport processes presented by Helmig [95], different primary variables can be chosen for the numerical treatment, where each of the sets has different properties with respect to its solvability and numerical stability. These aspects of the different presented variants and simplifications will be discussed within this section.

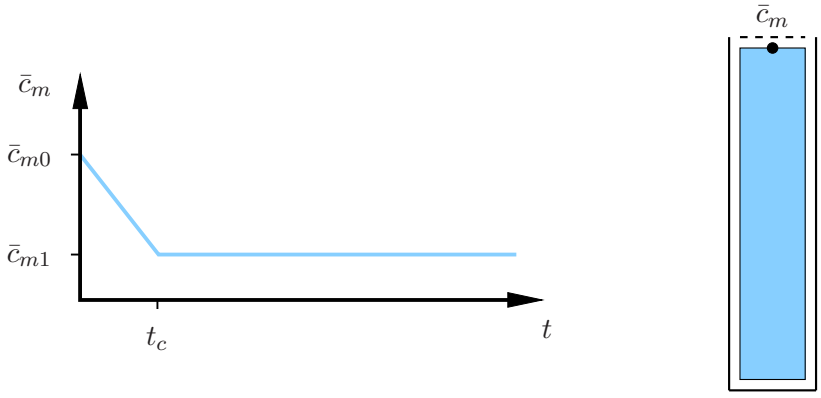

Figure 5.1: Left: Chemical loading, the concentration of the external solution is decreased from $\bar{c}^{\gamma}_{m0}$ to $\bar{c}^{\gamma}_{m1}$ within 50 s. Right: Sketch of the geometry with the observed upper node.

To compare the variants, a 2-d setup of a 1-d swelling experiment is computed. Therein, as depicted in Figure 5.1, a $1 \times 0.2\,\mathrm{mm}^2$ hydrogel column is chemically loaded by decreasing the concentration $\bar{c}^{\gamma}_m$ of the external solution from $\bar{c}^{\gamma}_{m0} = 0.9\,\mathrm{mol/l}$ to $\bar{c}^{\gamma}_{m1} = 0.1\,\mathrm{mol/l}$ within $t_c = 50\,\mathrm{s}$. Note that this range is chosen as the maximum concentration change, which can be handled by all variants. The material parameters used during the computations are summarised in Table 5.1. Therein, the unit 'eq/l' used in the table for the fixed charges concentration denotes the equivalence to one mole of electrons. Note that a monovalent salt solution such as Na^+Cl^- has been used for convenience in all the following simulations. The computations always start from an undeformed initial state, where the initial osmotic pressure π_0 is added to the purely mechanical solid extra stress $\mathbf{T}^S_{E_{mech.0}}$, cf. (4.34). Moreover, concerning the discretisation of the geometry, 2×40 stable quadrilateral extended *Taylor-Hood* elements are used with the approximations as given in Section 4.3.3.

During the computations, the upper node depicted on the right-hand side in Figure 5.1 is observed to plot the vertical displacement curve, i. e. the swelling of the hydrogel strip. Concerning the boundary conditions, the displacement on the left, right and the bottom boundaries are fixed in the direction perpendicular to the surface. In addition, there is neither a flux of the overall fluid over these boundaries nor ion diffusion. Thus, there is also no electric current flowing over these surfaces. At the upper boundary, the concentrations $\bar{c}^{\gamma}_m$ of the dissolved ions are decreased and, thus, the chemical potentials change as well. Concerning the pressure boundary conditions of the overall fluid volume balance, either the hydraulic pressure $\bar{p}$ or the osmotic pressure difference $\Delta\pi$ is applied and for the *Poisson* equation, the deformation-dependent electric potential $\mathcal{E}$ is used as the boundary condition.

c^{fc}_{m0S}	=	0.2 eq/l	n^S_{0S}	=	0.25
λ^S	=	0.04 N/mm^2	μ^S	=	0.10 N/mm^2
γ^{FR}	=	$1 \cdot 10^{-5}$ N/mm^3	k^F	=	$1.07 \cdot 10^{-8}$ mm/s
D^+	=	$0.5 \cdot 10^{-3}$ mm^2/s	D^-	=	$0.8 \cdot 10^{-3}$ mm^2/s
M^+_m	=	$22.99 \cdot 10^{-3}$ kg/mol	M^-_m	=	$40.08 \cdot 10^{-3}$ kg/mol
R	=	8.3144 J/K mol	θ	=	298 K
F	=	96 485.33 C/mol	$\kappa^{p,c,\varepsilon}$	=	1.0
z^+	=	+1	z^-	=	−1
z^{fc}	=	−1	ϵ^F	=	100.0 C/N mm^2
$\bar{c}_{m0}$	=	0.90 mol/l	$\bar{c}_{m1}$	=	0.10 mol/l

Table 5.1: Set of material parameters used for the comparison of the primary variable sets and the simplifications.

5.1.1 Comparison of the variants I – IV

Firstly, the four possible sets of primary variables are compared. The results of the computations are shown in Figure 5.2 and Figure 5.3. Therein and in what follows, the blue-coloured lines always correspond to the variants I and II with the chemical potentials μ^γ_m as primary variables and the red lines correspond to the variants III and IV given in the molar concentrations c^γ_m. Moreover, the lines with the crosses represent the variants I and III with the hydraulic pressure $\mathcal{P}$ as primary variables while the ones without the crosses belong to the variants II and IV formulated the overall pressure p. Note that this indication with and without cross refers throughout this section to the corresponding formulations.

On the left-hand side in Figure 5.2, the vertical displacement of the observed upper node is plotted. It can be seen, that the red curves of the variants formulated in the molar concentrations totally match independent of the pressure primary variable, while the curves obtained by the chemical potentials differ. A closer look reveals, that the progress of vertical displacement of variant II formulated in the overall pressure is very close to the variants III and IV.

The plots on the right-hand side in Figure 5.2 show a cut of the molar concentrations through the domain from the bottom to the top boundary. Several different time steps are plotted simultaneously to be able to follow the development of the concentrations in the domain. Therein, it can be seen that the concentration distributions within the domain computed by variants I/II and III/IV are pairwise equal. This result may have been expected, because, in contrast to the vertical displacement curve, where the pressure formulation has a great influence, the molar concentrations in the variants I/II and III/IV

are computed in the same manner, i. e. either as an internal variable via the relations (4.11) or as a primary variable.

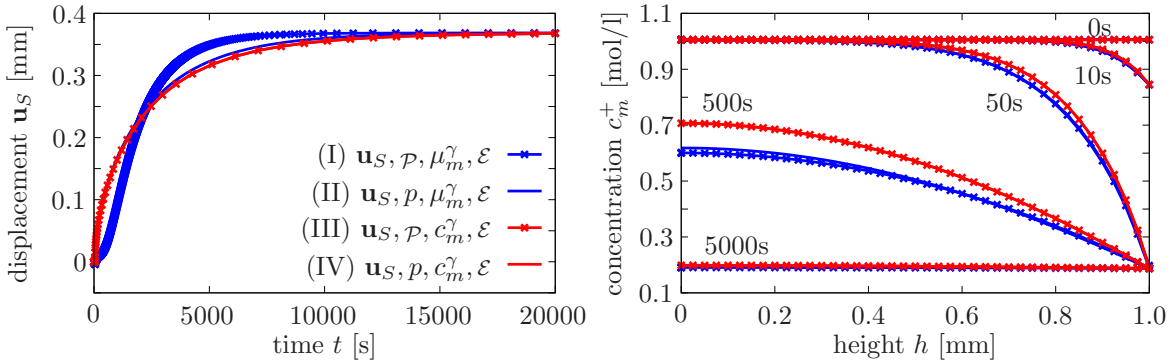

Figure 5.2: On the left-hand side, the vertical displacement of the observed node by use of the different sets of primary variables is depicted and, on the right-hand side, the cation concentration distribution in the domain at different times.

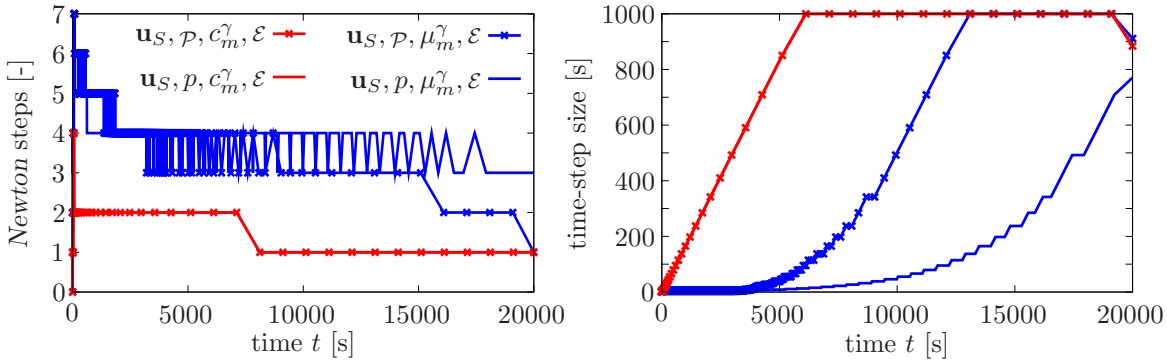

Figure 5.3: Numerical aspects of the computations. On the left-side, the number of *Newton* iterations over time is shown and the time-step size evolution on the right-hand side.

In Figure 5.3, two graphs concerning numerical aspects are depicted. In particular, on the left-hand side, the number of *Newton* steps required to obtain convergence is plotted over the simulation time. Also here, the curves are pairwise similar. Both variants with the chemical potentials as primary variables need more *Newton* steps to reach equilibrium, while the computations with the molar concentrations initially require two *Newton* steps, later only one is required. This effects also the time-step sizes[3], as one can see on the right-hand side of the same figure. While the variants corresponding to the red curves increase the time-step size with each new time step, the blue ones increase the time-step size very slowly. As a result of the higher number of *Newton* steps and the smaller time-step sizes, the computation times differ strongly. In particular, while the simulations with

[3]As has been pointed out in Section 4.3.6, the time integration within this thesis is carried out by use of the implicit *Euler* method. Since this is a single-step time integration scheme, there are no error estimators available such as in the two-step *Runge-Kutta* methods. Thus, the time-step size is controlled by the number of *Newton* iterations required until convergence is obtained.

the variants I and II need 71 minutes to run through the whole computation, the variants III and IV need only 13 seconds. Please note that this is not a mistake.

The reason of this discrepancy in computation time is twofold. Firstly, in the set I and II given in the chemical potentials, the concentrations of the ions are computed from the square root of exponential functions. Secondly, for the material time derivative $(c_m^\gamma)'_S$ of the molar concentrations, the second derivative of the solid displacement $\mathbf{u}_S$ is required, cf. $(4.13)_2$. Moreover, as denoted in the literature, the weakly imposed *Dirichlet* boundary conditions have a certain stabilisation effect.

5.1.2 Possible simplifications

The same numerical experiment, as mentioned in the introduction of this section, has also been performed via the simplifications S I, S II[4]. It is the intention of this section to compare and discuss the results computed by the reduced sets of primary variables with the full set of primary variables. Therefore, the variant IV is chosen as the reference, since this set seems to be most stable, cf. Section 5.1.1, and most accurate, cf. Section 5.2.2.

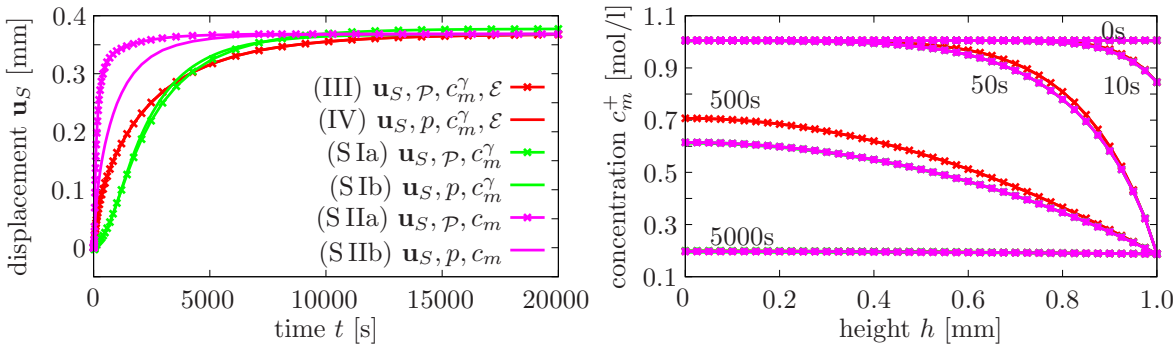

Figure 5.4: On the left-side, the vertical displacement of the observed node by use of the different simplifications plotted and, on the right-side, the cation concentration distribution in the domain at different times.

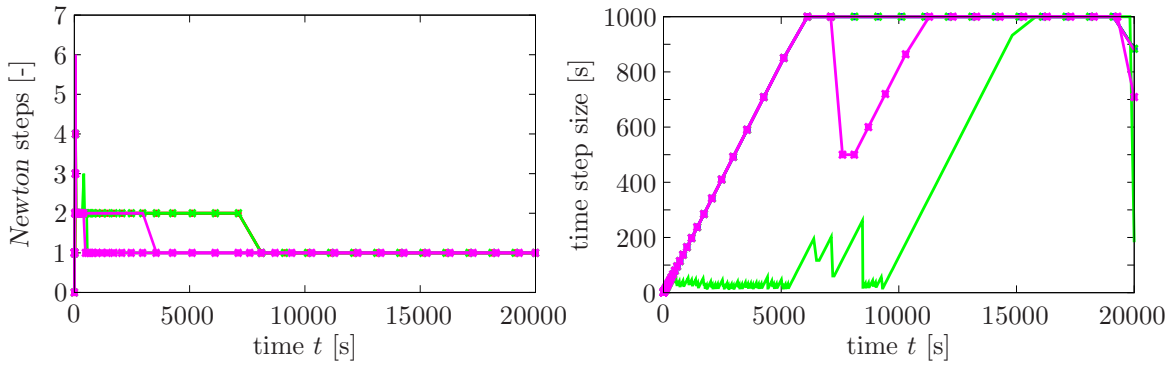

Figure 5.5: Numerical aspects of the computations. On the left-side, the number of *Newton* iterations over time is plotted and the time step size evolution on the right-hand side.

[4]Simplification S III is compared in the Appendix B.1

In Figure 5.4, the results obtained by variant IV are compared with the simplifications S I and S II. Therein, again the evolution of the vertical displacement of the upper observed node is plotted. The red lines belong to the variants III and IV, i. e. these are the same red curves as given in the previous section. In addition, the green lines correspond to the simplification I, the model without a net electric current, and the magenta lines correspond to the simplification S II, where additionally the electroneutrality condition is fulfilled strongly at each material point. Again in this situation, each variant has a representation in the hydraulic pressure (a) and in the overall pressure (b).

As one can see in Figure 5.4, by neglecting the overall electric current in the variant IV, the corresponding displacement curves get the same shape as the variants I and II expressed in the chemical potentials, cf. Figure 5.2. Moreover, by additionally assuming electroneutrality, the swelling process takes place much faster. Thus, the displacement curve is much more steep at the beginning and the equilibrium is reached earlier. This is even more the case by use of the hydraulic pressure $\mathcal{P}$ as the primary variable of the fluid. Recall that there is no difference in the variants III and IV if the hydraulic pressure or the overall pressure is chosen as the primary variable. But by use of simplification S I, there is a small difference before reaching the equilibrium level and even more in case of simplification S II. Following this, the choice of the pressure primary variable has a greater influence the more restrictions are added to the model. Looking at the distribution of the cation concentration c_m^+ within the domain at different times, on finds that the variants III and IV have certain distribution and all simplifications have a certain value. The reason is that the no-net-electric-current condition is used in all of them and, thus, the gradient of the electric potential, a driving force in the diffusion process, is computed from internal variables.

In Figure 5.5, the evolution of the *Newton* steps and the time-step sizes are plotted. Therein, it can be seen that the model tends to be more linear, the more additional assumptions are incorporated. Therefore, the simplification S II needs less *Newton* steps to reach convergence. Note that the curves of the variants III and IV lay exactly under the ones of simplification S Ia and S Ib. Concerning the time-step sizes, the curves of the variants III, IV and simplification S Ia formulated in the hydraulic pressure lay also exactly on each other. Thus, simplification S Ib formulated in the overall pressure p needs 89 s, while the other possibilities need 13 s.

As a result, it can be concluded that the more assumptions are incorporated into the model, the sooner the equilibrium state is reached. But note that the computations by four primary variables without the electric potential $\mathcal{E}$ are much more sensitive and, thus, unstable. This may be caused by the exclusion of the electric potential, but by nevertheless computing the ion concentrations individually. As a result, small deviations from the electroneutrality may occur, which are not captured by any restriction. This sensitivity is also the reason, why the variants I and II can not be simplified. The simulations of this set of primary variables do not run without the *Poisson* equation. As has already been mentioned above, the reason is that the molar concentrations are computed as internal variables.

5.2 Comparison with an experiment

In reality, it can be observed that the components of a chemical solution do not behave as predicted by use of the chemical potentials. The reason is that the chemical potential is based on the ideal gas law, where it is assumed that the individual atoms or molecules have a huge distance among each other and, thus, very low interactions, cf. Appendix A. This is not the case in a chemical solution. Here, due to the lower distances and higher interactions, the behaviour differs from an ideal gas. Note that in case of strong electrolytes such as, e. g., Na^+Cl^- and $Ca^{2+}Cl_2^-$, the deviations from the ideal behaviour can already be observed in case of very low concentrations, which is generally referred to as an ideal solution, cf. Figure 5.6. However, the difference from the ideal behaviour is captured by the activity coefficient f^β, which leads together with the molar concentration to the activity a^β. Since the activity coefficient of the liquid solvent can be considered as constant, i. e. $f^L \approx 1 = \text{const.}$, only the solutes have a non-constant activity coefficient, cf. also the discussion about activity and osmotic coefficients in Appendix A.2. Moreover, in case of ions in solution, i. e. for electrolytes, only a common activity coefficient $f^\pm$ can be measured. Thus,

$$\mu_m^L = \mu_{m0}^L + R\theta \ln c_m^L \qquad \text{and} \qquad \breve{\mu}_m^\gamma = \underbrace{\mu_{m0}^\gamma + R\theta \ln c_m^\gamma}_{\mu_m^\gamma} + \underbrace{R\theta \ln f^\pm}_{\mu_{ma}^\gamma}, \tag{5.1}$$

where $\breve{(\cdot)}$ denotes the quantities having an activity part $(\cdot)_a$. Based on the *Debye-Hückel* theory describing the electrostatic interactions of electrolytes, Hamer & Wu [87] postulated the following ansatz for the activity coefficient:

$$\log f^\pm := -\frac{A\,|z^+ z^-|\,\sqrt{I}}{1 + B\sqrt{I}} + C\,I + D\,I^2 + E\,I^3\,. \tag{5.2}$$

Therein, log is the logarithm to the base 10, the first term on the right-hand side represents the actual *Debye-Hückel* term, I is the ionic strength given by (2.21), A is the dielectric constant of the solvent, and the variables B to E have no distinct physical meaning and, thus, denote purely empirical and material dependent coefficients. Inserting (5.2) into (5.1) leads to

$$\breve{\mu}_m^\gamma = \mu_{m0}^\gamma + R\theta \ln c_m^\gamma + R\theta \ln 10 \Big(-\frac{A\,|z^+ z^-|\,\sqrt{I}}{1 + B\sqrt{I}} + C\,I + D\,I^2 + E\,I^3 \Big)\,. \tag{5.3}$$

By integration of the above chemical potential of the solutes with respect to the corresponding concentration c_m^γ, the so-called activity part of the *Helmholtz* free energy of φ^γ is obtained:

$$\begin{aligned} \Psi_{Fa}^\gamma &= R\theta \int_{c_m^\gamma} \ln f^\pm \,\mathrm{d}c_m^\gamma \\ &= R\theta \frac{2}{(z^\gamma)^2} \ln 10 \Big[-\frac{A\,|z^+ z^-|}{B^3} \big[B^2 I - 2\,B\sqrt{I} + 2 \ln\big(1 + B\sqrt{I}\big) \big] + \\ &\qquad + \tfrac{1}{2} C\,I^2 + \tfrac{1}{3} D\,I^3 + \tfrac{1}{4} E\,I^4 \Big]\,. \end{aligned} \tag{5.4}$$

Given the standard portion μ_m^β and the activity portion of the chemical potentials μ_{ma}^γ as well as of the *Helmholtz* free energies Ψ_F^β and Ψ_{Fa}^γ, the osmotic pressure of the component can be calculated from equation (3.51) by use of $\check{\mu}_m^\gamma$ and Ψ_{Fa}^γ, i. e.

$$\check{\pi}^\gamma = R\theta\, c_m^\gamma + R\theta \left(c_m^\gamma \ln f^{\pm} - \Psi_{Fa}^\gamma \right), \tag{5.5}$$

which leads to the overall pressure via relation (3.55):

$$\check{\pi} := \pi^L + \sum_\gamma \check{\pi}^\gamma = \sum_\beta \left(c_m^\beta \mu_m^\beta - \Psi_F^\beta \right) + \sum_\gamma \left(c_m^\gamma \mu_{ma}^\gamma - \Psi_{Fa}^\gamma \right). \tag{5.6}$$

Note in passing that due to the electroneutrality of the overall aggregate, the activity coefficients cannot be measured separately. Thus, the common activity coefficient $f^{\pm}$ always depends on both concentrations. Following this, it is not consistent with the assumption (3.37), that Ψ_F^γ only depends on its own concentration c_m^γ (or density ρ_F^γ). Concerning the osmotic coefficient, the following considerations hold. Recalling that the osmotic coefficient has been introduced for experimental reasons as a factor in front of the logarithmic function, cf. Appendix A.2.2, the resulting function cannot be integrated and, therefore, the osmotic coefficient cannot be introduced in such a consistent manner as the activity coefficient.

5.2.1 Influence of the activity coefficients

In this subsection, the influence of the activity coefficients will be evaluated. To be able to compare the obtained results with the previous ones, the same material parameters, the same geometry and also the same chemical loading are used for this numerical experiment.

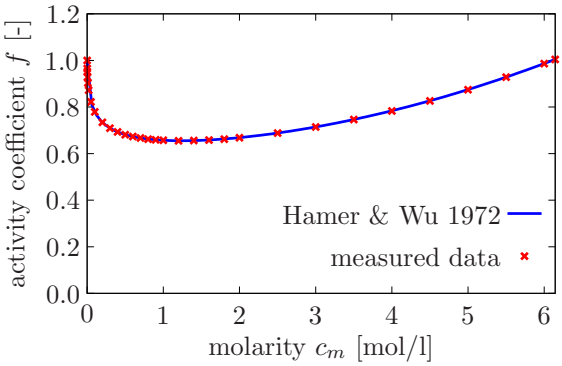

Figure 5.6: Measured data compared to the fitted curve by Hamer & Wu [87] in the range of pure solvent to saturated Na^+Cl^- solution.

As has been mentioned already in the previous section, the concentration-dependent activity coefficients are computed based on the *Debye-Hückel* theory by (5.2) proposed by Hamer & Wu [87]. In their publication, the authors collected the measured osmotic and activity coefficients of several electrolyte solutions and extended the *Debye-Hückel* equation to fit the corresponding curve of the activity coefficient in the complete range from

pure solvent to saturated solutions. The measured data as well as the activity coefficient computed by (5.2) are plotted in Figure 5.6. Therein, the following values have been taken from Hamer & Wu [87] for the empirical constants:

$$\begin{aligned} A &= 0.5102\,, \qquad B = 1.4495\,, \qquad C = 2.0442 \cdot 10^{-2}\,, \\ D &= 5.7927 \cdot 10^{-3}\,, \qquad E = -2.8860 \cdot 10^{-4}\,. \end{aligned} \tag{5.7}$$

By use of these values, the activity coefficient of the solutes of a Na^+Cl^- solution is computed. Moreover, in Figure 5.6, it can clearly be seen that $f^{\pm}$ rapidly deviates from one even for very dilute solutions. This is generally the case for strong electrolytes such as Na^+Cl^-, since the electric effects have a much higher range of influence than other effects. For other solutes, cf. [87]. In addition, Goldberg [78, 79] lists further values of the activity coefficients $f^{\pm}$ for uni-uni- and uni-bivalent compounds.

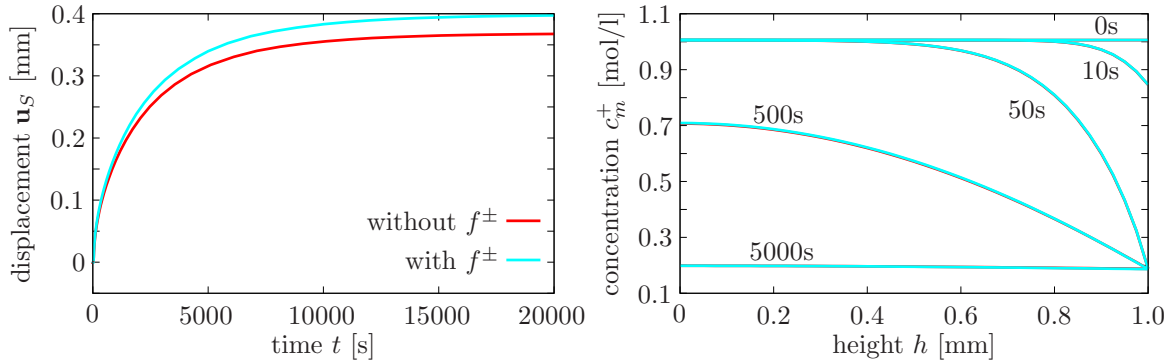

Figure 5.7: Vertical displacement of the observed node on the left and cation concentration c_m^+ distribution in the domain at different times on the right. Red line: variant IV. Cyan line: variant IV with activities.

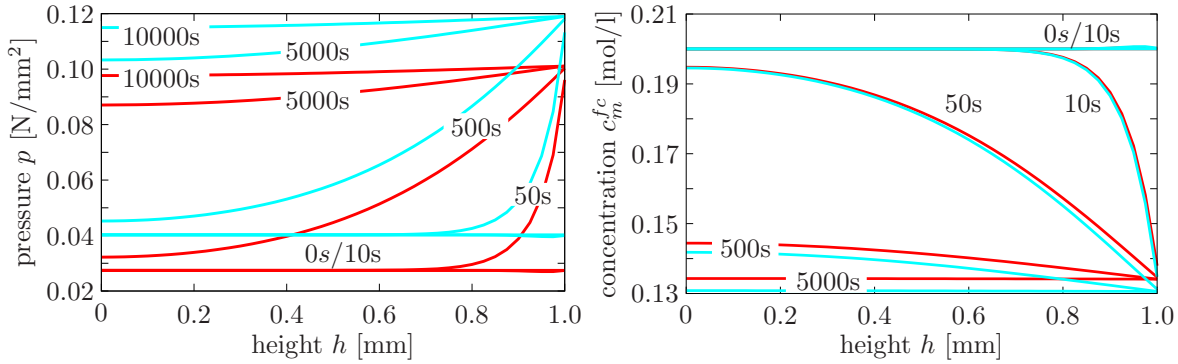

Figure 5.8: On the left-hand side, the overall pressure p distribution in the domain is depicted and, on the right-hand side, the distribution of the fixed charges c_m^{fc} in the domain at different times. Red line: variant IV. Cyan line: variant IV with activities.

The initial and boundary conditions corresponding to the primary variables of the model variant IV based on the above derived chemical potentials and osmotic pressures are

obtained in the same manner as (4.3), (4.5) and (4.6), i. e.

$$\begin{aligned} c_m^\gamma &= \frac{1}{2\,|z^\gamma|}\sqrt{\left(z^{fc}\,c_m^{fc}\right)^2 - 4\,z^+z^-\left(\frac{\bar f^\pm}{f^\pm}\,\bar c_m^\gamma\right)^2} - \frac{z^{fc}\,c_m^{fc}}{2\,z^\gamma}\,, \\ \Delta\pi &= R\theta\left[(c_m^+ + c_m^-) - (\bar c_m^+ + \bar c_m^-)\right] + R\theta\sum_\gamma\left[(c_m^\gamma \ln f^\pm - \bar c_m^\gamma \ln \bar f^\pm) - (\Psi_{Fa}^\gamma - \bar\Psi_{Fa}^\gamma)\right], \\ \Delta\mathcal{E} &= \frac{R\theta}{z^\gamma F}\ln\frac{\bar f^\pm\,\bar c_m^\gamma}{f^\pm\,c_m^\gamma}\,. \end{aligned} \tag{5.8}$$

In order to obtain the above conditions $(5.8)_1$ and $(5.8)_3$, it has been assumed that $f^\pm$ and $\bar f^\pm$ are stepwise constant functions.

The results of the vertical displacement and the cation concentration distribution are plotted in Figure 5.7. It can be seen that there is a distinct difference in the overall swelling behaviour of the hydrogel. The increase in the final volume in this 1-d situation is nearly 10%. Since the concentration distribution within the domain does not change, cf. Figure 5.7 on the right, the difference in the volume change results only from the change in the osmotic pressure, cf. Figure 5.8 on the left. Because of the higher deformation, the concentration of the fixed charges changes accordingly, cf. Figure 5.8 on the right, and thus, the anion concentration increases to maintain the electroneutrality condition.

Having a closer look at the boundary conditions (4.3), these results can be expected. More precisely, since the average of the inner and the average of the outer concentrations are in the same range, the ratio of the activity coefficients is approximately one ($\bar f^\pm / f^\pm \approx 1$). Thus, the values of the concentrations are almost unmodified compared to the ideal case. In contrast, the osmotic pressure difference $\Delta\pi$, cf. (4.5), at the boundary does definitely change.

5.2.2 Simulation of a swelling experiment

In order to validate the model derived within this thesis, a swelling experiment given in the literature (Frijns *et al.* [76]) will be simulated. Again, variant IV is chosen for the validation but including the previously introduced concentration-dependent activity coefficients.

The swelling experiment is performed as follows. A specimen of approximately 1 mm height is cut off from the intervertebral disc of a dog. During the experiment, the specimen is confined in the circumferential direction by a testing chamber. At the upper boundary, the loading piston including the displacement transducer is placed, while the bottom of the chamber is carried out as a glass filter. This filter is permeable for the Na^+Cl^- solution such that the specimen can be chemically loaded.

Thus, for the numerical simulation, a geometry of $0.1 \times 1.06\,\mathrm{mm}^2$ with the actual height of the specimen under consideration is discretised by 1×120 quadrilateral *Taylor-Hood* elements, cf. Figure 5.9. Starting from a zero-displacement initial condition, where the initial osmotic pressure is carried by the solid matrix, the sample is chemically loaded

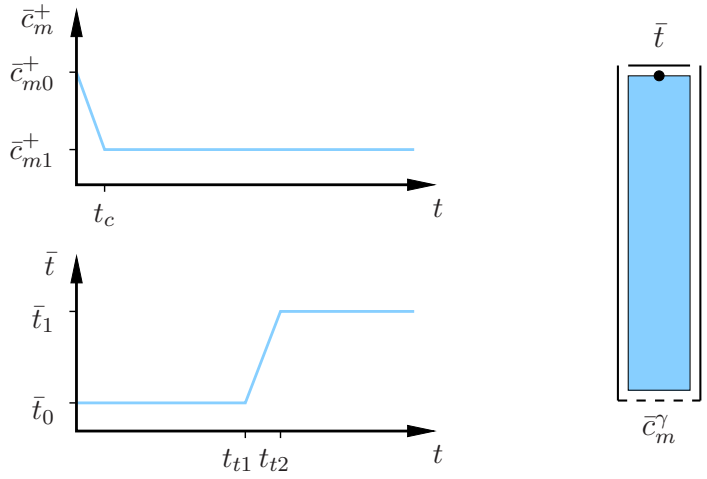

Figure 5.9: Upper left: Chemical loading, the concentration of the external solution is decreased from $\bar{c}_{m0}^+$ to $\bar{c}_{m1}^+$ until t_c. Lower left: The mechanical load at the upper boundary is increased within t_{t1} and t_{t2}. Right: Sketch of the geometry with the observed upper node.

c_{m0S}^{fc}	=	0.126 eq/l	n_{0S}^S	=	0.238
λ^S	=	0.45 N/mm^2	μ^S	=	0.195 N/mm^2
γ^{FR}	=	$1 \cdot 10^{-5}$ N/mm^3	k^F	=	$2.3 \cdot 10^{-9}$ mm/s
D^+	=	$0.49 \cdot 10^{-3}$ mm^2/s	D^-	=	$0.78 \cdot 10^{-3}$ mm^2/s
M_m^+	=	$22.99 \cdot 10^{-3}$ kg/mol	M_m^-	=	$40.08 \cdot 10^{-3}$ kg/mol
R	=	8.3144 J/K mol	θ	=	298 K
F	=	96 485.33 C/mol	$\kappa^{p,c,\varepsilon}$	=	1.0
z^+	=	+1	z^-	=	−1
z^{fc}	=	−1	ϵ^F	=	100.0 C/N mm^2
$\bar{c}_{m0}$	=	0.458 mol/l	$\bar{c}_{m1}$	=	0.146 mol/l

Table 5.2: Set of material parameters used for the simulation of the swelling experiment.

at the bottom by decreasing the ion concentration from $\bar{c}_{m0}^+ = 0.458\,\text{mol/l}$ to $\bar{c}_{m1}^+ = 0.146\,\text{mol/l}$ within $t_c = 50\,\text{s}$. After the corresponding equilibrium state is reached at $t_{t1} = 21600\,\text{s}$ (6 h), the mechanical load on the specimen at the upper boundary is increased from $\bar{t}_0 = 0.0\,\text{N/mm}^2$ to $\bar{t}_1 = 0.117\,\text{N/mm}^2$ within two seconds.

The respective set of material parameters used for this computation are taken from the above mentioned literature and are also summarised for convenience in Table 5.2. Note that instead of using osmotic coefficients, the computations have been performed by use of the concentration-dependent activity coefficients. Therefore, to fit the needs of the specimen, the parameters concerning the activity of the medium are "hand-fitted" as

follows:

$$A = 0.5108\,, \qquad B = 0.0495\,, \qquad C = 1.1044\,, \\ D = 5.7927 \cdot 10^{-3}\,, \qquad E = -2.8860 \cdot 10^{-4}\,. \tag{5.9}$$

Note that there are many chemical substances in the intervertebral disc contributing to the activity and also to the osmotic pressure. Thus, the values of the empirical constants corresponding to a pure Na^+Cl^- solution need to be modified. Moreover, as discussed by Chahine *et al.* [35], there is a residual osmotic pressure in the range of high concentrations, which suggests that the solid matrix has also a contribution to π.

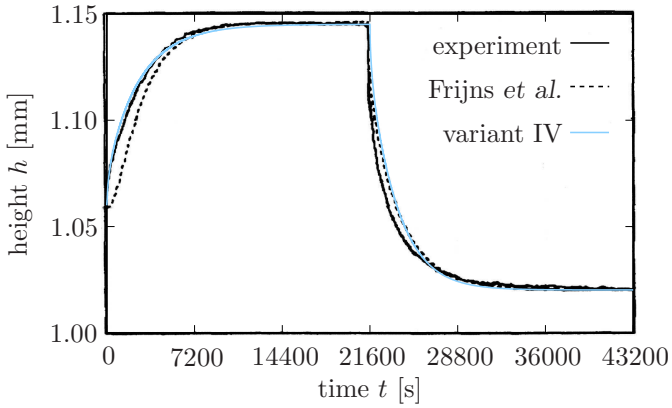

Figure 5.10: Comparison of the swelling and compression experiment (black, continuous) with the computation by Frijns *et al.* [76] (black, dashed) and the one performed by use the proposed model (green, variant IV).

However, as depicted in Figure 5.10, the simulation of the swelling experiment by the model presented in this contribution with the variant IV of the primary variable sets agrees quite well with the swelling experiment. Moreover, by use of the concentration-dependent activity coefficient, no additional osmotic coefficients are needed. Finally, note that Frijns *et al.* [76] used a formulation in the chemical potentials quite similar to the variant I and, thus, according to the results given in Section 5.1.1, the dashed black line exhibits the same behaviour as the curve corresponding to the variant I in Figure 5.2 left.

5.3 Electric stimulation

The effects of an electric loading of a charged, hydrated porous material will be computed within this section. Such materials are newly used in robotics as artificial muscles, cf. Bar-Cohen [8]. This ionic electroactive polymers (EAP) react to externally applied fields by diffusion and osmosis. As a result of the non-uniformly distributed ion concentrations, the osmotic pressure also varies within the domain.

To keep things simple, again a 2-d geometry is simulated under 1-d loading conditions. More precisely, the 2-d geometry sketched on the right-hand side in Figure 5.11 is fixed at its left and right boundaries, i. e. no movements perpendicular to these edges are possible, while additionally the vertical displacement is fixed at the middle nodes. There is neither

a fluid nor an ion efflux over these boundaries. Moreover, the upper and lover boundaries are in contact with the external bathing solution with the constant molar concentrations $c_m^+ = c_m^- = 0.09\,\text{mol/l}$, and these boundaries are also loaded electrically by $\mathcal{E}_t = +10\,\text{mV}$ at the top and by $\mathcal{E}_b = -10\,\text{mV}$ at the bottom within $t_\varepsilon = 2\,\text{s}$, cf. Figure 5.11. This results in an electric loading by 20 mV. The set of material parameters used during these computations is summarised in Table 5.3. The $0.1 \times 1.0\,\text{mm}^2$ is discretised by 2×40 quadrilateral *Taylor-Hood* elements.

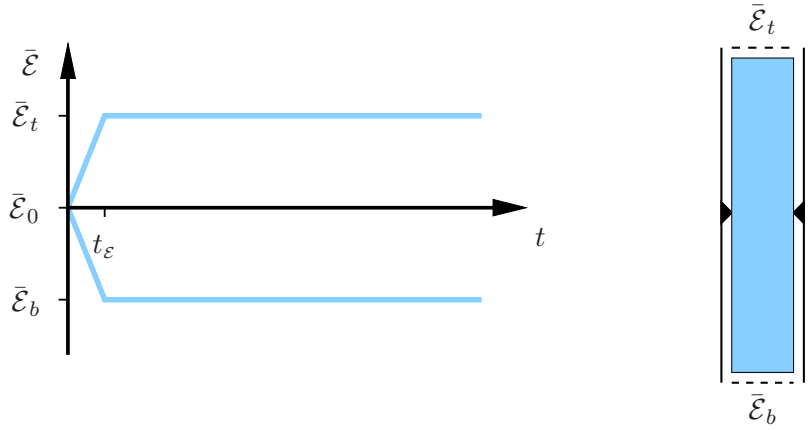

Figure 5.11: Left: Electric loading, at the top $\bar{\mathcal{E}}_t$ and at the bottom side, $\bar{\mathcal{E}}_b$is applied within 2 s. Right: Sketch of the geometry with the boundary conditions.

c_{m0S}^{fc}	=	0.02 eq/l	n_{0S}^S	=	0.25
λ^S	=	0.04 N/mm^2	μ^S	=	0.10 N/mm^2
γ^{FR}	=	$1 \cdot 10^{-5}$ N/mm^3	k^F	=	$1.07 \cdot 10^{-8}$ mm/s
D^+	=	$0.5 \cdot 10^{-3}$ mm^2/s	D^-	=	$0.8 \cdot 10^{-3}$ mm^2/s
M_m^+	=	$22.99 \cdot 10^{-3}$ kg/mol	M_m^-	=	$40.08 \cdot 10^{-3}$ kg/mol
R	=	8.3144 J/K mol	θ	=	298 K
F	=	96 485.33 C/mol	$\kappa^{p,c,\varepsilon}$	=	1.0
z^+	=	+1	z^-	=	−1
z^{fc}	=	−1	ϵ^F	=	100.0 C/N mm^2
$\bar{c}_{m0}$	=	0.09 mol/l	$\bar{\mathcal{E}}_t, \bar{\mathcal{E}}_b$	=	±10.0 mV

Table 5.3: Set of material parameters used for the electric stimulation.

In Figure 5.12, the results concerning the concentrations are plotted. On the left figure, the anion concentration is given. It can clearly be seen that at the boundary, where the negative electric potential is applied, i. e. at the cathode, the anion concentration increases, while at the opposite side, at the anode, the concentration of the anions decreases. Of

course, the opposite is the case for the cations. On the right-hand side in Figure 5.12, the electroneutrality, i. e. the sum of all molar concentrations times the corresponding valences, is plotted. As the electroneutrality condition is weakly fulfilled by use of the *Poisson* equation, the sum of the concentrations is not strictly zero anymore. Instead, it changes its value similar to the anion concentration over the time until an equilibrium state is reached. At this state, the net charge of the overall aggregate is negative at the cathode and positive at the anode. Between both of the loaded edges, the net charge changes linearly. Note that in contrast to Wallmersperger [168], a deforming solid skeleton has been considered herein, where the electric potential boundary conditions depend on the current state of the domain.

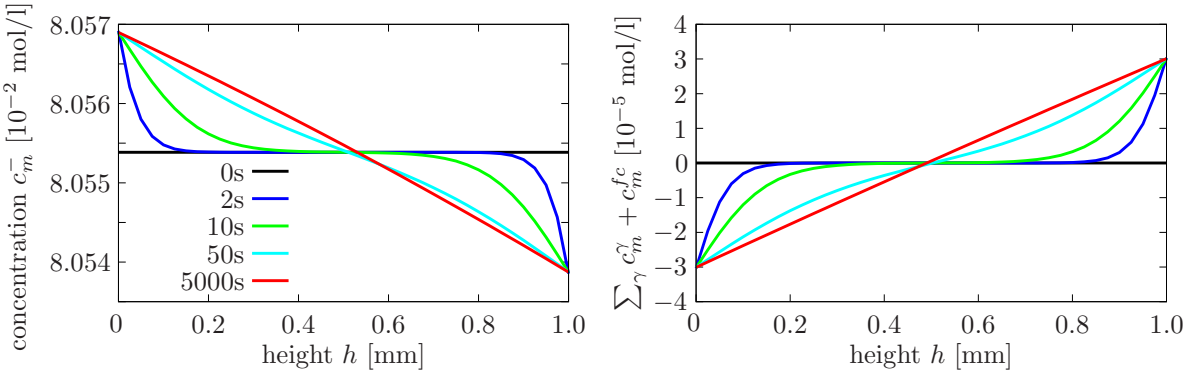

Figure 5.12: Anion concentration c_m^- within the domain at different times on the left-hand side and overall electroneutrality distribution on the right-hand side.

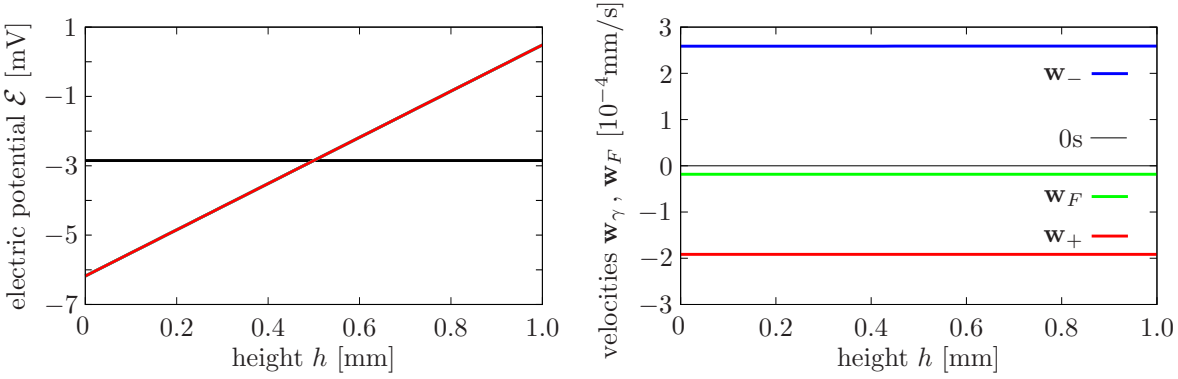

Figure 5.13: Left: electric potential $\mathcal{E}$ within the domain. It immediately reaches it equilibrium value. Right: velocities $\mathbf{w}_\gamma$ of the ions and the overall fluid $\mathbf{w}_F$.

In contrast to the concentrations, which gradually reach their equilibrium values by diffusion processes, the state of the electric variables changes immediately. As it can be seen in Figure 5.13, the electric potential does not change after the loading process. Thus, the equilibrium state is reached together with the stationary loading conditions. And also the fluid and ion flows reach their final values instantly. This contrary ion movements, where the anions flow to the cathode and the cations flow to the anode, results in an electric current from the upper boundary with the higher potential to the lower potential at the bottom, cf. equation (4.21).

5.4 3-d finite swelling of a hydrogel cylinder

In the next two sections, the capabilities of the theoretical model and its numerical implementation will be demonstrated by two 3-d examples. Note that both of the following simulations are based on the variant IV. The first example is the numerical simulation of a real free swelling experiment of a hydrogel cylinder exhibiting finite deformations. Such an experiment has been carried out by the group of Jacques Huyghe at the Biomedical Engineering department of the Eindhoven University of Technology. In this experiment, a soot-coloured cylindrical block was cut out of a hydrogel stick made in a test-tube and was thereafter immediately placed in a sodium chloride solution. The concentration in the new solution compared to the previous state was so low and, as a result, the osmotic pressure was so high that the hydrogel cylinder went through an enormous volumetric change until it reached its final equilibrium state, cf. Figure 5.14.

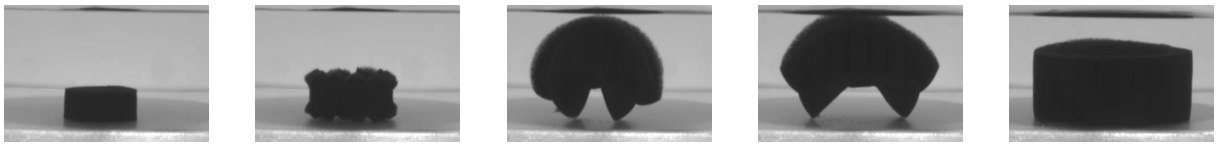

Figure 5.14: Free selling experiment of a soot-coloured hydrogel disc.

The aim of this numerical example is to simulate this experiment including the finite deformations as accurate as possible. It is clear that non-homogeneities as well as instabilities, which have not been implemented into this computation, play an important role during this experiment.

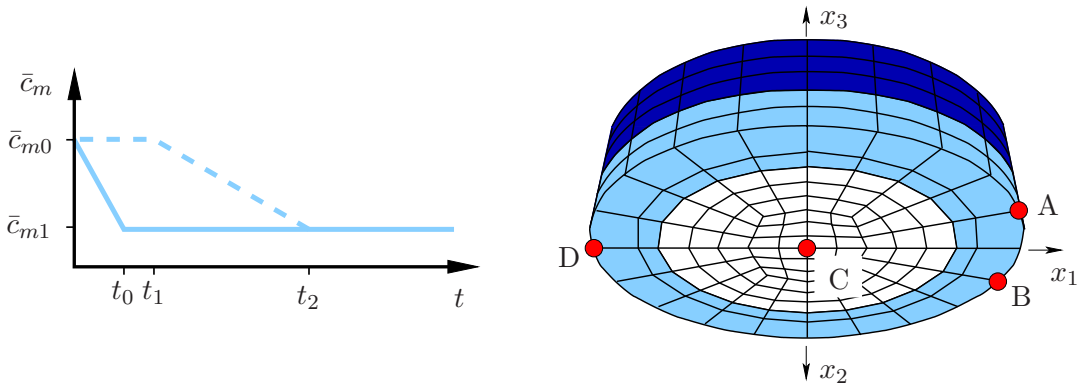

Figure 5.15: Chemical loading and geometry of the 3-d free swelling simulation. The solid concentration curve on the left side belongs to the dark blue boundary on the right side, while the dashed line belongs to the white surface. The light blue area in between is a transition zone between both concentrations.

To simulate this experimental setup, a slightly elliptic geometry with the radii $1.7 \times 1.5\,\mathrm{mm}^2$ and the height of 0.9 mm is discretised by 1.530 hexahedral *Taylor-Hood* elements. The elliptic form of the geometry has been chosen to avoid a radial symmetry. According to the discretisation described in Section 4.3.3, this results in a system with

29.865 DOF. The concentration curve of the external solution and a bottom view of the geometry of the disc are given in Figure 5.15. Therein, to mimic the contact conditions with the underground, only the boundary nodes denoted by the red circles have *Dirichlet* boundary conditions applied for the displacement. In particular, the nodes A and B are only fixed in the vertical direction, i. e. x_3, the centre node C has zero displacement in both horizontal directions, i. e. x_1 and x_2, and, finally, the node D is fixed in x_2 and x_3 direction. Thus, a minimum of displacement conditions have been set at the boundary such that the problem is statically determined.

c^{fc}_{m0S}	=	0.3 eq/l	n^S_{0S}	=	0.25
λ^S	=	0.02 N/mm^2	μ^S	=	0.14 N/mm^2
γ^{FR}	=	$1 \cdot 10^{-5}$ N/mm^3	k^F	=	$1.07 \cdot 10^{-7}$ mm/s
D^+	=	$0.5 \cdot 10^{-3}$ mm^2/s	D^-	=	$0.8 \cdot 10^{-3}$ mm^2/s
M^+_m	=	$22.99 \cdot 10^{-3}$ kg/mol	M^-_m	=	$40.08 \cdot 10^{-3}$ kg/mol
R	=	8.3144 J/K mol	θ	=	298 K
F	=	96 485.33 C/mol	$\kappa^{p,c,\varepsilon}$	=	3.0
z^+	=	+1	z^-	=	−1
z^{fc}	=	−1	ϵ^F	=	100.0 C/N mm^2
$\bar{c}^+_{m0}$	=	1.0 mol/l	$\bar{c}^+_{m1}$	=	0.05 mol/l

Table 5.4: Set of material parameters used for the swelling simulation of the hydrogel cylinder.

To apply the concentration boundary conditions, as can be seen in Figure 5.15 on the right-hand side, the surface of the overall geometry has been split into three regions. The upper dark blue surface is directly in contact with the external bathing solution. Thus, the concentration at this boundary follows the continuous blue line in the graph on the left-hand side in Figure 5.15, i. e. the concentration is immediately decreased from $\bar{c}^+_{m0} = 1.0\,\text{mol/l}$ to $\bar{c}^+_{m1} = 0.05\,\text{mol/l}$ within $t_0 = 175\,\text{s}$. In contrast, the white surface underneath the cylinder initially rests on the ground. On this account it, is not in contact with the external bathing solution and, therefore, the concentration does not change here from the beginning. Instead, at time $t_2 = 135\,\text{s}$, when the hydrogel cylinder has such a high bending that the bottom lifts off the ground, the concentration is decreased here to the same value of $\bar{c}_{m1} = 0.05\,\text{mol/l}$ within 350 s until $t_3 = 485\,\text{s}$. Finally, to avoid numerical difficulties resulting from a jump of the concentration value at different adjacent boundaries, the light blue surface of the disc denotes the transition zone between the concentration value of the dark blue surface and the value corresponding to the white surface. The material parameters used during the simulation are summarised in Table 5.4.

In Figure 5.16, the simulation results are depicted. Therein, the deformation of the mesh

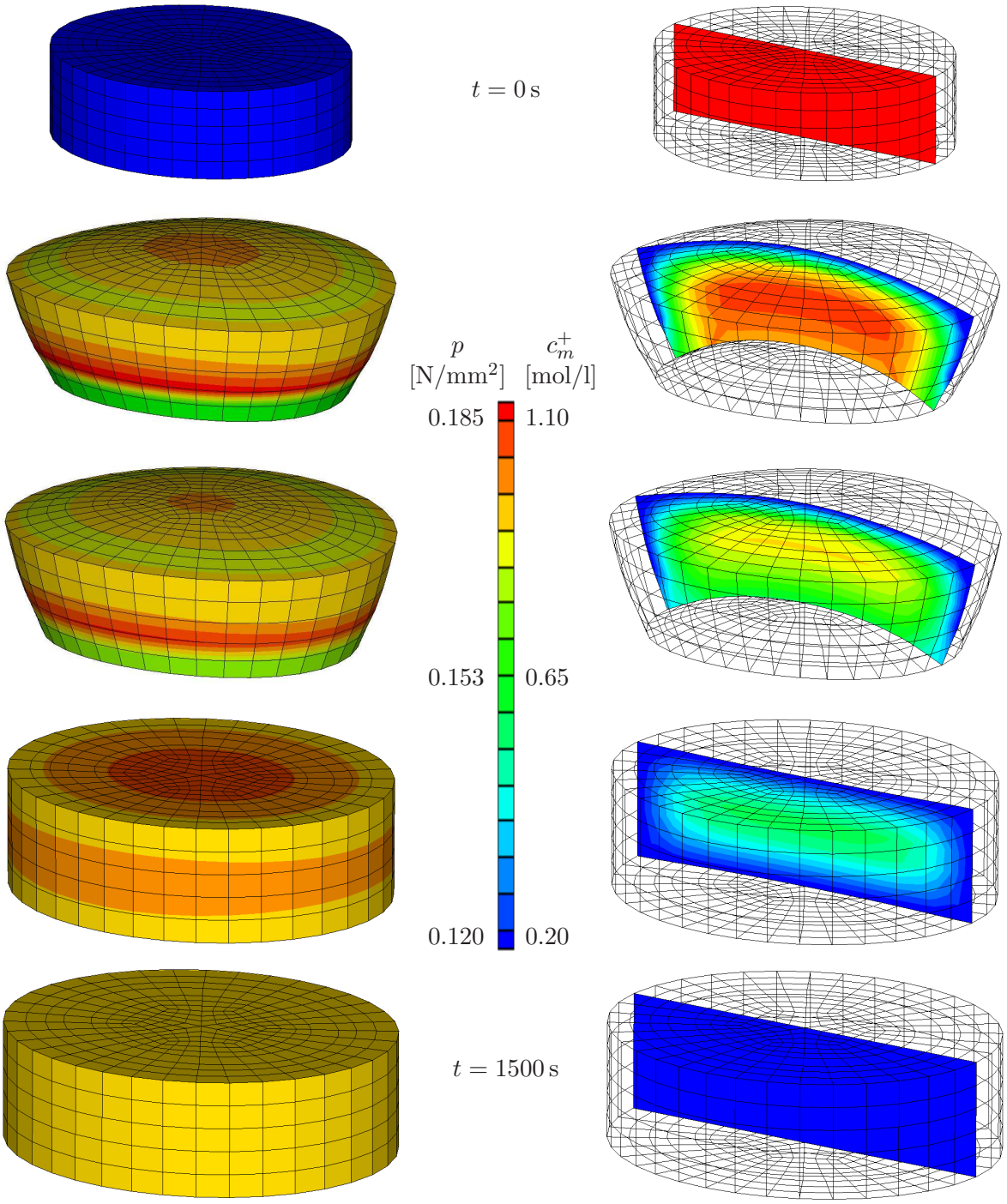

Figure 5.16: The overall pressure (l. h. s.) and the molar cation concentration (r. h. s.) evolution during the deformation of the hydrogel.

corresponds to the deformation of the medium at different times, i. e. $t = 0\,\mathrm{s}$, $t = 238\,\mathrm{s}$, $t = 376\,\mathrm{s}$, $t = 530\,\mathrm{s}$ and $t = 1500\,\mathrm{s}$. More precisely, on the left-hand side, the contour plot at the surface shows the overall pressure evolution and, on the right-hand side, the surface mesh is plotted along with a slice through the domain showing the molar concentration

distribution of the cations within the hydrogel disc. As one can see, the highest bending occurs around $t = 238\,\mathrm{s}$. Thereafter, the hydrogel slowly decreases its bending until $t = 530\,\mathrm{s}$, where it reaches a uniform strain at the upper and the bottom boundary. After that time it keeps swelling equally in each spatial direction such that it reaches its final equilibrium state at $t = 1500\,\mathrm{s}$. Moreover, in the second and third row in Figure 5.16, it can be seen that the concentrations do not change equally at the upper and the bottom boundaries. More precisely, the concentration is lower at the upper side and increases linearly along the boundary until the maximum value is reached at the bottom. Thus, the osmotic pressure is higher at the top side and decreases gradually to the bottom. This discrepancy in the pressure is the reason of the bending behaviour of the hydrogel disc. However, compared with to the photos of the real experiment in Figure 5.14, a similar behaviour could be simulated by the model presented within this thesis.

5.5 3-d bending of an EAP gripper

The intention of this last numerical example is to simulate the bending of an ionic electroactive polymer (EAP) under an electric field. Thus, a gripper made from an ionic EAP is electrically stimulated at two different sides to achieve a 3-d material response.

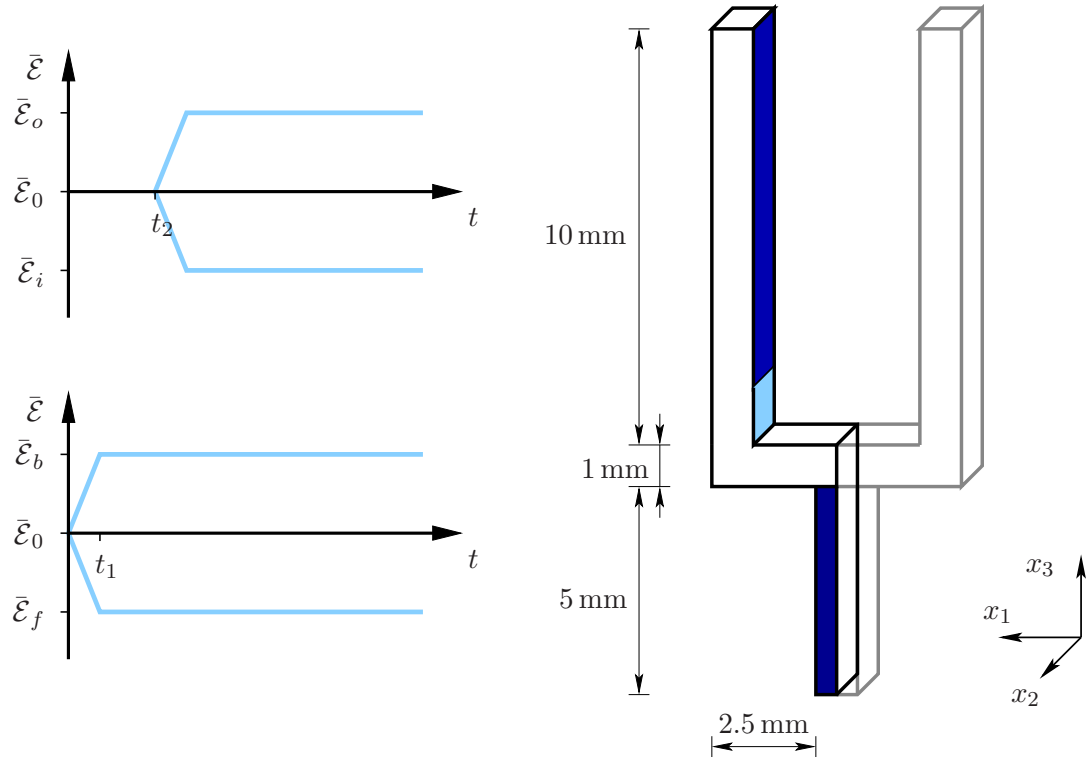

Figure 5.17: Electric stimulation of the upper part of the gripper follows the upper left curves and the electric stimulation of the lower part follows the lower left curves.

As depicted on the right-hand side in Figure 5.17, only one half of the system is considered because of the symmetry of the geometry as well as the boundary conditions. This

geometry is discretised by 258 *Taylor-Hood* elements, which leads to 6802 DOF. During the simulation, the following boundary conditions are applied. The EAP is spatially fixed at its bottom surface in the x_3 direction and at its symmetry surface in the x_1 direction. In addition, to fix the gripper spatially, one node at the bottom surface has been fixed in the x_2 direction. Moreover, following the experimental setups concerning ionic EAP, they are always placed in an ionic solution. Therefore, at each boundary, except at the symmetry and the bottom surface of the geometry, the constant molar concentration $\bar{c}_m^+ = \bar{c}_m^- = 1.0\,\text{mol/l}$ of the external solution together with the appropriate osmotic pressure is applied.

c_{m0S}^{fc}	=	0.3 eq/l	n_{0S}^{S}	=	0.25
λ^S	=	0.02 N/mm^2	μ^S	=	0.14 N/mm^2
γ^{FR}	=	$1 \cdot 10^{-5}$ N/mm^3	k^F	=	$2.07 \cdot 10^{-8}$ mm/s
D^+	=	$0.5 \cdot 10^{-3}$ mm^2/s	D^-	=	$0.8 \cdot 10^{-3}$ mm^2/s
M_m^+	=	$22.99 \cdot 10^{-3}$ kg/mol	M_m^-	=	$40.08 \cdot 10^{-3}$ kg/mol
R	=	8.3144 J/K mol	θ	=	298 K
F	=	96 485.33 C/mol	$\kappa^{p,c}$	=	22.0
z^+	=	+1	κ^{ε}	=	10.0
z^{fc}	=	−1	z^-	=	−1
$\bar{c}_{m0}$	=	1.0 mol/l	ϵ^F	=	100.0 C/N mm^2

Table 5.5: Set of material parameters used for the electric stimulation of the electroactive polymer.

The actual electric stimulation is performed in two steps. Firstly, the lower part of the gripper is stimulated at the surfaces with normals in the x_2 direction forcing the upper part to move in x_2 direction. This is done by applying the positive potential $\bar{\mathcal{E}}_b$ at the reverse side and the negative one $\bar{\mathcal{E}}_f$ at the front side within $t_1 = 4\,\text{s}$. Note that the anionic EAP always swell at the cathode side, i. e. the back side in the current configuration, and shrink at the anode side. Thus, the upper part of the gripper will move in the positive x_2 direction. Secondly, the upper part is stimulated at $t_2 = 450\,\text{s}$. In particular, the positive electric potential $\bar{\mathcal{E}}_o$ is applied at the outer surface and the negative potential $\bar{\mathcal{E}}_i$ is applied at the inner surface, both of them are again linearly increased within 4 s. Thus, the bending will take place in the negative x_1 direction such that the gripper is closed. The surfaces, where the electric potential is applied, are marked by the dark blue colour in Figure 5.17. Moreover, again to avoid numerical problems resulting from too high jumps in the electric potentials, a transition zone has been implemented in the upper part marked by the light blue colour. Note in passing, that in this example for the boundary condition of the electric potential, another penalty factor ($\kappa^{\varepsilon} = 10.0$) has been used as for the overall pressure and the molar concentration ($\kappa^{p,c} = 22.0$). The material

parameters used during the computation are summarised in Table 5.5.

The results of the simulation are given in Figure 5.18. Therein, the deformation of the gripper is depicted at several times. In particular, the two upper pictures show the initial condition at time $t = 0\,\mathrm{s}$ and the state after the first electric stimulation is fully applied ($t = 4\,\mathrm{s}$). Underneath, the deformation at time $t = 450\,\mathrm{s}$ is shown, before the second stimulation is applied and also the corresponding state with the fully applied electric load ($t = 454\,\mathrm{s}$) is shown. The bottom picture shows the final equilibrium state at $t = 741\,\mathrm{s}$, where the deformation is fully evolved. As has been pointed out before, anionic EAPs swell at the cathode, where the positive electric potential $\bar{\mathcal{E}}$ is applied, and shrink at the opposite side. Note that from this results, the difference between an ionic EAP and an electric EAP becomes clear. While the electronic EAP immediately reacts to the externally applied field via *Coulomb* forces, the ionic EAP responses via ion diffusion resulting from potential differences. Thus, the ionic EAPs are relatively slow compared to their electronic counterparts but they need a low voltage to be activated.

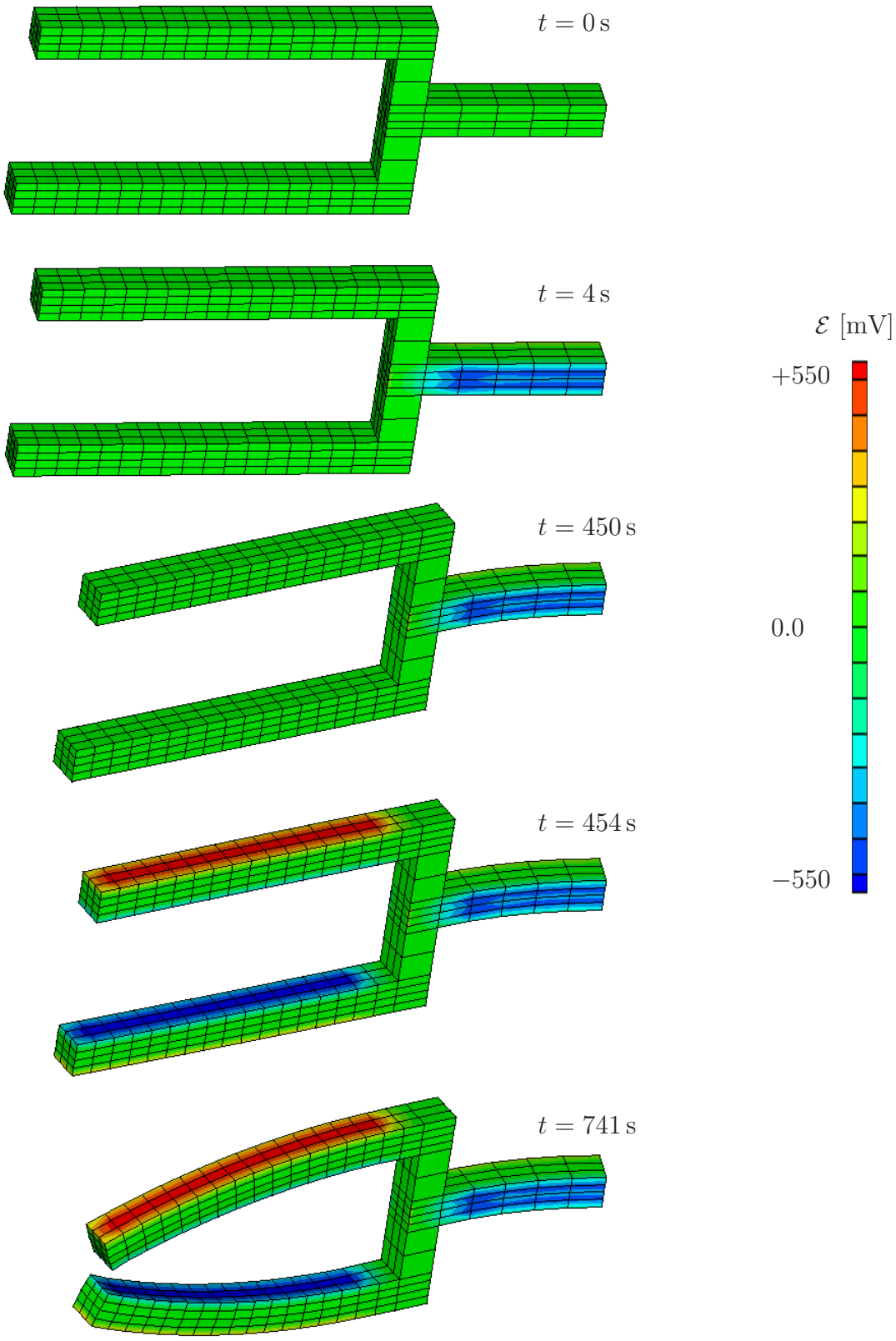

Figure 5.18: Bending of an electroactive polymer under an electric field.

Chapter 6:
Summary and future aspects

6.1 Summary

Throughout this work, a new integral and consistent continuum-mechanical theory has been derived to model swelling and electroosmosis of chemically and electrically active materials. Considering that this kind of materials generally consists of a charged solid matrix and a charged fluid, i. e. two immiscible phases, the overall aggregate has been modelled within the TPM. In contrast, particularly the fluid mixture with its miscible components has been modelled within the frame of the TM without using the concept of volume fractions of the fluid components, since they always occupy the entire fluid volume.

Based on this partition of the overall aggregate, the entropy inequality has been rearranged within the constitutive theory and the *Helmholtz* free energy of the overall fluid has been introduced. By evaluation of the entropy principle following the *Coleman-Noll* procedure, the definitions of the chemical potentials and the osmotic pressures representing the results of the classical thermodynamics could be derived. Moreover, the electric potential is introduced as a *Lagrange*an multiplier acting on the charge balances of the respective constituents. As a result, a novel model is derived, which is capable to describe all the phenomena within these materials resulting from the combination of deformation, osmosis, diffusion and electric current. The primary difference is, besides the individual description of the fluid components by the molar concentrations c_m^γ and the overall pressure p, the usage of the *Poisson*-equation to compute the electric potential.

The governing set of PDE has been investigated numerically within the FEM. Therein, different primary variable combinations could be chosen for the numerical scheme. Some of these primary variables such as the chemical potentials and the hydraulic pressure have continuous *Dirichlet* boundary conditions, which can be treated in the usual manner by strong imposition. In contrast, the molar concentrations, the overall pressure and the electric potential exhibit a jump over the boundary and, therefore, need to be computed from the respective equilibrium conditions depending on the current state of the medium. Thus, to avoid unsound oscillations of the results, a strategy from the field of free-surface flows has newly been adopted to this continuum-mechanical multifield problem. Therein, simultaneously four deformation-dependent boundary conditions have been imposed weakly by incorporation into the weak form of the corresponding balance relation via a penalty-like method.

From these numerical investigations of the primary variable sets, it could be observed that they differ slightly in their results and in their numerical efficiency. While both formulations in concentrations have exactly the same deformation behaviour regardless of the

choice of the pressure primary variable, the formulations in the chemical potentials exhibit a different deformation evolution. In particular, variant I given in the hydraulic pressure has a nearly horizontal tangent at the beginning of the displacement curve, whereas the displacement curve of the formulation in the overall pressure leans against the curves of the concentration formulation. Moreover, regarding the number of the *Newton* steps and the time step sizes, the formulations in the molar concentrations are more efficient. This can also concluded from the computation times. Here, the chemical potential formulations need 300 times longer than their counterparts. This may be caused by the condition that the concentrations and their derivatives are computed from square roots of exponential functions and that the second derivative of the solid displacement is required. Considering additional restrictions like no net electric current and strong electroneutrality, the general set of primary variables could be reduced. Because of stability reasons, these procedure could only be applied to the concentration formulations. From these reductions it could be concluded that the more assumptions are included into the model, the faster the swelling process takes place. Moreover, it has been found that the activity coefficients only influence the osmotic pressure and not the molar concentrations. The first applied restriction of no electric current, exhibited results similar to the formulation in the chemical potentials. By comparing the numerical results with a swelling-compression experiment, the derived model based on the molar concentrations has been validated. Therein, this model lead to more accurate results than other models found in the literature.

From the above considerations, it can be concluded that even though the programming effort for the weakly fulfilled boundary conditions may be higher, the simulation results are *more accurate* and numerically *more stable*. In addition, the computations are much *faster* than models using primary variables continuous over the boundary. Thus, the usage of basic and measurable variables such as the overall pore-pressure, the molar concentrations and the electric potentials instead of abstract quantities like the (electro-)chemical potentials is preferred.

6.2 Future aspects

The osmotic pressure of the overall aggregate has been measured in the literature, which differs from the computed one within this dissertation. However, even though this behaviour may be captured by the empirical coefficients within the activity portion of the chemical potentials, the difference may be caused by the hydrophilic character of the solid matrix, i. e. within the material a certain amount of water is bounded and does not contribute to the solvent, cf. Huyghe [105], Huyghe *et al.* [106], Loret & Simões [124].

As it has already been mentioned, the materials under consideration generally exhibit non-elastic behaviour. This is in the context of geomechanical materials plasticity, whereas in the area of biomechanical materials, the response of the solid matrix will be viscoelastic. Following this, the solid matrix could be specified more precisely. Moreover, the anisotropy of the solid matrix like in the case of the intervertebral discs could also be accounted for. Note that within this thesis only homogeneous materials have been considered. But the experience shows that the materials in nature have generally non-homogeneously

distributed material properties. This could also be regarded in future works.

Concerning the computation time of the numerical simulations by use of this model, it would be of great benefit to derive and program the analytical (consistent) tangent corresponding to the system of five PDEs implemented here.

Moreover, by use of a discontinuous *Galerkin* scheme, the primary variables would be able to exhibit jumps at the element boundaries. This would be of great benefit for the numerical stability of the system as well as for the discontinuous boundary conditions. Note that especially in cases such as the selling disc, where two different concentration boundary conditions need to be applied at adjacent boundaries like the bottom side and the circumferential surface, the conditions at this boundary lead to a jump of the primary variable along the boundary and, thus, to very steep gradients at this corner. However, also in this situation the discontinuous *Galerkin* scheme would improve the stability of the system and would enable the application of such boundary conditions.

Appendix A:
Chemical potential and the activity and osmotic coefficients

A.1 Background of the chemical potential

In textbooks about chemical thermodynamics like, for example, Klotz & Rosenberg [115], Ott & Boerio-Goates [141] and Prigogine & Defay [142], a general formulation of the chemical potential is given, which is independent of any ideality assumption and without any statement what type of component of the solution is considered, the solvent or the solute:

$$\mu^\beta \;=\; \mu_0^\beta + \bar{R}^\beta \theta \,\ln a^\beta \,. \tag{A.1}$$

Therein, μ_0^β is the standard chemical potential at standard state[1] and $\bar{R}^\beta$ denotes the specific gas constant, which is related to the universal gas constant

$$R \;=\; \bar{R}^\beta \, M_m^\beta \tag{A.2}$$

via the molar mass M_m^β. In the above representation of the chemical potential, the activity a^β is the product of the density ρ_F^β and the activity coefficient f^β, i. e.

$$a^\beta \;=\; f^\beta \rho_F^\beta \,, \tag{A.3}$$

where the activity coefficient f^β describes the deviation of the behaviour of an ideal solution, cf. Section A.2 for a more detailed introduction of the activity coefficient. Moreover, the mass specific chemical potential can be transformed to a molar quantity by multiplication with the molar mass and by use of (2.15):

$$\mu_m^\beta \;=\; \mu^\beta \, M_m^\beta \;=\; \mu_{m0}^\beta \;+\; R\theta \,\ln\, a^\beta \qquad \text{where} \qquad \left\{ \begin{array}{lcl} \mu_{m0}^\beta & = & \mu_0^\beta \, M_m^\beta \\ a^\beta & = & f^\beta \, c_m^\beta \end{array} \right. . \tag{A.4}$$

Note that to obtain a non-dimensional quantity, the term within the logarithmic function is divided by a standard value such as $\rho_{F0}^\beta = 1$ or $c_{m0}^\beta = 1$.

Remark: In chemical thermodynamics, the chemical potential is derived by inserting the ideal gas law

$$p^\beta = R\theta \, \frac{n_m^\beta}{v} \,, \tag{A.5}$$

[1] In chemistry, generally $\theta = 289\,\mathrm{K}$ and $p = 101,3\,\mathrm{kPa}$ (atmospheric pressure) is chosen as the standard state.

into the partial molar *Gibbs* free enthalpy $\xi(\theta, p)$ in case of constant temperatures

$$\frac{\partial \xi(p)}{\partial n_m^\beta} = \mathrm{d}\mu_p^\beta = \frac{v^F}{n_m^\beta}\,\mathrm{d}p^\beta = \frac{R\theta}{p^\beta}\,\mathrm{d}p^\beta \tag{A.6}$$

and integrating the result with respect to pressure, cf., for example, Adam *et al.* [2]. Note that the choice of the thermodynamical potential does not matter for the above equation, cf. Hille [96]. In the range of very low pressures, gases are in an ideal state with large distances among them, where the interactions between the molecules are negligible. Following this, the chemical potential of a component of an ideal gas mixture[2] is given by the partial pressure p^β belonging to the component, i. e.:

$$\mu_p^\beta = \mu_{p0}^\beta + R\theta \ln \frac{p^\beta}{p_0^\beta}\,. \tag{A.7}$$

Therein, p_0^β is a standard value generally chosen as 1 bar and is therefore cancelled in what follows. For ideal solutions, i. e. ideal fluid mixtures, one generally acts on the assumption that they behave like an ideal gas. Hence, the corresponding chemical potential looks rather similar. But, in contrast, two different kinds of components are involved in a solution. One of them contributes in a very large amount to the solution and the other ones are available only in minimal percentages. While the first is called solvent, the second kind of component is called solute. The maximum amount of a solute in a solution is given by its solubility, cf. Klotz & Rosenberg [115]. Based on this two natures of the components in a solution, two different chemical potentials are derived by transformation of the upper equation. Firstly, *Raoult*'s law for the solvent $p^\beta = x^\beta\, p_0^\beta$ is used, which indicates that the partial pressure of the solvent in an ideal solution is proportional to its mole fraction times vapour pressure in pure state p_0^β. The vapour pressure is the pressure at a certain temperature at which the solvent would undergo a phase transition from a fluid to a gas phase. By inserting this law into the chemical potential, one obtains

$$\mu_x^L = \mu_{x0}^L + R\theta \ln x_m^L\,. \tag{A.8}$$

Therein, standard potential is given by $\mu_{x0}^L = \mu_{p0}^\beta + R\theta \ln p_0^\beta$. Furthermore, the chemical potential for the solutes is derived by inserting the ideal gas law into (A.7). Thus,

$$\mu_m^\gamma = \mu_{m0}^\gamma + R\theta \ln c_m^\gamma\,, \tag{A.9}$$

is the relation for the solutes, where the standard potential is given by $\mu_{m0}^\gamma = \mu_{p0}^\gamma + R\theta \ln R\theta$.

All the representations of the chemical potentials expressed in different variables, i. e. the molar fraction c_m^γ, the density ρ_F^γ and the molar fraction x_m^β, have been plotted in Figure A.1 within the range of a pure solvent (0 mol/l) and a saturated Na^+Cl^- solution (6.14 mol/l). From this, it gets obvious that they only differ by a constant value. This difference is captured by the standard potential.

[2] An ideal gas mixture is a mixture of gases at very low pressure.

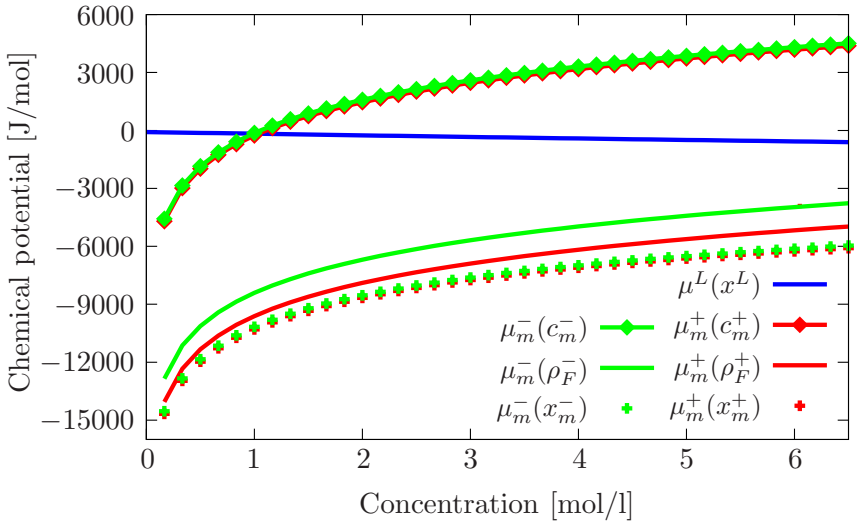

Figure A.1: Comparison of chemical potentials expressed in different scales, i. e. (A.1) with $(A.3)_1$, (A.8) and (A.9). The graphs reveal that the potentials only differ by a constant value. Here, the same standard potentials have been used.

Note, furthermore, that by use of these scales, the chemical potential of the solvent decreases with increasing concentration of the solutes since $\ln x^L \leq 0$ and has its maximum value at its pure state. In contrast, the potentials of the solutes increase with increasing concentration. □

A.2 Activity and osmotic coefficients

A.2.1 *Debye-Hückel* theory & activity coefficients

As has already been mentioned, with the chemical potentials in their standard form, one is only able to describe ideal solutions with evanescent concentrations. The main reason is that the chemical potentials are based on the ideal gas law (A.5), which does not account for any interactions between the molecules. Therefore, this theory is only valid in cases of low pressures or concentrations with a minimum of interaction within the components. *Van der Waals* was the first, who found a relation[3] for gases which is able to map their

[3] In 1873, van der Waals [165] derived the empirical equation

$$\left(p^\beta + \frac{a}{\tilde{V}_m^{\beta}}\right)(\tilde{V}_m^\beta - b) = R\theta$$

in his PhD thesis. Therein, the two parameters a and b are obtained from the specific critical point of the gas φ^β, i. e. the critical temperature θ_c^β and the critical pressure p_c^β, via the relations

$$b = \frac{R}{8}\frac{\theta_c^\beta}{p_c^\beta} \quad \text{and} \quad a = \frac{27\,R^2}{64}\frac{\theta_c^{\beta 2}}{p_c^\beta} \quad \text{and from this} \quad \tilde{V}_m^\beta = \frac{3\,R}{8}\frac{\theta_c^\beta}{p_c^\beta}.$$

behaviour correctly, even the critical point, where there is no distinction between the liquid and the gas phase. For a more detailed introduction, cf., for example, Adam *et al.* [2], Klotz & Rosenberg [115].

Taking into account that in gases the distances between the atoms or molecules are grater than in fluids or in mixtures of fluids, the error made by using the ideal gas law for fluid mixtures can be quite large. In order to capture the increasing interactions between the molecules in ranges of higher concentrations, the theory has to be extended. The effect of non-ideal behaviour is even higher in case of solutions with charged ions (electrolyte solutions), since the electrostatic effects outrange by far other effects like attraction forces between uncharged particles. The latter forces are referred to as *van der Waals* forces.

Considering firstly the solutes in a solution, generally described by their concentration (or density) in the solution, their deviation from the ideal behaviour is captured by use of the activity (A.3). Therein, the activity coefficient f^γ has to fulfil the limiting laws

$$\lim_{\rho_F^\gamma \to 0} \frac{a^\gamma}{\rho_F^\gamma} = 1 \quad \text{or} \quad \lim_{c_m^\gamma \to 0} \frac{a^\gamma}{c_m^\gamma} = 1\,. \tag{A.10}$$

Therefore, it follows from the above considerations for the limit of an ideal case:

$$\lim_{\rho_F^\gamma, c_m^\gamma \to 0} f^\gamma \;=\; 1\,. \tag{A.11}$$

The activity can be computed based on the ideas of the *Debye-Hückel* theory for strong electrolytes (Debye & Hückel [42]). This theory is in its original form only valid for ionic strengths up to 10^{-2} mol/l. Therefore, Hückel extended the corresponding relation by an additional term linear in the ionic strength I. Finally, Hamer & Wu [87] appended two terms, a quadratic and a cubic in the ionic strength, which leads to

$$\log f^+ \;=\; \log f^- \;=\; \log f^\pm \;=\; -\frac{A\,|z^+ z^-|\,\sqrt{I}}{1 + B\sqrt{I}} \;+\; C\,I \;+\; D\,I^2 \;+\; E\,I^3\,, \tag{A.12}$$

wherein the coefficients A, B, C and D are purely empirical solute-specific coefficients without any specific physical meaning. Note that the activity coefficient of an electrolyte in solution can not be measured individually. Considering that the solute was electrically neutral before it dissolved in the solvent, it will be electrically neutral in the solution as well, i. e. the cations and the anions always appear together in the solution, and, therefore, $f^\pm$ is the common activity coefficient for both, the cations and the anions.

In their contribution, Hamer & Wu measured and collected data from the literature to obtain the values for the activity and osmotic coefficients in aqueous solutions of uni-univalent electrolytes. If one is in search of the corresponding values for bi-univalent electrolytes, they can be found in Goldberg [78] and Goldberg [79]. Note furthermore that it is not possible to measure the activity of a single electrolyte. This is because always both ions dissociate in an electrolyte solution and, also, the condition that the solution as well as the original substances have been electrically neutral before the dissociation and will be electrically neutral thereafter as well. Therefore, one can only find the mean activity values for both ions.

A.2.2 Osmotic coefficients

In case of non-electrolyte solutes, the activity of the solvent can be calculated from the ones of the solutes via the *Gibbs-Duhem* equation, cf. Staples & Nuttall [157],

$$\sum_{\beta} n_m^{\beta} \, \mathrm{d}\mu_m^{\beta} \; = \; 0 \, , \tag{A.13}$$

where μ_m^{β} is the molar chemical potential discussed in detail in the previous section. Above relation can be transformed to yield

$$x_m^L \, \mathrm{d} \ln a^L \; = \; - \sum_{\gamma} x_m^{\gamma} \, \mathrm{d} \ln a^{\gamma} \tag{A.14}$$

with the aid of the mole fraction (2.17) and the chemical potential (A.9) such that a^L can be computed from the known values of x^{γ} and a^{γ}. Recall also that x^L is known via equation (2.18). But note that, because of the electrostatic effects, the activity of electrolytes is a quite sensitive quantity to measure solution nonlinearities. Therefore, calculating the activity corresponding to the solute via (A.14) would lead to incorrect results, cf. Table A.1. To circumvent this problem, Bjerrum [16] introduced in 1918 a new quantity ϕ^L, called the osmotic coefficient. As opposed to $f^{\pm}$, this coefficient is considered not in the logarithmic function but outside:

$$\mu_x^L \; = \; \mu_{x0}^L + \phi^L R\theta \, \ln x_m^L \, . \tag{A.15}$$

By comparison of the above relation with the chemical potential (A.8), one finds

$$\phi^L \; = \; \frac{\ln a^L}{\ln x^L} \, . \tag{A.16}$$

Following this, the osmotic coefficient can be computed from the activity of the liquid component measured by, for example, osmotic pressure experiments, where the measured osmotic pressure is compared to the computed one[4]. Note that the osmotic coefficient has to satisfy the limiting rule

$$\lim_{x^L \to 1} \phi^L = 1 \, . \tag{A.17}$$

The sensitivity of the different coefficients with respect to the concentration or the non-ideality of the solution can be seen by an example given in Klotz & Rosenberg [115]. Therein, the activity coefficients of the components of an electrolyte solution of potassium nitrate, i. e. $K^+NO_3^-$ dissociated in $H_2^+O^{2-}$, are compared with the osmotic coefficient of the solvent. As one can see in Table A.1, the activities of the dissolved ions alter in a much higher magnitude than the activity of the solvent. In contrast, the osmotic coefficient of

[4]By integration of the chemical potential of the solvent one obtains, cf. Klotz & Rosenberg [115],

$$\pi^L = - \frac{R\theta}{\tilde{V}_m^L} \, \ln a^L$$

which can be replaced in (A.16).

$K^+NO_3^-$ [mol/l]	$f^{\pm}$ [-]	f^L [-]	ϕ^L [-]
0.01	0.8993	1.00001	0.9652
0.05	0.7941	1.00005	0.9252
0.10	0.7259	1.00020	0.8965
1.00	0.3839	1.00560	0.6891

Table A.1: Activity coefficients of the solute and the solvent of a potassium nitrate ($K^+NO_3^-$) solution at different concentrations compared with the osmotic coefficient ϕ^L.

the solvent varies in almost the same manner, which makes ϕ^L from the experimental point of view a much more handy variable. Following this, it is assumed in this contribution that

$$f^L \approx 1 = \text{const.} \tag{A.18}$$

Following the above considerations about the osmotic coefficients, one finds that the activity f^L can not be converted into ϕ^L. This is one of the reasons, why it is not possible to introduce ϕ^L in a thermodynamically consistent manner. Moreover, it is also not possible to introduce the osmotic pressure consistently as given in Section 3.2.6.

Appendix B:
Additional model comparison and relations

B.1 Comparison with simplification S III

In this section, the results obtained by the simplification S III will briefly be compared to the results given in Section 5.1.1 and Section 5.1.2. As has already been mentioned, the simplification S III corresponds to the model presented in Ehlers & Acartürk [58]. Note that this model is not consistent with the thermodynamical assumptions made in Section 3.2.2. The geometry, the discretisation and the material parameters corresponding to this numerical example are already discussed in Section 5.1.

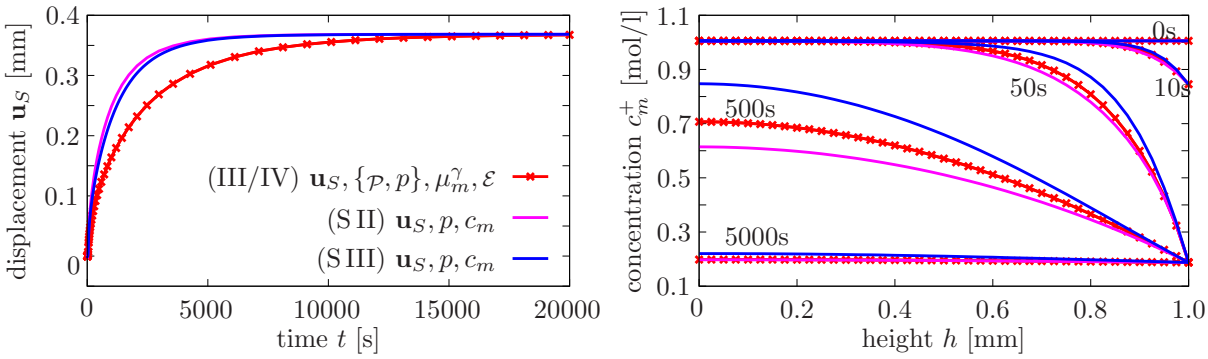

Figure B.1: Comparison of Variant III/IV (red with cross) and S II (magenta) with S III (blue). On the left-hand side, the vertical displacement of the observed node is depicted and, on the right-hand side, the cation concentration distribution within the domain at different times.

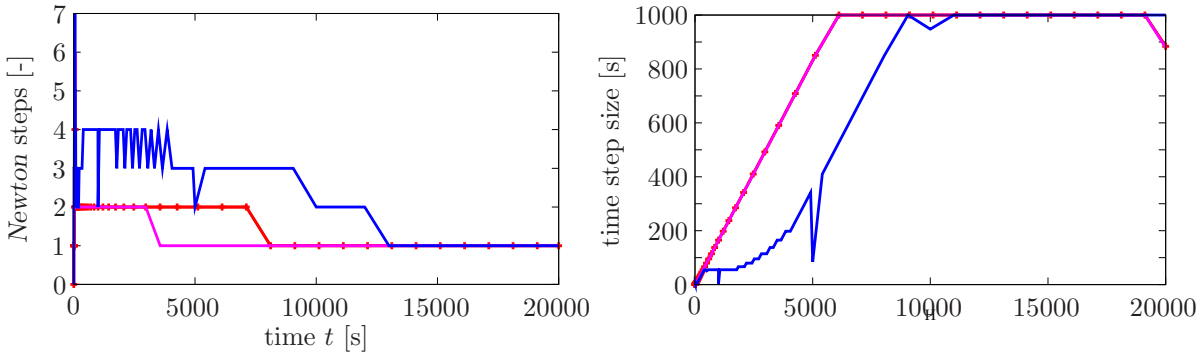

Figure B.2: Numerical aspects of the computations. On the left-hand side, the number of *Newton* iterations over time are shown and the time step size evolution on the right-hand side.

From the displacement curve on the left in Figure B.1, it can be seen that the consideration of a non-constant chemical potential of the liquid solvent has a relatively low influence on the deformation. In contrast, the concentrations within the domain are higher than the concentrations computed by the other variants.

Moreover, from the numerical point of view, by use of S III more *Newton* iterations are required to reach equilibrium and, thus, the time step size increases relatively slow. Following this, the simplification S III is less stable than S II. If one is interested in a reduced set of equations, then S II should be preferred.

B.2 Some further relations

Gradient of $\mathcal{E}$ formulated in the hydraulic pressure

$$\begin{aligned} F \operatorname{grad} \mathcal{E} \;=\; & \frac{z^{fc} D^L}{(z^+)^2 D^+ c_m^+ \,+\, (z^-)^2 D^- c_m^- \,+\, (z^{fc})^2 D^L c_m^{fc}} \operatorname{grad} \mathcal{P} \,+ \\ & + \frac{z^+ D^+ \rho_F^+ \,+\, z^- D^- \rho_F^- \,-\, z^{fc} D^L \rho^{FR}}{(z^+)^2 D^+ c_m^+ \,+\, (z^-)^2 D^- c_m^- \,+\, (z^{fc})^2 D^L c_m^{fc}} \, \mathbf{g} \,- \\ & - \frac{z^+ c_m^+ \,-\, z^{fc} c_m^{fc}}{(z^+)^2 D^+ c_m^+ \,+\, (z^-)^2 D^- c_m^- \,+\, (z^{fc})^2 D^L c_m^{fc}} \, R\theta \operatorname{grad} c_m^+ \,- \\ & - \frac{z^- c_m^- \,-\, z^{fc} c_m^{fc}}{(z^+)^2 D^+ c_m^+ \,+\, (z^-)^2 D^- c_m^- \,+\, (z^{fc})^2 D^L c_m^{fc}} \, R\theta \operatorname{grad} c_m^- \,. \end{aligned} \tag{B.1}$$

Time-integration of the mass balance

Starting from

$$(\rho^\alpha)'_\alpha \,+\, \rho^\alpha \operatorname{div} \mathbf{x}'_\alpha \;=\; 0 \,, \tag{B.2}$$

the divergence term is replaced by

$$(\det \mathbf{F}_\alpha)'_\alpha \;=\; \det \mathbf{F}_\alpha \operatorname{div} \mathbf{x}'_\alpha \,. \tag{B.3}$$

Thereafter, one obtains by separation of the variables

$$\int_0^t \Big(\frac{\rho^\alpha}{(\rho^\alpha)'_\alpha} \,+\, \frac{\det \mathbf{F}_\alpha}{(\det \mathbf{F}_\alpha)'_\alpha} \Big) \, \mathrm{d}t \;=\; 0 \,. \tag{B.4}$$

which is time-integrated. One obtains

$$\ln(\rho^\alpha) - \ln(\rho^\alpha_{0\alpha}) \,+\, \ln(\det \mathbf{F}_\alpha) - \ln(\det \mathbf{F}_{\alpha 0}) \;=\; 0 \,. \tag{B.5}$$

With the aid of the exponential function one obtains

$$\rho^\alpha \;=\; \rho^\alpha_{0\alpha} \, (\det \mathbf{F}_\alpha)^{-1} \,. \tag{B.6}$$

Bibliography

[1] Acartürk, A.; Ehlers, W. & Abbas, I.: Modelling of swelling phenomena in charged hydrated porous media. *PAMM* **4** (2004), 296–297.

[2] Adam, G.; Läuger, P. & Stark, G.: *Physikalische Chemie und Biophysik*, 3rd edn. Springer-Verlag, Berlin 1995.

[3] Ammann, M.: *Parallel Finite Element Simulations of Localization Phenomena in Porous Media*. Dissertation, Report No. II-11 of the Institute of Applied Mechanics (CE), Universität Stuttgart 2005.

[4] Anderson, G. M. & Crerar, D. A.: *Thermodynamics in Geochemistry: The Equilibrium Model*. Oxford University Press, New York 1992.

[5] Apel, N.: *Approaches to the Description of Anisotropic Material Behaviour at Finite Elastic and Plastic Defomations - Theory and Numerics*. Dissertation, Report No. I-12 of the Institute of Applied Mechanics (CE), Universität Stuttgart 2004.

[6] Atkin, R. J. & Craine, R. E.: Continuum theories of mixtures: Basic theory and historical development. *The Quarterly Journal of Mechanics and Applied Mathematics* **29** (1976), 209–244.

[7] Avci, A.: *Modelliereung und Simulation polyelektrolytischer Materialien im Rahmen der Theorie Poröser Medien*. Studienarbeit, Bericht Nr. 08-II-04 aus dem Institut für Mechanik (Bauwesen), Universität Stuttgart 2008.

[8] Bar-Cohen, Y.: *Electroactive Polymer (EAP) Actuators as Artificial Muscles: Reality, Potential, and Challenges*, 2nd edn. SPIE-International Society for Optical Engineering, Bellingham 2001.

[9] Barrett, R.; Berry, M.; Chan, T. F.; Demmel, J.; Donato, J.; Dongarra, J.; Eijkhout, V.; Pozo, R.; Romine, C. & der Vorst, H. V.: *Templates for the Solution of Linear Systems: Building Blocks for Iterative Methods*, 2nd edn. SIAM, Philadelphia 1994.

[10] Bathe, K.-J.: *Finite Element Procedures*, 2 edn. Prentice-Hall, New Jersey 1996.

[11] Bennethum, L. S.: Charge neutrality - Does it exist? In Huyghe, J. M.; Raats, P. A. C. & Cowin, S. C. (eds.), *Physicochemical and Electrochemical Interactions in Porous Media*, Springer, Doodrecht, The Netherlands 2005, pp. 259–265.

[12] Bennethum, L. S. & Cushman, J. H.: Multicomponent, multiphase thermodynamics of swelling porous media with electroquasistatics - I: Macroscale field equations. *Transport in Porous Media* **47** (2002), 309–336.

[13] Bennethum, L. S. & Cushman, J. H.: Multicomponent, multiphase thermodynamics of swelling porous media with electroquasistatics - II: Constitutive theory. *Transport in Porous Media* **47** (2002), 337–362.

[14] Biot, M. A.: General theory of three-dimensional consolidation. *Journal of Applied Physics* **12** (1941), 155–164.

[15] Bishop, A. W.: The effective stress principle. *Teknisk Ukeblad* **39** (1959), 859–863.

[16] Bjerrum, N.: Die Dissoziation der starken Elektrolyte. *Zeitschrift für Elektrochemie* **24** (1918), 321–328.

[17] Blome, K.-P.: *Ein Mehrphasen-Stoffmodell für Böden mit Übergang auf Interface-Gesetze*. Dissertation, Bericht Nr. II-10 aus dem Institut für Mechanik (Bauwesen), Universität Stuttgart 2003.

[18] Bluhm, J.: *A consistent model for saturated and empty porous media*. Habilitation, Forschungsberichte aus dem Fachbereich Bauwesen, Heft 74, Universität-GH Essen 1997.

[19] Bluhm, J.: Modelling of saturated thermo-elastic porous solids with different phase transitions. In Ehlers, W. & Bluhm, J. (eds.), *Porous Media: Theory, Experiments and Numerical Applications*, Springer-Verlag, Berlin 2002, pp. 87–118.

[20] Boehler, J. P.: Introduction of the invariant formulation of anisotropic constitutive equations. In Boehler, J. P. (ed.), *Applications of Tensor Functions in Solid Mechanics*, CISM Courses and Lectures No. 292, Springer-Verlag, Wien 1987, pp. 13–30.

[21] de Boer, R.: *Vektor- und Tensorrechung für Ingenieure*. Springer-Verlag, Berlin 1982.

[22] de Boer, R.: *Theory of Porous Media*. Springer-Verlag, Berlin 2000.

[23] de Boer, R.: *Trends in continuum mechanics of porous media*. Springer, Dodrecht, The Netherlands 2005.

[24] de Boer, R. & Ehlers, W.: *Theorie der Mehrkomponentenkontinua mit Anwendungen auf bodenmechanische Probleme*. Forschungsberichte aus dem Fachbereich Bauwesen, Heft 40, Universität-GH Essen 1986.

[25] de Boer, R. & Ehlers, W.: The development of the concept of effective stresses. *Acta Mechanica* **83** (1990), 77–92.

[26] Bowen, R. M.: Toward a thermodynamics and mechanics of mixtures. *Archive for Rational Mechanics and Analysis* **24** (1967), 370–403.

[27] Bowen, R. M.: Theory of mixtures. In Eringen, A. C. (ed.), *Continuum Physics, Volume III – Mixtures and EM Field Theories*, Academic Press, London 1976, pp. 1–127.

[28] Bowen, R. M.: Incompressible porous media models by use of the theory of mixtures. *International Journal of Engineering Science* **18** (1980), 1129–1148.

[29] Bowen, R. M.: Compressible porous media models by use of the theory of mixtures. *International Journal of Engineering Science* **20** (1982), 697–735.

[30] Bowen, R. M. & Wiese, J. C.: Diffusion in mixtures of elastic materials. *International Journal of Engineering Science* **7** (1969), 689–722.

[31] Boyle, R.: *Shadowrun: The Shadows Have Evolved*, 4th edn. Fantasy Productions 2005, URL www.shadowrun4.com.

[32] Braess, D.: *Finite Elemente*. Springer-Verlag, Berlin 1997.

[33] Brenan, K. E.; Campbell, S. L. & Petzold, L. R.: *Numerical Solution of Initial-Value Problems in Differential-Algebraic Equations*. SIAM, Philedelphia 1996.

[34] Brezzi, F. & Bathe, K.-J.: A discourse on the stability conditions for mixed finite element formulations. *Computer Methods in Applied Mechanics and Engineering* **82** (1990), 27–57.

[35] Chahine, N. O.; Chen, F. H.; Hung, C. T. & Ateshian, G. A.: Direct measurement of osmotic pressure of glycosaminoglycan solutions by membrane osmometry at room temperature. *Biophysical Journal* **89** (2005), 1543–1550.

[36] Chapelle, D. & Bathe, K. J.: The inf-sup test. *Computer & Structures* **47** (1993), 537–545.

[37] Chen, Y.; Chen, X. & Hisada, T.: Non-linear finite element analysis of mechanical electrochemical phenomena in hydrated soft tissues based on triphasic theory. *International Journal for Numerical Methods in Engineering* **65** (2006), 147–173.

[38] Coleman, B. D. & Noll, W.: The thermodynamics of elastic materials with heat conduction and viscosity. *Archive for Rational Mechanics and Analysis* **13** (1963), 167–178.

[39] Cross, J. J.: Mixtures of fluids and isotropic solids. *Archive of Mechanics* **25** (1973), 1025–1039.

[40] Danilov, A.: *Numerical treatment of dynamics in porous media*. Master Thesis, Report No. 04-II-5 of the Institute of Applied Mechanics (CE), Universität Stuttgart 2004.

[41] De, S. K. & Aluru, N. R.: A chemo-electro-mechanical mathematical model for simulation of ph sensitive hydrogels. *Mechanics of Materials* **36** (2004), 395–410.

[42] Debye, P. & Hückel, E.: Zur Theorie der Elektrolyte. I. Gefrierpunktserniedrigung und verwandte Erscheinungen. *Physikalische Zeitschrift* **24** (1923), 185–206.

[43] Delesse, M.: Pour déterminer la composition des roches. *Annales des mines, 4. séries* **13** (1848), 379–388.

[44] Diebels, S.: *Mikropolare Zweiphasenmodelle: Formulierung auf der Basis der Theorie Poröser Medien*. Habilitationsschrift, Bericht Nr. II-4 aus dem Institut für Mechanik (Bauwesen), Universität Stuttgart 2000.

[45] Diebels, S.: Micropolar mixture models on the basis of the Theory of Porous Media. In Ehlers, W. & Bluhm, J. (eds.), *Porous Media: Theory, Experiments and Numerical Applications*, Springer-Verlag, Berlin 2002, pp. 121–145.

[46] Diebels, S.; Ellsiepen, P. & Ehlers, W.: Error-controlled *Runge-Kutta* time integration of a viscoplastic hybrid two-phase model. *Technische Mechanik* **19** (1999), 19–27.

[47] Donnan, F. G.: Theorie der Membrangleichgewichte und Membranpotentiale bei Vorhandensein von nicht dialysierenden Elektrolyten. Ein Beitrag zur physikalisch-chemischen Physiologie. *Zeitschrift für Elektrochemie und Angewandte Physikalische Chemie* **17** (1911), 572–581.

[48] Dowell, E. H. & Hall, K. C.: Modeling of fluid-structure interaction. *Annual Reviews of Fluid Mechanics* **33** (2001), 445–490.

[49] Drumheller, D. S. & Bedford, A.: On the mechanics and thermodynamics of fluid mixtures. *Archive for Rational Mechanics and Analysis* **71** (1979), 345–355.

[50] Ehlers, W.: On thermodynamics of elasto-plastic porous media. *Archive of Mechanics* **41** (1989), 73–93.

[51] Ehlers, W.: *Poröse Medien – ein kontinuumsmechanisches Modell auf der Basis der Mischungstheorie*. Habilitationsschrift, Forschungsberichte aus dem Fachbereich Bauwesen, Heft 47, Universität-GH Essen 1989.

[52] Ehlers, W.: Toward finite theories of liquid-saturated elasto-plastic porous media. *International Journal of Plasticity* **7** (1991), 443–475.

[53] Ehlers, W.: Constitutive equations for granular materials in geomechanical context. In Hutter, K. (ed.), *Continuum Mechanics in Environmental Sciences and Geophysics*, CISM Courses and Lectures No. 337, Springer-Verlag, Wien 1993, pp. 313–402.

[54] Ehlers, W.: Grundlegende Konzepte in der Theorie Poröser Medien. *Technische Mechanik* **16** (1995), 63–76.

[55] Ehlers, W.: A single-surface yield function for geomaterials. *Archive of Applied Mechanics* **65** (1995), 246–259.

[56] Ehlers, W.: Foundations of multiphasic and porous materials. In Ehlers, W. & Bluhm, J. (eds.), *Porous Media: Theory, Experiments and Numerical Applications*, Springer-Verlag, Berlin 2002, pp. 3–86.

[57] Ehlers, W.: *Supplement to the COMMAS Courses*. Institute of Applied Mechanics (CE), Universität Stuttgart 2008, URL `www.mechbau.uni-stuttgart.de/ls2`.

[58] Ehlers, W. & Acartürk, A.: The role of implicit dirichlet boundary conditions for numerically stable computations of swelling phenomena. *Computational Mechanics* (2008), in press.

[59] Ehlers, W. & Blome, P.: A triphasic model for unsaturated soil based on the theory of porous media. *Mathematical and Computer Modelling* **37** (2003), 507–513.

[60] Ehlers, W. & Eipper, G.: Finite elastic deformations in liquid-saturated and empty porous solids. *Transport in Porous Media* **34** (1999), 179–191.

[61] Ehlers, W. & Ellsiepen, P.: Theoretical and numerical methods in environmental continuum mechanics based on the Theory of Porous Media. In Schrefler, B. A. (ed.), *Environmental Geomechanics*, CISM Courses and Lectures No. 417, Springer-Verlag, Wien 2001, pp. 1–81.

[62] Ehlers, W.; Ellsiepen, P.; Blome, P.; Mahnkopf, D. & Markert, B.: *Theoretische und numerische Studien zur Lösung von Rand- und Anfangswertproblemen in der Theorie Poröser Medien*. Forschungsbericht zum DFG-Projekt Eh 107/6-2, Bericht Nr. 99-II-1 aus dem Institut für Mechanik (Bauwesen), Universität Stuttgart 1999.

[63] Ehlers, W.; Karajan, N. & Markert, B.: A porous media model describing the inhomogeneous behaviour of the human intervertebral disc. *Materialwissenschaften und Wekstofftechnik* **37** (2006), 546–551.

[64] Ehlers, W.; Karajan, N. & Markert, B.: An extended biphasic model for charged hydrated tissues with application to the intervertebral disc. *Biomechanics and Modeling in Mechanobiology* (2008), in press.

[65] Ehlers, W. & Markert, B.: A linear viscoelastic biphasic model for soft tissues based on the Theory of Porous Media. *ASME Journal of Biomechanical Engineering* **123** (2001), 418–424.

[66] Ehlers, W.; Markert, B. & Acartürk, A.: Swelling phenomena of hydrated porous materials. In *Poromechanics III, Proceedings of the 3rd Biot Conference on Poromechanics*, Abousleiman, Y. N.; Cheng, A. H.-D. & Ulm, F. J., eds., Balkema Publishers, Leiden 2005, pp. 781–786.

[67] Einstein, A.: Zur Elektrodynamik bewegter Körper. *Annalen der Physik und Chemie* **17** (1905), 891–921.

[68] Eipper, G.: *Theorie und Numerik finiter elastischer Deformationen in fluidgesättigten porösen Festkörpern*. Dissertation, Bericht Nr. II-1 aus dem Institut für Mechanik (Bauwesen), Universität Stuttgart 1998.

[69] Ellison, W. J.; Lamkaouchi, K. & Moreau, J. M.: Water: a dielectric reference. *Journal of Molecular Liquids* **68** (1996), 171–279.

[70] Ellsiepen, P.: *Zeit- und ortsadaptive Verfahren angewandt auf Mehrphasenprobleme poröser Medien*. Dissertation, Bericht Nr. II-3 aus dem Institut für Mechanik (Bauwesen), Universität Stuttgart 1999.

[71] Eringen, A. C.: A mixture theory of electromagnetism and superconductivity. *International Journal of Engineering Science* **36** (1998), 525–543.

[72] Eringen, A. C. & Maugin, G. A.: *Electrodynamics of Continua I.* Springer-Verlag, New York 1990.

[73] Felippa, C. A. & Park, K. C.: Staggered transient analysis procedures for coupled mechanical systems: Formulation. *Computer Methods in Applied Mechanics and Engineering* **24** (1980), 61–111.

[74] Felippa, C. A.; Park, K. C. & Farhat, C.: Partitioned analysis of coupled mechanical systems. *Computer Methods in Applied Mechanics and Engineering* **190** (2001), 3247–3270.

[75] Fillunger, P.: *Erdbaumechanik?* Self-published by the author 1936.

[76] Frijns, A. J. H.; Huyghe, J. M. & Janssen, J. D.: A validation of the quadriphasic mixture theory for intervertebral disc tissue. *International Journal of Engineering Science* **35** (1997), 1419–1429.

[77] Ghadiani, S. R.: *A Multiphasic Contiuum Mechanical Model for Design Investigations of an Effusion-Cooled Rocket Thrust Chamber.* Dissertation,, Report No. II-13 of the Institute of Applied Mechanics (CE), Universität Stuttgart 2005.

[78] Goldberg, R. N.: Evaluated activity and osmotic coefficients for aqueous solutions: Bi-univalent compounds of Zinc, Cadmium and Ethylene Bis(trimethylammonium) Chloride and Iodide. *Journal of Physical and Chemical Reference Data* **10** (1981), 1–55.

[79] Goldberg, R. N.: Evaluated activity and osmotic coefficients for aqueous solutions: Thirty-six uni-bivalent electrolytes. *Journal of Physical and Chemical Reference Data* **10** (1981), 671–764.

[80] Graf, T.: *Zur Diskretisierung der Navier-Stokes-Gleichung.* Diplomarbeit, Bericht Nr. 01-II-11 aus dem Institut für Mechanik (Bauwesen), Universität Stuttgart 2001.

[81] Graf, T.: *Multiphasic flow processes in deformable porous media under consideration of fluid phase transitions.* Dissertation, Report No. II-17 of the Institute of Applied Mechanics (Civil Engineering), Universität Stuttgart 2008.

[82] Grant, C.; Twigg, P.; Egan, A.; Moody, A.; Smith, A.; Eagland, D.; Crowther, N. & Britland, S.: Poly(vinyl alcohol) hydrogel as a biocompatible viscoelastic mimetic for articular cartilage. *Biotechnology Progress* **22** (2006), 1400–1406.

[83] Green, A. E. & Naghdi, P. M.: Remarks on a paper by R. M. Bowen. *Archive for Rational Mechanics and Analysis* **27** (1967), 175–180.

[84] Grot, R. A.: Relativistic continuum physics: Electromagnetic interactions. In Eringen, A. C. (ed.), *Continuum Physics, Volume III – Mixtures and EM Field Theories*, Academic Press, London 1976, pp. 222–312.

[85] Gu, W. A.; Lai, W. M. & Mow, V. C.: Transport of multi-electrolytes in charged hydrated biological soft tissues. *Transport in Porous Media* **34** (1999), 143–157.

[86] Gu, W. Y.; Lai, W. M. & Mow, V. C.: A triphasic analysis of negative osmotic flows through charged hydrated soft tissues. *Journal of Biomechanics* **30** (1997), 71–78.

[87] Hamer, W. J. & Wu, Y.-C.: Osmotic coefficients and mean activity coefficients of uni-univalent electrolytes in water at 25°C. *Journal of Physical and Chemical Reference Data* **1** (1972), 1047–1097.

[88] Hansbo, P.: Lagrangian incompressible flow computations in three dimensions by use of space-time finite elements. *International Journal for Numerical Methods in Fluids* **20** (1995), 989–1001.

[89] Hansbo, P. & Hermansson, J.: Nitsche's method for coupling non-matching meshes in fluid-structure vibration problems. *Computational Mechanics* **32** (2003), 134–139.

[90] Haupt, P.: *Continuum Mechanics and Theory of Materials*. Springer-Verlag, Berlin 2000.

[91] Hayes, W. C. & Bodine, A. J.: Flow-independent vicoelastic properties of articular cartilage matrix. *Journal of Biomechanics* **11** (1978), 407–419.

[92] Heider, Y.: *Numerical simulation of wave prapagation in saturated porous media*. Master Thesis, Report No. 07-II-03 of the Institute of Applied Mechanics (CE), Universität Stuttgart 2007.

[93] Heidug, W. K. & Wong, S.: Hydration swelling of water-absorbing rocks: A constitutive model. *International Journal for Numerical and Analytical Methods in Geomechanics* **20** (1996), 403–430.

[94] Heinrich, G. & Desoyer, K.: Theorie dreidimensionaler Setzungsvorgänge in Tonschichten. *Ingenieur-Archiv* **30** (1961), 225–253.

[95] Helmig, R.: *Multiphase Flow and Transport Processes in the Subsurface*. Springer-Verlag, Berlin 1997.

[96] Hille, T. S.: *Beschreibung elektro-chemischen Materialverhaltens anhand klassischer Potentialtheorien in der Theorie Poröser Medien*. Diplomarbeit, Bericht Nr. 04-II-3 aus dem Institut für Mechanik (Beuwesen), Universität Stuttgart 2004.

[97] Hirt, C. W.; Amsden, A. A. & Cook, J. L.: An arbitrary Lagrangian-Eulerian computing method for all flow speeds. *Journal of Computational Physics* **14** (1974), 227–253.

[98] Hirt, C. W.; Cook, J. L. & Butler, T. D.: A Lagrangian method for calculating the dynamics of an incompressible fluid with free surface. *Journal of Computational Physics* **5** (1970), 103–124.

[99] Holzapfel, G. A.: *Nonlinear Solid Mechanics: A Continuum Approach for Engineering*. John Wiley & Sons, Chichester 2001.

[100] Hon, Y. C.; Lu, M. W.; Xue, W. M. & Zhou, X.: A new formulation and computation of the triphasic model for mechano-electrochemical mixtures. *Computational Mechanics* **24** (1999), 155–165.

[101] Huang, C.-Y.; Mow, V. C. & Ateshian, G. A.: The role of flow-independent viscoleasticity in the biphasic tensile and compressive responses of articular cartilage. *Transcations of the ASME* **123** (2001), 410–417.

[102] Hueckel, T.: Chemo-plasticity of clays subjected to stress and flow of a single contaminant. *International Journal for Numerical and Analytical Methods in Geomechanics* **21** (1997), 43–72.

[103] Hutter, K. & Jönk, K. D.: *Continuum Methods of Physical Modeling*. Springer-Varlag, Berlin 2004.

[104] Hutter, K.; van de Ven, A. A. F. & Ursescu, A.: *Electromagnetic Field Matter Interactions in Thermoelastic Solids and Viscous Fluids*. Springer, Berlin 2006.

[105] Huyghe, J. M.: Intra-extrafibrillar mixture formulation of soft charged hydrated tissues. *Journal of Theoretical and Applied Mechanics* **37** (1999), 519–536.

[106] Huyghe, J. M.; Houben, G. B.; Drost, M. R. & van Donkelaar, C. C.: An ionised/non-ionised dual porosity model of intervertebral disc tissue. *Biomechanics and Modeling in Mechanobiology* **2** (2003), 3–19.

[107] Huyghe, J. M. & Janssen, J. D.: Quadriphasic mechanics of swelling incompressible porous media. *International Journal of Engineering Science* **35** (1997), 793–802.

[108] Huyghe, J. M. & Janssen, J. D.: Thermo-chemo-electro-mechanical formulation of saturated charged porous solids. *Transport in Porous Media* **34** (1999), 129–141.

[109] Huyghe, J. M.; Molenaar, M. M. & Baaijens, F. P. T.: Poromechanics of compressible charged porous media using the theory of mixtures. *ASME Journal of Biomechanical Engineering* **129** (2007), 776–785.

[110] Kaasschieter, E. F.; Frijns, A. J. H. & Huyghe, J. M. R. J.: Mixed finite element modelling of cartilaginous tissues. *Mathematics and Computers in Simulation* **61** (2003), 549–560.

[111] Karajan, N.; Ehlers, W. & Markert, B.: An anisotropic porous media model of the intervertebral disc. *PAMM* **3** (2003), 180–181.

[112] Karajan, N.; Ehlers, W. & Markert, B.: Suitable initial conditions for multiphasic FE computations of spinal discs. *PAMM* **6** (2006), 133–134.

[113] Karajan, N.: *An Extended Biphasic Description of the Inhomogeneous and Anisotropic Intervertebral Disc*. Dissertation, Report No. II-19 of the Institute of Applied Mechanics (Civil Engineering), Universität Stuttgart 2009.

[114] Kisiday, J.; Jin, M.; Kurz, B.; Hung, H.; Semino, C.; Zhang, S. & Grodzinsky, A. J.: Self-assembling peptide hydrogel fosters chondrocyte extracellular matrix production and cell division: Implications for cartilage tissue repair. *PNAS* **99** (2002), 9996–10001.

[115] Klotz, I. M. & Rosenberg, R. M.: *Chemical Thermodynamics: Basic Theory and Methods*, 6th edn. John Wiley & Sons, New York 2000.

[116] Lai, W. M.; Hou, J. S. & Mow, V. C.: A triphasic theory for the swelling and deformation behaviours of articular cartilage. *ASME Journal of Biomechanical Engineering* **113** (1991), 245–258.

[117] Lai, W. M.; Mow, V. C.; Sun, D. D. & Ateshian, G. A.: On the electric potentials inside a charged soft hydrated biological tissue: Streaming potential vs. diffusion potential. *ASME Journal of Biomechanical Engineering* **122** (2000), 336–346.

[118] Lanir, Y.: Biorheology and fluidflux in swelling tissues. I. Bicomponent theory for small deformations, including concentration effects. *Biorheology* **24** (1987), 173–187.

[119] Li, H.; Luo, R. & Lam, K. Y.: Modeling and simulation of deformation of hydrogels responding to electric stimulus. *Journal of Biomechanics* **40** (2007), 1091–1098.

[120] Li, H.; Yuan, Z.; Lam, K. Y.; Lee, H. P.; Chen, J.; Hanes, J. & Fu, J.: Model development and numerical simulation of electric-stimulus-responsive hydrogels subject to an externally applied electric field. *Biosensors and Bioelectronics* **19** (2004), 1097–1107.

[121] Liu, I.-S.: Method of Lagrange multipliers for exploitation of the entropy principle. *Archive for Rational Mechanics and Analysis* **46** (1972), 131–148.

[122] van Loon, R.; Huyghe, J. M.; Wijlaars, M. W. & Baaijens, F. P. T.: 3D FE implementation of an incompressible quariphasic mixture model. *International Journal for Numerical Methods in Engineering* **57** (2003), 1243–1258.

[123] Loret, B.; Hueckel, T. & Gajo, A.: Chemo-mechanical coupling in saturated porous media: elastic-plastic behaviour of homoionic expansive clays. *International Journal of Solids and Structures* **39** (2002), 2773–2806.

[124] Loret, B. & Simões, F. M. F.: Articular cartilage with intra- and extrafibrillar waters: a chemo-mechanical model. *Mechanics of Materials* **36** (2004), 515–541.

[125] Low, P. F.: Structural component of the swelling pressure of clays. *Langmiur* **3** (1987), 18–25.

[126] Mabuma, J.: *Modelling and simulation of swelling phenomena by use of chemical potentials*. Master thesis, Report No. 07-II-04 of the Institute of Applied Mechanics (CE), Universität Stutgart 2007.

[127] Mahnkopf, D.: *Lokalisierung fluidgesättigter poröser Festkörper bei finiten elastoplastischen Deformationen*. Dissertation, Bericht Nr. II-5 aus dem Institut für Mechanik (Bauwesen), Universität Stuttgart 2000.

[128] Mak, A. F.: The apparent viscoelastic behaviour of articular cartilage – the contributions from the intrinsic matrix viscoelasticity and interstitial fluid flows. *ASME Journal of Biomechanical Engineering* **108** (1986), 123–130.

[129] Malakpoor, K.: *Mixed Finite Element for Swelling of Cartilaginous Tissues*. Ph. D. thesis, Technische Universiteit Eindhoven 2007.

[130] Markert, B.: *Porous media viscoelasticity with application to polymeric foams*. Dissertation, Report No. II-12 of the Institute of Applied Mechanics (Civil Engineering), Universität Stuttgart 2005.

[131] Markert, B.: A constitutive approach to 3-d nonlinear fluid flow through finite deformable porous continua. *Transport in Porous Media* **70** (2007), 427–450.

[132] di Martino, A.; Vaccaro, A.; Lee, J. Y.; Denaro, V. & Lim, M. R.: Nucleus pulposus replacement: Basic science and indications for clinical use. *Spine* **30** (2005), 16–22.

[133] Maugin, G. A.: *Continuum Mechanics of Electromagnetic Solids*, vol. 33 of *North-Holland Series in Applied Mathematics and Mechanics*. Elsevier Science Publishers B.V., Amsterdam 1988.

[134] Maugin, G. A.; Pouget, J.; Drouot, R. & Collet, B.: *Nonlinear Electromechanical Couplings*. Nonlinear Science: Theory and Applications, John Wiley & Sons, Chichester 1992.

[135] Mow, V. C.; Ateshian, G. A.; Lai, W. M. & Gu, W. Y.: Effects of fixed charges on the stress-relaxation behavior of hydrated soft tissues in a confined compression problem. *International Journal of Solids and Structures* **35** (1998), 4945–4962.

[136] Mow, V. C.; Kuei, S. C.; Lai, W. M. & Armstrong, C. G.: Biphasic creep and relaxation of articular cartilage in compression: theory and experiments. *ASME Journal of Biomechanical Engineering* **102** (1980), 73–84.

[137] Mow, V. C. & Ratcliffe, A.: Structure and function of articular cartilage and meniscus. In Mow, V. C. & Hayes, W. C. (eds.), *Basic Orthopaedic Biomechanics*, 2nd edn., Lippincott-Raven Publishers, Philadelphia 1997, pp. 113–176.

[138] Nörtemann, K.; Hilland, J. & Kaatze, U.: Dielectric properties of aqueous NaCl solutions at microwave frequencies. *The Journal of Physical Chemistry A* **101** (1997), 6864–6869.

[139] O'Handley, R. C.: *Modern Magnetic Materials: Priciples and Applications*. John Wiley & Sons, New York 2000.

[140] van Olphen, H.: *An Itroduction to Clay Colloid Chemistry: for Clay Technologists, Geologists, and Soil Scientists*. Krieger Publications 1991.

[141] Ott, J. B. & Boerio-Goates, J.: *Chemical Thermodynamics: Principles and Applications*. Elsevier 2000.

[142] Prigogine, I. & Defay, R.: *Chemical Thermodynamics*. Longmans, Green and Co., London 1954.

[143] Radovitzky, R. & Ortiz, M.: Lagrangian finite element analysis of Newtonian fluid flows. *International Journal for Numerical Methods in Engineering* **43** (1998), 607–619.

[144] Ramaswamy, B. & Kawahara, M.: Lagrangian finite element analysis applied to viscous free surface fluid flow. *International Journal for Numerical Methods in Fluids* **7** (1987), 953–984.

[145] Ricken, T. & Ustohalova, V.: Modeling of thermal mass transfer in porous media with applications to the organic phase transition in landfills. *Computational Materials Science* **32** (2005), 498–508.

[146] Samson, E.; Marchand, J.; Robert, J.-L. & Bournazel, J.-P.: Modelling ion diffusion mechanisms in porous media. *International Journal for Numerical Methods in Engineering* **46** (1999), 2043–2060.

[147] Scardovelli, R. & Zaleski, S.: Direct numerical simulation of free-surface and interfacial flow. *Annual Review of Fluid Mechanics* **31** (1999), 567–603.

[148] Schanz, M. & Diebels, S.: A comparative study of Biot's theory and the linear theory of porous media for wave propagation problems. *Acta Mechanica* **161** (2003), 213–235.

[149] Scholz, B.: *Application of a micropolar model to the localization phenomena in granular materials*. Dissertation, Report No. II-15 of the Institute of Applied Mechanics (CE), Universität Stuttgart 2007.

[150] Schröder, J.: *Theoretische und algorithmische Konzepte zur phänomenologischen Beschreibung anisotropen Materialverhaltens*. Dissertation, Bericht Nr. I-1 aus dem Institut für Mechanik (Bauwesen), Universität Stuttgart 1996.

[151] Schröder, J.; Neff, P. & Balzani, D.: A variational approach for materially stable anisotropic hyperelasticity. *International Journal of Solids and Structures* **42** (2005), 4352–4371.

[152] Schwarz, H. R.: *Numerische Mathematik*. B. G. Teuner, Stuttgart 1997.

[153] Sherwood, J. D.: Biot poroelasticity of a chemically active shale. *Proceedings of the Royal Society of London A* **440** (1993), 365–377.

[154] Skempton, A. W.: Significance of Terzaghi's concept of effective stress (Terzaghi's discovery of effective stress). In Bjerrum, L.; Casagrande, A.; Peck, R. B. & Skempton, A. W. (eds.), *From Theory to Practice in Soil Mechanics*, John Wiley & Sons, New York 1960, pp. 42–53.

[155] Snijders, H.; Huyghe, J. M. & Janssen, J. D.: Triphasic finite element model for swelling porous media. *International Journal for Numerical Methods in Fluids* **20** (1995), 1039–1046.

[156] Spencer, A. J. M.: Constitutive theory for strongly anisotropic solids. In Spencer, A. J. M. (ed.), *Continuum Theory of the Mechanics of Fibre-Reinforced Composites*, CISM Courses and Lectures No. 282, Springer-Verlag, Wien 1984, pp. 1–32.

[157] Staples, B. R. & Nuttall, R. L.: The activity and osmotic coefficients of aqueous Calcium Chloride at 298.15 K. *Journal of Physical and Chemical Reference Data* **6** (1977), 385–407.

[158] Steeb, H.: *Fehlerschätzer für FE-Berechnungen bei entfestigenden Materialien*. Dissertation, Bericht Nr. 37 aus dem Institut für Baustatik, Universität Stuttgart 2002.

[159] Sun, D. N.; Gu, W. Y.; Guo, X. E. & Mow, W. M. L. V. C.: A mixed finite element formulation of triphasic mechano-electrochemical theory for charged, hydrated biological soft tissues. *International Journal for Numerical Methods in Engineering* **45** (1999), 1375–1402.

[160] Terzaghi, K.: Die Berechnung der Durchlässigkeitsziffer des Tones aus dem Verlauf der hydrodynamischen Spannungserscheinungen. *Sitzungsberichte der Kaiserlichen Akademie der Wissenschaften, Mathematisch-Naturwissenschaftliche Klasse, Abteilung 2a* **132** (1923), 125–138.

[161] Tezduyar, T. E.: Finite element methods for flow problems with moving boundaries and interfaces. *Archives of Computational Methods in Engineering* **8** (2001), 83–130.

[162] Truesdell, C. & Noll, W.: The non-linear field theories of mechanics. In Flügge, S. (ed.), *Handbuch der Physik*, vol. III/3, Springer-Verlag, Berlin 1965, pp. 1–598.

[163] Truesdell, C. & Toupin, R. A.: The classical field theories. In Flügge, S. (ed.), *Handbuch der Physik*, vol. III/1, Springer-Verlag, Berlin 1960, pp. 226–902.

[164] Volk, W.: *Untersuchung des Lokalisierungsverhaltens mikropolarer poröser Medien mit Hilfe der Cosserat-Theorie*. Dissertation, Bericht Nr. II-2 aus dem Institut für Mechanik (Bauwesen), Universität Stuttgart 1999.

[165] van der Waals, J. D.: *Over de Continuiteit van den Gas- en Vloeistoftoestand*. Academisch proefschrift, Sijthoff, Leiden 1873.

[166] Wall, W. A.: *Fluid-Struktur-Interaktion mit stabilisierten Finiten Elementen*. Dissertation, Bericht Nr. 31 aus dem Institut für Baustatik, Universität Stuttgart 1999.

[167] Wall, W. A.; Genkinger, S. & Ramm, E.: A strong coupling partitioned approach for fluid-structure interaction with free surfaces. *Computers & Fluids* **36** (2007), 169–183.

[168] Wallmersperger, T.: *Modellierung und Simulation stimulierbarer polyelektrolytischer Gele*. Dissertation, Institut für Statik und Dynamik der Luft- und Raumfahrtkonstruktionen, University of Stuttgart 2003.

[169] Woltman, R.: *Beyträge zur Hydraulischen Architektur*. Dritter Band, Johann Christian Dietrich, Göttingen 1794.

[170] Zhou, X.; Hon, Y. C.; Sun, S. & Mak, A. F. T.: Numerical simulation of the steady-state deformation of a smart hydrogel under external electric field. *Smart Material Structures* **11** (2002), 459–467.

[171] Zienkiewicz, O. C.; Qu, S.; Taylor, R. L. & Nakazawa, S.: The patch test for mixed formulations. *International Journal for Numerical Methods in Engineering* **23** (1986), 1873–1883

[172] Zienkiewicz, O. C. & Taylor, R. L.: *The Finite Element Method*, 5th edn. Butterworth-Heinemann, Oxford 2000.

[173] Zienkiewicz, O. C.; Taylor, R. L.; Sherwin, S. J. & Peiró, J.: On discontinuous galerkin methods. *International Journal for Numerical Methods in Engineering* **58** (2003), 1119–1148.

Curriculum vitae

Name:	Ayhan Yusuf Acartürk
Date of Birth:	30th October 1970
Place of Birth:	Stuttgart, Germany
Nationality:	German
Martial Status:	Unmarried
Education:	1976 – 1981 Elementary School: Konya, Turkey
	1981 – 1988 Secondary School: Realschule der Stadt Frechen
	1988 – 1991 Ingenieurbüro Boll & Partner, Stuttgart Trained as Engineering Draughtsman
	1991 – 1993 High School: Technische Oberschule Stuttgart
Community Service:	1994 – 1995 Community Service at Stiftung Wilhelmspflege, Stuttgart
Studies:	1995 – 2001 Civil Engineering at the University of Stuttgart
Professional Occupation:	2002 – 2008 Research Associate Institute of Applied Mechanics (Civil Engineering) University of Stuttgart
	since 2008 Development Engineer TWT - Science & Innovation Neuhausen a. d. F.

Released report series:

II-1 Gernot Eipper: *Theorie und Numerik finiter elastischer Deformationen in fluidgesättigten porösen Festkörpern*, June 1998.

II-2 Wolfram Volk: *Untersuchung des Lokalisierungsverhaltens mikropolarer poröser Medien mit Hilfe der Cosserat-Theorie*, May 1999.

II-3 Peter Ellsiepen: *Zeit- und ortsadaptive Verfahren angewandt auf Mehrphasenprobleme poröser Medien*, July 1999.

II-4 Stefan Diebels: *Mikropolare Zweiphasenmodelle: Formulierung auf der Basis der Theorie Poröser Medien*, March 2000.

II-5 Dirk Mahnkopf: *Lokalisierung fluidgesättigter poröser Festkörper bei finiten elastoplastischen Deformationen*, March 2000.

II-6 Heiner Müllerschön: *Spannungs-Verformungsverhalten granularer Materialien am Beispiel von Berliner Sand*, August 2000.

II-7 Stefan Diebels (Ed.): *Zur Beschreibung komplexen Materialverhaltens: Beiträge anläßlich des 50. Geburtstages von Herrn Prof. Dr.-Ing. Wolfgang Ehlers*, August 2001.

II-8 Jack Widjajakusuma: *Quantitative Prediction of Effective Material Parameters of Heterogeneous Materials*, June 2002.

II-9 Alexander Droste: *Beschreibung und Anwendung eines elastisch-plastischen Materialmodells mit Schädigung für hochporöse Metallschäume*, October 2002.

II-10 Peter Blome: *Ein Mehrphasen-Stoffmodell für Böden mit Übergang auf Interface-Gesetze*, October 2003.

II-11 Martin Ammann: *Parallel Finite Element Simulations of Localization Phenomena in Porous Media*, April 2005.

II-12 Bernd Markert: *Porous Media Viscoelasticity with Application to Polymeric Foams*, July 2005.

II-13 Saeed Reza Ghadiani: *A Multiphasic Continuum Mechanical Model for Design Investigations of an Effusion-Cooled Rocket Thrust Chamber*, September 2005.

II-14 Wolfgang Ehlers & Bernd Markert (Eds.): *Proceedings of the 1st GAMM Seminar on Continuum Biomechanics*, September 2005.

II-15 Bernd Scholz: *Application of a Micropolar Model to the Localization Phenomena in Granular Materials: General Model, Sensitivity Analysis and Parameter Optimization*, November 2007.

II-16 Wolfgang Ehlers & Nils Karajan (Eds.): *Proceedings of the 2nd GAMM Seminar on Continuum Biomechanics*, December 2007.

II-17 Tobias Graf: *Multiphasic Flow Processes in Deformable Porous Media under Consideration of Fluid Phase Transitions*, June 2008.

II-18 Ayhan Acartürk: *Simulation of Charged Hydrated Porous Materials*, March 2009.

II-19 Nils Karajan: *An Extended Biphasic Description of the Inhomogeneous and Anisotropic Intervertebral Disc*, March 2009.

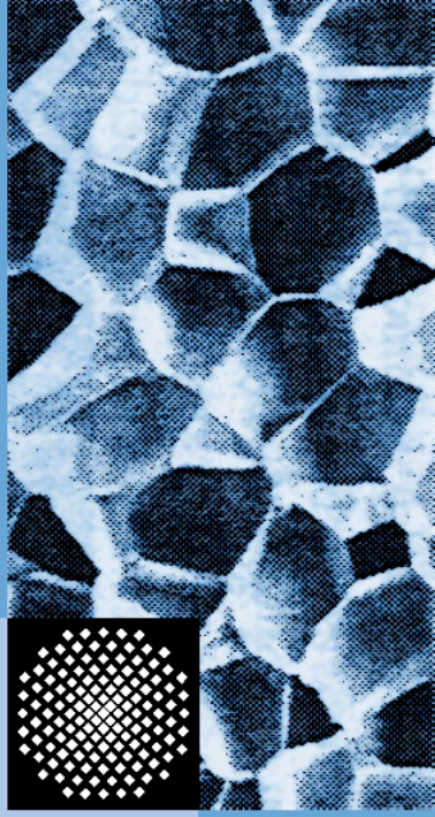

VGE
Verlag Glückauf Essen

ISBN 3–937399–18–6
(D 93 – Dissertation, Universität Stuttgart)